

附件

## 内蒙古自治区重点实验室 2023 年度 工作报表

实验室名称：内蒙古自治区马铃薯产业融合发展企业重点  
实验室  
实验室主任：仲乃琴  
主管部门：呼伦贝尔市科学技术局  
依托单位：呼伦贝尔恒屹农牧业股份有限公司  
通讯地址：呼伦贝尔市海拉尔区  
邮政编码：021000  
联系人：志恒  
联系电话：13904703429  
E-mail 地址：zhiheng0616@163.com

2023 年 12 月 29 日填报

2023 年制

## 一、基本信息

实验室名称	中文：内蒙古自治区马铃薯产业融合发展企业重点实验室			
	英文：Key Laboratory of Integrated Development Enterprises in the Potato Industry			
实验室简介	<p>内蒙古自治区马铃薯产业融合发展企业重点实验室于2022年6月在“内蒙古自治区马铃薯肥料农药高效利用技术企业重点实验室”原有的基础上进行优化和调整，由原来单一与中国科学院微生物研究所合作，调整扩增为集合“内蒙古自治区马铃薯种薯绿色繁育技术院士专家工作站”、中国科学院微生物研究所、自治区农牧业产业化重点龙头企业“呼伦贝尔恒屹农牧业股份有限公司”、东华大学、青岛农业大学食品研究院、呼伦贝尔市新型研发机构“呼伦贝尔恒屹马铃薯产业研究院有限公司”等科研平台、基地组建。</p> <p>内蒙古自治区马铃薯产业融合发展企业重点实验室，以马铃薯产业融合发展领域的关键技术问题为目标，突破产业重大共性关键技术，推动马铃薯产业链科技成果转化和技术创新。</p>			
研究方向 (据实增删)	研究方向1	马铃薯肥料高效利用与化肥替代技术		
	研究方向2	马铃薯化学农药控失及绿色防控技术		
	研究方向3	加工专用型马铃薯新品种选育		
	研究方向4	马铃薯主粮化与高值化精深加工关键技术		
	研究方向5	畜禽粪污农作物秸秆快速腐熟技术		
实验室主任	姓名	仲乃琴	出生年月	1965.05.15
	职称	正高级	专业领域	农业生物技术
	任职时间	2018年	在依托单位职务	中科院微生物所

学术 委员会 主任	姓名	方荣祥	出生年月	1946.01.19
	职称	正高级	专业领域	植物病毒学
	任职时间	2018年	所在单位及职务	中科院微生物所

## 二、重点实验室年度情况

实验室 经费 (万元)	经费构成	运行费 (万元)	科研经费 (万元)	仪器设备购 置费 (万元)	合计
	国家	0	0	0	0
	部门 (地方)	0	180	0	180
	依托单位	98.8	250	5.85	354.65
	合计	98.8	430	5.85	534.65
科研 条件 (当前 情况)	实验室面积		2016 平方米		
	科研仪器、设备累计		65 台	120 万元	
	大型仪器、设备 (50 万元 以上) 累计		0 台	0 万元	
科研 情况	承担国家自然科学基金		0 项	经费	0 万元
	承担自治区自然科学基金		0 项	经费	0 万元
	承担自治区科技计划项目		1 项	经费	100 万元
	承担地市级项目 (课题)		1 项	经费	80 万元
	承担横向项目 (课题)		2 项	经费	50 万元
	合计		4		230
人才	固定人员		28 人		

队伍	高级职称	6人	中级职称	4人	初级职称	0人	
	流动人员		16人				
	高级职称	4人	中级职称	4人	初级职称	0人	
	院士		固定	1人	百千万人才	固定	0人
			流动	0人		流动	0人
	杰青或优青		固定	人	长江学者	固定	0人
			流动	1人		流动	0人
	其他国家级人才		固定	0人	省部级人才计划	固定	0人
流动			0人	流动		2人	
运行管理	管理制度	10项	是否全部实施		是 <input checked="" type="checkbox"/> 否 <input type="checkbox"/>		
	组建学术委员会	是 <input checked="" type="checkbox"/> 否 <input type="checkbox"/>	召开会议次数		1次		
开放共享	开放课题	2项	经费合计		50万元		
	仪器设施对外开放机时	86小时	开展科普活动		1次		

### 三、成果统计

获奖情况	国家级奖励	一等奖	0项		二等奖	0项	
	省、部级科技奖励	一等奖	1项	二等奖	0项	三等奖	0项
	行业科技奖励	一等奖	0项	二等奖	0项	三等奖	0项
论文专著	发表论文	共计	6篇	SCI	0篇	EI	6篇
	专著	国内出版	0部		国外出版	0部	



知识 产权	发明专利	国际	3 项	国内	1 项
	其它专利	国际	0 项	国内	0 项
	标准规范	国际标准	0 个	国家标准	0 个
		行业标准	0 个	团体标准	1 个
产学研 合作	与高校、院所 合作	1 项	合作经费	24 万元	
	与企业合作	0 项	合作经费	0 万元	
行业 支撑	成果转移转化	1 项	转移转化收入	100 万元	
	行业技术服务	0 项	服务收入	0 万元	

注：以上各表中所有数据指截止到统计年度所得数据或统计年度当年情况，项目经费指每个项目的总经费。

#### 四、实验室本年度建设情况

简要介绍实验室本年度研发条件与能力、科研水平与贡献、团队建设与人才培养、开放交流与运行管理等情况。存在的不足及下一步工作计划。

##### 一、研发条件与能力

2023 年依托单位呼伦贝尔恒屹农牧业股份有限公司为实验室共计投入 354.65 万元，其中，日常运行经费 27.68 万元，仪器设备经费 5.85 万元，人才培养与引进经费 71.12 万元（包括实验室固定人员工资），科研经费 250 万元。

2017 年本实验室依托单位呼伦贝尔恒屹农牧业股份有限公司与中国科学院微生物所开始合作，2019 年正式签订了全面科技合

作协议，2021 年续签，并新增了约定大型仪器实现开放共享，为共同研发肥药高效利用及替代技术提供科研保障，本实验室及其依托单位可根据科研需求可随时免费预约使用。例如：磷屏扫描仪、红外双色扫描仪、高速转盘式激光共聚焦显微镜, 荧光显微镜，qRT-PCR 仪，全自动核酸提取仪，高通量植物样品粉碎系统等设备。

依托单位购置并建成了完整的病毒分子检测平台、微生物分离平台、脱毒苗组培平台，包括 eppendorf 冷冻离心机 1 台、博日基因扩增仪 1 台、上海天能凝胶成像系统 1 台、北京六一琼脂糖水平电泳仪 1 台、知信制冰机 1 台、奥浦两档体式显微镜 1 台，土壤速测仪 1 台，超净工作台 20 个等 60 余台（套），价值（原值）120 余万元。设备对于进行马铃薯组培苗、种薯的病毒检测、土壤病原菌的分子鉴定，具备良好的检出能力，为企业马铃薯的种薯品质提供技术保障。

内蒙古自治区马铃薯产业融合发展企业重点实验室于 2022 年 6 月在“内蒙古自治区马铃薯肥料农药高效利用技术企业重点实验室”原有的基础上进行优化和调整，由原来单一与中国科学院微生物研究所合作，调整扩增为集合“内蒙古自治区马铃薯种薯绿色繁育技术院士专家工作站”、中国科学院微生物研究所、自治区农牧业产业化重点龙头企业“呼伦贝尔恒屹农牧业股份有限公司”、东华大学、青岛农业大学食品研究院、呼伦贝尔市新型研发机构“呼伦贝

尔恒屹马铃薯产业研究院有限公司”等科研平台、基地组建。

内蒙古自治区马铃薯产业融合发展企业重点实验室，以马铃薯产业融合发展领域的关键技术问题为目标，突破产业重大共性关键技术，推动马铃薯产业链科技成果转化和技术创新。

截止至 2023 年 12 月 31 日，实验室的主要研究方向承担国家和自治区各级各类项目共 9 项，其中，国家级项目 1 项为国家发改委项目；中国科学院项目 1 项；自治区级项目共 6 项，包括自治区应用技术与开发项目 1 项，院士工作站建设 1 项，自治区科技创新引导奖励资金 2 项；关键技术攻关 2 项，呼伦贝尔市级项目 5 项。

## 二、科研水平与贡献

**马铃薯新品种选育工作：**通过三年的育种工作，实验室已收集鉴定了几十份优质马铃薯亲本资源，2023 年，本站依托呼伦贝尔恒屹农牧业股份有限公司与呼伦贝尔农牧科学研究合作，开展“加工专用型马铃薯新品种选育”研究工作，现已对目标品种“恒屹 1 号、恒屹 2 号”进行 DUS 测试，其淀粉含量在 18%左右或干物质含量 20 左右，还原糖含量低于 0.4%，平均单产 2.3 吨/亩以上，抗晚疫病，抗退化等综合形状表现突出。2024 年预申请登记目标新品种 1-2 个。

**病毒检测工作：**开展马铃薯病毒检测，利用 PCR 技术鉴定马铃薯样品的病毒含量,培训相关技术人员 1-2 名，使其能够掌握病毒检

测技术的操作程序，鉴定种植区域马铃薯病毒病主要病源，分析土壤理化性质，制定了防控方案；对马铃薯种苗、种薯、土壤进行病害、病毒等检测，严控种苗、种薯质量；同时开展肥药减施增效、土传病害防控等功能菌剂技术开发，进行技术的展示及应用，培训相关技术人员 1-2 名。

**种质资源库建设工作：**2023 年我们成功地建成了种质资源库，并实现了正常运行。该资源库收藏了马铃薯种质资源共计 70 余份，种质资源库的建设，不仅丰富了我地区种质资源的保存手段和管理方式，还有力地推动了农业科技创新和产业升级。未来，我们将继续优化和完善种质资源库及其管理水平，进一步提高我地区在种质资源保护和利用方面的水平，为农业现代化做出更大的贡献。

**组培室育苗工作：**在 2023 年，我们的马铃薯组培室在繁育种苗方面取得了显著的成果。今年，我们共繁育了种苗 500 万株，较去年增长了 21% 左右。这些种苗均经过精心培育和筛选，以保证其生长状况良好，符合农业生产的各项标准。为了更好地满足对高品质马铃薯的需求我们将继续优化培育技术，提高种苗质量及成活率。同时，也将加强与相关科研机构的合作与交流，吸收先进的农业科技成果，为农业生产提供更优质的服务。

**成果应用示范及转化工作：**实验室以具有自主知识产权的环保肥料增效剂、农药控失剂、高效叶面肥、拌种菌剂等为核心技术，在本企业建立多点试验示范，而且将肥料增效剂用于小麦生产示范基

地上。同时，在呼伦贝尔陈巴尔虎旗鄂温克苏木绿野农场建立 1 个有机肥中试线和农田示范基地，打造有机肥生产样板车间，生产有机肥 100 吨，示范农田 1000 亩，并将该技术在呼伦贝尔地区进行应用推广，发表相关学术论文 2 篇。

## 二、科研水平与贡献之成果

### (1) 发表研究论文 6 篇

- 《产胞外多糖菌株的分离鉴定及其功能研究》，茹素龙、赵永龙、王紫薇、曹晶晶、汪志琴、赵盼、仲乃琴，微生物学刊
- 《疮痂链霉菌拮抗菌 HD9-1 的筛选及功能评价》，周敬轩、赵永龙、赵盼、曹晶晶、汪志琴、刘璐、仲乃琴，微生物学通报，
- Effects of a Nanonetwork-Structured Soil Conditioner on Microbial Community Structure, Jingjing Cao、Pan Zhao 、Dongfang Wang、Yonglong Zhao、Zhiqin Wang、Naiqin Zhong, **Biology 2023, 12, 668**
- Phosphorus accumulation aggravates potato common scab and to be controlled by phosphorus-solubilizing bacteria , Jingjing Cao 、Zhiqin Wang、Jiahe Wu、 Pan Zhao、Chengchen Li、 Xiaobo Li 、Lu Liu 、Yonglong Zhao、Naiqin Zhong, **Science Bulletin 68 (2023) 2316–2320**
- Alkali-Activated Potassium Persulfate Treatment of Sugarcane Filter Cake for the Rapid Production of Fulvic-like-Acid Fertilizer.  
Dongqing Cai, Xianghai Kong, Xiaojiang Zhang, Jinghong Ye, He Xu,

Yanping Zhu, and Dongfang Wang, **ACS Sustainable Chemistry & Engineering, 2023, 11, 13678-13687.**

- Accelerated spent coffee grounds humification by heat/base co-activated persulfate and products' fertilization evaluation

Yanping Zhu, Keyi Zhang, Qing Hu, Weijia Liu, Yi Qiao, Dongqing Cai, Pengjin Zhu, Dongfang Wang, He Xu, Shihu Shu\*, Naiyun Gao, **Environmental Technology & Innovation, 2023, 32, 103393.**

## (2) 专利：申请 4 项、年度授权 4 项

申请四项：

- 1、植物抗性诱导制剂及其应用，2023104994462
- 2、磷酸根盐在制备促疮痂链霉菌生长的菌剂中的应用，

2023111604413

- 3、一株植物乳杆菌 LWQ17 及其应用，202311409402.2
- 4、一株戊糖片球菌 LWQ1 及其应用，2023114092972

(国际专利授权 3 项)

《Annealing treatment based on modified starch and its preparation method and application》**OCTROOINUMMER , 2031143**

《Magnetic microsphere-immobilized protease, instant high-nitrogen-soluble index plant protein and their

preparation method》OCTROOINUMMER ， 2031144

《Slow digestion of starch as well as the preparation method, sand and application》THEREOFOCTROOINUMMER ， 2031145

### （国内专利授权 1 项）

1、《一种微生物菌剂、制备方法及其应用》，呼伦贝尔恒屹农牧业股份有限公司，ZL 2018 1 0113513.1

### 三、团队建设与人培养

2023 年共引进了不同层次人才 13 人（本科毕业生 5 人，专科毕业生 8 人），同时与中国科学院微生物研究所、青岛农业大学、东华大学技术团队开展合作，为加强工作站科学发展提供有力人才支撑。

### 四、开放交流与运行管理

2023 年 8 月公司组织各种植基地场长、技术员参加内蒙古呼伦贝尔马铃薯单产提升培训班。

2023 年 8 月参加上海交通大学种质创新研究团队调研座谈会。

2023 年 10 月与 HZPC 团队开展交流合作洽谈会。

2023 年 11 月参加上海交通大学转移转化对接会。

2023 年 11 月与 HZPC 团队签约合作。

在过去的一年中，内蒙古自治区马铃薯产业融合发展企业重点实验室始终坚持高标准、严要求，确保实验室的各项工作有序进行。

首先，在人员管理方面，我们注重培养专业素养高、创新能力强的人才队伍。通过制定科学的培训计划和激励机制，激发员工的工作热情和创造力。同时，我们加强团队建设，促进员工之间的交流与合作，形成良好的工作氛围。

其次，在设备管理方面，我们注重设备的维护和更新。定期对设备进行检查和保养，确保其正常运行。对于老旧设备，我们及时进行更新换代，提高实验室的整体装备水平。此外，我们还加强与外部机构的合作与交流，引进先进的实验设备和技术，提升实验室的科研能力。在安全管理方面，我们始终坚持“安全第一”的原则。制定完善的安全管理制度和应急预案，确保实验室的安全运行。同时，我们加强员工的安全意识培训，提高大家对安全问题的重视程度。对于存在的安全隐患，我们及时进行排查整改，确保实验室的安全稳定。

最后，在财务管理方面，我们注重合理使用经费。制定科学的预算方案，严格按照预算进行开支。同时，我们加强与财务部门的沟通协作，确保经费使用的合法性和规范性。对于重大项目的经费使用，我们进行严格的审计和监督，确保资金的有效利用。

## 五、存在问题与下一步计划

1、由于 2023 年优化重组后，实验室规模日益增大，目前实验室面积已不能满足各项实验要求，需要寻找合适的地理位置重



新建设重点实验室和流动专家生活区。

2、实验室人才引进和管理制度仍需完善。目前的科技体制，激励机制、人才引进和评价机制不够完善，有待进一步加强。

### 下一步计划

1、单位进一步加大实验室科研经费投入力度，每年企业投入100万元以上专项经费支持实验室开放课题开展，吸引专家在公司开展科研工作，从而提升实验室的研究能力和水平，解决制约企业发展的技术瓶颈问题。

2、深入开展马铃薯化肥农药减施增效技术的研发和示范，优化土传病害绿色防控技术，熟化和产业化更多在国内具有较高影响力的肥药高效和替代技术产品，为马铃薯化肥农药有效减施提供技术支撑。

3、积极参与更多科研项目，争取国家、自治区、呼伦贝尔市科技专项经费支持（尤其是200万元以上的自治区重大专项）；

4、力争2025年新建3000平方米以上的现代化组培室，目前前期土地手续正在进行中。

5、更新、引进智能化组培设备6-10台件，采取集约化生产，降低人工费用，达到节本增效目的。

## 五、审核意见

实验室承诺所填内容属实，数据准确可靠。

实验室主任：



2023 年 12 月 31 日

依托单位审核意见

依托单位负责人（签字）：

依托单位（公章）



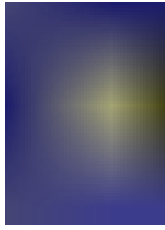
2023 年 12 月 31 日

主管部门审核意见

主管部门负责人（签字）：

主管部门（公章）

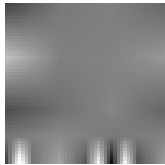
年 月 日



微生物学报  
*Acta Microbiologica Sinica*  
ISSN 0001-6209, CN 11-1995/Q

## 《微生物学报》网络首发论文

题目：产胞外多糖菌株的分离鉴定及其功能研究  
作者：茹素龙，赵永龙，王紫薇，曹晶晶，汪志琴，赵盼，仲乃琴  
DOI：10.13343/j.cnki.wsxb.20230202  
收稿日期：2023-03-24  
网络首发日期：2023-06-02  
引用格式：茹素龙，赵永龙，王紫薇，曹晶晶，汪志琴，赵盼，仲乃琴. 产胞外多糖菌株的分离鉴定及其功能研究[J/OL]. 微生物学报.  
<https://doi.org/10.13343/j.cnki.wsxb.20230202>



**网络首发：**在编辑部工作流程中，稿件从录用到出版要经历录用定稿、排版定稿、整期汇编定稿等阶段。录用定稿指内容已经确定，且通过同行评议、主编终审同意刊用的稿件。排版定稿指录用定稿按照期刊特定版式（包括网络呈现版式）排版后的稿件，可暂不确定出版年、卷、期和页码。整期汇编定稿指出版年、卷、期、页码均已确定的印刷或数字出版的整期汇编稿件。录用定稿网络首发稿件内容必须符合《出版管理条例》和《期刊出版管理规定》的有关规定；学术研究成果具有创新性、科学性和先进性，符合编辑部对刊文的录用要求，不存在学术不端行为及其他侵权行为；稿件内容应基本符合国家有关书刊编辑、出版的技术标准，正确使用和统一规范语言文字、符号、数字、外文字母、法定计量单位及地图标注等。为确保录用定稿网络首发的严肃性，录用定稿一经发布，不得修改论文题目、作者、机构名称和学术内容，只可基于编辑规范进行少量文字的修改。

**出版确认：**纸质期刊编辑部通过与《中国学术期刊（光盘版）》电子杂志社有限公司签约，在《中国学术期刊（网络版）》出版传播平台上创办与纸质期刊内容一致的网络版，以单篇或整期出版形式，在印刷出版之前刊发论文的录用定稿、排版定稿、整期汇编定稿。因为《中国学术期刊（网络版）》是国家新闻出版广电总局批准的网络连续型出版物（ISSN 2096-4188，CN 11-6037/Z），所以签约期刊的网络版上网络首发论文视为正式出版。

DOI: 10.13343/j.cnki.wsxb.20230202

(研究报告)

# 产胞外多糖菌株的分离鉴定及其功能研究

茹素龙<sup>1</sup>, 赵永龙<sup>2,3</sup>, 王紫薇<sup>4</sup>, 曹晶晶<sup>2,3</sup>, 汪志琴<sup>2,3</sup>, 赵盼<sup>2,3,5</sup>, 仲乃琴<sup>2,3,5\*</sup>

1 宁夏大学农学院, 宁夏 银川 750021

2 中国科学院微生物研究所, 北京 100101

3 中国科学院农业微生物先进技术工程实验室, 北京 100101

4 山西农业大学植物保护学院, 山西 晋中 030600

5 内蒙古自治区马铃薯肥料农药高效利用技术企业重点实验室, 内蒙古呼伦贝尔 021000

**摘要:** 微生物产生的胞外多糖 (EPS) 可促进大粒径土壤团聚体形成, 高产 EPS 的菌株在土壤改良、促进作物生长方面具有较好的应用前景。【目的】从土壤样品中筛选高产胞外多糖的细菌, 研究其在土壤改良、环境适应性、广谱抗病等方面的功能, 为制备土壤改良型功能菌剂提供候选菌株。【方法】采用蒽酮硫酸法测定菌株胞外多糖的产量, 通过形态学观察、生理生化试验及 16S rRNA 基因序列测定确定其分类地位, 结合土壤培养试验研究菌株对土壤团聚体形成的影响。【结果】获得 3 株胞外多糖产量大于 500 mg/L 的细菌, 经鉴定 A-5 为地衣芽孢杆菌 (*Bacillus licheniformis*), XJ-3 为萎缩芽孢杆菌 (*Bacillus atrophaeus*), KW3-10 为耐盐芽孢杆菌 (*Bacillus halotolerans*)。菌株 A-5、XJ-3、KW3-10 处理后, 土壤大团聚体 (>0.25 mm) 含量较对照分别提高了 4.07、2.14、3.16 倍。3 株菌株对疮痂链霉菌 (*Streptomyces scabies*)、尖孢镰刀菌 (*Fusarium oxysporum*)、茄链格孢菌 (*Alternaria solani*) 和立枯丝核菌 (*Rhizoctonia solani*) 等多种植物病原菌具有明显的抑制效果, 可耐受 pH5-9 和 NaCl 含量 1%-9% 的盐碱环境, 促进植物生长, 其中 KW3-10 的代谢产物中 IAA 含量为 25.58 mg/L。【结论】菌株 A-5、XJ-3、KW3-10 可显著促进土壤团粒结构形成, 具有较好的广谱抗病性和促生长特性, 可作为高效复合功能菌剂的候选菌株。

资助项目: 中国科学院战略性先导科技专项 (XDA13020601, XDA28030202); 广东省重点领域研发计划 (2020B0202010005); 内蒙古自治区关键技术攻关计划 (2021GG0300)

This work was supported by the Strategic Priority Research Program of the Chinese Academy of Sciences (XDA13020601, XDA28030202), the Guangdong Province Key Field R&D Program Project (2020B0202010005), and the Inner Mongolia Autonomous Region Key Technology Tackling Plan Project (2021GG0300)

\*Corresponding author. E-mail: nqzhong@im.ac.cn

Received: 2023-03-24; Accepted: 2023-05-23; Published online:

**关键词:** 胞外多糖, 土壤团聚体, 芽孢杆菌, 土壤改良

# Isolation, identification, and functional characterization of exopolysaccharide-producing strains

RU Sulong<sup>1</sup>, ZHAO Yonglong<sup>2,3</sup>, WANG Ziwei<sup>4</sup>, CAO Jingjing<sup>2,3</sup>, WANG Zhiqin<sup>2,3</sup>, ZHAO Pan<sup>2,3,5</sup>, ZHONG Naiqin<sup>2,3,5\*</sup>

1 School of Agriculture, Ningxia University, Yinchuan 750021, Ningxia, China

2 Institute of Microbiology, Chinese Academy of Sciences, Beijing 100101, China

3 Engineering Laboratory for Advanced Technology of Agricultural Microbiology, Chinese Academy of Sciences, Beijing 100101, China

4 College of Plant Protection, Shanxi Agricultural University, Jinzhong 030600, Shanxi, China

5 The Enterprise Key Laboratory of Advanced Technology for Potato Fertilizer and Pesticide, Hulunbuir 021000, Inner Mongolia, China

**Abstract:** Exopolysaccharides (EPS) produced by microorganisms can promote the formation of large soil aggregates. EPS-producing strains have good application prospects in improving soil and promoting crop growth. **[Objective]** We isolated the bacteria with high yields of exopolysaccharides from soil samples and studied their soil-improving function, environmental adaptability, and broad-spectrum disease resistance, aiming to provide candidate strains for the preparation of soil-improving microbial agents. **[Methods]** The yield of EPS was determined by anthrone-sulfuric acid method. The taxonomic status of the strain was determined by morphological observation, physiological and biochemical tests, and 16S rRNA gene sequencing. Soil culture experiments were carried out to evaluate the effect of the strain on the formation of soil aggregates. **[Results]** Three strains of bacteria with EPS yields greater than 500 mg/L were obtained. A-5 was identified as *Bacillus licheniformis*, XJ-3 as *B. atrophaeus*, and KW3-10 as *B. halotolerans*. After treatment with these strains, the content of soil macroaggregates (>0.25 mm) increased by 4.07, 2.14, and 3.16 times, respectively. The three strains exerted significant inhibitory effects on plant pathogens such as *Streptomyces scabies*, *Fusarium oxysporum*, *Alternaria solani*, and *Rhizoctonia solani*. They could tolerate the saline-alkali environment with pH 5–9 and NaCl content of 1%–9% and promoted plant growth. The content of indole acetic acid in the metabolites of KW3-10 was 25.58 mg/L. **[Conclusion]**

Strains A-5, XJ-3, and KW3-10 can significantly promote the formation of soil aggregates and demonstrate broad-spectrum disease resistance and remarkable growth-promoting performance, serving as candidates for the preparation of efficient compound microbial agents.

**Keywords:** exopolysaccharides, soil aggregate, *Bacillus*, soil improvement

土壤团聚体是土壤结构的基本单元，其数量和粒径分布决定土壤的肥沃程度，稳定性决定土壤承受被破坏的能力<sup>[1]</sup>。多糖是土壤有机质的组成成分之一，占总有机质的 5%-30%，可通过游离羟基的离子键和氢键与土壤颗粒结合，形成稳定的团聚体<sup>[2]</sup>。胞外多糖 (exopolysaccharides, EPS) 是一些微生物生长代谢过程中分泌到细胞壁外的水溶性多糖，对土壤大团聚体 (>0.25 mm) 的形成及植物生长发育具有显著的促进作用<sup>[3]</sup>。Chenu<sup>[4]</sup>和 Vadakattu<sup>[5]</sup>等研究发现，EPS 可促进边际土壤颗粒的聚集，形成有效团聚体，从而提高土壤结构的稳定性和持水能力。EPS 不仅能提高植物根部土壤团聚体的稳定性，还能增加土壤孔隙度，改善透气性，利于植物根系生长和营养吸收，从而提高土壤养分的利用效率<sup>[6-8]</sup>，并可将有机碳封闭在团聚体中，增强其迟效性<sup>[9]</sup>。邓照亮等<sup>[10]</sup>研究结果表明，抑病型土壤的水稳定性大团聚体含量明显高于导病型土壤，砖红壤和砂壤的抑病型土壤中粒径大于 2 mm 的团聚体是导病型土壤的 1.87 倍、2.38 倍；康贻军等人<sup>[11]</sup>用两种产胞外多糖的细菌浸种，有效提高了土壤水稳性团聚体(>0.25 mm)比例，促进番茄幼苗生长，降低青枯病危害程度。可见，产胞外多糖细菌对于改良土壤结构，调节土壤生态、促进作物增产具有重要作用。但是目前应用于土壤改良的菌种资源十分有限，加之 EPS 的形成对环境温度、土壤 pH 值和盐度的变化十分敏感<sup>[12-13]</sup>，迫切需要筛选胞外多糖产量高、兼具抗病、耐盐碱，且环境稳定性强的菌株，为复合功能菌剂的研发和产业化应用提供候选菌种资源。

本研究从土壤样品中定向分离和筛选高产 EPS 的细菌，明确其分类地位，研究菌株对土壤水稳性大粒径团聚体形成的促进作用，探究其环境适应性和对土壤的改良作用，测定其对致病性链霉菌 *S. scabies* 等多种病原菌的广谱拮抗效果，以期获得具有推广应用前景的功能菌株。

## 1 材料与方法

### 1.1 材料

#### 1.1.1 病原菌样品

疮痂链霉菌 (*Streptomyces scabies*)、尖孢镰刀菌 (*Fusarium oxysporum*)、立枯丝核菌 (*Rhizoctonia solani*) 购自中国科学院微生物研究所菌种保藏管理中心，馆藏编号分别为 CGMCC4.1765、CGMCC3.18025、CGMCC3.2888；盆栽基质采用  $1 \times 10^5$  Pa 灭菌 30 min 的营养土和蛭石。

#### 1.1.2 供试土壤样品

土壤培养试验供试土样采自黑龙江省三江平原北大荒集团友谊农场 (46°13'-46°47'N,

131°21'-131°21'E), pH 8.16, 总磷 0.77 g/kg, 全氮 0.761 g/kg, 全钾 2.17%, 有机质 29.7 g/kg。

### 1.1.3 主要培养基与试剂

LB 培养基(g/L): 蛋白胨 10, 酵母提取物 5, NaCl 10, 用去离子水定容至 1 L, pH 调整至 7.0-7.2, 121 °C 灭菌 20 min。

有氮培养基(g/L): 蔗糖 10, (NH<sub>4</sub>)<sub>2</sub>SO<sub>4</sub> 1, MgSO<sub>4</sub>·7H<sub>2</sub>O 0.5, NaCl 0.1, K<sub>2</sub>HPO<sub>4</sub> 2, 酵母提取物 0.5, 用去离子水定容至 1 L, 调 pH 为 7, 固体培养基添加 20 琼脂, 113 °C 灭菌 30 min。

PDA 固体培养基(g/L): 马铃薯块茎 200 切碎, 沸水煮 20 min, 用纱布过滤除渣, 加入葡萄糖 20, 琼脂 15, 用去离子水定容至 1 L, 调 pH 至 7.0-7.2, 113 °C 灭菌 20 min。

King 氏培养基(g/L): 蛋白胨 20, K<sub>2</sub>HPO<sub>4</sub> 1.725, 丙三醇 15 mL, MgSO<sub>4</sub>·7H<sub>2</sub>O 1.5, 色氨酸 0.1, 用去离子水定容至 1 L, 调 pH 至 7.2, 121 °C 灭菌 20 min。

比色液: 将 20 mL 0.025 mol/L 的 FeCl<sub>3</sub> 缓缓加入 30 mL 浓硫酸中, 搅拌均匀。

B5 营养液(g/L): KNO<sub>3</sub> 2.5, MgSO<sub>4</sub>·7H<sub>2</sub>O 0.25, NaH<sub>2</sub>PO<sub>4</sub>·H<sub>2</sub>O 0.15, CaCl<sub>2</sub>·2H<sub>2</sub>O 0.15, (NH<sub>4</sub>)<sub>2</sub>SO<sub>4</sub> 0.135, FeSO<sub>4</sub>·7H<sub>2</sub>O 0.028, EDTA·Na<sub>2</sub> 0.037, MnSO<sub>4</sub>·4H<sub>2</sub>O 0.004, ZnSO<sub>4</sub>·7H<sub>2</sub>O 0.0008, 去离子水定容至 1 L。

PKO 培养基(g/L): 葡萄糖 10, (NH<sub>4</sub>)<sub>2</sub>SO<sub>4</sub> 0.5, NaCl 0.3, KCl 0.3, MgSO<sub>4</sub>·7H<sub>2</sub>O 0.1, MgSO<sub>4</sub>·H<sub>2</sub>O 0.03, FeSO<sub>4</sub> 0.03, Ca<sub>3</sub>(PO<sub>4</sub>)<sub>2</sub> 5, 酵母提取物 0.5, 琼脂 20, 用去离子水定容至 1 L, 调 pH 至 7.0, 113 °C 灭菌 20 min。

蒽酮溶液(g/mL): 称取 0.2 蒽酮, 定容至 100 mL 浓硫酸中, 临用前配制。

### 1.1.4 供试作物

由本实验室培育 30 d 的马铃薯脱毒试管苗 (品种: 夏波蒂)。

## 1.2 目标菌株的分离

采集上海松江区、广西环江县严重板结的农田土壤样品, 和宁夏西吉县板结土壤中马铃薯病薯表面土壤样品, 取 1 g 置于 50 mL 离心管中, 加入 10 mL 无菌水充分震荡。吸取 100 μL 上述悬浮液均匀涂布于 LB 固体培养基上, 28 °C 培养 24 h; 挑选细菌单菌落进行划线纯化, 并将所得菌株接种于液体 LB 培养基中, 37 °C 振荡培养备用。

## 1.3 产 EPS 菌的初筛

将分离所得的菌株涂布于固体有氮培养基中, 37 °C 培养 48 h。用灭菌牙签挑取菌落, 挑选黏度较大的菌株。

## 1.4 多糖含量的测定

将初筛获得的菌株分别于 37 °C 振荡(200 r/min)培养 48 h, 采用乙醇沉淀法提取发酵液粗多糖, 并采用硫酸-蒽酮法测定多糖含量。



葡萄糖标准曲线制作：分别吸取 50  $\mu\text{g}/\text{mL}$  的葡萄糖溶液 0、0.5、1、1.5、2、2.5 mL 于 25 mL 比色管中，加去离子水至 2.5 mL，分别加入 5 mL 的蒽酮溶液，置沸水浴中保温 10 min。采用分光光度计测定  $OD_{620}$  值。以葡萄糖浓度为横坐标， $OD$  值为纵坐标绘制葡萄糖标准曲线。

样品多糖含量的测定：待测菌株培养液 8 000 r/min 离心 10 min，用 Sevag 法<sup>[14]</sup>提取 EPS，分别取 EPS 溶液 0.1 mL 于比色管中，加入去离子水 2.4 mL，混匀，采用硫酸-蒽酮法测定多糖含量。

### 1.5 菌株形态观察

将待测菌液均匀涂布于 LB 固体培养基上，37  $^{\circ}\text{C}$  培养 24 h 后镜检观察菌落形态，分别采用日立冷场发射扫描电子显微镜 SU8010 和蔡司荧光倒置显微镜 Observer Z1 观察菌体形态。

### 1.6 菌株革兰氏染色

将待测菌液滴至载玻片上，自然晾干后轻微烘烤，用草酸铵结晶紫染色 1 min，自来水冲洗 30 s，加碘液于涂面约 1 min，再次水洗，用吸水纸吸干水分，加 95% 酒精数滴，轻轻摇动进行脱色，20 s 后水洗，吸去水分，番红染色液（稀）染 2 min，自来水冲洗，干燥后镜检。

### 1.7 菌株生理生化特性分析

采用 API 50 CHB G+ 芽胞杆菌鉴定试剂盒测定菌株理化性质，依据 API 50CH 试验条说明书判读测试结果。

将待测菌种分别接种于 pH 值为 3.0、5.0、7.0、9.0、11.0，NaCl 浓度分别为 1%、3%、5%、7%、9%、11% 的液体 LB 培养基中，37  $^{\circ}\text{C}$ 、200 r/min 振荡培养 12 h 后测定其  $OD_{600}$  值，分析菌株耐盐碱特性<sup>[15]</sup>。

### 1.8 分子系统学分析

采用 16S rRNA 基因片段通用引物 (27F: 5'-AGAGTTTGATCCTGGCTCAG-3', 1492R: 5'-CTACGGCTACCTTGTACGA-3') 进行测序 (北京博迈德生物工程股份有限公司)，PCR 反应体系 (20  $\mu\text{L}$ ): 2 $\times$ T5 Super PCR Mix 10  $\mu\text{L}$ ，菌株基因组 DNA (200 ng/ $\mu\text{L}$ ) 2  $\mu\text{L}$ ，正、反向引物 (10  $\mu\text{mol}/\text{L}$ ) 各 1  $\mu\text{L}$ ，ddH<sub>2</sub>O 6  $\mu\text{L}$ 。PCR 反应条件：95  $^{\circ}\text{C}$  5 min；95  $^{\circ}\text{C}$  30 s，55  $^{\circ}\text{C}$  30 s，72  $^{\circ}\text{C}$  2 min，35 个循环；72  $^{\circ}\text{C}$  10 min。测序结果在 National Center for Biotechnology Information (NCBI) 上进行比对，采用 MEGA 7.0 软件构建系统发育树。

### 1.9 土壤培养试验

挖取 0-15 cm 土层土壤，自然风干后，碾碎过孔径为 0.25 mm 的筛。在容积为 1 300 mL 的组培瓶底部垫 150 g 石英砂 (约 1 cm 厚)，称取 500 g 过筛土样装入组培瓶中，用纱网将土壤与石英砂隔开，121  $^{\circ}\text{C}$  灭菌 45 min。将参试菌株接种于 500 mL LB 液体培养中培养 4-5 d，至芽孢形成，离心弃上清，将菌体用无菌水洗涤 2 次，分别取 10<sup>7</sup> CFU/mL 菌体均匀接种



入土壤中，加无菌水至土壤饱和含水量 60%，室温培养箱 37 °C 培养 120 d，样品送至青岛斯坦德衡立环境技术研究院有限公司测定不同粒径水稳性土壤团聚体含量。

试验设置 4 个处理，CK（过筛土样+无菌水），处理 1（过筛土样+A-5），处理 2（过筛土样+XJ-3），处理 3（过筛土样+ KW3-10），每个处理重复 3 次。

### 1.10 菌株溶磷及促生长特性分析

菌株在 PKO 固体培养基上 28 °C 培养 7 d，观察菌株溶磷效果。

吸取 100 μL 菌液接种于 King 氏液体培养基中，37 °C、200 r/min 培养 48 h，离心收集上清液，用 SalKowski 比色法定性检测菌液中的生长素(IAA)，参照李振东等的方法测算 IAA 浓度<sup>[16]</sup>。

### 1.11 广谱抑菌效果测定

吸取 100 μL 疮痂链霉菌(*S. scabies*)孢子悬浮液均匀涂布于 PDA 固体培养基，吸取上述细菌培养液 6 μL 滴于其上，28 °C 培养 7 d 后测量抑菌圈直径。

在 PDA 培养基上接种大丽轮枝菌、立枯丝核菌和尖孢镰刀菌，在其两侧间隔 1 cm 处分别接种 6 μL 目标菌株培养液，并以单独接种病原菌的处理为对照，28 °C 培养 4 d 观察抑菌效果。

### 1.12 马铃薯疮痂病盆栽防控效果验证

在高 10 cm、直径为 17 cm 的花盆中装满蛭石与营养土（蛭石：营养土=4：1），将 2 L B5 营养液均匀浇入花盆，移栽培养 30 d 的马铃薯夏波蒂脱毒组培苗，每盆 3 株，置于相同环境培养，10 d 后每株幼苗根部接种 100 mL  $1 \times 10^7$  CFU/mL 的 *S. scabies* 孢子悬浮液，间隔 15 d 后接种目标菌悬浮液(30 mL/盆， $1 \times 10^8$  CFU/mL)，不接种任何菌株的处理为 CK1，仅接种 *S. scabies* 的处理为 CK2。每个处理重复 3 次，每周浇水 1 次，每次浇 2 L。马铃薯收获以后，依据疮痂病分级标准统计发病率、病情指数，计算防治效果。

病害分级标准<sup>[17]</sup>：0 级为薯皮健康，无病斑；1 级为病斑面积占块茎总表面积的 0-1/6；2 级为病斑面积占块茎总表面积的 1/6-1/3；3 级为病斑面积占块茎总表面积的 1/3-1/2；4 级为病斑面积占块茎总表面积的 1/2 以上。

发病率(%)=发病块茎数/总块茎数×100%；

病情指数= $\sum$ (各病级块茎数×该病级数代表值)/(调查个体总和×最高病级数)×100；

相对防效(%)=(对照组病情指数-处理组病情指数)/对照组病情指数×100%。

参照 Wanner Leslie A<sup>[18]</sup>的方法，以基质环境为模板，依据 *S. scabies* 的关键致病基因 *TxtA* 序列设计引物，正向引物：5'-CACGTACGCGCAGTTCAATG-3'；反向引物：5'-AGATGATGTAGGCGGGAC-3'。采用 ABI 7500Real-Time PCR System 仪扩增土壤中 *TxtA* 的生物量，试验重复 3 次。

### 1.13 数据处理

采用 Excel 和 Origin 2021b 软件处理相关数据，运用 MEGA 7.0 软件构建菌株系统发育树。

## 2 结果与分析

### 2.1 高产 EPS 菌株筛选

分别从采自上海松江区、广西环江县、宁夏西吉县的严重板结土壤样品中，分离获得 3 株表面湿润、黏度较大、产胞外多糖高的细菌，编号分别为 A-5、XJ-3，KW3-10。采用硫酸-蒽酮法制作葡萄糖标准曲线，葡萄糖浓度和吸光度之间的线性方程为  $Y=0.0125X+0.0424$ ， $R^2=0.9983$ ，标准曲线满足分析测试要求。测定结果如图 1 所示，培养 72 h 时，A-5 培养液中 EPS 产量最高，达 1 439.23 mg/L，XJ-3 与 KW3-10 菌株 EPS 产量分别为 735.34 mg/L 和 838.77 mg/L。

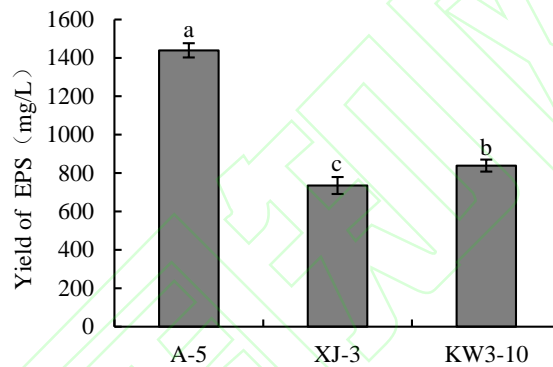
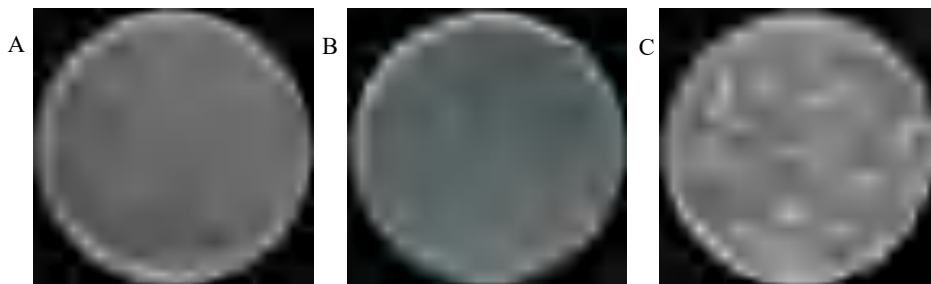


图 1 菌株胞外多糖 (EPS) 产量

Figure 1 EPS yield of strain. The presented values are the means of three determinations, with standard deviations indicated; Means with different letters are significantly different at  $P < 0.05$ .

### 2.2 菌株形态学观察

如图 2 所示，扫描电镜下观察发现，3 株菌均为杆状细菌，菌体两端钝圆，边缘整齐，表面湿润，革兰氏染色呈阳性，且周围有丝状分泌物。其中 A-5 菌落白色圆形，半透明，宽度 0.60-0.95  $\mu\text{m}$ ，长度 1.5-2.4  $\mu\text{m}$ ；XJ-3 菌落乳白色圆形，半透明，有荚膜，宽度约为 0.55-1.00  $\mu\text{m}$ ，长度为 1.6-2.4  $\mu\text{m}$ ；菌株 KW3-10 菌落乳白色圆形，不透明，宽度 0.50-0.95  $\mu\text{m}$ ，长度 1.5-3.5  $\mu\text{m}$ 。



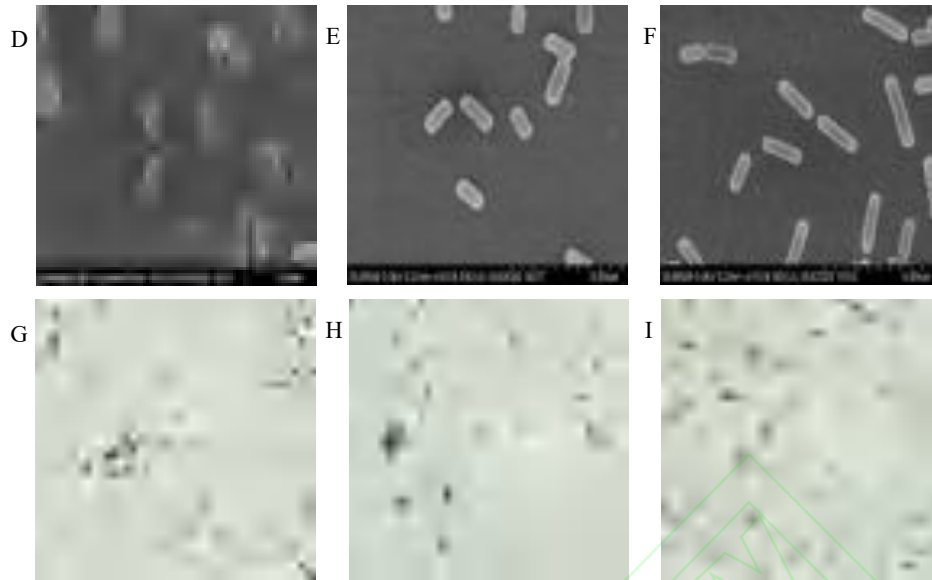


图2 菌株 A-5、XJ-3、KW3-10 的形态特征

Figure 2 Morphological characteristics of A-5, XJ-3, KW3-10. A: A-5 colonies; B: XJ-3 colonies; C: KW3-10 colonies; D: A-5 bacteria; E: XJ-3 bacteria; F: KW3-10 bacteria; G: A-5 Gram staining; H: XJ-3 Gram staining; I: KW3-10 Gram staining.

### 2.3 菌株生理生化特性分析

由表 1 所示，菌株 A-5、XJ-3、KW3-10 均可利用 D-核糖、D-葡萄糖、D-果糖、D-甘露糖、山梨醇、D-蔗糖、D-纤维二糖、肌醇、水杨苷、D-麦芽糖、D-海藻糖、淀粉作为唯一碳源，代谢产物可降解苦杏仁苷；不能利用 D-阿拉伯糖、赤藻糖醇、L-木糖、D-核糖醇、L-山梨糖、卫矛醇、D-乳糖、D-松三糖、木糖醇、葡萄糖酸钾。API 50CH 鉴定结果显示，3 株待测菌株均为芽胞杆菌，其中 A-5 初步鉴定为地衣芽孢杆菌，鉴定率为 99.5%；XJ-3 与 KW3-10 初步鉴定为枯草-解淀粉芽孢杆菌，鉴定率分别为 77.4%、89.9%。

表 1 菌株的生理生化特性

Table 1 Physiological and biochemical characters of strains

Test items	Results			Test items	Results		
	A-5	XJ-3	KW3-10		A-5	XJ-3	KW3-10
Negative control	-	-	-	Esculin ferric citrate	+	+	+
Glycerol	+	+	+	Salicin	+	+	+
Erythritol	-	-	-	cellobiose	+	+	+
D-Arabinose	-	-	-	D- maltose	+	+	+
L-Arabinose	+	+	+	D- lactose	-	-	-
D-ribose	+	+	+	D-disaccharide	-	-	+
D-xylose	+	-	+	D- sucrose	+	+	+
L-Xylose	-	-	-	D-Trehalose dihydrate	+	+	+
D-Ribitol	-	-	-	Synanthrin	+	-	+
D-Galactose	+	-	-	D-Raffinose	+	-	+
D-glucose	+	+	+	amylum	+	+	+
D-Fructose	+	+	+	glycogen	+	+	+
D-Mannose	+	+	+	Xylitol	-	-	-

L-Sorbose	-	-	-	D-Gentiobiose	+	-	-
L-rhamnose	+	-	-	Melezitose	-	-	-
Dulcitol	-	-	-	D-Lyxose	-	-	-
Inositol	+	+	+	D-Tagatose	+	+	+
D-Mannitol	+	+	+	D-fucose	-	-	-
Sorbitol	+	+	+	L-fucose	-	-	-
Methyl alpha-D-Mannopyranoside	-	-	-	D-arabinitol	-	-	-
Methyl-a-D-glucopyranoside	+	+	+	L-Arabitol	-	-	-
N-Acetyl glucosamine	-	-	-	Potassium gluconate	-	-	-
Nitrilosides	+	+	+	2-Keto-potassium gluconate	-	-	-
hydroquinone O-β-D-glucopyranoside	+	+	+	5-Keto-potassium gluconate	-	-	-

+: Positive; -: Negative.

## 2.4 基于 16S rRNA 的分子生物学鉴定

将菌株 A-5、XJ-3 和 KW3-10 的 16S rRNA 序列在 NCBI 中进行比对，发现三者分别与地衣芽孢杆菌、萎缩芽孢杆菌与耐盐芽孢杆菌的同源性达到 99.9% 以上，运用 MEGA 7.0 软件构建系统发育树。结果如图 3 所示，A-5 与 *Bacillus paralicheniformis* QT391<sup>T</sup> 在同一分支，XJ-3 与 *Bacillus atrophaeus* B-1<sup>T</sup> 在同一分支，KW3-10 与 *Bacillus halotolerans* NOK83<sup>T</sup> 在同一分支，结合形态学和生理生化特性分析结果，将 A-5、XJ-3 和 KW3-10 分别鉴定为地衣芽孢杆菌 (*Bacillus licheniformis*)、萎缩芽孢杆菌 (*Bacillus atrophaeus*)、耐盐芽孢杆菌 (*Bacillus halotolerans*)。

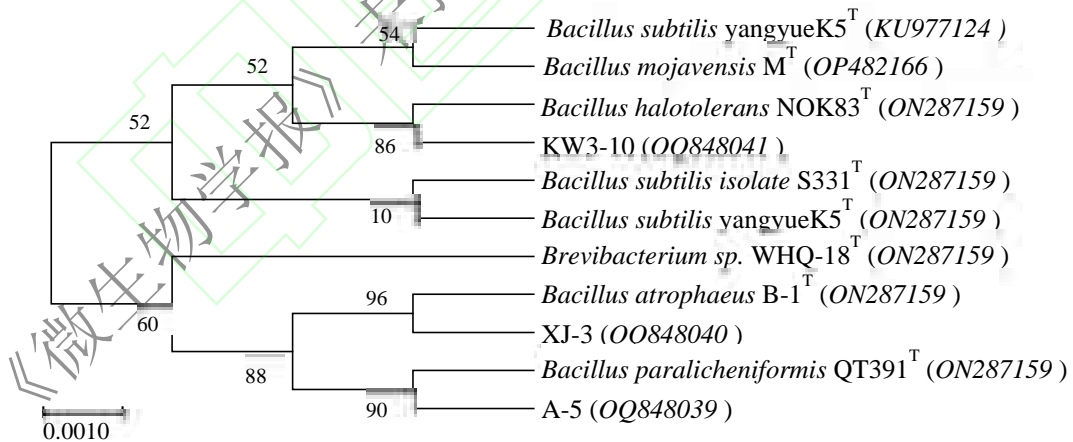


图 3 基于 16S rRNA 基因序列构建菌株的系统发育树

Figure 3 Phylogenetic tree of Strains constructed based on the 16S rRNA gene sequences. Numbers in parentheses are GenBank accession numbers; The bootstrap values are shown at the node; The scale bar indicates 0.050 substitutions per nucleotide position.

## 2.5 土壤培养试验

菌株处理土壤样品 120 d 后, 不同粒径的土壤团聚体分布如图 4A 所示, 接种 A-5、XJ-3 和 KW3-10 的处理组, 粒径大于 2 mm 的土壤团聚体比例分别较 CK 提高了 1.97%、0.53%、1.60%, 差异均达到极显著水平 ( $P<0.01$ ); 粒径大于 0.25 mm 的土壤团聚体比例分别较 CK 提高了 4.07、2.14、3.16 倍, 其中 XJ-3 和 KW3-10 处理达到显著水平 ( $P<0.05$ ); 粒径大于 0.053 mm 的土壤团聚体比例均较 CK 略有增加, 其中 XJ-3 差异达到显著水平。与 CK 相比, 各处理粒径小于 0.053 mm 的土壤团聚体比例均有所下降, 其中 XJ-3 和 KW3-10 差异达到显著水平。结果表明, 胞外多糖具有较好的胶结能力, 可以将小团聚体聚集形成稳定的大团聚体。

土壤多糖含量测定结果如图 4B 所示。3 组处理的土壤多糖含量均有所增加, 分别较 CK 提高了 28.87%、21.09% 和 12.93%, 其中菌株 A-5 处理的差异达显著水平, XJ-3 处理的差异达极显著水平。

各处理对土壤 pH 变化的影响如图 4C 所示。与 CK 相比, 接种 A-5、XJ-3、KW3-10 的土壤 pH 值分别下降了 0.49、0.84、0.85, 差异均达到极显著水平。推测参试细菌能通过代谢产生有机酸, 利用质子置换盐碱土壤中的阳离子, 从而降低土壤的 pH 值。

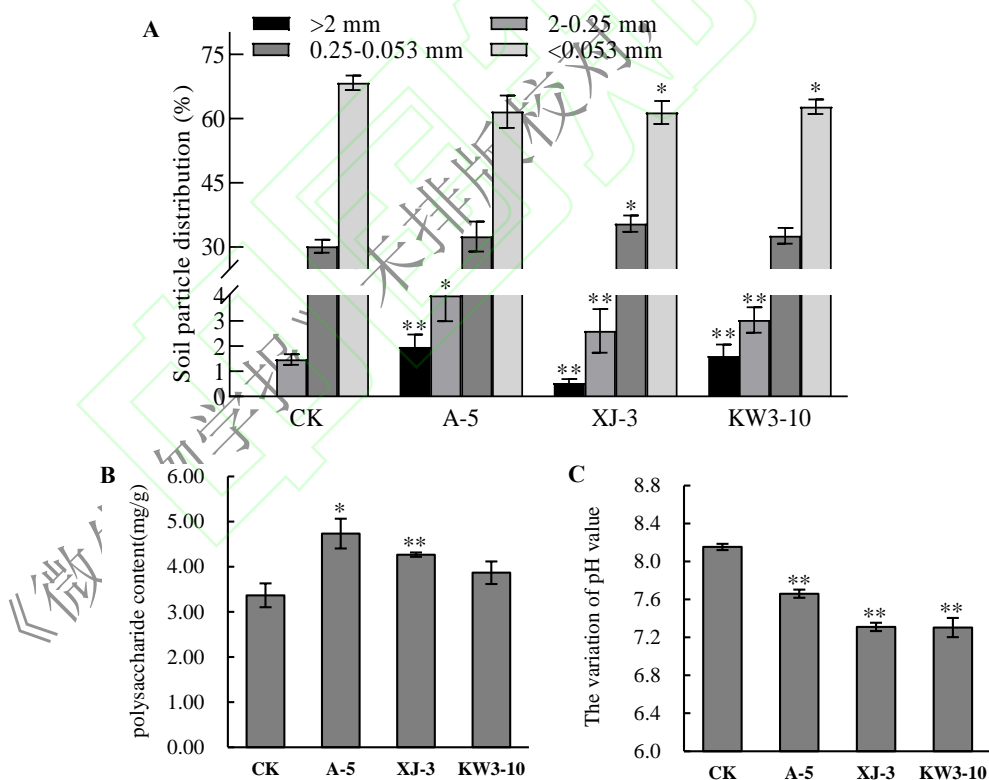


图 4 土壤培养试验结果

Figure 4 Soil culture test results. A: Effects of different strains on soil aggregates distribution in the soil culture experiment; B: The Effect of Strains on the Content of Soil Polysaccharides; C: The effect of strains on soil pH. The presented values are the means of three determinations, with standard deviations indicated; \*:  $P<0.05$ , \*\*:  $P<0.01$ .

## 2.6 菌株耐盐碱特性分析

为了探究参试菌株对盐碱环境的适应性，我们分别将其接种于 NaCl 含量 1%-11%、pH1-13 的 LB 液体培养基中，28 °C，培养 24 h 后观察发现（图 5），3 株菌对极端盐碱环境均具有较强的耐受性，其中菌株 A-5 和 KW3-10，在 NaCl 浓度为 1%-3% 的条件下可正常生长，在 NaCl 浓度为 7%-9% 的条件下可较好生长；XJ-3 和 KW3-10 最高可耐受 NaCl 浓度 11% 的高盐环境（培养 24 h 后，KW3-10 菌液的  $OD_{600}$  值可达 0.896）。在 pH 为 5-7 的环境中，3 株菌均可正常生长，KW3-10 可耐受 pH11 的极端高碱环境。

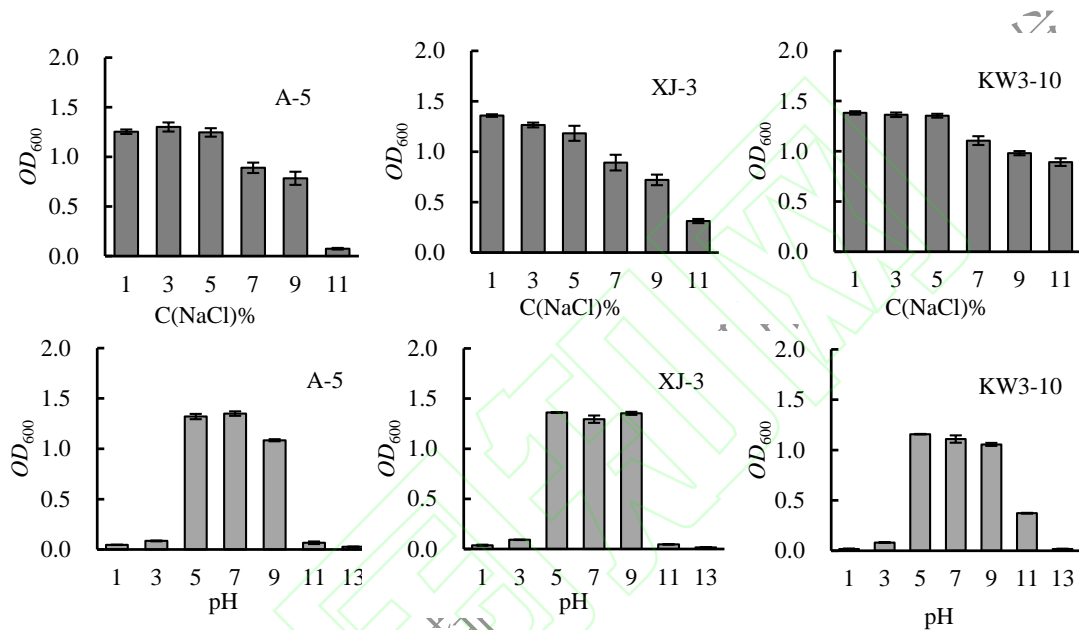


图 5 菌株 A-5, XJ-3, KW3-10 的耐盐碱范围

Figure 5 Salt-alkali tolerance range of A-5, XJ-3, KW3-10. The presented values are the means of three determinations, with standard deviations indicated.

## 2.7 参试菌株产 IAA 能力与溶解磷能力比较

将 3 株目标菌在 King 氏液体培养基中培养 24 h，将上清液与比色液进行混合，3 株菌的混合液均呈显粉红色，对照标准曲线  $Y=8.8218X$ ， $R^2=0.9918$  计算，菌株 IAA 的产量（图 6A）分别为 2.68、8.09、25.58 mg/L。

在 KPO 培养基上培养发现，A-5 菌落周围形成明显的透明圈，表明其具有较好的溶磷能力（图 6B）；KW3-10 菌落周围虽没有形成透明圈，但其生长繁殖明显好于 XJ-3。

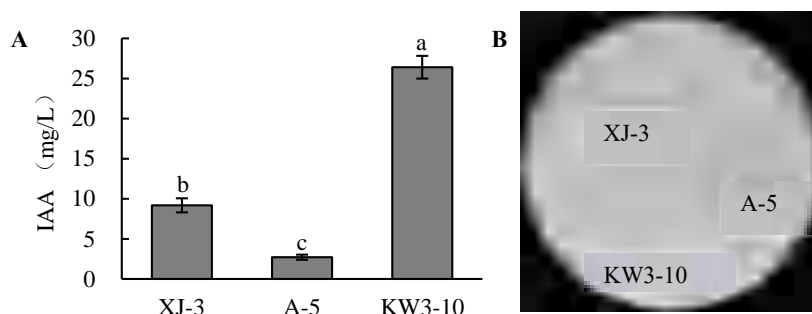




图 6 菌株 A-5, XJ-3, KW3-10 代谢产物中生长素测定与溶解磷能力

Figure 6 Determination of auxin in metabolites of strains A-5, XJ-3, KW3-10 and their ability to phosphate solubilizing. A: Auxin assay in strain A-5, XJ-3, KW3-10 metabolites; B: Phosphate solubilizing ability of strains. The presented values are the means of three determinations, with standard deviations indicated; Means with different letters are significantly different at  $P < 0.05$ .

## 2.8 菌株促生长效果测定

菌体浇施马铃薯幼苗, 培养 60 d 后统计 SPAD、株高、茎粗, 数据汇总如图 7 所示。3 株菌处理的植株长势均优于对照, 其中, A-5 处理后的 SPAD 值、株高、茎径较对照分别增加了 23.42%, 21.35% 和 20.73%, 差异均达到极显著水平; XJ-3 的株高与茎径较对照分别增加了 28.83%、36.96%, 差异达到显著水平, SPAD 值增加 17.00%, 但差异不显著; KW3-10 处理的 SPAD 值、株高与茎径分别较对照增加了 29.15%、34.81% 和 56.54%, 差异均达到显著水平。可见, 3 株菌均对植株具有良好的促生长效果 (图 7A-D)。

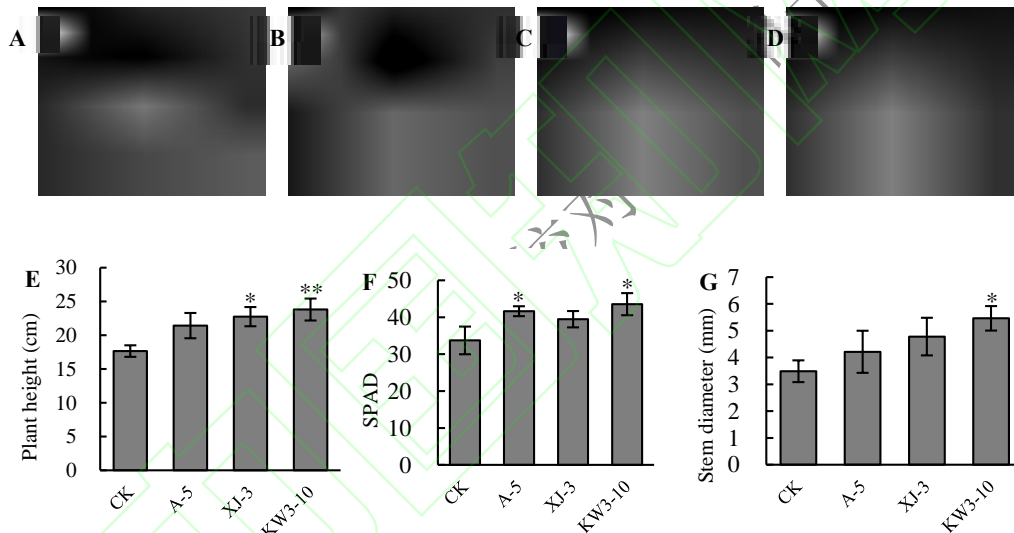


图 7 菌株 A-5, XJ-3, KW3-10 促生能力分析

Figure 7 Analysis of growth-promoting ability of strains. A: water treatment; B-D: The order of pouring A-5, XJ-3 and KW3-10 bacterial liquid; E: Plant height after 60 d; F: SPAD after 60 d; G: Stem diameter after 60 d. The presented values are the means of three determinations, with standard deviations indicated; \*:  $P < 0.05$ , \*\*:  $P < 0.01$ .

## 2.9 菌株广谱抗性分析

为了进一步挖掘被试菌株的广谱生防功能, 通过平板对峙试验测试了其对于 4 种植物病原菌的拮抗效果。结果如图 8 所示, A-5, XJ-3, KW3-10 的 72 h 培养液对疮痂链霉菌(*S. scabies*)的抑菌圈直径分别约为 20、49、56 mm; A-5 对尖孢镰刀菌(*Fusarium xysporum*)、茄链格孢菌(*Alternaria solani*)和立枯丝核菌(*Rhizoctonia solani*)均具有的抑菌率分别约为 50.97%、25.66%、2.44%, XJ-3 的抑菌率分别约为 37.65%、46.9%、63.41%, KW3-10 的抑菌率分别为 48.05%、64.91%、60.98%, 推测 3 株芽孢杆菌均具有较好的广谱抗性。

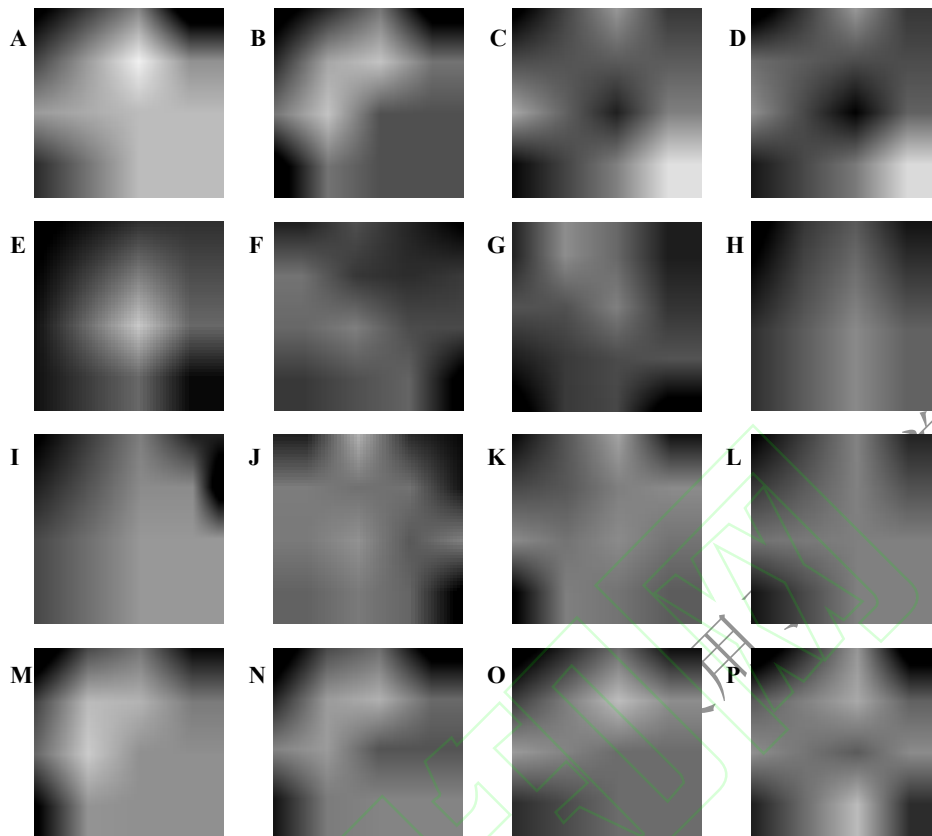


图 8 菌株 A-5, XJ-3, KW3-10 的广谱抗性

Figure 8 Broad-spectrum resistance of A-5, XJ-3, KW3-10. B, C, D: A-5, XJ-3, KW3-10 antagonize *Streptomyces scabies*; F, G, H: A-5, XJ-3, KW3-10 antagonize *Fusarium oxysporum*; J, K, L: A-5, XJ-3, KW3-10 antagonize *Alternaria solani*; N, O, P: A-5, XJ-3, KW3-10 antagonize *Rhizoctonia solani*.

## 2.10 盆栽防病试验

为了验证平板试验结果的准确性, 本文采用高感马铃薯疮痂病品种夏波蒂作为参试植物, 通过盆栽试验, 人为分别接种致病链霉菌 *S. scabies*、致病链霉菌 *S. scabies*+产胞外多糖细菌, 结果如表 2 和图 9 所示, 水处理组 (CK1) 的微型薯均未发病; 病原菌 *S. scabies* 处理组 (CK2) 发病率为 100%, 病情指数为 55.88; *S. scabies* 与 A-5 共处理组发病率为 50%, 病情指数 17.5, 相对防效达 68.68%; *S. scabies* 和 XJ-3 共处理组发病率为 55.56%, 病情指数为 20.83, 相对防效为 62.72%; *S. scabies* 和 KW3-10 共处理组发病率为 61.11%, 病情指数为 22.22, 相对防效达 60.24%。

*TxtA* 是致病性链霉菌 *S. scabies* 的主要致病基因, *TxtA* 在基质中的相对丰度反映了基质中疮痂链霉菌的数量。图 9F 所示, 菌株 A-5、XJ-3 和 KW3-10 处理组中致病菌的相对丰度显著低于 CK2, 与上述结果一致, 表明 3 个目标菌对 *S. scabies* 均有较好的抑制效果。



表 2 马铃薯疮痂病情统计

Table 2 Statistics of potato scab

Treatment	Number of grains	Sickness					Occurrence rate	Disease index	Relative control effects
		0	1	2	3	4			
CK1	16	16	0	0	0	0	0	0	-
CK2	17	0	6	4	4	3	100%	55.88	-
A-5	20	10	7	2	1	0	50%	17.5	68.68%
XJ-3	18	8	8	0	1	1	55.56%	20.83	62.72%
KW3-10	18	7	8	2	0	1	61.11%	22.22	60.24%

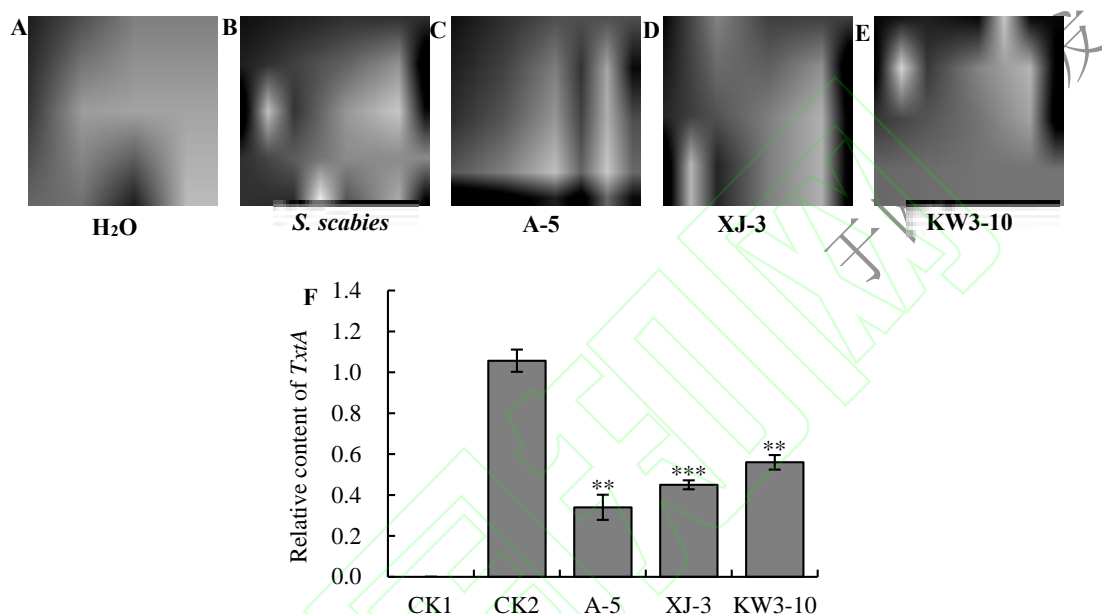


图 9 盆栽防病试验结果

Figure 9 Pot disease inhibition test results. A: Control; B: Pathogen treatment; C, D, E: Pathogen+target bacteria treatment F: Detection of pathogenic gene *TxtA*. The presented values are the means of three determinations, with standard deviations indicated; \*:  $P < 0.05$ , \*\*:  $P < 0.01$ , \*\*\*:  $P < 0.001$ .

### 3 讨论

一些产胞外多糖、生态适应性强、对环境友好的芽孢杆菌，能通过竞争、拮抗和提高植物抗病性等方式抵御病原菌的入侵，促进农作物增产，具有潜在的产业化应用可能性<sup>[19]</sup>。Vardharajula<sup>[20]</sup>等人在土壤中接种高产 EPS 的解淀粉芽孢杆菌 (*Bacillus amyloliquefaciens*) HYD-B17、地衣芽孢杆菌 (*Bacillus licheniformis*) HYTAPB18 及枯草芽孢杆菌 (*Bacillus subtilis*) RMPB44 后，土壤中小团聚体的胶结性提高，水稳定性大团聚体数量显著增多。张文平<sup>[21]</sup>等通过优化蜡样芽孢杆菌 DT-10 的发酵条件，获得较高产量的 EPS。枯草芽孢杆菌沙漠亚种 GBW HF-98 在盐碱胁迫下，可以通过产胞外多糖改善土壤团粒结构，调整土壤的盐碱性，从而促进番茄生长<sup>[22]</sup>。

近年来，随着化肥农药的大量施用和养分的不平衡富集，土壤生态环境持续恶化，农作物土传病害加剧危害，尤其由致病性链霉菌(*Streptomyces scabies*)引起的块根块茎类作物

的疮痂病在世界范围普遍发生，危害程度逐年加重<sup>[23-26]</sup>。我国马铃薯疮痂病年发病面积超过 40 万  $\text{hm}^2$ ，平均病株率约 30%，导致块茎商品性和耐储性大幅下降，病原菌土传和种传，难以防控，已严重威胁到产业的可持续发展<sup>[27]</sup>。微生物制剂具有对环境友好、促进作物生长、广谱抗病等多种功能，越来越受到人们的重视，可能是未来实现马铃薯疮痂病等主要土传病害有效防控的重要途径。虽然有一些学者分离鉴定了疮痂链霉菌的拮抗菌，并在盆栽或田间试验中取得了一定的防效，但真正用于生产的菌株非常有限，且防治效果并不理想。

2022 年农业部颁布的微生物肥料行业标准 GB/T 41728-2022 明确规定，地衣芽孢杆菌对人畜和环境友好，可免作毒理学试验，直接添加在肥料中应用于农业生产。本研究从严重板结的土壤样品中分离获得的地衣芽孢杆菌 A-5，培养液胞外多糖含量高达 1439.23  $\text{mg/L}$ ，在土壤中定殖力强，处理后土壤多糖为 4.73  $\text{mg/g}$ ，粒径  $>0.25 \text{ mm}$  的团聚体数量比对照提高 4.07 倍，不仅具有很好的耐盐碱特性和调节土壤 pH 的作用，还具有较好的广谱抗病功能，尤其对马铃薯疮痂病的盆栽防效达到 68.68%，可作为土壤改良型抑病功能菌剂的候选菌株，具有较好的应用前景。值得一提的是 A-5 虽然在平板对峙试验中抑菌圈直径最小（20 mm），但其解磷和产 EPS 能力显著优于其他 2 株菌，盆栽试验对疮痂链霉菌的抑制效果最佳，相对防效达 68.68%，我们推测菌株对疮痂病抑制效果可能与其解磷或产胞外多糖性能相关，其相关性和作用机理有待进一步研究和验证。

## 参考文献

- [1] AZIZI A, GILANDEH YA, MESRI-GUNDOSHMIAN T, SALEH-BIGDELI AA, MOGHADDAM HA. Classification of soil aggregates: a novel approach based on deep learning[J]. Soil and Tillage Research, 2020, 199: 104586.
- [2] 刘艳, 马茂华, 吴胜军, 冉义国, 王小晓, 黄平. 干湿交替下土壤团聚体稳定性研究进展与展望[J]. 土壤, 2018, 50(5):853-865.
- [2] LIU Y, MA MH, WU SJ, RAN YG, WANG XX, HUANG P. Soil aggregates as affected by wetting-drying cycle: a review[J]. Soils, 2018, 50(5):853-865 (in Chinese).
- [3] CHANTIGNY MH, ANGERS DA, PRÉVOST D, VÉZINA LP, CHALIFOUR FP. Soil aggregation and fungal and bacterial biomass under annual and perennial cropping systems[J]. Soil Science Society of America Journal, 1997, 61(1): 262-267.
- [4] CHENU C, ROBERSON EB. Diffusion of glucose in microbial extracellular polysaccharide as affected by water potential[J]. Soil Biology and Biochemistry, 1996, 28(7): 877-884.
- [5] VADAKATTU VSR, JAMES J, GUPTA. Soil aggregation: influence on microbial biomass and implications for biological processes[J]. Soil Biology and Biochemistry, 2015, 80: A3-A9.

- [6] OADES JM. Soil organic matter and structural stability: mechanisms and implications for management[J]. *Plant and Soil*, 1984, 76(1): 319-337.
- [7] SIX J, ELLIOTT ET, PAUSTIAN K. Soil macroaggregate turnover and microaggregate formation: a mechanism for C sequestration under no-tillage agriculture[J]. *Soil Biology and Biochemistry*, 2000, 32(14): 2099-2103.
- [8] ALAMI Y, ACHOUAK W, MAROL C, HEULIN T. Rhizosphere soil aggregation and plant growth promotion of sunflowers by an exopolysaccharide-producing *Rhizobium* sp. strain isolated from sunflower roots[J]. *Applied and Environmental Microbiology*, 2000, 66(8): 3393-3398.
- [9] SANDHYA V, ALI SZ. The production of exopolysaccharide by *Pseudomonas putida* GAP-P45 under various abiotic stress conditions and its role in soil aggregation[J]. *Microbiology*, 2015, 84(4): 512-519.
- [10] 邓照亮. 海南连作香蕉抑病型和导病型土壤团聚体组成及生物学特性研究[D]. 南京农业大学, 2017.
- [10] DENG ZL. Study on composition of soil aggregates and biological characteristics of suppressive and conducive soils of continuous cropping bananas in hainan[D]. Nanjing Agricultural University, 2017 (in Chinese).
- [11] 康贻军, 沈敏, 王欢莉, 赵庆新, 殷士学. 两株植物根际促生菌对番茄青枯病的生物防治效果评价[J]. *中国生物防治学报*, 2012, 28(2): 255-261.
- [11] KANG YJ, SHEN M, WANG HL, ZHAO QX, YIN TX. Biological control of tomato bacterial wilt caused by *Ralstonia solanacearum* with *Erwinia persicinus* RA2 and *Bacillus pumilus* WP8[J]. *Chinese Journal of Biological Control*, 2012, 28(2): 255-261 (in Chinese).
- [12] JIAO YQ, CODY GD, HARDING AK, WILMES P, SCHRENK M, WHEELER KE, BANFIELD JF, THELEN MP. Characterization of extracellular polymeric substances from acidophilic microbial biofilms[J]. *Applied and Environmental Microbiology*, 2010, 76(9): 2916-2922.
- [13] UPADHYAY SK, SINGH JS, SINGH DP. Exopolysaccharide-producing plant growth-promoting rhizobacteria under salinity condition[J]. *Pedosphere*, 2011, 21(2): 214-222.
- [14] CHENG R, WANG L, LI J, FU R, WANG S, ZHANG J. *In vitro* and *in vivo* anti-inflammatory activity of a succinoglycan riclin from *Agrobacterium* sp. ZCC3656[J]. *Journal of Applied Microbiology*, 2019, 127(6): 1716-1726.
- [15] 曹晶晶, 熊惘梓, 钞亚鹏, 赵盼, 汪志琴, 仲乃琴. 极耐盐碱固氮菌的分离鉴定及固氮特性研究[J]. *微生物学报*, 2021, 61(11): 3483-3495.
- [15] CAO JJ, XIONG MZ, (CHAO/MIAO) YP, ZHAO P, WANG ZQ, ZHONG NQ. Isolation and identification of extremely salt-tolerant azotobacter and its nitrogen-fixing characteristics[J]. *Acta Microbiologica Sinica*, 2021, 61(11): 3483-3495 (in Chinese).
- [16] 李振东, 陈秀蓉, 李鹏, 满百膺. 珠芽蓼内生菌 Z5 产 IAA 和抑菌能力测定及其鉴定[J]. *草业学报*, 2010, 19(2): 61-68.
- [16] LI ZD, CHEN XR, LI P, MAN BY. Identification of *Polygonum viviparum* endophytic bacteria Z5 and

determination of the capacity to secrete IAA and antagonistic capacity towards pathogenic fungi[J]. *Acta Prataculturae Sinica*, 2010, 19(2): 61-68 (in Chinese).

[17] 石莹莹, 赵盼, 宋双伟, 熊桐梓, 莫乘宝, 仲乃琴. 马铃薯疮痂病拮抗菌 YN-2-2 的分离与鉴定[J]. *微生物学通报*, 2020, 47(8): 2425-2435.

[17] SHI YY, ZHAO P, SONG SW, XIONG MZ, MO CB, ZHONG NQ. Isolation and characterization of the antagonistic bacterium YN-2-2 against potato common scab[J]. *Microbiology China*, 2020, 47(8): 2425-2435 (in Chinese).

[18] WANNER LA, KIRK WW. *Streptomyces* - from basic microbiology to role as a plant pathogen[J]. *American Journal of Potato Research*, 2015, 92(2): 236-242.

[19] 马佳, 李颖, 胡栋, 彭杰丽, 贾楠, 张翠绵, 王旭, 王占武. 芽胞杆菌生物防治作用机理与应用研究进展[J]. *中国生物防治学报*, 2018, 34(4): 639-648.

[19] MA J, LI Y, HU D, PENG JL, JIA N, ZHANG CM, WANG X, WANG ZW. Progress on mechanism and applications of *Bacillus* as a biocontrol microbe[J]. *Chinese Journal of Biological Control*, 2018, 34(4): 639-648 (in Chinese).

[20] VARDHARAJULA S, ALISK Z. Exopolysaccharide production by drought tolerant bacillus spp. and effect on soil aggregation under drought stress[J]. *Journal of Microbiology, Biotechnology and Food Sciences*, 2014, 4(1): 51-57.

[21] 张文平, 李昆太, 黄林, 魏赛金, 程新. 产胞外多糖菌株的筛选及其对土壤团聚体的影响[J]. *江西农业大学学报*, 2017, 39(4): 772-779.

[21] ZHANG WP, LI KT, HUANG L, WEI SJ, CHENG X. Screening of exopolysaccharide-producing bacteria and their effects on aggregation in soil[J]. *Acta Agriculturae Universitatis Jiangxiensis (Natural Sciences Edition)*, 2017, 39(4): 772-779 (in Chinese).

[22] 李慧芬, 方安然, 冯海霞, 黄剑, 赵明珠, 周波. 胞外多糖产生菌的筛选鉴定及其促生改土作用[J]. *微生物学通报*, 2023, 50(5): 1941-1957.

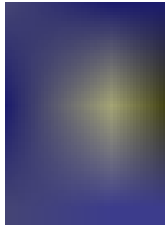
[22] LI HF, FANG AR, FENG HX, HUANG J, ZHAO MZ, ZHOU B. Screening and identification of extracellular polysaccharide-producing strain and the influence on soil quality and crop growth[J]. *Microbiology China*, 2023, 50(5): 1941-1957 (in Chinese).

[23] ZHAO P, LIU L, CAO JJ, WANG ZQ, ZHAO YL, ZHONG NQ. Transcriptome analysis of tryptophan-induced resistance against potato common scab[J]. *International Journal of Molecular Sciences*, 2022, 23(15): 8420.

[24] 陈文轩, 李茜, 王珍, 孙兆军. 中国农田土壤重金属空间分布特征及污染评价[J]. *环境科学*, 2020, 41(6): 2822-2833.

[24] CHEN WX, LI Q, WANG Z, SUN ZJ. Spatial distribution characteristics and pollution evaluation of heavy metals in arable land soil of China[J]. *Environmental Science*, 2020, 41(6): 2822-2833 (in Chinese). [万方]

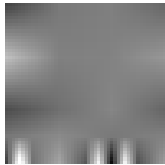
- [25] 张晓云, 丛蓉, 赵卫松, 曲远航, 苏振贺, 郭庆港, 鹿秀云, 李社增, 马平. 30 亿 CFU/g 芽胞杆菌可湿性粉剂的研制及其对马铃薯黄萎病和疮痂病的防治效果[J]. 农药学学报, 2023, 25(1)140-149.
- [25] ZHANG XY, CONG R, ZHAO WS, QU YH, SU ZH, GUO QG, LU XY, LI SZ, MA P. Development of 3 billion CFU/g *Bacillus* wettable powder and its control efficacy on potato *Verticillium* wilt and scab[J]. Chinese Journal of Pesticide Science, 2023, 25(1)140-149 (in Chinese).
- [26] 赵永龙, 赵盼, 曹晶晶, 汪志琴, 刘璐, 仲乃琴. 疮痂链霉菌拮抗菌定向筛选及其功能评价[J]. 微生物学报, 2022, 62(7): 2624-2641.
- [26] ZHAO YL, ZHAO P, CAO JJ, WANG ZQ, LIU L, ZHONG NQ. Targeted screening and functional evaluation of the bacterial antagonists to *Streptomyces* scabies[J]. Acta Microbiologica Sinica, 2022, 62(7): 2624-2641 (in Chinese).
- [27] 王敏, 吕和平, 高彦萍, 吴雁斌, 张武, 梁宏杰. 微生物菌肥在马铃薯疮痂病防治上的应用效果[J]. 甘肃农业科技, 2021, 52(10): 27-31.
- [27] WANG M, LÜ HP, GAO YP, WU YB, ZHANG W, LIANG HJ. Application effect of microbial fertilizer on potato scab control[J]. Gansu Agricultural Science and Technology, 2021, 52(10): 27-31 (in Chinese).



微生物学报  
*Acta Microbiologica Sinica*  
ISSN 0001-6209, CN 11-1995/Q

## 《微生物学报》网络首发论文

题目：产胞外多糖菌株的分离鉴定及其功能研究  
作者：茹素龙, 赵永龙, 王紫薇, 曹晶晶, 汪志琴, 赵盼, 仲乃琴  
DOI: 10.13343/j.cnki.wsxb.20230202  
收稿日期: 2023-03-24  
网络首发日期: 2023-06-02  
引用格式: 茹素龙, 赵永龙, 王紫薇, 曹晶晶, 汪志琴, 赵盼, 仲乃琴. 产胞外多糖菌株的分离鉴定及其功能研究[J/OL]. 微生物学报.  
<https://doi.org/10.13343/j.cnki.wsxb.20230202>



**网络首发:** 在编辑部工作流程中, 稿件从录用到出版要经历录用定稿、排版定稿、整期汇编定稿等阶段。录用定稿指内容已经确定, 且通过同行评议、主编终审同意刊用的稿件。排版定稿指录用定稿按照期刊特定版式(包括网络呈现版式)排版后的稿件, 可暂不确定出版年、卷、期和页码。整期汇编定稿指出版年、卷、期、页码均已确定的印刷或数字出版的整期汇编稿件。录用定稿网络首发稿件内容必须符合《出版管理条例》和《期刊出版管理规定》的有关规定; 学术研究成果具有创新性、科学性和先进性, 符合编辑部对刊文的录用要求, 不存在学术不端行为及其他侵权行为; 稿件内容应基本符合国家有关书刊编辑、出版的技术标准, 正确使用和统一规范语言文字、符号、数字、外文字母、法定计量单位及地图标注等。为确保录用定稿网络首发的严肃性, 录用定稿一经发布, 不得修改论文题目、作者、机构名称和学术内容, 只可基于编辑规范进行少量文字的修改。

**出版确认:** 纸质期刊编辑部通过与《中国学术期刊(光盘版)》电子杂志社有限公司签约, 在《中国学术期刊(网络版)》出版传播平台上创办与纸质期刊内容一致的网络版, 以单篇或整期出版形式, 在印刷出版之前刊发论文的录用定稿、排版定稿、整期汇编定稿。因为《中国学术期刊(网络版)》是国家新闻出版广电总局批准的网络连续型出版物(ISSN 2096-4188, CN 11-6037/Z), 所以签约期刊的网络版上网络首发论文视为正式出版。



DOI: 10.13343/j.cnki.wsxb.20230202

(研究报告)

# 产胞外多糖菌株的分离鉴定及其功能研究

茹素龙<sup>1</sup>, 赵永龙<sup>2,3</sup>, 王紫薇<sup>4</sup>, 曹晶晶<sup>2,3</sup>, 汪志琴<sup>2,3</sup>, 赵盼<sup>2,3,5</sup>, 仲乃琴<sup>2,3,5\*</sup>

1 宁夏大学农学院, 宁夏 银川 750021

2 中国科学院微生物研究所, 北京 100101

3 中国科学院农业微生物先进技术工程实验室, 北京 100101

4 山西农业大学植物保护学院, 山西 晋中 030600

5 内蒙古自治区马铃薯肥料农药高效利用技术企业重点实验室, 内蒙古呼伦贝尔 021000

**摘要:** 微生物产生的胞外多糖 (EPS) 可促进大粒径土壤团聚体形成, 高产 EPS 的菌株在土壤改良、促进作物生长方面具有较好的应用前景。【目的】从土壤样品中筛选高产胞外多糖的细菌, 研究其在土壤改良、环境适应性、广谱抗病等方面的功能, 为制备土壤改良型功能菌剂提供候选菌株。【方法】采用蒽酮硫酸法测定菌株胞外多糖的产量, 通过形态学观察、生理生化试验及 16S rRNA 基因序列测定确定其分类地位, 结合土壤培养试验研究菌株对土壤团聚体形成的影响。【结果】获得 3 株胞外多糖产量大于 500 mg/L 的细菌, 经鉴定 A-5 为地衣芽孢杆菌 (*Bacillus licheniformis*), XJ-3 为萎缩芽孢杆菌 (*Bacillus atrophaeus*), KW3-10 为耐盐芽孢杆菌 (*Bacillus halotolerans*)。菌株 A-5、XJ-3、KW3-10 处理后, 土壤大团聚体 (>0.25 mm) 含量较对照分别提高了 4.07、2.14、3.16 倍。3 株菌株对疮痂链霉菌 (*Streptomyces scabies*)、尖孢镰刀菌 (*Fusarium oxysporum*)、茄链格孢菌 (*Alternaria solani*) 和立枯丝核菌 (*Rhizoctonia solani*) 等多种植物病原菌具有明显的抑制效果, 可耐受 pH5-9 和 NaCl 含量 1%-9% 的盐碱环境, 促进植物生长, 其中 KW3-10 的代谢产物中 IAA 含量为 25.58 mg/L。【结论】菌株 A-5、XJ-3、KW3-10 可显著促进土壤团粒结构形成, 具有较好的广谱抗病性和促生长特性, 可作为高效复合功能菌剂的候选菌株。

资助项目: 中国科学院战略性先导科技专项 (XDA13020601, XDA28030202); 广东省重点领域研发计划 (2020B0202010005); 内蒙古自治区关键技术攻关计划 (2021GG0300)

This work was supported by the Strategic Priority Research Program of the Chinese Academy of Sciences (XDA13020601, XDA28030202), the Guangdong Province Key Field R&D Program Project (2020B0202010005), and the Inner Mongolia Autonomous Region Key Technology Tackling Plan Project (2021GG0300)

\*Corresponding author. E-mail: nqzhong@im.ac.cn

Received: 2023-03-24; Accepted: 2023-05-23; Published online:

**关键词:** 胞外多糖, 土壤团聚体, 芽孢杆菌, 土壤改良

# Isolation, identification, and functional characterization of exopolysaccharide-producing strains

RU Sulong<sup>1</sup>, ZHAO Yonglong<sup>2,3</sup>, WANG Ziwei<sup>4</sup>, CAO Jingjing<sup>2,3</sup>, WANG Zhiqin<sup>2,3</sup>, ZHAO Pan<sup>2,3,5</sup>, ZHONG Naiqin<sup>2,3,5\*</sup>

1 School of Agriculture, Ningxia University, Yinchuan 750021, Ningxia, China

2 Institute of Microbiology, Chinese Academy of Sciences, Beijing 100101, China

3 Engineering Laboratory for Advanced Technology of Agricultural Microbiology, Chinese Academy of Sciences, Beijing 100101, China

4 College of Plant Protection, Shanxi Agricultural University, Jinzhong 030600, Shanxi, China

5 The Enterprise Key Laboratory of Advanced Technology for Potato Fertilizer and Pesticide, Hulunbuir 021000, Inner Mongolia, China

**Abstract:** Exopolysaccharides (EPS) produced by microorganisms can promote the formation of large soil aggregates. EPS-producing strains have good application prospects in improving soil and promoting crop growth. **[Objective]** We isolated the bacteria with high yields of exopolysaccharides from soil samples and studied their soil-improving function, environmental adaptability, and broad-spectrum disease resistance, aiming to provide candidate strains for the preparation of soil-improving microbial agents. **[Methods]** The yield of EPS was determined by anthrone-sulfuric acid method. The taxonomic status of the strain was determined by morphological observation, physiological and biochemical tests, and 16S rRNA gene sequencing. Soil culture experiments were carried out to evaluate the effect of the strain on the formation of soil aggregates. **[Results]** Three strains of bacteria with EPS yields greater than 500 mg/L were obtained. A-5 was identified as *Bacillus licheniformis*, XJ-3 as *B. atrophaeus*, and KW3-10 as *B. halotolerans*. After treatment with these strains, the content of soil macroaggregates (>0.25 mm) increased by 4.07, 2.14, and 3.16 times, respectively. The three strains exerted significant inhibitory effects on plant pathogens such as *Streptomyces scabies*, *Fusarium oxysporum*, *Alternaria solani*, and *Rhizoctonia solani*. They could tolerate the saline-alkali environment with pH 5–9 and NaCl content of 1%–9% and promoted plant growth. The content of indole acetic acid in the metabolites of KW3-10 was 25.58 mg/L. **[Conclusion]**



Strains A-5, XJ-3, and KW3-10 can significantly promote the formation of soil aggregates and demonstrate broad-spectrum disease resistance and remarkable growth-promoting performance, serving as candidates for the preparation of efficient compound microbial agents.

**Keywords:** exopolysaccharides, soil aggregate, *Bacillus*, soil improvement

土壤团聚体是土壤结构的基本单元，其数量和粒径分布决定土壤的肥沃程度，稳定性决定土壤承受被破坏的能力<sup>[1]</sup>。多糖是土壤有机质的组成成分之一，占总有机质的 5%-30%，可通过游离羟基的离子键和氢键与土壤颗粒结合，形成稳定的团聚体<sup>[2]</sup>。胞外多糖 (exopolysaccharides, EPS) 是一些微生物生长代谢过程中分泌到细胞壁外的水溶性多糖，对土壤大团聚体 (>0.25 mm) 的形成及植物生长发育具有显著的促进作用<sup>[3]</sup>。Chenu<sup>[4]</sup>和 Vadakattu<sup>[5]</sup>等研究发现，EPS 可促进边际土壤颗粒的聚集，形成有效团聚体，从而提高土壤结构的稳定性和持水能力。EPS 不仅能提高植物根部土壤团聚体的稳定性，还能增加土壤孔隙度，改善透气性，利于植物根系生长和营养吸收，从而提高土壤养分的利用效率<sup>[6-8]</sup>，并可将有机碳封闭在团聚体中，增强其迟效性<sup>[9]</sup>。邓照亮等<sup>[10]</sup>研究结果表明，抑病型土壤的水稳定性大团聚体含量明显高于导病型土壤，砖红壤和砂壤的抑病型土壤中粒径大于 2 mm 的团聚体是导病型土壤的 1.87 倍、2.38 倍；康贻军等人<sup>[11]</sup>用两种产胞外多糖的细菌浸种，有效提高了土壤水稳性团聚体(>0.25 mm)比例，促进番茄幼苗生长，降低青枯病危害程度。可见，产胞外多糖细菌对于改良土壤结构，调节土壤生态、促进作物增产具有重要作用。但是目前应用于土壤改良的菌种资源十分有限，加之 EPS 的形成对环境温度、土壤 pH 值和盐度的变化十分敏感<sup>[12-13]</sup>，迫切需要筛选胞外多糖产量高、兼具抗病、耐盐碱，且环境稳定性强的菌株，为复合功能菌剂的研发和产业化应用提供候选菌种资源。

本研究从土壤样品中定向分离和筛选高产 EPS 的细菌，明确其分类地位，研究菌株对土壤水稳性大粒径团聚体形成的促进作用，探究其环境适应性和对土壤的改良作用，测定其对致病性链霉菌 *S. scabies* 等多种病原菌的广谱拮抗效果，以期获得具有推广应用前景的功能菌株。

## 1 材料与方法

### 1.1 材料

#### 1.1.1 病原菌样品

疮痂链霉菌 (*Streptomyces scabies*)、尖孢镰刀菌 (*Fusarium oxysporum*)、立枯丝核菌 (*Rhizoctonia solani*) 购自中国科学院微生物研究所菌种保藏管理中心，馆藏编号分别为 CGMCC4.1765、CGMCC3.18025、CGMCC3.2888；盆栽基质采用  $1 \times 10^5$  Pa 灭菌 30 min 的营养土和蛭石。

#### 1.1.2 供试土壤样品

土壤培养试验供试土样采自黑龙江省三江平原北大荒集团友谊农场 (46°13'-46°47'N,

131°21'-131°21'E), pH 8.16, 总磷 0.77 g/kg, 全氮 0.761 g/kg, 全钾 2.17%, 有机质 29.7 g/kg。

### 1.1.3 主要培养基与试剂

LB 培养基(g/L): 蛋白胨 10, 酵母提取物 5, NaCl 10, 用去离子水定容至 1 L, pH 调整至 7.0-7.2, 121 °C 灭菌 20 min。

有氮培养基(g/L): 蔗糖 10, (NH<sub>4</sub>)<sub>2</sub>SO<sub>4</sub> 1, MgSO<sub>4</sub>·7H<sub>2</sub>O 0.5, NaCl 0.1, K<sub>2</sub>HPO<sub>4</sub> 2, 酵母提取物 0.5, 用去离子水定容至 1 L, 调 pH 为 7, 固体培养基添加 20 琼脂, 113 °C 灭菌 30 min。

PDA 固体培养基(g/L): 马铃薯块茎 200 切碎, 沸水煮 20 min, 用纱布过滤除渣, 加入葡萄糖 20, 琼脂 15, 用去离子水定容至 1 L, 调 pH 至 7.0-7.2, 113 °C 灭菌 20 min。

King 氏培养基(g/L): 蛋白胨 20, K<sub>2</sub>HPO<sub>4</sub> 1.725, 丙三醇 15 mL, MgSO<sub>4</sub>·7H<sub>2</sub>O 1.5, 色氨酸 0.1, 用去离子水定容至 1 L, 调 pH 至 7.2, 121 °C 灭菌 20 min。

比色液: 将 20 mL 0.025 mol/L 的 FeCl<sub>3</sub> 缓缓加入 30 mL 浓硫酸中, 搅拌均匀。

B5 营养液(g/L): KNO<sub>3</sub> 2.5, MgSO<sub>4</sub>·7H<sub>2</sub>O 0.25, NaH<sub>2</sub>PO<sub>4</sub>·H<sub>2</sub>O 0.15, CaCl<sub>2</sub>·2H<sub>2</sub>O 0.15, (NH<sub>4</sub>)<sub>2</sub>SO<sub>4</sub> 0.135, FeSO<sub>4</sub>·7H<sub>2</sub>O 0.028, EDTA·Na<sub>2</sub> 0.037, MnSO<sub>4</sub>·4H<sub>2</sub>O 0.004, ZnSO<sub>4</sub>·7H<sub>2</sub>O 0.0008, 去离子水定容至 1 L。

PKO 培养基(g/L): 葡萄糖 10, (NH<sub>4</sub>)<sub>2</sub>SO<sub>4</sub> 0.5, NaCl 0.3, KCl 0.3, MgSO<sub>4</sub>·7H<sub>2</sub>O 0.1, MgSO<sub>4</sub>·H<sub>2</sub>O 0.03, FeSO<sub>4</sub> 0.03, Ca<sub>3</sub>(PO<sub>4</sub>)<sub>2</sub> 5, 酵母提取物 0.5, 琼脂 20, 用去离子水定容至 1 L, 调 pH 至 7.0, 113 °C 灭菌 20 min。

蒽酮溶液(g/mL): 称取 0.2 蒽酮, 定容至 100 mL 浓硫酸中, 临用前配制。

### 1.1.4 供试作物

由本实验室培育 30 d 的马铃薯脱毒试管苗 (品种: 夏波蒂)。

## 1.2 目标菌株的分离

采集上海松江区、广西环江县严重板结的农田土壤样品, 和宁夏西吉县板结土壤中马铃薯病薯表面土壤样品, 取 1 g 置于 50 mL 离心管中, 加入 10 mL 无菌水充分震荡。吸取 100 μL 上述悬浮液均匀涂布于 LB 固体培养基上, 28 °C 培养 24 h; 挑选细菌单菌落进行划线纯化, 并将所得菌株接种于液体 LB 培养基中, 37 °C 振荡培养备用。

## 1.3 产 EPS 菌的初筛

将分离所得的菌株涂布于固体有氮培养基中, 37 °C 培养 48 h。用灭菌牙签挑取菌落, 挑选黏度较大的菌株。

## 1.4 多糖含量的测定

将初筛获得的菌株分别于 37 °C 振荡(200 r/min)培养 48 h, 采用乙醇沉淀法提取发酵液粗多糖, 并采用硫酸-蒽酮法测定多糖含量。

葡萄糖标准曲线制作：分别吸取 50  $\mu\text{g}/\text{mL}$  的葡萄糖溶液 0、0.5、1、1.5、2、2.5 mL 于 25 mL 比色管中，加去离子水至 2.5 mL，分别加入 5 mL 的蒽酮溶液，置沸水浴中保温 10 min。采用分光光度计测定  $OD_{620}$  值。以葡萄糖浓度为横坐标， $OD$  值为纵坐标绘制葡萄糖标准曲线。

样品多糖含量的测定：待测菌株培养液 8 000 r/min 离心 10 min，用 Sevag 法<sup>[14]</sup>提取 EPS，分别取 EPS 溶液 0.1 mL 于比色管中，加入去离子水 2.4 mL，混匀，采用硫酸-蒽酮法测定多糖含量。

### 1.5 菌株形态观察

将待测菌液均匀涂布于 LB 固体培养基上，37  $^{\circ}\text{C}$  培养 24 h 后镜检观察菌落形态，分别采用日立冷场发射扫描电子显微镜 SU8010 和蔡司荧光倒置显微镜 Observer Z1 观察菌体形态。

### 1.6 菌株革兰氏染色

将待测菌液滴至载玻片上，自然晾干后轻微烘烤，用草酸铵结晶紫染色 1 min，自来水冲洗 30 s，加碘液于涂面约 1 min，再次水洗，用吸水纸吸干水分，加 95% 酒精数滴，轻轻摇动进行脱色，20 s 后水洗，吸去水分，番红染色液（稀）染 2 min，自来水冲洗，干燥后镜检。

### 1.7 菌株生理生化特性分析

采用 API 50 CHB G+ 芽胞杆菌鉴定试剂盒测定菌株理化性质，依据 API 50CH 试验条说明书判读测试结果。

将待测菌种分别接种于 pH 值为 3.0、5.0、7.0、9.0、11.0，NaCl 浓度分别为 1%、3%、5%、7%、9%、11% 的液体 LB 培养基中，37  $^{\circ}\text{C}$ 、200 r/min 振荡培养 12 h 后测定其  $OD_{600}$  值，分析菌株耐盐碱特性<sup>[15]</sup>。

### 1.8 分子系统学分析

采用 16S rRNA 基因片段通用引物 (27F: 5'-AGAGTTTGATCCTGGCTCAG-3', 1492R: 5'-CTACGGCTACCTTGTACGA-3') 进行测序 (北京博迈德生物工程股份有限公司)，PCR 反应体系 (20  $\mu\text{L}$ ): 2 $\times$ T5 Super PCR Mix 10  $\mu\text{L}$ ，菌株基因组 DNA (200 ng/ $\mu\text{L}$ ) 2  $\mu\text{L}$ ，正、反向引物 (10  $\mu\text{mol}/\text{L}$ ) 各 1  $\mu\text{L}$ ，ddH<sub>2</sub>O 6  $\mu\text{L}$ 。PCR 反应条件：95  $^{\circ}\text{C}$  5 min；95  $^{\circ}\text{C}$  30 s，55  $^{\circ}\text{C}$  30 s，72  $^{\circ}\text{C}$  2 min，35 个循环；72  $^{\circ}\text{C}$  10 min。测序结果在 National Center for Biotechnology Information (NCBI) 上进行比对，采用 MEGA 7.0 软件构建系统发育树。

### 1.9 土壤培养试验

挖取 0-15 cm 土层土壤，自然风干后，碾碎过孔径为 0.25 mm 的筛。在容积为 1 300 mL 的组培瓶底部垫 150 g 石英砂 (约 1 cm 厚)，称取 500 g 过筛土样装入组培瓶中，用纱网将土壤与石英砂隔开，121  $^{\circ}\text{C}$  灭菌 45 min。将参试菌株接种于 500 mL LB 液体培养中培养 4-5 d，至芽孢形成，离心弃上清，将菌体用无菌水洗涤 2 次，分别取 10<sup>7</sup> CFU/mL 菌体均匀接种

入土壤中，加无菌水至土壤饱和含水量 60%，室温培养箱 37 °C 培养 120 d，样品送至青岛斯坦德衡立环境技术研究院有限公司测定不同粒径水稳性土壤团聚体含量。

试验设置 4 个处理，CK（过筛土样+无菌水），处理 1（过筛土样+A-5），处理 2（过筛土样+XJ-3），处理 3（过筛土样+ KW3-10），每个处理重复 3 次。

### 1.10 菌株溶磷及促生长特性分析

菌株在 PKO 固体培养基上 28 °C 培养 7 d，观察菌株溶磷效果。

吸取 100 μL 菌液接种于 King 氏液体培养基中，37 °C、200 r/min 培养 48 h，离心收集上清液，用 SalKowski 比色法定性检测菌液中的生长素(IAA)，参照李振东等的方法测算 IAA 浓度<sup>[16]</sup>。

### 1.11 广谱抑菌效果测定

吸取 100 μL 疮痂链霉菌(*S. scabies*)孢子悬浮液均匀涂布于 PDA 固体培养基，吸取上述细菌培养液 6 μL 滴于其上，28 °C 培养 7 d 后测量抑菌圈直径。

在 PDA 培养基上接种大丽轮枝菌、立枯丝核菌和尖孢镰刀菌，在其两侧间隔 1 cm 处分别接种 6 μL 目标菌株培养液，并以单独接种病原菌的处理为对照，28 °C 培养 4 d 观察抑菌效果。

### 1.12 马铃薯疮痂病盆栽防控效果验证

在高 10 cm、直径为 17 cm 的花盆中装满蛭石与营养土（蛭石：营养土=4：1），将 2 L B5 营养液均匀浇入花盆，移栽培养 30 d 的马铃薯夏波蒂脱毒组培苗，每盆 3 株，置于相同环境培养，10 d 后每株幼苗根部接种 100 mL  $1 \times 10^7$  CFU/mL 的 *S. scabies* 孢子悬浮液，间隔 15 d 后接种目标菌悬浮液(30 mL/盆， $1 \times 10^8$  CFU/mL)，不接种任何菌株的处理为 CK1，仅接种 *S. scabies* 的处理为 CK2。每个处理重复 3 次，每周浇水 1 次，每次浇 2 L。马铃薯收获以后，依据疮痂病分级标准统计发病率、病情指数，计算防治效果。

病害分级标准<sup>[17]</sup>：0 级为薯皮健康，无病斑；1 级为病斑面积占块茎总表面积的 0-1/6；2 级为病斑面积占块茎总表面积的 1/6-1/3；3 级为病斑面积占块茎总表面积的 1/3-1/2；4 级为病斑面积占块茎总表面积的 1/2 以上。

发病率(%)=发病块茎数/总块茎数×100%；

病情指数= $\sum$ (各病级块茎数×该病级数代表值)/(调查个体总和×最高病级数)×100；

相对防效(%)=(对照组病情指数-处理组病情指数)/对照组病情指数×100%。

参照 Wanner Leslie A<sup>[18]</sup>的方法，以基质环境为模板，依据 *S. scabies* 的关键致病基因 *TxtA* 序列设计引物，正向引物：5'-CACGTACGCGCAGTTCAATG-3'；反向引物：5'-AGATGATGTAGGCGGGAC-3'。采用 ABI 7500Real-Time PCR System 仪扩增土壤中 *TxtA* 的生物量，试验重复 3 次。

### 1.13 数据处理

采用 Excel 和 Origin 2021b 软件处理相关数据，运用 MEGA 7.0 软件构建菌株系统发育树。

## 2 结果与分析

### 2.1 高产 EPS 菌株筛选

分别从采自上海松江区、广西环江县、宁夏西吉县的严重板结土壤样品中，分离获得 3 株表面湿润、黏度较大、产胞外多糖高的细菌，编号分别为 A-5、XJ-3，KW3-10。采用硫酸-蒽酮法制作葡萄糖标准曲线，葡萄糖浓度和吸光度之间的线性方程为  $Y=0.0125X+0.0424$ ， $R^2=0.9983$ ，标准曲线满足分析测试要求。测定结果如图 1 所示，培养 72 h 时，A-5 培养液中 EPS 产量最高，达 1 439.23 mg/L，XJ-3 与 KW3-10 菌株 EPS 产量分别为 735.34 mg/L 和 838.77 mg/L。

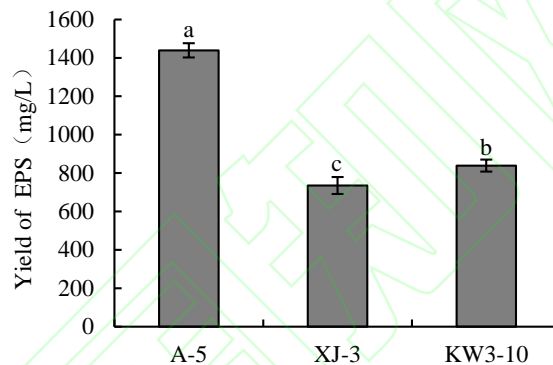
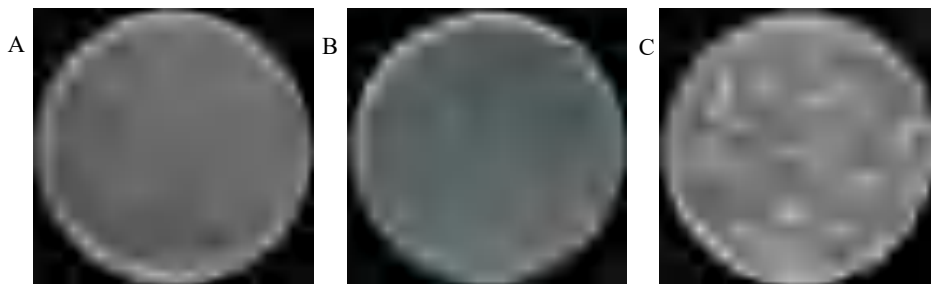


图 1 菌株胞外多糖 (EPS) 产量

Figure 1 EPS yield of strain. The presented values are the means of three determinations, with standard deviations indicated; Means with different letters are significantly different at  $P < 0.05$ .

### 2.2 菌株形态学观察

如图 2 所示，扫描电镜下观察发现，3 株菌均为杆状细菌，菌体两端钝圆，边缘整齐，表面湿润，革兰氏染色呈阳性，且周围有丝状分泌物。其中 A-5 菌落白色圆形，半透明，宽度 0.60-0.95  $\mu\text{m}$ ，长度 1.5-2.4  $\mu\text{m}$ ；XJ-3 菌落乳白色圆形，半透明，有荚膜，宽度约为 0.55-1.00  $\mu\text{m}$ ，长度为 1.6-2.4  $\mu\text{m}$ ；菌株 KW3-10 菌落乳白色圆形，不透明，宽度 0.50-0.95  $\mu\text{m}$ ，长度 1.5-3.5  $\mu\text{m}$ 。





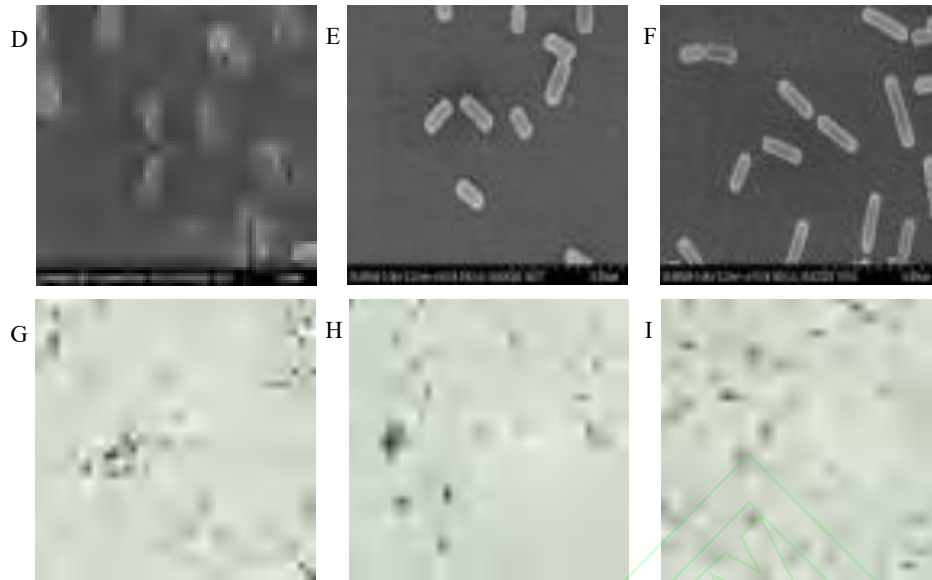


图2 菌株 A-5、XJ-3、KW3-10 的形态特征

Figure 2 Morphological characteristics of A-5, XJ-3, KW3-10. A: A-5 colonies; B: XJ-3 colonies; C: KW3-10 colonies; D: A-5 bacteria; E: XJ-3 bacteria; F: KW3-10 bacteria; G: A-5 Gram staining; H: XJ-3 Gram staining; I: KW3-10 Gram staining.

### 2.3 菌株生理生化特性分析

由表 1 所示，菌株 A-5、XJ-3、KW3-10 均可利用 D-核糖、D-葡萄糖、D-果糖、D-甘露糖、山梨醇、D-蔗糖、D-纤维二糖、肌醇、水杨苷、D-麦芽糖、D-海藻糖、淀粉作为唯一碳源，代谢产物可降解苦杏仁苷；不能利用 D-阿拉伯糖、赤藻糖醇、L-木糖、D-核糖醇、L-山梨糖、卫矛醇、D-乳糖、D-松三糖、木糖醇、葡萄糖酸钾。API 50CH 鉴定结果显示，3 株待测菌株均为芽胞杆菌，其中 A-5 初步鉴定为地衣芽孢杆菌，鉴定率为 99.5%；XJ-3 与 KW3-10 初步鉴定为枯草-解淀粉芽孢杆菌，鉴定率分别为 77.4%、89.9%。

表 1 菌株的生理生化特性

Table 1 Physiological and biochemical characters of strains

Test items	Results			Test items	Results		
	A-5	XJ-3	KW3-10		A-5	XJ-3	KW3-10
Negative control	-	-	-	Esculin ferric citrate	+	+	+
Glycerol	+	+	+	Salicin	+	+	+
Erythritol	-	-	-	cellobiose	+	+	+
D-Arabinose	-	-	-	D- maltose	+	+	+
L-Arabinose	+	+	+	D- lactose	-	-	-
D-ribose	+	+	+	D-disaccharide	-	-	+
D-xylose	+	-	+	D- sucrose	+	+	+
L-Xylose	-	-	-	D-Trehalose dihydrate	+	+	+
D-Ribitol	-	-	-	Synanthrin	+	-	+
D-Galactose	+	-	-	D-Raffinose	+	-	+
D-glucose	+	+	+	amylum	+	+	+
D-Fructose	+	+	+	glycogen	+	+	+
D-Mannose	+	+	+	Xylitol	-	-	-

L-Sorbose	-	-	-	D-Gentiobiose	+	-	-
L-rhamnose	+	-	-	Melezitose	-	-	-
Dulcitol	-	-	-	D-Lyxose	-	-	-
Inositol	+	+	+	D-Tagatose	+	+	+
D-Mannitol	+	+	+	D-fucose	-	-	-
Sorbitol	+	+	+	L-fucose	-	-	-
Methyl alpha-D-Mannopyranoside	-	-	-	D-arabinitol	-	-	-
Methyl-a-D-glucopyranoside	+	+	+	L-Arabitol	-	-	-
N-Acetyl glucosamine	-	-	-	Potassium gluconate	-	-	-
Nitrilosides	+	+	+	2-Keto-potassium gluconate	-	-	-
hydroquinone O-β-D-glucopyranoside	+	+	+	5-Keto-potassium gluconate	-	-	-

+: Positive; -: Negative.

#### 2.4 基于 16S rRNA 的分子生物学鉴定

将菌株 A-5、XJ-3 和 KW3-10 的 16S rRNA 序列在 NCBI 中进行比对，发现三者分别与地衣芽孢杆菌、萎缩芽孢杆菌与耐盐芽孢杆菌的同源性达到 99.9% 以上，运用 MEGA 7.0 软件构建系统发育树。结果如图 3 所示，A-5 与 *Bacillus paralicheniformis* QT391<sup>T</sup> 在同一分支，XJ-3 与 *Bacillus atrophaeus* B-1<sup>T</sup> 在同一分支，KW3-10 与 *Bacillus halotolerans* NOK83<sup>T</sup> 在同一分支，结合形态学和生理生化特性分析结果，将 A-5、XJ-3 和 KW3-10 分别鉴定为地衣芽孢杆菌 (*Bacillus licheniformis*)、萎缩芽孢杆菌 (*Bacillus atrophaeus*)、耐盐芽孢杆菌 (*Bacillus halotolerans*)。

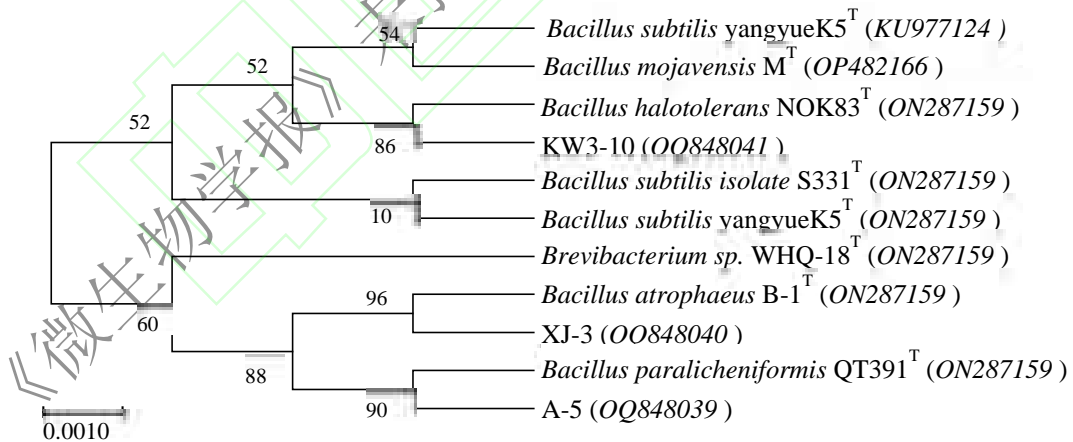


图 3 基于 16S rRNA 基因序列构建菌株的系统发育树

Figure 3 Phylogenetic tree of Strains constructed based on the 16S rRNA gene sequences. Numbers in parentheses are GenBank accession numbers; The bootstrap values are shown at the node; The scale bar indicates 0.050 substitutions per nucleotide position.

## 2.5 土壤培养试验

菌株处理土壤样品 120 d 后, 不同粒径的土壤团聚体分布如图 4A 所示, 接种 A-5、XJ-3 和 KW3-10 的处理组, 粒径大于 2 mm 的土壤团聚体比例分别较 CK 提高了 1.97%、0.53%、1.60%, 差异均达到极显著水平 ( $P<0.01$ ); 粒径大于 0.25 mm 的土壤团聚体比例分别较 CK 提高了 4.07、2.14、3.16 倍, 其中 XJ-3 和 KW3-10 处理达到显著水平 ( $P<0.05$ ); 粒径大于 0.053 mm 的土壤团聚体比例均较 CK 略有增加, 其中 XJ-3 差异达到显著水平。与 CK 相比, 各处理粒径小于 0.053 mm 的土壤团聚体比例均有所下降, 其中 XJ-3 和 KW3-10 差异达到显著水平。结果表明, 胞外多糖具有较好的胶结能力, 可以将小团聚体聚集形成稳定的大团聚体。

土壤多糖含量测定结果如图 4B 所示。3 组处理的土壤多糖含量均有所增加, 分别较 CK 提高了 28.87%、21.09% 和 12.93%, 其中菌株 A-5 处理的差异达显著水平, XJ-3 处理的差异达极显著水平。

各处理对土壤 pH 变化的影响如图 4C 所示。与 CK 相比, 接种 A-5、XJ-3、KW3-10 的土壤 pH 值分别下降了 0.49、0.84、0.85, 差异均达到极显著水平。推测参试细菌能通过代谢产生有机酸, 利用质子置换盐碱土壤中的阳离子, 从而降低土壤的 pH 值。

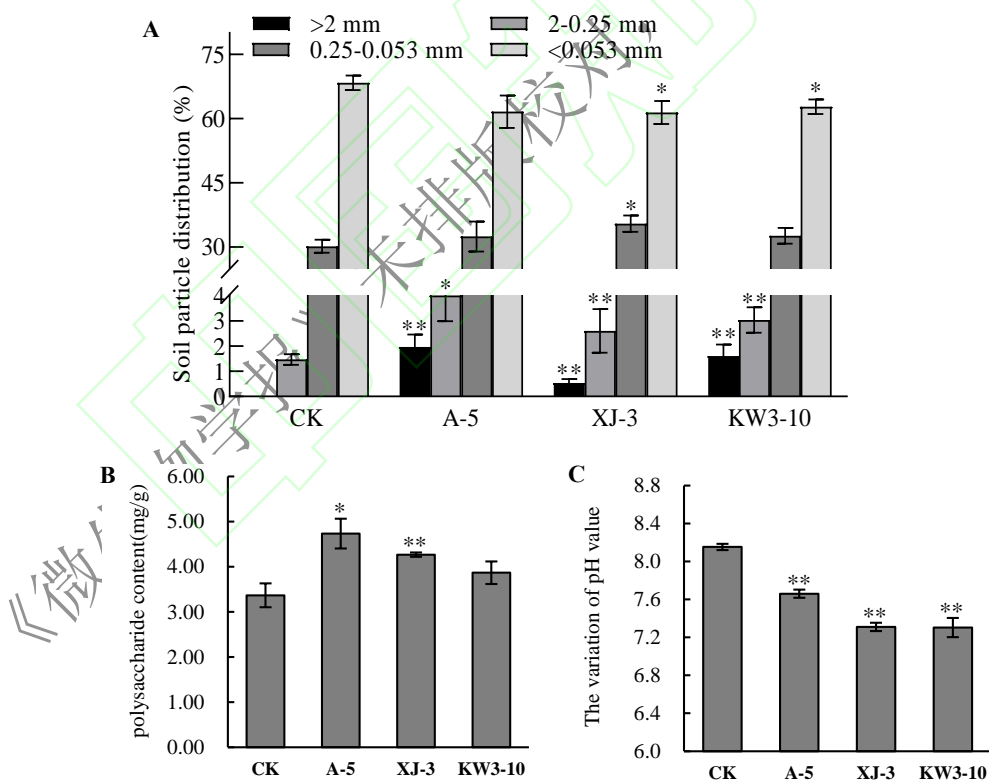


图 4 土壤培养试验结果

Figure 4 Soil culture test results. A: Effects of different strains on soil aggregates distribution in the soil culture experiment; B: The Effect of Strains on the Content of Soil Polysaccharides; C: The effect of strains on soil pH. The presented values are the means of three determinations, with standard deviations indicated; \*:  $P<0.05$ , \*\*:  $P<0.01$ .



## 2.6 菌株耐盐碱特性分析

为了探究参试菌株对盐碱环境的适应性，我们分别将其接种于 NaCl 含量 1%-11%、pH1-13 的 LB 液体培养基中，28 °C，培养 24 h 后观察发现（图 5），3 株菌对极端盐碱环境均具有较强的耐受性，其中菌株 A-5 和 KW3-10，在 NaCl 浓度为 1%-3% 的条件下可正常生长，在 NaCl 浓度为 7%-9% 的条件下可较好生长；XJ-3 和 KW3-10 最高可耐受 NaCl 浓度 11% 的高盐环境（培养 24 h 后，KW3-10 菌液的  $OD_{600}$  值可达 0.896）。在 pH 为 5-7 的环境中，3 株菌均可正常生长，KW3-10 可耐受 pH11 的极端高碱环境。

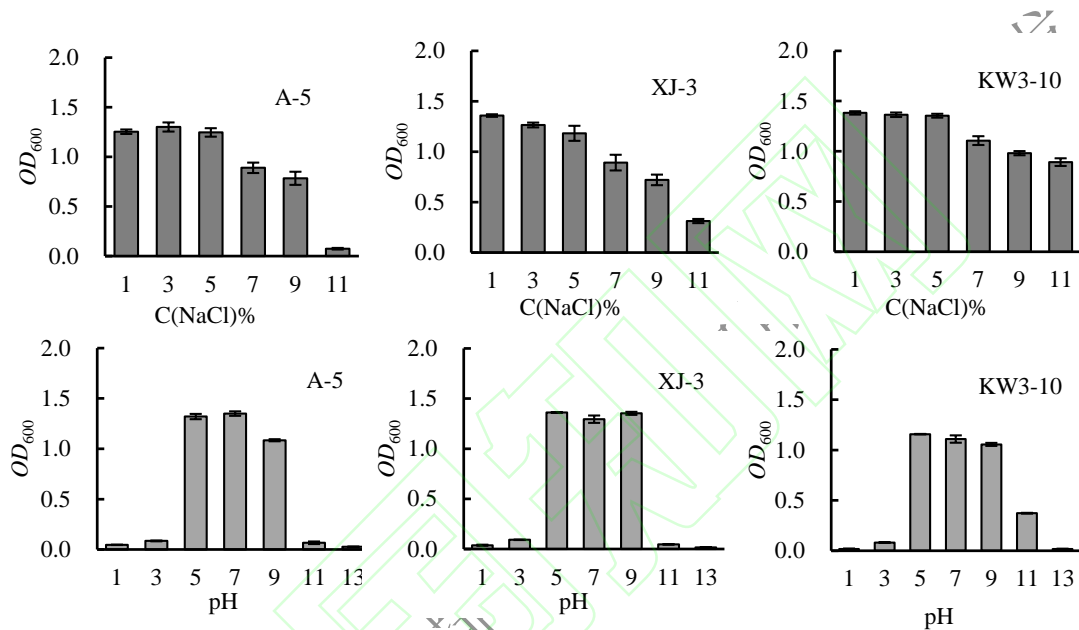


图 5 菌株 A-5, XJ-3, KW3-10 的耐盐碱范围

Figure 5 Salt-alkali tolerance range of A-5, XJ-3, KW3-10. The presented values are the means of three determinations, with standard deviations indicated.

## 2.7 参试菌株产 IAA 能力与溶解磷能力比较

将 3 株目标菌在 King 氏液体培养基中培养 24 h，将上清液与比色液进行混合，3 株菌的混合液均呈显粉红色，对照标准曲线  $Y=8.8218X$ ， $R^2=0.9918$  计算，菌株 IAA 的产量（图 6A）分别为 2.68、8.09、25.58 mg/L。

在 KPO 培养基上培养发现，A-5 菌落周围形成明显的透明圈，表明其具有较好的溶磷能力（图 6B）；KW3-10 菌落周围虽没有形成透明圈，但其生长繁殖明显好于 XJ-3。

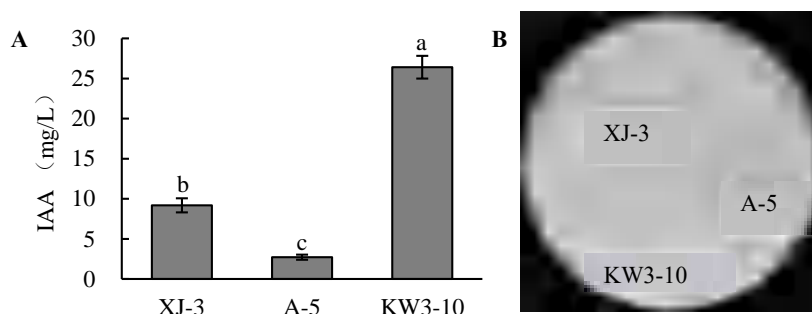


图 6 菌株 A-5, XJ-3, KW3-10 代谢产物中生长素测定与溶解磷能力

Figure 6 Determination of auxin in metabolites of strains A-5, XJ-3, KW3-10 and their ability to phosphate solubilizing. A: Auxin assay in strain A-5, XJ-3, KW3-10 metabolites; B: Phosphate solubilizing ability of strains. The presented values are the means of three determinations, with standard deviations indicated; Means with different letters are significantly different at  $P < 0.05$ .

## 2.8 菌株促生长效果测定

菌体浇施马铃薯幼苗, 培养 60 d 后统计 SPAD、株高、茎粗, 数据汇总如图 7 所示。3 株菌处理的植株长势均优于对照, 其中, A-5 处理后的 SPAD 值、株高、茎径较对照分别增加了 23.42%, 21.35% 和 20.73%, 差异均达到极显著水平; XJ-3 的株高与茎径较对照分别增加了 28.83%、36.96%, 差异达到显著水平, SPAD 值增加 17.00%, 但差异不显著; KW3-10 处理的 SPAD 值、株高与茎径分别较对照增加了 29.15%、34.81% 和 56.54%, 差异均达到显著水平。可见, 3 株菌均对植株具有良好的促生长效果 (图 7A-D)。

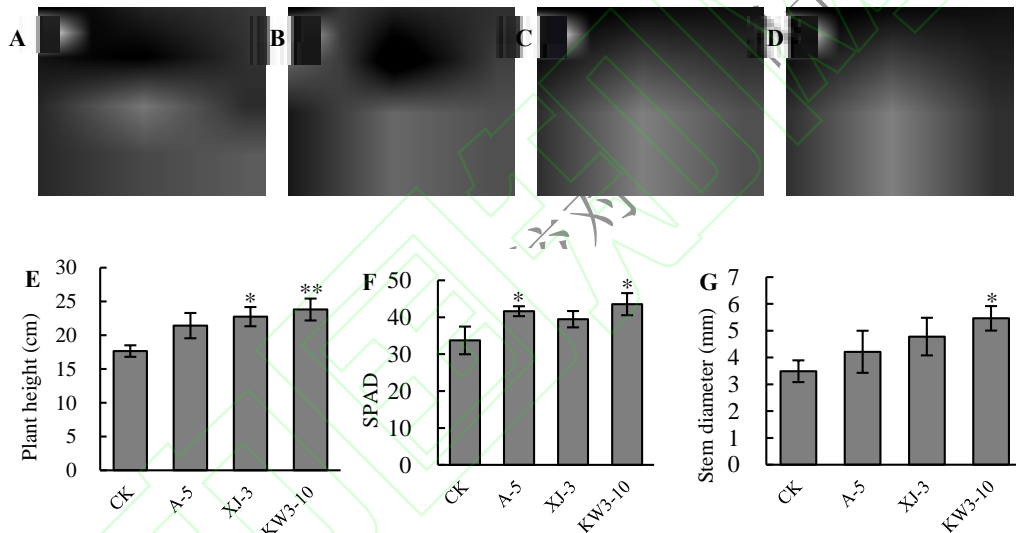


图 7 菌株 A-5, XJ-3, KW3-10 促生能力分析

Figure 7 Analysis of growth-promoting ability of strains. A: water treatment; B-D: The order of pouring A-5, XJ-3 and KW3-10 bacterial liquid; E: Plant height after 60 d; F: SPAD after 60 d; G: Stem diameter after 60 d. The presented values are the means of three determinations, with standard deviations indicated; \*:  $P < 0.05$ , \*\*:  $P < 0.01$ .

## 2.9 菌株广谱抗性分析

为了进一步挖掘被试菌株的广谱生防功能, 通过平板对峙试验测试了其对于 4 种植物病原菌的拮抗效果。结果如图 8 所示, A-5, XJ-3, KW3-10 的 72 h 培养液对疮痂链霉菌(*S. scabies*)的抑菌圈直径分别约为 20、49、56 mm; A-5 对尖孢镰刀菌(*Fusarium oxysporum*)、茄链格孢菌(*Alternaria solani*)和立枯丝核菌(*Rhizoctonia solani*)均具有的抑菌率分别约为 50.97%、25.66%、2.44%, XJ-3 的抑菌率分别约为 37.65%、46.9%、63.41%, KW3-10 的抑菌率分别为 48.05%、64.91%、60.98%, 推测 3 株芽孢杆菌均具有较好的广谱抗性。

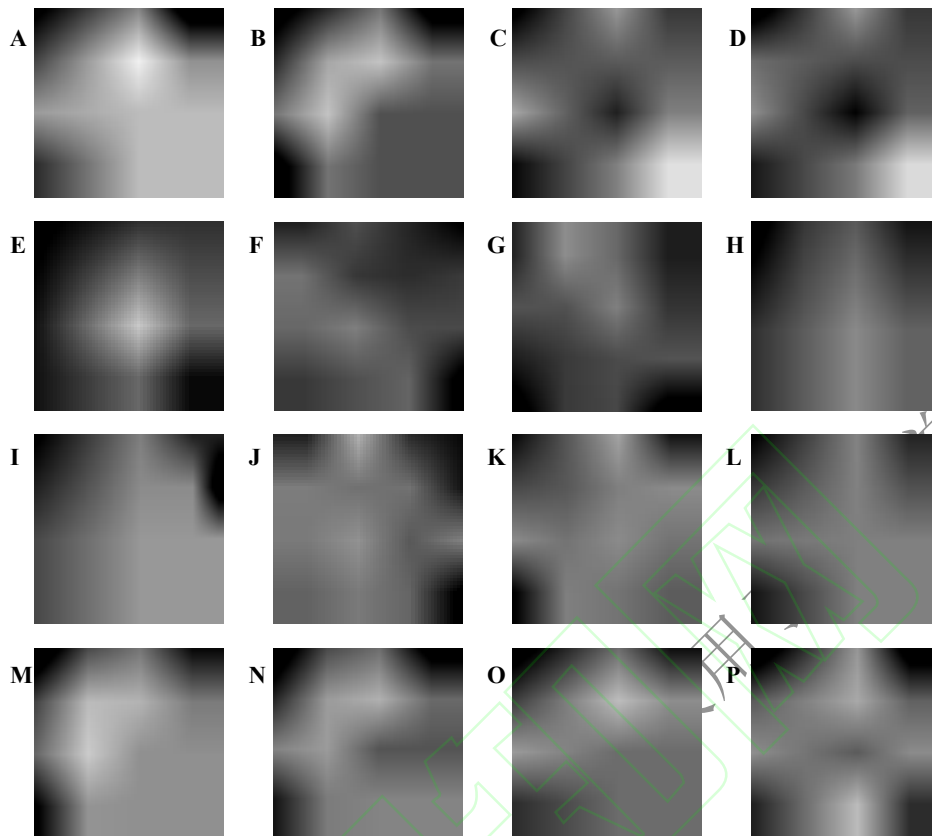


图 8 菌株 A-5, XJ-3, KW3-10 的广谱抗性

Figure 8 Broad-spectrum resistance of A-5, XJ-3, KW3-10. B, C, D: A-5, XJ-3, KW3-10 antagonize *Streptomyces scabies*; F, G, H: A-5, XJ-3, KW3-10 antagonize *Fusarium oxysporum*; J, K, L: A-5, XJ-3, KW3-10 antagonize *Alternaria solani*; N, O, P: A-5, XJ-3, KW3-10 antagonize *Rhizoctonia solani*.

## 2.10 盆栽防病试验

为了验证平板试验结果的准确性, 本文采用高感马铃薯疮痂病品种夏波蒂作为参试植物, 通过盆栽试验, 人为分别接种致病链霉菌 *S. scabies*、致病链霉菌 *S. scabies*+产胞外多糖细菌, 结果如表 2 和图 9 所示, 水处理组 (CK1) 的微型薯均未发病; 病原菌 *S. scabies* 处理组 (CK2) 发病率为 100%, 病情指数为 55.88; *S. scabies* 与 A-5 共处理组发病率为 50%, 病情指数 17.5, 相对防效达 68.68%; *S. scabies* 和 XJ-3 共处理组发病率为 55.56%, 病情指数为 20.83, 相对防效为 62.72%; *S. scabies* 和 KW3-10 共处理组发病率为 61.11%, 病情指数为 22.22, 相对防效达 60.24%。

*TxtA* 是致病性链霉菌 *S. scabies* 的主要致病基因, *TxtA* 在基质中的相对丰度反映了基质中疮痂链霉菌的数量。图 9F 所示, 菌株 A-5、XJ-3 和 KW3-10 处理组中致病菌的相对丰度显著低于 CK2, 与上述结果一致, 表明 3 个目标菌对 *S. scabies* 均有较好的抑制效果。

表 2 马铃薯疮痂病情统计

Table 2 Statistics of potato scab

Treatment	Number of grains	Sickness					Occurrence rate	Disease index	Relative control effects
		0	1	2	3	4			
CK1	16	16	0	0	0	0	0	0	-
CK2	17	0	6	4	4	3	100%	55.88	-
A-5	20	10	7	2	1	0	50%	17.5	68.68%
XJ-3	18	8	8	0	1	1	55.56%	20.83	62.72%
KW3-10	18	7	8	2	0	1	61.11%	22.22	60.24%

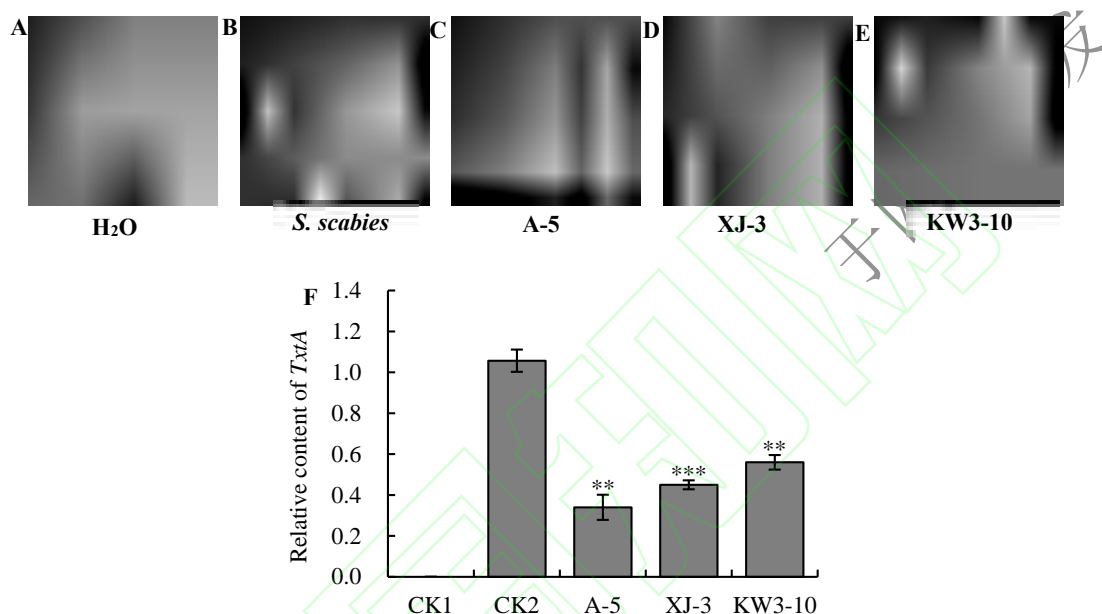


图 9 盆栽防病试验结果

Figure 9 Pot disease inhibition test results. A: Control; B: Pathogen treatment; C, D, E: Pathogen+target bacteria treatment F: Detection of pathogenic gene *TxtA*. The presented values are the means of three determinations, with standard deviations indicated; \*:  $P < 0.05$ , \*\*:  $P < 0.01$ , \*\*\*:  $P < 0.001$ .

### 3 讨论

一些产胞外多糖、生态适应性强、对环境友好的芽孢杆菌，能通过竞争、拮抗和提高植物抗病性等方式抵御病原菌的入侵，促进农作物增产，具有潜在的产业化应用可能性<sup>[19]</sup>。Vardharajula<sup>[20]</sup>等人在土壤中接种高产 EPS 的解淀粉芽孢杆菌 (*Bacillus amyloliquefaciens*) HYD-B17、地衣芽孢杆菌 (*Bacillus licheniformis*) HYTAPB18 及枯草芽孢杆菌 (*Bacillus subtilis*) RMPB44 后，土壤中小团聚体的胶结性提高，水稳定性大团聚体数量显著增多。张文平<sup>[21]</sup>等通过优化蜡样芽孢杆菌 DT-10 的发酵条件，获得较高产量的 EPS。枯草芽孢杆菌沙漠亚种 GBW HF-98 在盐碱胁迫下，可以通过产胞外多糖改善土壤团粒结构，调整土壤的盐碱性，从而促进番茄生长<sup>[22]</sup>。

近年来，随着化肥农药的大量施用和养分的不平衡富集，土壤生态环境持续恶化，农作物土传病害加剧危害，尤其由致病性链霉菌(*Streptomyces scabies*)引起的块根块茎类作物

的疮痂病在世界范围普遍发生，危害程度逐年加重<sup>[23-26]</sup>。我国马铃薯疮痂病年发病面积超过 40 万  $\text{hm}^2$ ，平均病株率约 30%，导致块茎商品性和耐储性大幅下降，病原菌土传和种传，难以防控，已严重威胁到产业的可持续发展<sup>[27]</sup>。微生物制剂具有对环境友好、促进作物生长、广谱抗病等多种功能，越来越受到人们的重视，可能是未来实现马铃薯疮痂病等主要土传病害有效防控的重要途径。虽然有一些学者分离鉴定了疮痂链霉菌的拮抗菌，并在盆栽或田间试验中取得了一定的防效，但真正用于生产的菌株非常有限，且防治效果并不理想。

2022 年农业部颁布的微生物肥料行业标准 GB/T 41728-2022 明确规定，地衣芽孢杆菌对人畜和环境友好，可免作毒理学试验，直接添加在肥料中应用于农业生产。本研究从严重板结的土壤样品中分离获得的地衣芽孢杆菌 A-5，培养液胞外多糖含量高达 1 439.23  $\text{mg/L}$ ，在土壤中定殖力强，处理后土壤多糖为 4.73  $\text{mg/g}$ ，粒径  $>0.25 \text{ mm}$  的团聚体数量比对照提高 4.07 倍，不仅具有很好的耐盐碱特性和调节土壤 pH 的作用，还具有较好的广谱抗病功能，尤其对马铃薯疮痂病的盆栽防效达到 68.68%，可作为土壤改良型抑病功能菌剂的候选菌株，具有较好的应用前景。值得一提的是 A-5 虽然在平板对峙试验中抑菌圈直径最小（20 mm），但其解磷和产 EPS 能力显著优于其他 2 株菌，盆栽试验对疮痂链霉菌的抑制效果最佳，相对防效达 68.68%，我们推测菌株对疮痂病抑制效果可能与其解磷或产胞外多糖性能相关，其相关性和作用机理有待进一步研究和验证。

## 参考文献

- [1] AZIZI A, GILANDEH YA, MESRI-GUNDOSHMIAN T, SALEH-BIGDELI AA, MOGHADDAM HA. Classification of soil aggregates: a novel approach based on deep learning[J]. Soil and Tillage Research, 2020, 199: 104586.
- [2] 刘艳, 马茂华, 吴胜军, 冉义国, 王小晓, 黄平. 干湿交替下土壤团聚体稳定性研究进展与展望[J]. 土壤, 2018, 50(5):853-865.
- [2] LIU Y, MA MH, WU SJ, RAN YG, WANG XX, HUANG P. Soil aggregates as affected by wetting-drying cycle: a review[J]. Soils, 2018, 50(5):853-865 (in Chinese).
- [3] CHANTIGNY MH, ANGERS DA, PRÉVOST D, VÉZINA LP, CHALIFOUR FP. Soil aggregation and fungal and bacterial biomass under annual and perennial cropping systems[J]. Soil Science Society of America Journal, 1997, 61(1): 262-267.
- [4] CHENU C, ROBERSON EB. Diffusion of glucose in microbial extracellular polysaccharide as affected by water potential[J]. Soil Biology and Biochemistry, 1996, 28(7): 877-884.
- [5] VADAKATTU VSR, JAMES J, GUPTA. Soil aggregation: influence on microbial biomass and implications for biological processes[J]. Soil Biology and Biochemistry, 2015, 80: A3-A9.

- [6] OADES JM. Soil organic matter and structural stability: mechanisms and implications for management[J]. *Plant and Soil*, 1984, 76(1): 319-337.
- [7] SIX J, ELLIOTT ET, PAUSTIAN K. Soil macroaggregate turnover and microaggregate formation: a mechanism for C sequestration under no-tillage agriculture[J]. *Soil Biology and Biochemistry*, 2000, 32(14): 2099-2103.
- [8] ALAMI Y, ACHOUAK W, MAROL C, HEULIN T. Rhizosphere soil aggregation and plant growth promotion of sunflowers by an exopolysaccharide-producing *Rhizobium* sp. strain isolated from sunflower roots[J]. *Applied and Environmental Microbiology*, 2000, 66(8): 3393-3398.
- [9] SANDHYA V, ALI SZ. The production of exopolysaccharide by *Pseudomonas putida* GAP-P45 under various abiotic stress conditions and its role in soil aggregation[J]. *Microbiology*, 2015, 84(4): 512-519.
- [10] 邓照亮. 海南连作香蕉抑病型和导病型土壤团聚体组成及生物学特性研究[D]. 南京农业大学, 2017.
- [10] DENG ZL. Study on composition of soil aggregates and biological characteristics of suppressive and conducive soils of continuous cropping bananas in hainan[D]. Nanjing Agricultural University, 2017 (in Chinese).
- [11] 康贻军, 沈敏, 王欢莉, 赵庆新, 殷士学. 两株植物根际促生菌对番茄青枯病的生物防治效果评价[J]. *中国生物防治学报*, 2012, 28(2): 255-261.
- [11] KANG YJ, SHEN M, WANG HL, ZHAO QX, YIN TX. Biological control of tomato bacterial wilt caused by *Ralstonia solanacearum* with *Erwinia persicinus* RA2 and *Bacillus pumilus* WP8[J]. *Chinese Journal of Biological Control*, 2012, 28(2): 255-261 (in Chinese).
- [12] JIAO YQ, CODY GD, HARDING AK, WILMES P, SCHRENK M, WHEELER KE, BANFIELD JF, THELEN MP. Characterization of extracellular polymeric substances from acidophilic microbial biofilms[J]. *Applied and Environmental Microbiology*, 2010, 76(9): 2916-2922.
- [13] UPADHYAY SK, SINGH JS, SINGH DP. Exopolysaccharide-producing plant growth-promoting rhizobacteria under salinity condition[J]. *Pedosphere*, 2011, 21(2): 214-222.
- [14] CHENG R, WANG L, LI J, FU R, WANG S, ZHANG J. *In vitro* and *in vivo* anti-inflammatory activity of a succinoglycan riclín from *Agrobacterium* sp. ZCC3656[J]. *Journal of Applied Microbiology*, 2019, 127(6): 1716-1726.
- [15] 曹晶晶, 熊惘梓, 钞亚鹏, 赵盼, 汪志琴, 仲乃琴. 极耐盐碱固氮菌的分离鉴定及固氮特性研究[J]. *微生物学报*, 2021, 61(11): 3483-3495.
- [15] CAO JJ, XIONG MZ, (CHAO/MIAO) YP, ZHAO P, WANG ZQ, ZHONG NQ. Isolation and identification of extremely salt-tolerant azotobacter and its nitrogen-fixing characteristics[J]. *Acta Microbiologica Sinica*, 2021, 61(11): 3483-3495 (in Chinese).
- [16] 李振东, 陈秀蓉, 李鹏, 满百膺. 珠芽蓼内生菌 Z5 产 IAA 和抑菌能力测定及其鉴定[J]. *草业学报*, 2010, 19(2): 61-68.
- [16] LI ZD, CHEN XR, LI P, MAN BY. Identification of *Polygonum viviparum* endophytic bacteria Z5 and



determination of the capacity to secrete IAA and antagonistic capacity towards pathogenic fungi[J]. Acta Prataculturae Sinica, 2010, 19(2): 61-68 (in Chinese).

[17] 石莹莹, 赵盼, 宋双伟, 熊桐梓, 莫乘宝, 仲乃琴. 马铃薯疮痂病拮抗菌 YN-2-2 的分离与鉴定[J]. 微生物学通报, 2020, 47(8): 2425-2435.

[17] SHI YY, ZHAO P, SONG SW, XIONG MZ, MO CB, ZHONG NQ. Isolation and characterization of the antagonistic bacterium YN-2-2 against potato common scab[J]. Microbiology China, 2020, 47(8): 2425-2435 (in Chinese).

[18] WANNER LA, KIRK WW. *Streptomyces* - from basic microbiology to role as a plant pathogen[J]. American Journal of Potato Research, 2015, 92(2): 236-242.

[19] 马佳, 李颖, 胡栋, 彭杰丽, 贾楠, 张翠绵, 王旭, 王占武. 芽胞杆菌生物防治作用机理与应用研究进展[J]. 中国生物防治学报, 2018, 34(4): 639-648.

[19] MA J, LI Y, HU D, PENG JL, JIA N, ZHANG CM, WANG X, WANG ZW. Progress on mechanism and applications of *Bacillus* as a biocontrol microbe[J]. Chinese Journal of Biological Control, 2018, 34(4): 639-648 (in Chinese).

[20] VARDHARAJULA S, ALISK Z. Exopolysaccharide production by drought tolerant bacillus spp. and effect on soil aggregation under drought stress[J]. Journal of Microbiology, Biotechnology and Food Sciences, 2014, 4(1): 51-57.

[21] 张文平, 李昆太, 黄林, 魏赛金, 程新. 产胞外多糖菌株的筛选及其对土壤团聚体的影响[J]. 江西农业大学学报, 2017, 39(4): 772-779.

[21] ZHANG WP, LI KT, HUANG L, WEI SJ, CHENG X. Screening of exopolysaccharide-producing bacteria and their effects on aggregation in soil[J]. Acta Agriculturae Universitatis Jiangxiensis (Natural Sciences Edition), 2017, 39(4): 772-779 (in Chinese).

[22] 李慧芬, 方安然, 冯海霞, 黄剑, 赵明珠, 周波. 胞外多糖产生菌的筛选鉴定及其促生改土作用[J]. 微生物学通报, 2023, 50(5): 1941-1957.

[22] LI HF, FANG AR, FENG HX, HUANG J, ZHAO MZ, ZHOU B. Screening and identification of extracellular polysaccharide-producing strain and the influence on soil quality and crop growth[J]. Microbiology China, 2023, 50(5): 1941-1957 (in Chinese).

[23] ZHAO P, LIU L, CAO JJ, WANG ZQ, ZHAO YL, ZHONG NQ. Transcriptome analysis of tryptophan-induced resistance against potato common scab[J]. International Journal of Molecular Sciences, 2022, 23(15): 8420.

[24] 陈文轩, 李茜, 王珍, 孙兆军. 中国农田土壤重金属空间分布特征及污染评价[J]. 环境科学, 2020, 41(6): 2822-2833.

[24] CHEN WX, LI Q, WANG Z, SUN ZJ. Spatial distribution characteristics and pollution evaluation of heavy metals in arable land soil of China[J]. Environmental Science, 2020, 41(6): 2822-2833 (in Chinese). [万方]

- [25] 张晓云, 丛蓉, 赵卫松, 曲远航, 苏振贺, 郭庆港, 鹿秀云, 李社增, 马平. 30 亿 CFU/g 芽胞杆菌可湿性粉剂的研制及其对马铃薯黄萎病和疮痂病的防治效果[J]. 农药学学报, 2023, 25(1):140-149.
- [25] ZHANG XY, CONG R, ZHAO WS, QU YH, SU ZH, GUO QG, LU XY, LI SZ, MA P. Development of 3 billion CFU/g *Bacillus* wettable powder and its control efficacy on potato *Verticillium* wilt and scab[J]. Chinese Journal of Pesticide Science, 2023, 25(1):140-149 (in Chinese).
- [26] 赵永龙, 赵盼, 曹晶晶, 汪志琴, 刘璐, 仲乃琴. 疮痂链霉菌拮抗菌定向筛选及其功能评价[J]. 微生物学报, 2022, 62(7): 2624-2641.
- [26] ZHAO YL, ZHAO P, CAO JJ, WANG ZQ, LIU L, ZHONG NQ. Targeted screening and functional evaluation of the bacterial antagonists to *Streptomyces* scabies[J]. Acta Microbiologica Sinica, 2022, 62(7): 2624-2641 (in Chinese).
- [27] 王敏, 吕和平, 高彦萍, 吴雁斌, 张武, 梁宏杰. 微生物菌肥在马铃薯疮痂病防治上的应用效果[J]. 甘肃农业科技, 2021, 52(10): 27-31.
- [27] WANG M, LÜ HP, GAO YP, WU YB, ZHANG W, LIANG HJ. Application effect of microbial fertilizer on potato scab control[J]. Gansu Agricultural Science and Technology, 2021, 52(10): 27-31 (in Chinese).



Article

# Transcriptome Analysis of Tryptophan-Induced Resistance against Potato Common Scab

Pan Zhao <sup>1,2,3,†,\*</sup>, Lu Liu <sup>1,2,†</sup>, Jingjing Cao <sup>1,2</sup>, Zhiqin Wang <sup>1,2</sup>, Yonglong Zhao <sup>1,2</sup> and Naiqin Zhong <sup>1,2,3,\*</sup>

<sup>1</sup> State Key Laboratory of Plant Genomics, Institute of Microbiology, Chinese Academy of Sciences, Beijing 100101, China; liulu202206@163.com (L.L.); caojingjing@im.ac.cn (J.C.); wangzq1210@163.com (Z.W.); ylzha097101@163.com (Y.Z.)

<sup>2</sup> Engineering Laboratory for Advanced Microbial Technology of Agriculture, Chinese Academy of Sciences, Beijing 100101, China

<sup>3</sup> The Enterprise Key Laboratory of Advanced Technology for Potato Fertilizer and Pesticide, Hulunbuir 021000, China

\* Correspondence: zhaop@im.ac.cn (P.Z.); nqzhong@im.ac.cn (N.Z.)

† These authors contributed equally to this work.

**Abstract:** Potato common scab (CS) is a worldwide soil-borne disease that severely reduces tuber quality and market value. We observed that foliar application of tryptophan (Trp) could induce resistance against CS. However, the mechanism of Trp as an inducer to trigger host immune responses is still unclear. To facilitate dissecting the molecular mechanisms, the transcriptome of foliar application of Trp and water (control, C) was compared under *Streptomyces scabies* (S) inoculation and uninoculation. Results showed that 4867 differentially expressed genes (DEGs) were identified under *S. scabies* uninoculation (C-vs-Trp) and 2069 DEGs were identified under *S. scabies* inoculation (S-vs-S+Trp). Gene ontology (GO) and Kyoto Encyclopedia of Genes and Genomes (KEGG) enrichment analyses indicated that Trp induced resistance related to the metabolic process, response to stimulus, and biological regulation. As phytohormone metabolic pathways related to inducing resistance, the expression patterns of candidate genes involved in salicylic acid (SA) and jasmonic acid/ethylene (JA/ET) pathways were analyzed using qRT-PCR. Their expression patterns showed that the systemic acquired resistance (SAR) and induced systemic resistance (ISR) pathways could be co-induced by Trp under *S. scabies* uninoculation. However, the SAR pathway was induced by Trp under *S. scabies* inoculation. This study will provide insights into Trp-induced resistance mechanisms of potato for controlling CS, and extend the application methods of Trp as a plant resistance inducer in a way that is cheap, safe, and environmentally friendly.

**Keywords:** *Solanum tuberosum*; common scab; transcriptome analysis; tryptophan; induced resistance

**Citation:** Zhao, P.; Liu, L.; Cao, J.; Wang, Z.; Zhao, Y.; Zhong, N. Transcriptome Analysis of Tryptophan-Induced Resistance against Potato Common Scab. *Int. J. Mol. Sci.* **2022**, *23*, 8420. <https://doi.org/10.3390/ijms23158420>

Academic Editor: Zsófia Bánfalvi

Received: 9 June 2022

Accepted: 26 July 2022

Published: 29 July 2022

**Publisher's Note:** MDPI stays neutral with regard to jurisdictional claims in published maps and institutional affiliations.



**Copyright:** © 2022 by the authors. Licensee MDPI, Basel, Switzerland. This article is an open access article distributed under the terms and conditions of the Creative Commons Attribution (CC BY) license (<https://creativecommons.org/licenses/by/4.0/>).

## 1. Introduction

The potato (*Solanum tuberosum*) is the fourth most important food crop in China after rice, wheat, and maize. In 2017, the potato-cultivated area was over 5.67 million hectares, and its production exceeded 99.15 million metric tons [1]. However, numerous diseases threaten the growth of potato, especially common scab (CS) disease [2]. CS in potato tubers results in skin lesions, leading to the production of unmarketable potatoes for fresh consumption, seeds and others [3–5]. In recent years, CS has caused a substantial economic loss worldwide and has become one of the most severe concerns for potato farmers [6–8].

CS is caused by the soil-borne Gram-positive, filamentous bacteria genus *Streptomyces* [9]. At least 12 species in *Streptomyces* have been reported to be able to produce scab symptoms [9–11], among which *S. scabies* is the first and best-characterized species

[9,12,13]. Thaxtomins are plant phytotoxins secreted by *Streptomyces* and are supposed to induce CS skin lesion symptoms [3,9,14]. As the predominant form of thaxtomins produced by *S. scabies*, thaxtomin A inhibits plant cellulose biosynthesis, especially cellobiose and celotriose biosynthesis [15–17]. The secretion of thaxtomin A in potato tubers alters plant physiologies, such as  $\text{Ca}^{2+}$ ,  $\text{H}^+$  inflowing, and polysaccharide deposition, resulting in tissue necrosis and reduced potato quality [10,18]. Genetic evidence has shown that eliminating critical genes of thaxtomin A synthesis, including *txtA*, *txtB* and *txtC*, negatively affects the pathogenicity of *S. scabies*. It is well-known that *txtA* and *txtB* encode two nonribosomal peptide synthetases, and *txtC* encodes cytochrome P450-type monooxygenase in thaxtomin A biosynthesis.[9,19–21].

Although the causal agent of CS is well-diagnosed, it is still challenging to control CS effectively. The applications of individual strategies, such as crop rotation, chemical fumigation, or fungicides, have all proven insufficient [10,22]. Meanwhile, chemical methods are expensive and environmentally unfriendly. Therefore, new nontoxic and cheap strategies need to be searched for. Plant immunity inducers, which are green biological agents able to control diseases, have attracted much attention around the world. Immunity inducers are a class of immune-active compounds that can induce resistance in plants and promote healthy plant growth. Induced resistance in plants is triggered by biological or chemical inducers that protects the plant's nonexposed parts against future attack by pathogenic microbes [23–25]. This resistance can be divided into induced systemic resistance (ISR), and systemic acquired resistance (SAR), induced by nonpathogenic microbes and pathogenic microbes, or based on the nature of the elicitor and the regulatory pathways involved [25]. SAR is dependent on the accumulation of phytohormone salicylic acid (SA) and pathogenesis-related (PR) proteins [26–29]. However, ISR is dependent of the phytohormone jasmonic acid/ethylene (JA/ET) [30,31]. Induced resistance is expressed not only locally at the site but also systemically in other parts of the plant that are separated from the inducer, enhancing the level of protection against a broad spectrum of attackers [32].

Plant-induced resistance provides a new strategy for controlling potato scab disease. In practice, foliar sprays of auxins and related molecules have been used for controlling CS [33–35]. Some chemicals act as elicitors or inducers that can trigger host immune responses [23,24]. For example, 2,4-dichlorophenoxyacetic acid (2,4-D), indole-3-acetic acid (IAA) [36], benzothiadiazole (BTH),  $\beta$ -aminobutyric acid (BABA), and acetylsalicylic acid (ASA) [33–35,37–41] have been used to suppress the development of CS. It has been reported that tryptophan (Trp), a precursor of auxin and secondary metabolites, could protect plants against some fungal, bacterial, and insect attacks [42–46]. Here, we found that the application of Trp could induce potato resistance to control CS. Considering that Trp is a relatively cheap chemical, this observation expanded the range of inducers that could be used to protect potato in the field. There are few reports stating that Trp application as an inducer can enhance the resistance of potato to CS. Thus, it is valuable to investigate the mechanisms of Trp-induced resistance against potato CS.

Transcriptome analysis is an important method for studying the expression of a large number of genes in a given tissue [47]. RNA transcript profiling can rapidly and effectively provide information for genome-wide transcript characterization, differential gene expression analysis, variant detection, and gene-specific expression. This technology is used to analyze the transcriptome in response to different biotic or abiotic stresses, including low-nitrogen stress [48], high-light stress [49], drought response to different soybean cultivars [50], salt stress [51,52], Cd stress [53], and sweet orange response to *Citrus tristeza virus* [54].

In this study, we analyzed transcriptome datasets from the leaves of potato plantlets. Leaves sprayed with Trp or water were examined from two groups (C-vs-Trp and S-vs-S+Trp) of potato plants. The differentially expressed genes (DEGs) of the two groups were identified to deepen the understanding of Trp-induced resistance to potato CS. These data

will be critical to identifying defense-related genes that are regulated by exogenous Trp and to prompting our understanding of potato–*S. scabies* interactions.

## 2. Results

### 2.1. Foliar Treatment of Trp Enhances Potato Resistance against CS

Although Trp has been reported to protect plants against some fungi and bacteria, foliar application of Trp to defend against the soil disease CS has not been reported. It was hypothesized that Trp may act as an inducer to enhance resistance to CS in potato. Therefore, a field trial was designed to test the effectiveness of Trp. The results of disease incidence and yield indicated that 100 mg/L Trp was the best concentration (Figure S1).

Thus, 100 mg/L Trp was sprayed on potato plants in pots during tuber initiation. At this time, tubers are easily infected by the bacteria. The potato tubers were harvested from pots and assessed for CS. Tubers > 2 g were washed under running water and scored for disease incidence, disease index, total tuber mass and control efficacy. Tubers inoculated with *S. scabies* (S) showed strong susceptibility to disease compared to the control (C), showing that the inoculation was very successful. As shown in Figure 1, the scabs on the surface of the tubers treated with *S. scabies* and Trp (S + Trp) were reduced compared to tubers treated with only *S. scabies*. Then, we scored the total tuber mass, disease incidence, disease index and control efficacy. As shown in Table 1, the tuber mass of Trp was the best. After inoculation with *S. scabies*, foliar application of Trp decreased the disease incidence and disease index. Compared with S, the disease incidence of S + Trp was decreased from 90% to 59.09% and the disease index of S + Trp tubers was decreased from 53 to 27.27. The control efficacy of S + Trp compared with S was 48.54%. These results suggest that foliar treatment with Trp could enhance potato resistance against CS.



**Figure 1.** Disease symptoms of potatoes in pots. C: *S. scabies*-uninoculated plants treated with water; Trp: *S. scabies*-uninoculated plants treated with Trp; S: *S. scabies*-inoculated plants treated with water; S + Trp: *S. scabies*-inoculated plants treated with Trp.

**Table 1.** Disease index and incidence assessment following foliar application of Trp on CS.

Treatment	Total Tuber Mass (g)	Disease Incidence (%)	Disease Index	Control Efficacy (%)
C	323.40 ± 7.82	0	0	–
Trp	370.51 ± 1.70	0	0	–
S	271.13 ± 5.85	90.00 ± 7.08	53.00 ± 6.95	–
S + Trp	342.67 ± 10.89	59.09 ± 2.53 **	27.27 ± 1.18 **	48.54 ± 8.27

The asterisks denote statistically significant differences, as determined by Student's *t*-test, \*\*  $p < 0.01$ . Three biological repetitions were performed.

### 2.2. Analyses of the Transcriptome Datasets

The quality of the total RNA was assessed using the Agilent Bioanalyser 2100 (Agilent Technologies, Santa Clara, CA, USA) prior to subsequent experiments. A total of 12 RNA libraries were sequenced in depth, ranging from 102.19 to 105.84 million raw reads (Table S1). After filtering (removal of low-quality, joint contamination, and excessive unknown bases), 122.11 GB of data (fq.gz) was generated in total. More than 97.78% and 89.49% of the clean reads reached the Q20 and Q30 levels, respectively. More than 78.64%

of the clean reads were mapped to the reference genome, including more than 58.61% unique reads (Table S2). The assessment of the filtered data indicated that the filtered sequences were high-quality.

The transcriptional levels were normalized using the fragments per kilobase per million reads (FPKM) method. Based on the criteria ( $|\text{fold change, FC}| \geq 2$  and  $Q\text{-value} \leq 0.001$ ), DEGs were defined. The number of DEGs was depicted as volcano plots (Figure 2a,b). Under *S. scabiei* uninoculation (C-vs-Trp), compared with C plants, 3158 DEGs were upregulated and 1709 were downregulated (Figure 2a). Under *S. scabiei* inoculation (S-vs-S+Trp), compared with the S-treated plants, we found that 1297 DEGs were upregulated and 772 were downregulated (Figure 2b). The C-vs-Trp group had more DEGs than the S-vs-S+Trp group. A Venn diagram analysis showed the unique and shared DEGs in the two groups (Figure 2c). In total, 810 DEGs were common between the two groups (Table S3). Among these 810 DEGs, 592 DEGs showed the same trends in gene expression, including 387 DEGs being upregulated and 205 downregulated, and the remaining 218 DEGs had different expression trends between the two groups. These DEGs were involved in the starch and sucrose metabolism pathway, metabolic pathway, and plant hormone signal transduction pathway. There were 486 upregulated DEGs and 324 downregulated DEGs in the C-vs-Trp group. These genes were mainly categorized as catalytic activity and metabolic process, and were mainly involved in metabolic pathways, biosynthesis of secondary metabolites pathways and plant hormone signal biosynthesis. There were 506 upregulated and 304 downregulated DEGs in the S-vs-S+Trp group. Most of the genes were categorized as catalytic activity, metabolic process, transporter activity, and so on. The pathways or biological processes included biological regulation, binding, RNA transport, and cutin biosynthesis. Furthermore, 4057 DEGs, including 2627 upregulated DEGs and 1385 downregulated DEGs, were specific to the C-vs-Trp group (Table S3). These DEGs were involved in plant hormone signal transduction, plant-pathogen interaction, glycan degradation, and wax biosynthesis. 1259 DEGs, including 807 upregulated DEGs and 452 downregulated DEGs, were specific to the S-vs-S+Trp group (Table S3). These DEGs were involved in the mRNA surveillance pathway, base excision repair, and non-homologous end-joining pathway. These results showed that more DEGs were upregulated when treated with Trp without pathogens.

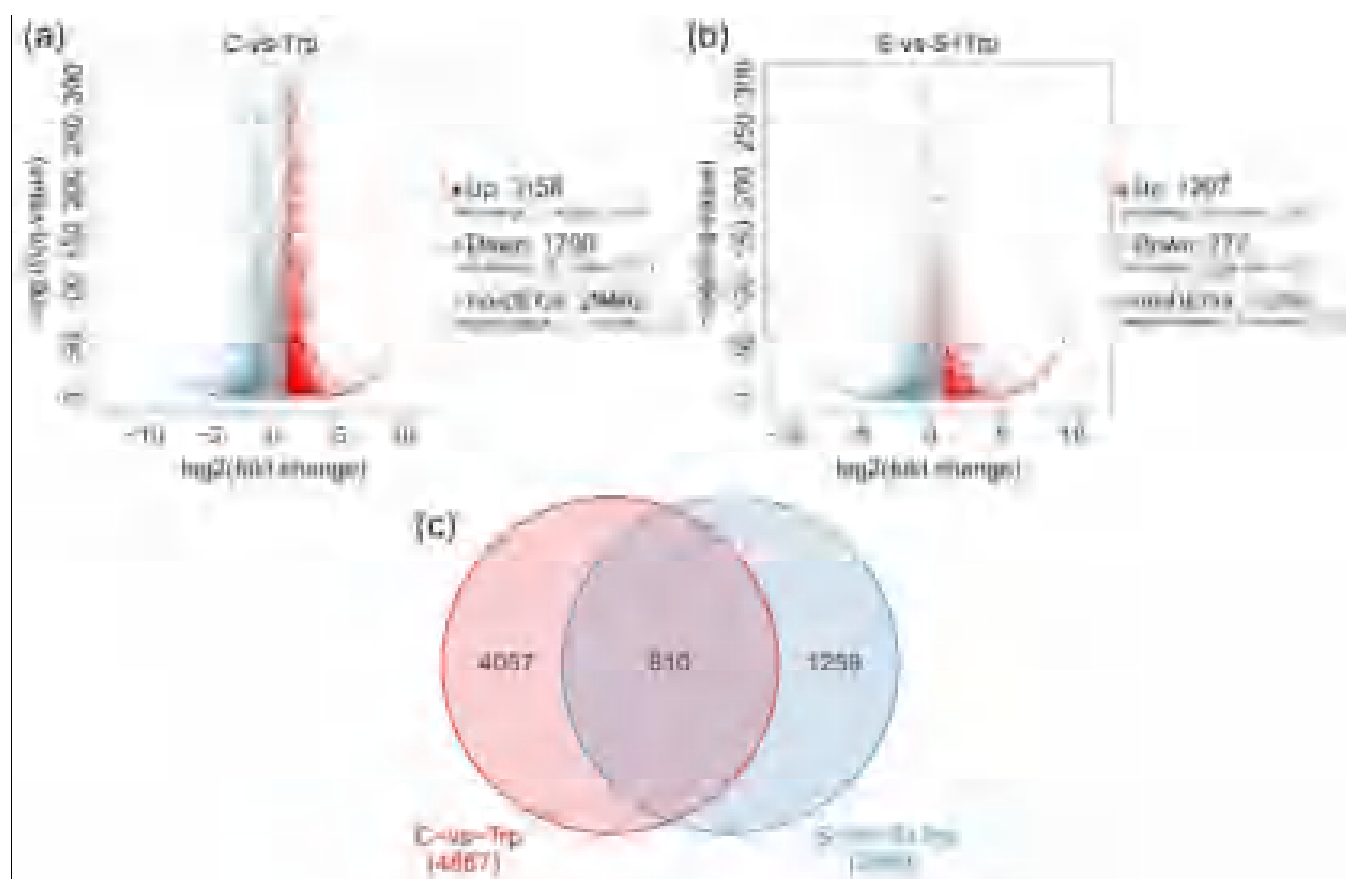


**Figure 2.** Volcano plot (a,b) and Venn diagram (c) of DEGs in the C-vs-Trp group and S-vs-S+Trp group.

### 2.3. GO and KEGG Enrichment Analyses of DEGs

Gene Ontology (GO) enrichment analysis was applied to categorize the DEGs (Figure 3). In the two groups, DEGs were classified into three GO categories: biological process (BP), cellular component (CC), and molecular function (MF). In the C-vs-Trp group, the BP category was mainly enriched in cellular process (721 DEGs), metabolic process (679 DEGs), response to stimulus (318 DEGs), biological regulation (274 DEGs), and regulation of biological process (242 DEGs); in the CC category, DEGs were mainly enriched in membrane (979 DEGs), membrane part (930 DEGs), cell (710 DEGs), cell part (679 DEGs) and organelle (509 DEGs); in the MF category, the top five items were catalytic activity (1435 DEGs), binding (1358 DEGs), transporter activity (177 DEGs), transcription regulator activity (110 DEGs) and molecular function regulator (84 DEGs). In the S-vs-S+Trp group, the DEGs enriched were similar to those in the C-vs-Trp group. In the BP category, the top five items were cellular process (368 DEGs), metabolic process (348 DEGs), biological regulation (100 DEGs), response to stimulus (100 DEGs), and regulation of biological process (94 DEGs); in the CC category, the top five items were membrane (342 DEGs), membrane part (330 DEGs), cell (315 DEGs), cell part (306 DEGs) and organelle (245 DEGs); in the MF category, the top five items were binding (568 DEGs), catalytic activity (559 DEGs), transporter activity (75 DEGs), transcription regulator activity (37 DEGs) and molecular function regulator (37 DEGs). The results showed the same categorization of BP and MF in the two groups. It was also clearly visible that more genes were upregulated than downregulated for each group (Figure S2). There was a slight difference between the two groups. For example, in the “response to stimulus” process, there were more upregulated genes than downregulated ones in C-vs-Trp group. However, there were more downregulated genes than upregulated ones in S-vs-S+Trp group. The genes related hormones,

stimulus, transcription regulator activity, and metabolic process should be given more attention in further research.

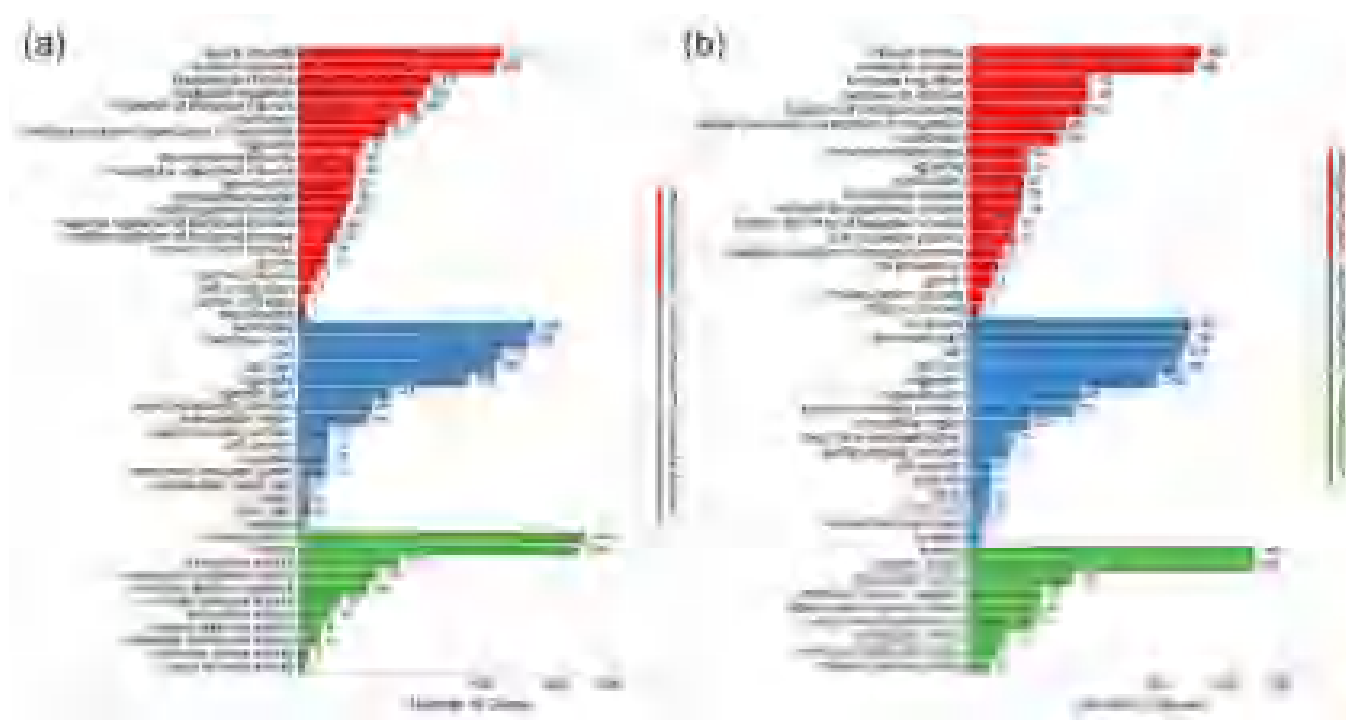


**Figure 3.** Gene Ontology (GO) enrichment analysis of DEGs in the C-vs-Trp (a) and S-vs-S+Trp (b) groups.

Kyoto Encyclopedia of Genes and Genomes (KEGG) enrichment analysis was performed to further understand the DEGs. In the diagrams, the significant results were based on the Rich factor (RF) and Q-value (the smaller the Q-value is, the more significant the results; the larger RF is, the more significant the results). In the C-vs-Trp group, the major pathways were plant hormone signal transduction (268 DEGs, 0.21 RF), sesquiterpenoid and triterpenoid biosynthesis (55 DEGs, 0.28 RF), other glycan degradation (50 DEGs, 0.27 RF) and cutin, suberine and wax biosynthesis (38 DEGs, 0.25 RF); in the S-vs-S+Trp group, the major pathways were sesquiterpenoid and triterpenoid biosynthesis (17 DEGs, 0.09 RF), mRNA surveillance pathway (34 DEGs, 0.07 RF), fatty acid metabolism (19 DEGs, 0.08 RF) and RNA degradation (39 DEGs, 0.07 RF) (Figure 4).

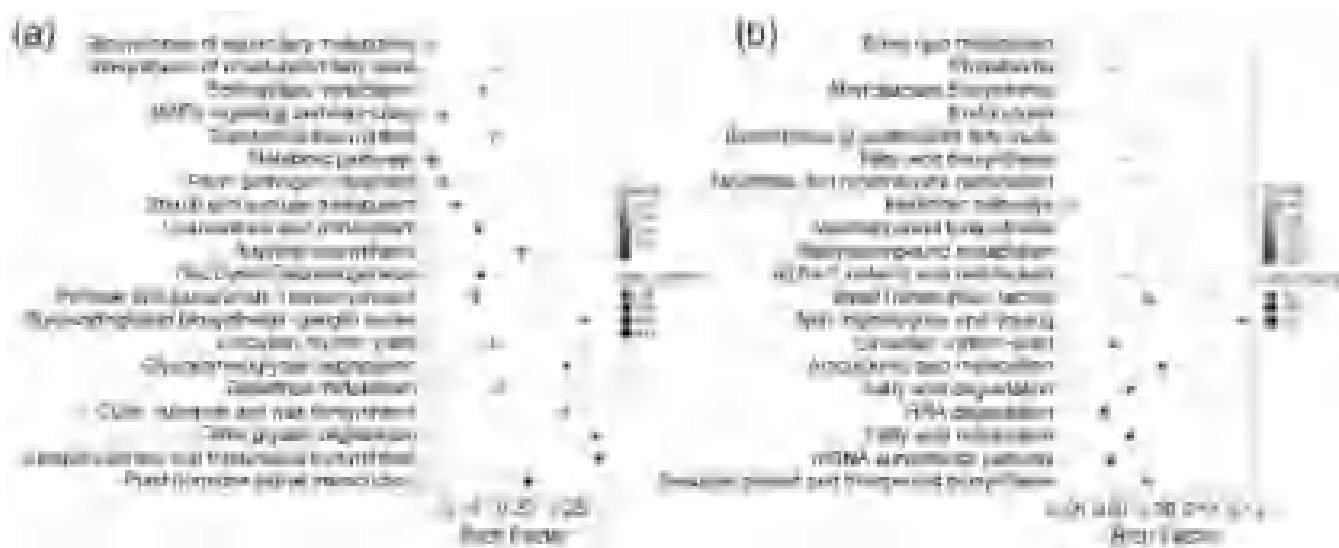


**Figure 4.** Kyoto Encyclopedia of Genes and Genomes (KEGG) pathway enrichment analysis of DEGs in the C-vs-Trp group (a) and S-vs-S+Trp (b) group. The X-axis represents the enrichment factor, and the Y-axis represents the pathway name. The depth of color represents the Q-value, and the size of the dot represents the number of DEGs.

2.4. Validation of RNA-seq Data by qRT-PCR

To validate the transcriptome sequencing results, qRT-PCR was performed to assess the expression levels of genes. A total of 18 genes were selected, of which 7 were differentially expressed in the two groups, 3 were only differentially expressed in the S-vs-S+Trp group, 6 were only differentially expressed in the C-vs-Trp group, and 2 were not DEGs in both groups. As shown in Figure 5, the qRT-PCR results were consistent with the transcriptome sequencing results. The results indicated that the obtained RNA-seq data are reliable.

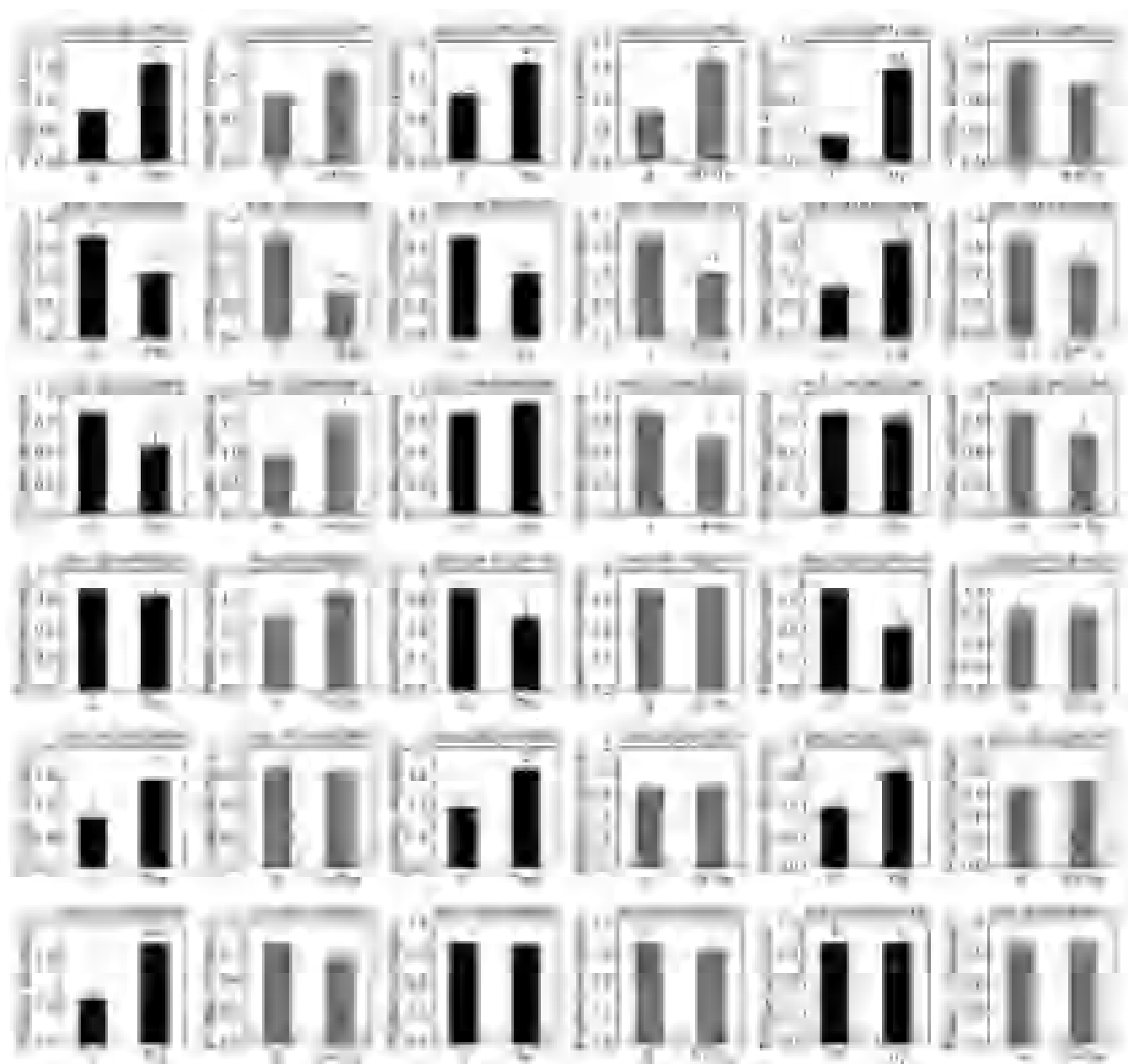


**Figure 5.** qRT-PCR validation of 18 DEGs. The asterisks denote statistically significant differences, as determined by Student's *t*-test, \*  $p < 0.05$ , \*\*  $p < 0.01$ . Three biological repetitions were performed.

### 2.5. Candidate Trp-Induced DEGs in Phytohormone Pathways

The genes in the phytohormone pathways were correlated with induced resistance. Based on functional annotation and pathway analysis, several candidate DEGs related to phytohormone pathways were found to be notable in both groups. These were SA-, JA- and ET-related genes, such as SA biosynthesis-related genes *ICS* (*isochorismate synthase*), *PAL* (*phenylalanine ammonia-lyase*), SA-responsive genes *PR1* (*pathogenesis-related protein 1*) and *NPR1* (*nonexpressor of pathogenesis related genes 1*), *NPR1* transcription factor gene *WRKY*, SA glucosylation genes *SAGT* (*salicylic acid glucosyltransferase*), JA biosynthesis-related genes *LOX* (*lipoxygenase*) and *OPR* (*12-oxophytodienoate reductase*), and ET biosynthesis-related genes *ACO* (*1-aminocyclopropane-1-carboxylate oxidase*) and *ACS* (*1-aminocyclopropane-1-carboxylate synthase*).

In the C-vs-Trp group, the expression of SA biosynthesis-related genes *ICS* and *PAL* was significantly induced by Trp. All the *SAGT* genes were downregulated. Furthermore, three *NPR1* genes, one *PR1* gene and six *WRKY* genes were upregulated. Foliar treatment



of Trp also induced the expression of JA biosynthesis-related genes. Seven *LOX* genes and two *OPR* genes were upregulated. The same results were seen in the ET-related genes. The expression of four *ACO* genes and seven *ACS* genes was induced (Table S4). Moreover, we selected some candidate genes with high FC values from the group and detected their relative expression levels by qRT-PCR (Figure 6a).

In the S-vs-S+Trp group, there were similar results in the expression of the SA biosynthesis-related genes. Two *ICS* genes and one *PAL* gene were upregulated. Three of the *SAGT* genes were downregulated. One *NPR1* gene, three *PR1* genes and two *WRKY* genes were upregulated. However, in the JA/ET biosynthesis-related genes, Trp downregulated genes expression. Four *LOX* genes were downregulated. The same results were seen in the ET pathway-related genes. The four *ACO* genes and one *ACS* gene were all downregulated (Table S4). Some genes with high FC values were selected to verify the differences in expression using qRT-PCR (Figure 6b).

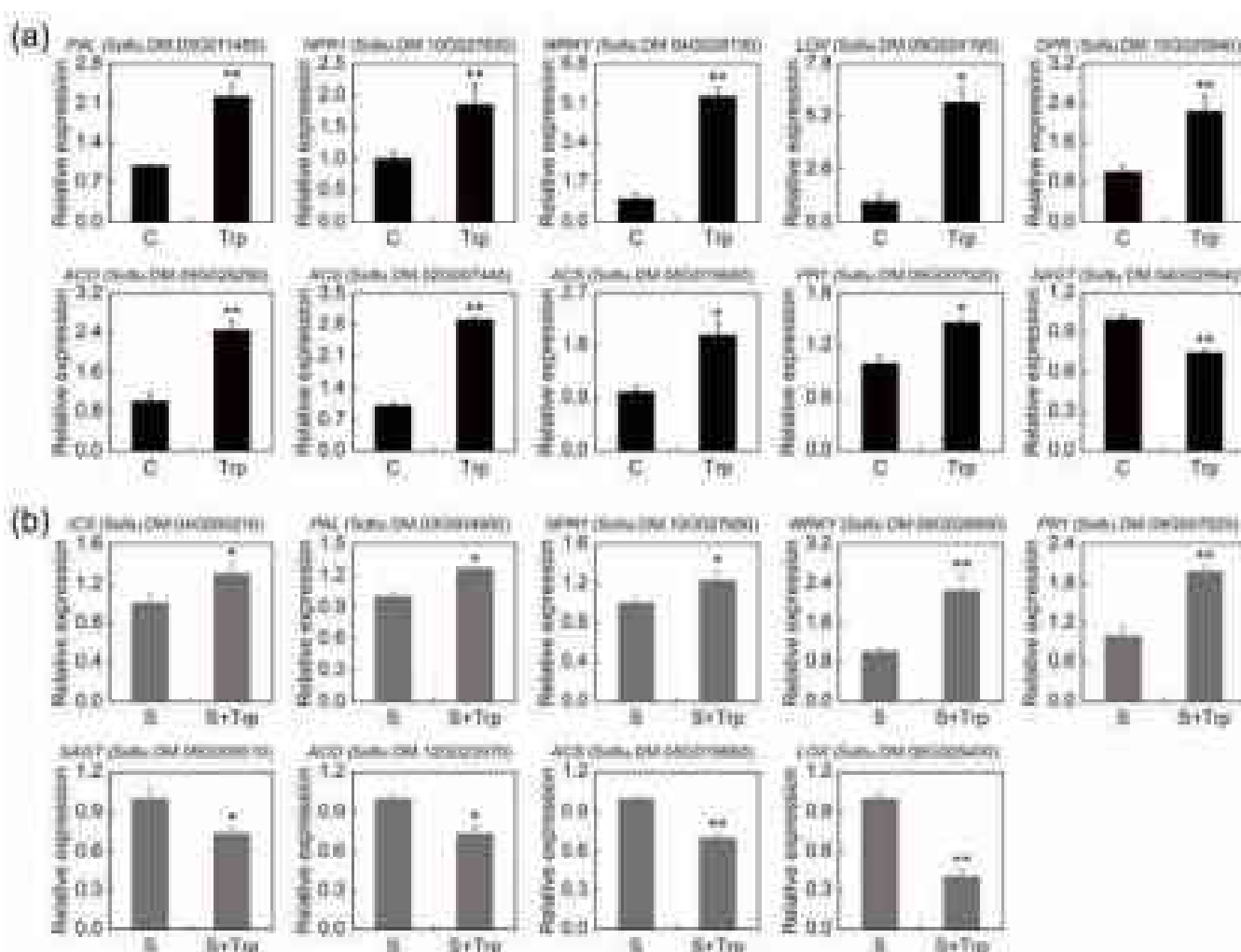


**Figure 6.** The relative expression of some candidate genes belonging to the C-vs-Trp group (a) and S-vs-S+Trp group (b) was detected by qRT-PCR. The asterisks denote statistically significant differences, as determined by Student's *t*-test, \*  $p < 0.05$ , \*\*  $p < 0.01$ . Three biological repetitions were performed.

### 3. Discussion

As a globally serious potato disease, CS is difficult to control via single management. Chemical methods are frequently used but expensive and environmentally unfriendly. The overuse or inappropriate use of chemical agents results in serious problems, espe-

cially environmental pollution and food safety, in agriculture [55,56]. Techniques to induce plant resistance represent a new and rapidly developing field of research and development [56]. To reduce the usage of chemical agents, we need to search for nontoxic and effective methods. Previous studies have reported that Trp could protect plants against some fungal, bacterial, and insect attacks [42–46]. In particular, Trp-derived secondary metabolites play important roles in defense responses, such as producing serotonin [57] and increasing the accumulation of camalexin, indole-carboxylic acid (ICA), and IAA [58,59]. Exogenous Trp can strongly inhibit the production of thaxtomin A by pathogenic *S. scabiei* in a liquid thaxtomin-inducing growth medium [60,61]. Thus, the foliar application of Trp induces a broad-spectrum resistance exhibiting a great potential to avoid plant diseases.

We found that foliar treatment with Trp enhances potato resistance to CS and can increase its yield (Figures 1 and S1). There are no reports that foliar application of Trp can control potato CS. Thus, it is of value to investigate the mechanisms of Trp-induced resistance against CS. We used transcriptome sequencing technology to analyze the mechanisms of the induced resistance of potato by foliar application of Trp against CS. A total of 4867 and 2069 DEGs were identified in the C-vs-Trp and S-vs-S+Trp groups, respectively. Based on GO and KEGG analyses, DEGs induced by Trp were found to be involved in the metabolic process, response to stimulus and biological regulation (Figures 3 and 4).

In view of the phytohormone pathways related to induced resistance, we analyzed key genes in hormone signaling pathways, such as SA, JA and ET. Induced resistance is an important mechanism by which plants enhance their defense ability via inducers in response to a broad range of pathogen attacks [30]. At present, the two forms of induced resistance, SAR and ISR, have been used in conventional agriculture against pathogens [62]. Via comparative transcriptome analysis, we found that SAR and ISR can be co-induced by Trp without pathogen treatment. Under *S. scabiei* treatment, SAR is the pathway induced by Trp treatment.

SAR is required for the accumulation of PR proteins (and transcripts) and SA [26–29]. In this study, we analyzed the hormones of SA-related DEGs. In the C-vs-Trp and S-vs-S+Trp groups, the expression of SA-related genes was induced by Trp. *ICS* and *PAL* expression was upregulated, suggesting that SA biosynthesis may be increased. The *SAGT* genes were also downregulated. *SAGT* enzymes convert most of the produced SA to SAG, which is stored in the vacuole. Knockout mutants of the Arabidopsis *SAGT* genes showed increased disease resistance and free SA levels [63]. *AtSGT1* gene overexpression results in a reduction in SA content and reduced plant resistance [64]. SAR is typically characterized by augmentation of SA and *PR* genes' activation. SAR-induced plants showed increased expression of SA-dependent *PR1* [29]. In our study, the expression of *PR1* genes in the two groups was upregulated by Trp. In fact, exogenous application of SA can activate *PR* gene expression and resistance in plants without pathogen inoculation [65,66]. These results imply that the SA signaling pathway is required to induce resistance by Trp.

ISR is mediated by a JA/ET-sensitive pathway and does not involve the accumulation of PR proteins or SA [30,31]. It is generally believed that this antagonism occurs between SA and JA, and we also analyzed the expression of SA. JA biosynthesis-related genes, including *LOX* and *OPR*, and ET synthesis-related genes, including *ACO* and *ACS*, were found. In the C-vs-Trp group, the expression of *LOX*, *OPR*, *ACO*, and *ACS* was shown to increase after treatment with Trp. Surprisingly, the expression of these responsive genes was downregulated by foliar treatment with Trp in the S-vs-S+Trp group. There were significant differences in the expression of these genes between the two groups. Both synergistic and antagonistic interactions between SA and JA have been reported [67]. The interaction between SA and JA is either concentration-dependent or tissue-specific and dynamic [68]. In our results, we presumed that Trp-mediated resistance is different with or without pathogen attack. Without pathogens, foliar treatment with Trp induced SA and JA increases at low levels. Therefore, the resistance induced by Trp overlaps with ISR and SAR. This was also found in a recent study showing that the SA- and JA-biosynthesis

pathways can be co-induced [69]. In contrast, in the S-vs-S+Trp group, SA biosynthesis-related genes were induced, and JA-related genes were downregulated. This showed that SAR was induced by Trp rather than ISR when the pathogen was inoculated. *NPR1* expression is consistent with *ICS* and *PAL*, which are SA biosynthesis genes. *NPR1* is a common regulator of ISR and SAR [66]. The SAR and ISR pathways are independent but have an overlapping requirement for *NPR1* [70]. In both groups, the expression of *NPR1* was increased. These results showed that Trp-mediated resistance required *NPR1* to regulate the SAR and ISR pathways in pathogen inoculation. This is different from Si-mediated LB resistance in potato that occurs through ET/JA- and *NPR1*- dependent signaling pathways [71]. In a study of SA- and JA-mediated gene expression, the *WRKY70* transcription factor was likely to be involved in mediating SA-JA crosstalk [72]. However, in our data, no *WRKY70* genes were found among the DEGs. Whether the other transcription factors play a role is unclear; we require further analysis of our data in future works.

There are many elicitors that can initiate the plant defense response [62]. These include many chemical compounds, such as SA, BTH, BABA, or PBZ, or biological compounds including metabolites, oligosaccharides, glycoproteins, glycopeptides, proteins, polypeptides, lipids, and other cellular components [56]. Amino acids, such as methionine, can activate the ROS defense pathway and induce defense-related genes [73]. Lower concentrations of JA and BTH enable the simultaneous expression of both SAR and ISR pathways [74]. The combination of ISR and SAR can increase protection against pathogens that are resisted through both pathways in addition to extending protection to a broader spectrum of pathogens than ISR/SAR alone [29]. Trp-induced resistance is unlike these elicitors. In the S-vs-S+Trp/C-vs-Trp groups, there are different signaling pathways involved in Trp-induced resistance. Further research, such as protein assays, plant hormone measurements, and cell assays, is needed to validate the functions of interesting genes.

In this study, we revealed that foliar treatment with Trp can induce resistance of potato against CS. Our results showed that Trp induced resistance through different pathways under different conditions. Under pathogen inoculation, SAR is the pathway induced by Trp treatment. Without pathogen inoculation, SAR and ISR can be co-induced by Trp. This study provides useful information for research into Trp-induced resistance mechanisms and extends the application of Trp as an alternative agent to control CS, especially considering the field conditions.

#### 4. Materials and Methods

##### 4.1. Determine the Proper Concentration of Trp

To determine the proper concentration of Trp, a series of concentrations solutions (50 mg/L, 100 mg/L, 200 mg/L, and 400 mg/L) were prepared in water. The field trial was arranged in a plot in which CS occurred year by year. The plot consisted of five subplots of the same area (4.2 m × 4 m) that sowed the same number of seeds at the same time. The different concentrations of Trp were sprayed on field potato plants 3 weeks after seed germination. Water was sprayed as the control. Trp solution or water was sprayed onto the leaves of different potato groups until runoff. Field tubers were harvested at 120 days after seeding and assessed for disease incidence and yield.

##### 4.2. Plant Materials

The CS-susceptible potato cultivar, Shepody, was used. The potato plantlets were multiplied through plant tissue culture technology and grown in pot trials. Briefly, stems of potato plantlets were cut into node explants of similar length. These single-node explants were cultured on solid Murashige and Skoog (M&S) medium (pH 5.8) at 24 °C in an 8 h/16 h light cycle. Two weeks later, five established non-embryogenic callus lines of similar size were selected and transferred into pots filled with the same amount of autoclaved vermiculite. The selected potato lines were maintained under the same growth conditions. In brief, the pots were cultured at 24 °C with a 16 h light/8 h dark photoperiod

and  $70 \mu\text{mol m}^{-2} \text{s}^{-1}$  photon flux density provided by fluorescent lamps. For further trials, there were 3 plots (diameter 25 cm) that 5 seedlings per pot to replicate each treatment.

#### 4.3. Pathogen Inoculation and Tryptophan Treatments

The *S. scabiei* strain 4.1765, a highly pathogenic isolate from the China General Microbiological Culture Collection (CGMCC), was used in our experiments. The *S. scabiei* strain was cultured on an oatmeal medium (OM) plate for 15 days at 28 °C. Then, the pathogenic colonies were inoculated into tryptic soy broth (TSB) and incubated at 28 °C in a rotary shaker (200 rpm) for three days. The cell pellets were harvested by centrifugation (10 min,  $5000 \times g$ ) and washed with sterile water. The bacterial cells were resuspended in fresh water to a final concentration of  $1 \times 10^9$  conidia/mL for inoculation. This concentration of the suspension was determined based on the relationship between amount of pathogenic *S. scabiei* and the incidence of CS on tubers [75,76]. Then, 10 mL inoculation buffer was poured near the roots of seedlings. Therefore, a total of 50 mL inoculation buffer was inoculated into each pot.

The potato plants were divided into two groups and maintained under the same growth conditions. One was subjected to *S. scabiei* infection, and another group was *S. scabiei* uninoculation. Twenty-one days post-inoculation, at which time the tubers initiate and bacteria are highly infectious [77,78], Trp solution or water was sprayed onto the leaves of different potato groups until runoff. The concentration of the tryptophan solution was set at 100 mg/L, because this relatively low concentration could effectively inhibit the spread of CS disease. For the *S. scabiei*-uninoculated plants, leaves were treated with tryptophan (Trp) and water (C). The same treatment of the leaves was performed in the *S. scabiei*-inoculated plants (S+Trp and S).

After 4 days treatment, two top leaves were collected from each plant. Leaves collected from 5 different plants in one pot were pooled together as one sample for RNA extraction. Three replicates were repeated for each sample.

#### 4.4. Disease Assessment

Tubers harvested 90 days after seedlings were planted in pots (3 pots, 5 plants per plot) were graded and assessed for CS. Tubers > 2 g were washed under running water and scored for the percentage of tuber area covered by scab.

The disease index was calculated by the following equation:

Disease index =  $[\sum(n \times 1 + n \times 2 + n \times 3 + n \times 4 + n \times 5)/(N \times 5)] \times 100$ . (n = number of tubers corresponding to the numerical grade. N = total number of potato tubers assessed. 5 = high score on the severity of scale). The percentage of tuber area covered: 0. No symptom of scab; 1. 0–12.5%; 2. 12.6–25%; 3. 26–50%; 4. 51–75%; 5. 76–100%.

Control efficacy = (disease index of control – disease index of treated)/disease index of control  $\times 100\%$ .

#### 4.5. RNA Extraction and RNA Sequencing

In total, twelve samples of four conditions were used for total RNA extraction and library construction. Total RNA was isolated using the RNeasy Plant Mini Kit (Qiagen, Hilden, Germany) and library construction and sequencing were conducted by The Beijing Genomics Institute (BGI, Beijing, China, <http://www.genomics.cn/index.html>; accessed on 6 May 2022). The BGISEQ-500 platform was used for RNA sequencing and generated raw data [79,80]. The raw reads of the transcriptome data were filtered with SOAP-nuke software to remove unsatisfactory reads with low quality, joint contamination, and excessive unknown bases.

The clean RNA-Seq data have been deposited in the SRA database under NCBI (Accession No. PRJNA611872).

#### 4.6. Data Mapping, Analysis and Functional Annotation

The filtered clean reads were saved as FASTQ data and aligned to the potato reference genome *S. tuberosum* group phureja DM1-3 v6.1 (<http://spuddb.uga.edu/>; accessed on 20 April 2022) by HISAT [81–83].

The updated reference genome was generated by adding the newly identified transcripts into the original potato reference sequences. The clean reads were mapped to the updated reference sequences by Bowtie 2 [82–84]. The abundance of transcripts was estimated using the FPKM [85] method.

DEGs were analyzed by DEGseq [86,87] with the parameters “FC  $\geq 2$ ” and “Q-value  $\leq 0.001$ ”. GO functional enrichment of DEGs was performed based on the GO database (<http://www.geneontology.org/>; accessed on 22 April 2022), and pathway enrichment of DEGs was performed based on the KEGG database (<http://www.genome.jp/kegg/>; accessed on 23 April 2022). Meanwhile, GO term enrichment and KEGG pathway enrichment analyses were conducted using the “phyper” function of the R package. FDR < 0.05 was defined as the threshold for significant enrichment.

#### 4.7. qRT-PCR Analysis

Total RNA was extracted using the Plant Total RNA Extraction kit (Tiangen, Beijing, China) according to the manufacturer’s instructions. cDNA was synthesized from 1  $\mu$ g total RNA using the TransScript® One-Step gDNA Removal and cDNA Synthesis Super-Mix (Transgene, Beijing, China). qRT-PCR was performed using the SYBR® Green Realtime PCR Master Mix (Toyobo, Osaka, Japan). All qRT-PCRs were analyzed using CFX96 Touch (Bio-Rad, Hercules, CA, USA) with three technical replicates and three biological replicates. The relative expression levels of selected genes were identified using the  $2^{-\Delta\Delta CT}$  method [88]. *StActin* (Soltu.DM.04G007480) was used as an internal control. The primers for qRT-PCR are shown in Table S5.

**Supplementary Materials:** The following supporting information can be downloaded at: [www.mdpi.com/article/10.3390/ijms23158420/s1](http://www.mdpi.com/article/10.3390/ijms23158420/s1)

**Author Contributions:** Conceptualization, P.Z. and N.Z.; methodology, L.L., J.C. and P.Z.; validation, L.L. and J.C.; data analysis, Z.W. and P.Z.; investigation, Y.Z., P.Z. and N.Z.; writing, L.L. and P.Z.; visualization, Z.W. and Y.Z.; supervision, P.Z. and N.Z.; project administration, P.Z. and N.Z.; funding acquisition, P.Z. and N.Z. All authors have read and agreed to the published version of the manuscript.

**Funding:** This research was funded by Key Area Research and Development Program of Guangdong Province in China (2020B0202010005), the Strategic Priority Research Program of the Chinese Academy of Sciences (XDA24020104, XDA28030202), the National Natural Science Foundation of China (31601622), Science and Technology Poverty Alleviation Project of The Chinese Academy of Sciences (KFJ-FP-201905, KFJ-FP-202001), and Key Technologies R & D Program of Inner Mongolia (2021GG0300).

**Institutional Review Board Statement:** Not applicable.

**Informed Consent Statement:** Not applicable.

**Data Availability Statement:** The clean data presented in this study are available in the Sequence Read Archive (SRA) database in NCBI (Accession No. PRJNA611872).

**Conflicts of Interest:** The authors declare no conflict of interest.

## References

1. FAOSTAT. Available online: <http://www.fao.org/faostat/en/#data/QC> (accessed on 6 May 2019).
2. Kirk, W.W. Introduction to 2013 symposium on bacterial diseases of potatoes. *Am. J. Potato Res.* **2015**, *92*, 215–217.
3. Loria, R.; Bukhalid, R.A.; Fry, B.A.; King, R.R. Plant pathogenicity in the genus *Streptomyces*. *Plant Dis.* **1997**, *81*, 836–846.
4. Wanner, L.A.; Kirk, W.W. *Streptomyces*-from basic microbiology to role as a plant pathogen. *Am. J. Potato Res.* **2015**, *92*, 236–242.

5. Santos-Cervantes, M.E.; Felix-Gastelum, R.; Herrera-Rodríguez, G.; Espinoza-Mancillas, M.G.; Mora-Romero, A.G.; Leyva-López, N.E. Characterization, pathogenicity and chemical control of *Streptomyces acidiscabies* associated to potato common scab. *Am. J. Potato Res.* **2017**, *94*, 14–25.
6. Hiltunen, L.H.; Weckman, A.; Ylhainen, A.; Rita, H.; Richter, E.; Valkonen, J.P.T. Responses of potato cultivars to the common scab pathogens, *Streptomyces scabies* and *S. turgidiscabies*. *Ann. Appl. Biol.* **2005**, *146*, 395–403.
7. Hill, J.; Lazarovits, G. A mail survey of growers to estimate potato common scab prevalence and economic loss in Canada. *Can. J. Plant Pathol.* **2005**, *27*, 46–52.
8. Wilson, C.R. A summary of common scab disease of potato research from Australia. In Proceedings of the International Potato Scab Symposium, Sapporo, Japan, 6–7 September 2004.
9. Loria, R.; Kers, J.; Joshi, M. Evolution of plant pathogenicity in *Streptomyces*. *Annu. Rev. Phytopathol.* **2006**, *44*, 469–487.
10. Dees, M.W.; Wanner, L.A. In search of better management of potato common scab. *Potato Res.* **2012**, *55*, 249–268.
11. Sarwar, A.; Latif, Z.; Zhang, S.; Zhu, J.; Zechel, D.L.; Bechthold, A. Biological control of potato common scab with rare isatropolone C compound produced by plant growth promoting *Streptomyces* A1RT. *Front. Microbiol.* **2018**, *9*, 1126.
12. Lambert, D.H.; Loria, R.; Labeda, D.P.; Saddler, G.S. Recommendation for the conservation of the name *Streptomyces scabies*. Request for an Opinion. *Int. J. Syst. Evol. Microbiol.* **2007**, *57*, 2447–2448.
13. Lambert, D.H.; Loria, R. *Streptomyces scabies* sp. nov., nom. rev. *Int. J. Syst. Evol. Microbiol.* **1989**, *39*, 387–392.
14. King, R.R.; Lawrence, C.H.; Calhoun, L.A. Chemistry of phytotoxins associated with *Streptomyces scabies* the causal organism of potato common scab. *J. Agric. Food Chem.* **1992**, *40*, 834–837.
15. King, R.R.; Lawrence, C.H.; Clark, M.C.; Calhoun, L.A. Isolation and characterization of phytotoxins associated with *Streptomyces scabies*. *J. Chem. Soc., Chem. Commun.* **1989**, *13*, 849–850.
16. Johnson, E.G.; Joshi, M.V.; Gibson, D.M.; Loria, R. Cello-oligosaccharides released from host plants induce pathogenicity in scab-causing *Streptomyces* species. *Physiol. Mol. Plant Pathol.* **2007**, *71*, 18–25.
17. Bischoff, V.; Cookson, S.J.; Wu, S.; Scheible, W.R. Thaxtomin A affects CESA-complex density, expression of cell wall genes, cell wall composition, and causes ectopic lignification in *Arabidopsis thaliana* seedlings. *J. Exp. Bot.* **2009**, *60*, 955–965.
18. Errakhi, R.; Dauphin, A.; Meimoun, P.; Lehner, A.; Rebutier, D.; Vatsa, P.; Briand, J.; Madiona, K.; Rona, J.P.; Barakate, M.; et al. An early Ca<sup>2+</sup> influx is a prerequisite to thaxtomin A-induced cell death in *Arabidopsis thaliana* cells. *J. Exp. Bot.* **2008**, *59*, 4259–4270.
19. Healy, F.G.; Krasnoff, S.B.; Wach, M.; Gibson, D.M.; Loria, R. Involvement of a cytochrome P450 monooxygenase in thaxtomin A biosynthesis by *Streptomyces acidiscabies*. *J. Bacteriol.* **2002**, *184*, 2019–2029.
20. Barry, S.M.; Kers, J.A.; Johnson, E.G.; Song, L.; Aston, P.R.; Patel, B.; Krasnoff, S.B.; Crane, B.R.; Gibson, D.M.; Loria, R.; et al. Cytochrome P450-catalyzed L-tryptophan nitration in thaxtomin phytotoxin biosynthesis. *Nat. Chem. Biol.* **2012**, *8*, 814–816.
21. Healy, F.G.; Wach, M.; Krasnoff, S.B.; Gibson, D.M.; Loria, R. The *txtAB* genes of the plant pathogen *Streptomyces acidiscabies* encode a peptide synthetase required for phytotoxin thaxtomin A production and pathogenicity. *Mol. Microbiol.* **2000**, *38*, 794–804.
22. Hosny, M.; Abo-Elyousr, K.A.M.; Asran, M.R.; Saeed, F.A. Chemical control of potato common scab disease under field conditions. *Arch. Phytopathol. Plant Prot.* **2014**, *47*, 2193–2199.
23. Kuć, J. Induced immunity to plant disease. *BioScience* **1982**, *32*, 854–860.
24. Klopper, J.W.; Tuzun, S.; Kuć, J.A. Proposed definition related to induced disease resistance. *Biocontrol Sci. Technol.* **1992**, *2*, 349–351.
25. Pieterse, C.M.J.; Zamioudis, C.; Berendsen, R.L.; Weller, D.M.; Van Wees, S.C.M.; Bakker, P.A.H.M. Induced systemic resistance by beneficial microbes. *Annu. Rev. Phytopathol.* **2014**, *52*, 347–375.
26. Cameron, R.K.; Dixon, R.A.; Lamb, C.J. Biologically induced systemic acquired resistance in *Arabidopsis thaliana*. *Plant J.* **1994**, *5*, 715–725.
27. Uknes, S.; Mauch-Mani, B.; Moyer, M.; Potter, S.; Williams, S.; Dincher, S.; Chandler, D.; Slusarenko, A.; Ward, E.; Ryals, J. Acquired resistance in *Arabidopsis*. *Plant Cell* **1992**, *4*, 645–656.
28. Ward, E.R.; Uknes, S.J.; Williams, S.C.; Dincher, S.S.; Wiederhold, D.L.; Alexander, D.C.; Ahl-Goy, P.; Métraux, J.P.; Ryals, J.A. Coordinate gene activity in response to agents that induce systemic acquired resistance. *Plant Cell* **1991**, *3*, 1085–1094.
29. Choudhary, D.K.; Prakash, A.; Johri, B.N. Induced systemic resistance (ISR) in plants: Mechanism of action. *Indian J. Microbiol.* **2007**, *47*, 289–297.
30. van Loon, L.C.; Bakker, P.A.H.M.; Pieterse, C.M.J. Systemic resistance induced by rhizosphere bacteria. *Annu. Rev. Phytopathol.* **1998**, *36*, 453–483.
31. Pieterse, C.M.J.; van Wees, S.C.M.; van Pelt, J.A.; Knoester, M.; Laan, R.; Gerrits, H.; Weisbeek, P.J.; van Loon, L.C. A novel signaling pathway controlling induced systemic resistance in *Arabidopsis*. *Plant Cell* **1998**, *10*, 1571–1580.
32. Walters, D.R.; Ratsep, J.; Havis, N.D. Controlling crop diseases using induced resistance: Challenges for the future. *J. Exp. Bot.* **2013**, *64*, 1263–1280.
33. McIntosh, A.H.; Bateman, G.L.; Chamberlain, K.; Dawson, G.W.; Burrell, M.M. Decreased severity of potato common scab after foliar sprays of 3,5-dichlorophenoxyacetic acid, a possible antipathogenic agent. *Ann. Appl. Biol.* **1981**, *99*, 275–281.
34. McIntosh, A.H.; Bateman, G.L.; Chamberlain, K. Substituted benzoic and picolinic acids as foliar sprays against potato common scab. *Ann. Appl. Biol.* **1988**, *112*, 397–401.

35. Tegg, R.S.; Gill, W.M.; Thompson, H.K.; Davies, N.W.; Ross, J.J.; Wilson, C.R. Auxin-induced resistance to common scab disease of potato linked to inhibition of thaxtomin A toxicity. *Plant Dis.* **2008**, *92*, 1321–1328.
36. Meyer, R.; Slater, V.; Dubery, I.A. A phytotoxic protein-lipopolysaccharide complex produced by *Verticillium dahliae*. *Phytochemistry* **1994**, *35*, 1449–1453.
37. Thompson, H.K.; Tegg, R.S.; Corkrey, R.; Wilson, C.R. Optimal rates of 2,4-dichlorophenoxyacetic acid foliar application for control of common scab in potato. *Ann. Appl. Biol.* **2014**, *165*, 293–302.
38. Bokshi, A.I.; Morris, S.C.; Deverall, B.J. Effects of benzothiadiazole and acetylsalicylic acid on  $\beta$ -1,3-glucanase activity and disease resistance in potato. *Plant Pathol.* **2003**, *52*, 22–27.
39. Bengtsson, T.; Weighill, D.; Proux-Wéra, E.; Levander, F.; Resjö, S.; Burra, D.D.; Moushib, L.I.; Hedley, P.E.; Liljeroth, E.; Jacobson, D.; et al. Proteomics and transcriptomics of the BABA-induced resistance response in potato using a novel functional annotation approach. *BMC Genom.* **2014**, *15*, 315.
40. Zimmerli, L.; Métraux, J.P.; Mauch-Mani, B.  $\beta$ -Aminobutyric acid-induced protection of Arabidopsis against the necrotrophic fungus *Botrytis cinerea*. *Plant Physiol.* **2001**, *126*, 517–523.
41. Conrath, U.; Beckers, G.J.M.; Langenbach, C.J.G.; Jaskiewicz, M.R. Priming for enhanced defense. *Annu. Rev. Phytopathol.* **2015**, *53*, 97–119.
42. Barth, C.; Jander, G. Arabidopsis myrosinases TGG1 and TGG2 have redundant function in glucosinolate breakdown and insect defense. *Plant J.* **2006**, *46*, 549–562.
43. Bednarek, P.; Osbourn, A. Plant-microbe interactions: Chemical diversity in plant defense. *Science* **2009**, *324*, 746–748.
44. Lu, H.P.; Luo, T.; Fu, H.W.; Wang, L.; Tan, Y.Y.; Huang, J.Z.; Wang, Q.; Ye, G.Y.; Gatehouse, A.M.R.; Lou, Y.G.; et al. Resistance of rice to insect pests mediated by suppression of serotonin biosynthesis. *Nat. Plants* **2018**, *4*, 338–344.
45. Miao, Y.; Xu, L.; He, X.; Zhang, L.; Shaban, M.; Zhang, X.; Zhu, L. Suppression of tryptophan synthase activates cotton immunity by triggering cell death via promoting SA synthesis. *Plant J.* **2019**, *2*, 329–345.
46. Legault, G.S.; Lerat, S.; Nicolas, P.; Beaulieu, C. Tryptophan regulates thaxtomin A and indole-3-acetic acid production in *Streptomyces scabiei* and modifies its interactions with radish seedlings. *Phytopathology* **2011**, *101*, 1045–1051.
47. Wilhelm, B.T.; Marguerat, S.; Watt, S.; Schubert, F.; Wood, V.; Goodhead, I.; Penkett, C.J.; Rogers, J.; Bähler, J. Dynamic repertoire of a eukaryotic transcriptome surveyed at single-nucleotide resolution. *Nature* **2008**, *453*, 1239–1243.
48. Yan, H.; Shi, H.; Hu, C.; Luo, M.; Xu, C.; Wang, S.; Li, N.; Tang, W.; Zhou, Y.; Wang, C.; et al. Transcriptome differences in response mechanisms to low-nitrogen stress in two wheat varieties. *Int. J. Mol. Sci.* **2021**, *22*, 12278.
49. Luo, Y.; Teng, S.; Yin, H.; Zhang, S.; Tuo, X.; Tran, L.S.P. Transcriptome analysis reveals roles of anthocyanin- and jasmonic acid-biosynthetic pathways in rapeseed in response to high light stress. *Int. J. Mol. Sci.* **2021**, *22*, 13027.
50. Xuan, H.; Huang, Y.; Zhou, L.; Deng, S.; Wang, C.; Xu, J.; Wang, H.; Zhao, J.; Guo, N.; Xing, H. Key soybean seedlings drought-responsive genes and pathways revealed by comparative transcriptome analyses of two cultivars. *Int. J. Mol. Sci.* **2022**, *23*, 2893.
51. Yu, Y.; Yu, M.; Zhang, S.; Song, T.; Zhang, M.; Zhou, H.; Wang, Y.; Xiang, J.; Zhang, X. Transcriptomic identification of wheat AP2/ERF transcription factors and functional characterization of *TaERF-6-3A* in response to drought and salinity stresses. *Int. J. Mol. Sci.* **2022**, *23*, 3272.
52. Ouertani, R.N.; Arasappan, D.; Abid, G.; Chikha, M.B.; Jardak, R.; Mahmoudi, H.; Mejri, S.; Ghorbel, A.; Ruhlman, T.A.; Jansen, R.K. Transcriptomic analysis of salt-stress-responsive genes in barley roots and leaves. *Int. J. Mol. Sci.* **2021**, *22*, 8155.
53. Yang, J.; Li, L.; Zhang, X.; Wu, S.; Han, X.; Li, X.; Xu, J. Comparative transcriptomics analysis of roots and leaves under Cd stress in *Calotropis gigantea* L. *Int. J. Mol. Sci.* **2022**, *23*, 3329.
54. Ramírez-Pool, J.A.; Xoconostle-Cázares, B.; Calderón-Pérez, B.; Ibarra-Laclette, E.; Villafán, E.; Lira-Carmona, R.; Ruiz-Medrano, R. Transcriptomic analysis of the host response to mild and severe CTV strains in naturally infected *Citrus sinensis* orchards. *Int. J. Mol. Sci.* **2022**, *23*, 2435.
55. Dai, W.B. Research on prevention and control of chinese agricultural ecological environment pollution to ensure food safety. *Adv. Mater. Res.* **2013**, *616–618*, 2247–2250.
56. Qiu, D.; Dong, Y.; Zhang, Y.; Li, S.; Shi, F. Plant immunity inducer development and application. *Mol. Plant-Microbe Interact.* **2017**, *30*, 355–360.
57. Ishihara, A.; Hashimoto, Y.; Tanaka, C.; Dubouzet, J.G.; Nakao, T.; Matsuda, F.; Nishioka, T.; Miyagawa, H.; Wakasa, K. The tryptophan pathway is involved in the defense responses of rice against pathogenic infection via serotonin production. *Plant J.* **2008**, *54*, 481–495.
58. Glawischnig, E. Camalexin. *Phytochemistry* **2007**, *68*, 401–406.
59. Frerigmann, H.; Piślewska-Bednarek, M.; Sánchez-Vallet, A.; Molina, A.; Glawischnig, E.; Gigolashvili, T.; Bednarek, P. Regulation of pathogen-triggered tryptophan metabolism in *Arabidopsis thaliana* by MYB transcription factors and indole glucosinolate conversion products. *Mol. Plant* **2016**, *9*, 682–695.
60. Babcock, M.J.; Eckwall, E.C.; Schottel, J.L. Production and regulation of potato-scab-inducing phytotoxins by *Streptomyces scabies*. *J. Gen. Microbiol.* **1993**, *139*, 1579–1586.
61. Lauzier, A.; Goyer, C.; Ruest, L.; Brzezinski, R.; Crawford, D.L.; Beaulieu, C. Effect of amino acids on thaxtomin A biosynthesis by *Streptomyces scabies*. *Can. J. Microbiol.* **2002**, *48*, 359–364.
62. Vallad, G.E.; Goodman, R.M. Systemic acquired resistance and induced systemic resistance in conventional agriculture. *Crop Sci.* **2004**, *44*, 1920–1934.

63. Noutoshi, Y.; Okazaki, M.; Shirasu, K. Imprimatins A and B: Novel plant activators targeting salicylic acid metabolism in *Arabidopsis thaliana*. *Plant Signal. Behav.* **2012**, *7*, 1715–1717.
64. Song, J.T.; Koo, Y.J.; Seo, H.S.; Kim, M.C.; Choi, Y.D.; Kim, J.H.; Choi, Y.D.; Kim, J.H. Overexpression of AtSGT1, an Arabidopsis salicylic acid glucosyltransferase, leads to increased susceptibility to *Pseudomonas syringae*. *Phytochemistry* **2008**, *69*, 1128–1134.
65. Friedrich, L.; Lawton, K.; Reuss, W.; Masner, P.; Specker, N.; Rella, M.G.; Meier, B.; Dincher, S.; Staub, T.; Uknes, S.; et al. A benzothiadiazole derivative induces systemic acquired resistance in tobacco. *Plant J.* **1996**, *10*, 61–70.
66. Dong, X. NPR1, all things considered. *Curr. Opin. Plant Biol.* **2004**, *7*, 547–552.
67. Kunkel, B.N.; Brooks, D.M. Cross-talk between signaling pathways in pathogen defense. *Curr. Opin. Plant Biol.* **2002**, *5*, 325–331.
68. Mur, L.A.J.; Kenton, P.; Atzorn, R.; Miersch, O.; Wasternack, C. The outcomes of concentration-specific interactions between salicylate and jasmonate signaling include synergy, antagonism, and oxidative stress leading to cell death. *Plant Physiol.* **2006**, *140*, 249–262.
69. Sudheeran, P.K.; Sela, N.; Carmeli-Weissberg, M.; Ovadia, R.; Panda, S.; Feygenberg, O.; Maurer, D.; Oren-Shamir, M.; Aharoni, A.; Alkan, N. Induced defense response in red mango fruit against *Colletotrichum gloeosporioides*. *Hortic. Res.* **2021**, *8*, 17.
70. van Wees, S.C.M.; de Swart, E.A.M.; van Pelt, J.A.; van Loon, L.C.; Pieterse, C.M.J. Enhancement of induced disease resistance by simultaneous activation of salicylate- and jasmonate-dependent defense pathways in *Arabidopsis thaliana*. *Proc. Natl. Acad. Sci. USA* **2000**, *97*, 8711–8716.
71. Xue, X.; Geng, T.; Liu, H.; Yang, W.; Zhong, W.; Zhang, Z.; Zhu, C.; Chu, Z. Foliar application of silicon enhances resistance against *Phytophthora infestans* through the ET/JA- and NPR1- dependent signaling pathways in potato. *Front. Plant Sci.* **2021**, *12*, 609870.
72. Li, J.; Brader, G.; Palva, E.T. The WRKY70 transcription factor: A node of convergence for jasmonate-mediated and salicylate-mediated signals in plant defense. *Plant Cell* **2004**, *16*, 319–331.
73. Boubakri, H.; Wahab, M.A.; Chong, J.; Gertz, C.; Gandoura, S.; Mliki, A.; Bertsch, C.; Soustre-Gacougnolle, I. Methionine elicits H<sub>2</sub>O<sub>2</sub> generation and defense gene expression in grapevine and reduces *Plasmopara viticola* infection. *J. Plant Physiol.* **2013**, *170*, 1561–1568.
74. Walling, L.L. Induced resistance: From the basic to the applied. *Trends Plant Sci.* **2001**, *6*, 445–447.
75. Manome, A.; Kageyama, A.; Kurata, S.; Yokomaku, T.; Koyama, O.; Kanagawa, T.; Tamaki, H.; Tagawa, M.; Kamagata, Y. Quantification of potato common scab pathogens in soil by quantitative competitive PCR with fluorescent quenching-based probes. *Plant Pathol.* **2008**, *57*, 887–896.
76. Qu, X.; Wanner, L.A.; Christ, B.J. Using the *txtAB* operon to quantify pathogenic *Streptomyces* in potato tubers and soil. *Phytopathology* **2008**, *98*, 405–412.
77. Adams, M.J.; Lapwood, D.H. Studies on the lenticel development, surface microflora and infection by common scab (*Streptomyces scabiei*) of potato tubers growing in wet and dry soils. *Ann. Appl. Biol.* **1978**, *90*, 335–343.
78. Khatri, B.B.; Tegg, R.S.; Brown, P.H.; Wilson, C.R. Temporal association of potato tuber development with susceptibility to common scab and *Streptomyces scabiei*-induced responses in the potato periderm. *Plant Pathol.* **2011**, *60*, 776–786.
79. Patch, A.M.; Nones, K.; Kazakoff, S.H.; Newell, F.; Wood, S.; Leonard, C.; Holmes, O.; Xu, Q.; Addala, V.; Creaney, J.; et al. Germline and somatic variant identification using BGISEQ-500 and HiSeq X Ten whole genome sequencing. *PLoS ONE* **2018**, *13*, e0190264.
80. Zhu, F.Y.; Chen, M.X.; Ye, N.H.; Qiao, W.M.; Gao, B.; Law, W.K.; Tian, Y.; Zhang, D.; Zhang, D.; Liu, T.Y.; et al. Comparative performance of the BGISEQ-500 and Illumina HiSeq4000 sequencing platforms for transcriptome analysis in plants. *Plant Methods* **2018**, *14*, 69.
81. Kim, D.; Langmead, B.; Salzberg, S.L. HISAT: A fast spliced aligner with low memory requirements. *Nat. Methods* **2015**, *12*, 357–360.
82. Li, S.; Tian, Y.; Wu, K.; Ye, Y.; Yu, J.; Zhang, J.; Liu, Q.; Hu, M.; Li, H.; Tong, Y.; et al. Modulating plant growth–metabolism coordination for sustainable agriculture. *Nature* **2018**, *560*, 595–600.
83. Tian, Y.; Fan, M.; Qin, Z.; Lv, H.; Wang, M.; Zhang, Z.; Zhou, W.; Zhao, N.; Li, X.; Han, C.; et al. Hydrogen peroxide positively regulates brassinosteroid signaling through oxidation of the BRASSINAZOLE-RESISTANT1 transcription factor. *Nat. Commun.* **2018**, *9*, 1063.
84. Langmead, B.; Salzberg, S.L. Fast gapped-read alignment with Bowtie 2. *Nat. Methods* **2012**, *9*, 357–359.
85. Catalanotto, C.; Pallotta, M.; ReFalo, P.; Sachs, M.S.; Vayssie, L.; Macino, G.; Cogoni, C. Redundancy of the two dicer genes in transgene-induced posttranscriptional gene silencing in *Neurospora crassa*. *Mol. Cell. Biol.* **2004**, *24*, 2536–2545.
86. Wang, L.; Feng, Z.; Wang, X.; Wang, X.; Zhang, X. DEGseq: An R package for identifying differentially expressed genes from RNA-seq data. *Bioinformatics* **2010**, *26*, 136–138.
87. Yang, Y.H.; Dudoit, S.; Luu, P.; Lin, D.M.; Peng, V.; Ngai, J.; Speed, T.P. Normalization for cDNA microarray data: A robust composite method addressing single and multiple slide systematic variation. *Nucleic Acids Res.* **2002**, *30*, e15.
88. Livak, K.J.; Schmittgen, T.D. Analysis of relative gene expression data using real-time quantitative PCR and the 2<sup>-ΔΔCT</sup> method. *Methods* **2001**, *25*, 402–408.



## Short Communication

## Phosphorus accumulation aggravates potato common scab and to be controlled by phosphorus-solubilizing bacteria

Jingjing Cao<sup>a,c,1</sup>, Zhiqin Wang<sup>a,c,1</sup>, Jiahe Wu<sup>a,c</sup>, Pan Zhao<sup>a,c,d</sup>, Chengchen Li<sup>b</sup>, Xiaobo Li<sup>b</sup>, Lu Liu<sup>a,c</sup>, Yonglong Zhao<sup>a,c</sup>, Naiqin Zhong<sup>a,c,d,\*</sup><sup>a</sup>State Key Laboratory of Plant Genomics, Institute of Microbiology, Chinese Academy of Sciences, Beijing 100101, China<sup>b</sup>Guangdong Provincial Key Laboratory of Crops Genetics and Improvement, Crop Research Institute, Guangdong Academy of Agricultural Sciences, Guangzhou 510640, China<sup>c</sup>Engineering Laboratory for Advanced Microbial Technology of Agriculture, Chinese Academy of Sciences, Beijing 100101, China<sup>d</sup>The Enterprise Key Laboratory of Advanced Technology for Potato Fertilizer and Pesticide, Hulunbuir 021000, China

## a r t i c l e i n f o

## Article history:

Received 9 March 2023

Received in revised form 25 May 2023

Accepted 31 August 2023

Available online 4 September 2023

© 2023 Science China Press. Published by Elsevier B.V. and Science China Press. All rights reserved.

As the fourth largest food crop, potato plays an important role in ensuring the stability of the human food supply [1,2]. However, potato common scab (CS) induced by pathogenic *Streptomyces* occurs globally, and the harm is increasing year by year [3]. Potato CS has become a key problem that urgently needs to be solved in the potato industry. The research on preventing potato CS has been carried out for more than 100 years [4], yet limited breakthroughs have been achieved so far. Therefore, the investigation of the main mechanism leading to CS and the effective strategy to control CS for industrialized applications is needed.

Previous research showed that potato CS disease is potentially affected by plant mineral nutrients including the exogenous application of fertilizer [5,6]. These studies demonstrated that macro- and microelements, e.g., nitrogen, phosphorus, calcium, iron, etc., affect the CS severity depending on their contents in soil or plant tissue [7]. Phosphorus is an essential nutrient element for the growth and the development of all crops, often supplied through application of phosphorus fertilizer. Since soil colloid has a strong effect on phosphorus adsorption and fixation, most phosphorus fertilizers (monoammonium phosphate and diammonium phosphate) combine with  $\text{Ca}^{2+}$ ,  $\text{Fe}^{2+}$ ,  $\text{Fe}^{3+}$ , and  $\text{Al}^{3+}$  in soil to form insoluble phosphate including  $\text{Ca}_3(\text{PO}_4)_2$  [8,9]. Here, we found for the first time that  $\text{Ca}_3(\text{PO}_4)_2$  enhances the growth and reproduction of the pathogen *S. scabies*. During the growth of the pathogen, organic acids are produced, and the protons released by organic acids combine with  $\text{Ca}_3(\text{PO}_4)_2$  to form  $\text{HPO}_4^{2-}$ , which supports the growth of *S. scabies*. We further screened one antagonistic bac-

terium with effective phosphorus-dissolving function to effectively prevent and control potato CS.

Firstly, to investigate the effects of soil phosphorus content on CS development, we conducted field experiments. These experiments were performed in two main potato varieties (Favorita and Qingshu) produced in areas in China, Huidong (HD) in Guangdong Province from 2020 to 2021 and Hailar (HLE) in Inner Mongolia Autonomous Region in the year 2021. Disease incidence rate and index are positively correlated with phosphate concentration, as the high phosphate fertilizer (HP) enhances both the rate and the index of CS, in comparison with low phosphate (LP) or moderate phosphate (MP). In line with this, the relative abundance of *S. scabies* in soil indicated by the DNA level of the gene *txtA* (the effector gene of *S. scabies*) is also higher in HP than LP (Fig. 1a). Altogether, these results suggested that there was a positive correlation between doses of phosphorous fertilizer and occurrence of CS in the field.

Given that phosphorous fertilizer was able to promote CS occurrence in the field, we further studied which phosphate states contribute to this consequence. Various types of phosphorous chemical components were supplemented in the medium (initial pH 7.0) to support *S. scabies* growth. On the media containing  $\text{KH}_2\text{PO}_4$  and  $\text{Ca}(\text{H}_2\text{PO}_4)_2$  as the only source of phosphorus, the growth of *S. scabies* peaked at 1.25 g/L of  $\text{KH}_2\text{PO}_4$  and 3.75 g/L of  $\text{Ca}(\text{H}_2\text{PO}_4)_2$ , respectively, and gradually decreased with higher concentrations (Fig. S1a online), indicating that excess of  $\text{H}_2\text{PO}_4^-$  was not benefit for further growth. Whereas the medium containing  $\text{CaHPO}_4$  or  $\text{K}_2\text{HPO}_4$  could support the growth of *S. scabies* until the highest phosphate concentration (Fig. 1b), suggesting that  $\text{HPO}_4^{2-}$  was easily absorbed and utilized by *S. scabies*. Interestingly, on the medium with insoluble  $\text{Ca}_3(\text{PO}_4)_2$ , the growth and reproduction of *S. scabies* was remarkably faster than on the media mentioned above, reaching high colony numbers (above 1000)

\* Corresponding author.

E-mail address: [nqzhong@im.ac.cn](mailto:nqzhong@im.ac.cn) (N. Zhong).<sup>1</sup> These authors contributed equally to this work.

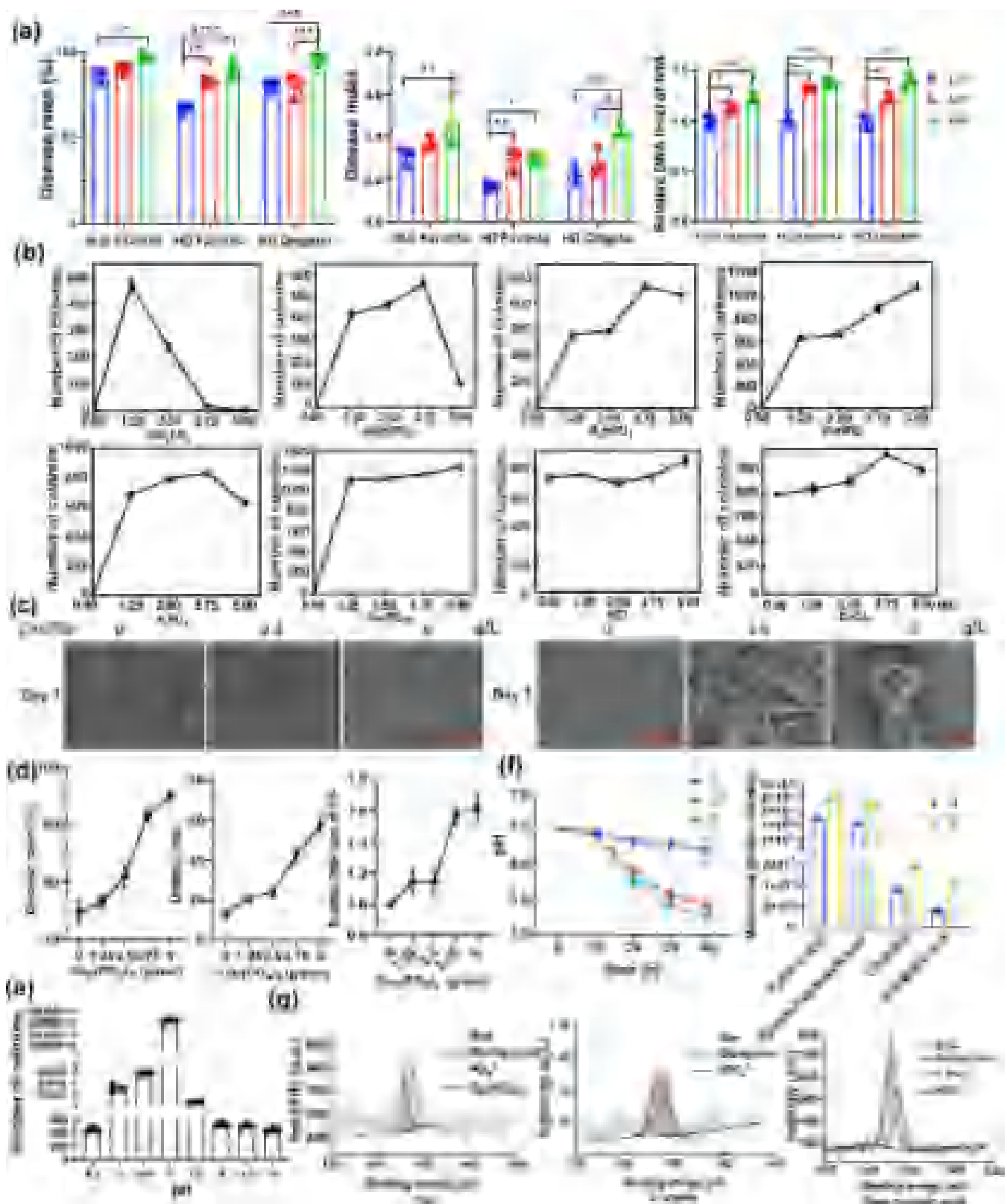


Fig. 1. High phosphorus fertilizer application increases the severity of potato CS disease. (a) The incidence and disease index of harvested potatoes in field experiments. Relative DNA levels of txtA were analyzed by qPCR with 16S DNA as an internal control. (b) Colony numbers of *S. scabies* on different phosphate media. (c) The growth of *S. scabies* mycelia and spores was observed by electron microscope at day 1 and 3 during culture. (d) Disease rates and disease index of harvested potatoes were calculated, and the relative DNA levels of txtA were analyzed. (e) The optimum pH for the growth of *S. scabies*. (f) The chemicals in the culturing medium after 48 h were analyzed via HPLC-MS. (g) The phosphorus state was analyzed by XPS in the media without *S. scabies*, with *S. scabies* or pure organic acid growing for 7 days. Pooled data from 3 plots for each experiment are shown with mean  $\pm$  standard deviation and were analyzed by unpaired t test (\*\*\*\* $P < 0.0001$ , \*\*\* $P < 0.001$ , \*\* $P < 0.01$ , \* $P < 0.05$ ). qPCR: quantitative polymerase chain reaction.

starting from 1.25 g/L of  $\text{Ca}_3(\text{PO}_4)_2$ .  $\text{K}_3\text{PO}_4$  could also support a rapid growth of *S. scabies*, even though not as pronounced as  $\text{Ca}_3(\text{PO}_4)_2$ . To exclude whether  $\text{Ca}^{2+}$  promotes the growth of *S. scabies*, gradually increasing amounts of  $\text{CaCl}_2$  or  $\text{KCl}$  were supplemented on top of  $\text{K}_2\text{HPO}_4$  which supplied  $\text{HPO}_4^{2-}$ . Additional  $\text{Ca}^{2+}$  or  $\text{K}^+$  only mildly enhanced the growth of *S. scabies* (Fig. 1b).

Then, scanning electron microscope was also employed to assess the growth of *S. scabies*. As shown in Fig. 1c, at day 1, only a few *S. scabies* spores germinated to form aerial hyphae in the absence of  $\text{Ca}_3(\text{PO}_4)_2$ , whereas all spores formed hyphae in the presence of 2.5 g/L of  $\text{Ca}_3(\text{PO}_4)_2$ . Aerial hyphae generated branches in the presence of 5 g/L of  $\text{Ca}_3(\text{PO}_4)_2$  at day 1, indicating that  $\text{Ca}_3(\text{PO}_4)_2$  promotes *S. scabies* spore germination and hyphae growth (Fig. 1c). At day 3, 2.5 g/L of  $\text{Ca}_3(\text{PO}_4)_2$  accelerated hyphae growth and reproduction with much higher hyphae intensity. When  $\text{Ca}_3(\text{PO}_4)_2$  was increased to 5 g/L, lots of new spores were formed. In sum,  $\text{Ca}_3(\text{PO}_4)_2$  promotes rapid growth and reproduction of *S. scabies*.

We next focused on  $\text{Ca}_3(\text{PO}_4)_2$  and tested its ability to drive CS in potato. Potatoes were cultured under gradually increased concentration of  $\text{Ca}_3(\text{PO}_4)_2$  and were inoculated with *S. scabies*. In line with the results from field experiments (Fig. 1d), CS severity was significantly exacerbated along with the increasing amount of  $\text{Ca}_3(\text{PO}_4)_2$  (Fig. S1b online). Similar results were observed when assessing the disease rates and disease index (Fig. 1d), as well as the relative DNA levels of *txtA* of *S. scabies* (Fig. 1d).

To further decipher the mechanism underlying how  $\text{Ca}_3(\text{PO}_4)_2$  promotes the growth and reproduction of *S. scabies*, the pH and metabolic products of the culturing medium were analyzed. The optimum initial pH value for *S. scabies* growth was determined to be 7.0 (Fig. 1e). The culturing medium became acidified after the addition of  $\text{Ca}_3(\text{PO}_4)_2$  (2.5 or 5 g/L), indicated by the decrease on pH to lower than 6.0 after 36 h (Fig. 1f, left panel). The analysis of the metabolic products by high-performance liquid chromatography-mass spectrometric (HPLC-MS) showed that the organic acid level was heightened in the medium containing  $\text{Ca}_3(\text{PO}_4)_2$  compared to that in the medium without  $\text{Ca}_3(\text{PO}_4)_2$  (Fig. 1f, right panel). More specifically, the organic acids produced along with the addition of  $\text{Ca}_3(\text{PO}_4)_2$  included pyruvic acid, pyrrole-2-carboxylic acid, L-Leucine and parabanic acid. We thus speculated whether these organic acids conferred  $\text{H}^+$  to  $\text{Ca}_3(\text{PO}_4)_2$  and generated  $\text{HPO}_4^{2-}$  which supported  $\text{Ca}_3(\text{PO}_4)_2$  promotes *S. scabies* spore germination and hyphae growth, as observed in Fig. 1b, c. To test this hypothesis, we performed X-ray photoelectron spectroscopy (XPS) to analyze the phosphate content in the media. In the medium containing  $\text{Ca}_3(\text{PO}_4)_2$  but without *S. scabies* as a control, both  $\text{Ca}_3(\text{PO}_4)_2$  and  $\text{PO}_4^{3-}$  were detected. While the inoculation of *S. scabies* altered the main phosphate state to  $\text{HPO}_4^{2-}$ , the pure organic acids could generation of different phosphate states, and the major state being  $\text{HPO}_4^{2-}$  (Fig. 1g). Meanwhile, the number of *S. scabies* spore germination in medium containing  $\text{Ca}_3(\text{PO}_4)_2$  higher than medium containing  $\text{CaHPO}_4$  (Fig. 1b). This showed that  $\text{HPO}_4^{2-}$  could promote the spores germination. Meanwhile, the  $\text{Ca}_3(\text{PO}_4)_2$  in medium advanced the hyphae growth (Fig. 1c). These results confirmed our speculation. In the field, the high  $\text{HPO}_4^{2-}$  and insoluble phosphorus from HP could result in potato CS more serious. In view of the concentration of  $\text{Ca}_3(\text{PO}_4)_2$  in field is lower than medium, we thought that the severity of the CS is due to spores germination number increased.

Next, to identify the antagonistic bacteria against *S. scabies* for controlling CS, we performed multiple rounds of screening with soil samples collected from different potato production areas across China, with the procedure listed in Fig. S2a. In total, 988 bacterial strains with the ability to antagonize *S. scabies* were isolated by cultured-based methods. Among them, *Bacillus* accounted for the largest proportion, about 77%; and *Pseudomonas* accounted for 8.62% (Fig. 2a). These antagonistic bacteria have application potential for disease control. In our field test, high phosphate fertilizer

(HP) enhanced both the rate and the index of CS. One of reason for this is that  $\text{Ca}_3(\text{PO}_4)_2$  promotes rapid growth and reproduction of *S. scabies*. However, whether HP affects the bacteria abundance in soil is unclear, especially the antagonistic bacteria such as *Bacillus* and *Pseudomonas*. The change of bacteria composition in soil with LP, MP, and HP was analyzed by high-throughput sequencing. The highest relative abundance of genus is uncultured\_bacterium\_c\_Sub group\_6. The relative abundances of the two genera (*Bacillus* and *Pseudomonas*), with potential antibacterial activities, were significantly decreased with increasing amounts of phosphorous fertilizer (Fig. 2b). Each sample (LP, MP, and HP) includes 79,857 reads on average, matched with about 1843 operational taxonomic units (OTUs). At the family level, the relative abundance of antagonistic bacteria, including Rhizobiaceae, Pseudomonadaceae, Bacillaceae, Berkelbacteria and Streptomycetaceae, was analyzed. The proportions of Pseudomonadaceae and Bacillaceae dropped the most with increasing amounts of phosphorus fertilizer, with 93% and 37%, respectively (Fig. 2b, left panel). An obvious decrease was also seen in *Pseudomonas* and *Bacillus* at the genus level, and the abundance of *Serratia* was largely diminished due to the high level of phosphorus (Fig. 2b, right panel). From antagonistic strains, we selected three antagonistic strains (namely DX-9, XJ-3, and HZ-9) belonging to *Bacillus* and one (SC-2) from *Pseudomonas*, which displayed the best antagonistic effect with an obvious inhibition zone, for further study (Fig. S2b online). We found that the supplementation of  $\text{Ca}_3(\text{PO}_4)_2$  shrunk their inhibition zone in a dose-dependent manner (Fig. 2c, Fig. S3 online). The relationship between inhibition rate and  $\text{Ca}_3(\text{PO}_4)_2$  concentration were conducted (Fig. 2d). With the concentration of  $\text{Ca}_3(\text{PO}_4)_2$  increased, the inhibition rate of antagonistic bacteria decreased. These results suggest that a high concentration of  $\text{Ca}_3(\text{PO}_4)_2$  could reduce the effect of beneficial bacterial antagonistic to potato. This benefits the growth and reproduction of *S. scabies*.

$\text{Ca}_3(\text{PO}_4)_2$  is converted from insoluble phosphorus to  $\text{HPO}_4^{2-}$  and promotes the growth of *S. scabies*. HP reduces the abundance of antagonistic bacteria against *S. scabies* and high level of  $\text{Ca}_3(\text{PO}_4)_2$  also inhibits their antagonistic effect. We therefore hypothesized that the CS disease could be controlled by reducing the concentration of  $\text{Ca}_3(\text{PO}_4)_2$  in soil. To test this hypothesis on the correlation between phosphorus context and disease occurrence, one particular round of screening was conducted to select the phosphorus-dissolving bacteria. The 4 strains with the best antagonistic effect were inoculated into the phosphorus-dissolving medium, and then the transparent circle in plate was selected as phosphorus-dissolving bacteria. After this test, one phosphorus-solubilizing strain DX-9 (*Bacillus atrophaeus*) and two non-phosphorus-solubilizing strains XJ-3 (*Bacillus atrophaeus*) and HZ-9 (*Paenibacillus polymyxa*) were selected from the screened bacteria to conduct pot experiments (Fig. S4a online). CS occurrence and severity were much lower in all bacteria-treated potatoes, in comparison with non-treated ones but inoculated with *S. scabies* (Fig. 2e, Fig. S4b online). *Bacillus* sp. DX-9, which can solubilize phosphorus, conferred a better protection against *S. scabies* than non-phosphorus-solubilizing bacteria XJ-3 and HZ-9. The disease index treated with DX-9 was significantly lower than those treated with XJ-3 and HZ-9 (Fig. 2e). In  $\text{Ca}_3(\text{PO}_4)_2$  culture condition,  $\text{Ca}_3(\text{PO}_4)_2$  was decomposed into  $\text{HPO}_4^{2-}$  and  $\text{H}_2\text{PO}_4^-$  by phosphate-solubilizing bacteria DX-9. After the culture of non-phosphate-solubilizing bacteria XJ-3, the medium contained  $\text{Ca}_3(\text{PO}_4)_2$  and  $\text{PO}_4^{3-}$ , which was consistent with the components in the control (Ctrl) of uncultured bacteria (Fig. 2f). Given that  $\text{Ca}_3(\text{PO}_4)_2$  promotes the growth of *S. scabies*, the decomposed  $\text{Ca}_3(\text{PO}_4)_2$  slowed down the amount of the pathogen. Under  $\text{Ca}_3(\text{PO}_4)_2$  plate, *S. scabies* and DX-9 possibly competed with each other to obtain better growth conditions. This was observed by scanning electron microscope (Fig. 2g). The results implied that the antagonistic *Bacillus* with phosphorus-solubilizing functions in our test are more effective in controlling potato CS.

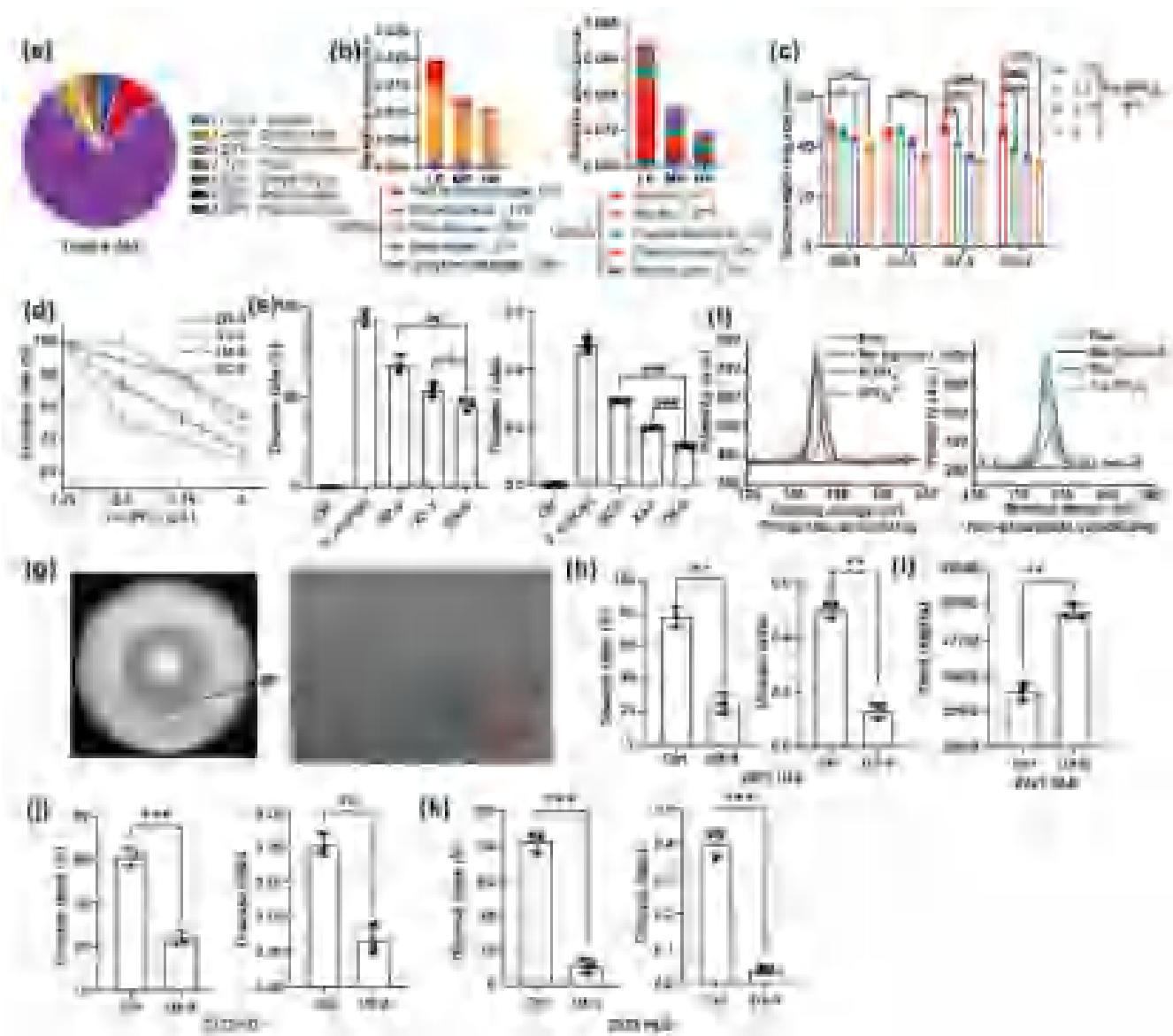


Fig. 2. Phosphate-solubilizing bacteria counteract CS more effectively than non-phosphate-solubilizing bacteria. (a) Taxonomic statistics of 988 antagonistic bacteria isolated from multiple potato fields in different areas in China. (b) The relative abundance and composition of the antagonistic bacteria in the near-rhizosphere soil were analyzed by high-throughput sequencing. (c)  $\text{Ca}_3(\text{PO}_4)_2$  diminishes the abundance of the antagonistic bacteria against *S. scabiei* and inhibits their antagonistic effect. (d)  $\text{Ca}_3(\text{PO}_4)_2$  inhibited the inhibition rate of antagonistic bacteria against *S. scabiei*. (e) The inhibitory effect towards CS disease of phosphate-solubilizing *Bacillus* sp. DX-9 and non-phosphate-solubilizing *Bacillus* spp. XI-3 and HZ-9. (f) The state of phosphorus in phosphate-solubilizing bacteria (DX-9) and non-phosphate-solubilizing bacteria (XI-3) after 7 days of growth in  $\text{Ca}_3(\text{PO}_4)_2$  medium was analyzed by XPS. (g) The growth of DX-9 and *S. scabiei* in control (without  $\text{Ca}_3(\text{PO}_4)_2$ ) and  $\text{Ca}_3(\text{PO}_4)_2$  media. (h–k) The *Bacillus* sp. DX-9 was applied in the field and the CS disease severity was assessed by disease rates and disease index, and the yield was measured. Pooled data from 3 plots are shown with mean  $\pm$  standard deviation and were analyzed by unpaired t test (\*\*\*  $P < 0.001$ , \*\*  $P < 0.01$ , \*  $P < 0.05$ ).

We then applied DX-9 to conduct the field experiments on farms in HLE and HD. Compared to the Ctrl, both disease incident rate and disease index in the field applied with DX-9 were significantly diminished (Fig. 2h, j, k). Accordingly, the tube yield in treated fields was dramatically increased (Fig. 2i). The field trials suggested that DX-9 can be utilized to control CS and increase the potato yield in large-scale productions.

Phosphorus fertilizer is conventionally regarded as a beneficial agent to plants. It is essential for crop growth and disease resistance [10]. Unexpectedly, we demonstrated here that a high amount of phosphorus fertilizer increases the incidence of potato CS (Fig. 1a). Likewise, Liu et al. [11] reported a similar conclusion that phosphorus addition is positively relevant to the severity of foliar fungal disease in Tibetan alpine meadows. The high phosphorus application leads to insoluble phosphorous (like  $\text{Ca}_3(\text{PO}_4)_2$ )

accumulation in soil [12], leading to increase of potato CS (Fig. 1a). We also tested whether rotation with non-Solanaceae crops for more than 5 years can alleviate CS. The incidence rate of CS was as high as 79% in a wasteland reclaimed in Erguna in Inner Mongolia with *Favorita* (Fig. S5 online), suggesting that simply crop rotation hardly solve the problem of CS.

In this study, the insoluble  $\text{Ca}_3(\text{PO}_4)_2$  promotes *S. scabiei* growth (Fig. 1c), resulting from *S. scabiei* secreting organic acids (Fig. 1f), which decompose insoluble  $\text{Ca}_3(\text{PO}_4)_2$  into  $\text{HPO}_4^{2-}$  (Fig. 1g). Phosphorus-solubilizing microorganisms can convert insoluble phosphorus compounds into soluble ones by producing organic acid, thus increasing the effectiveness of phosphorus absorption [13,14]. From our results, the culture medium of non-phosphate-solubilizing only contained  $\text{Ca}_3(\text{PO}_4)_2$  and  $\text{PO}_4^{3-}$  (Fig. 2f). But the culture medium of pure organic acids includes  $\text{HPO}_4^{2-}$  and  $\text{H}_2\text{PO}_4^-$

(Fig. 1g). We speculate that maybe non-phosphate-solubilizing microorganisms could not generate enough organic acids to decomposed the  $\text{Ca}_3(\text{PO}_4)_2$ . Therefore, *S. scabies* also has the capability to secrete organic acids like phosphorus-solubilizing microorganisms which facilitating the solubility of  $\text{Ca}_3(\text{PO}_4)_2$ .

The phosphorous-solubilizing bacterium, *Bacillus* sp. DX-9, was screened in this study which was proved to counteract CS disease, especially in the field experiments. The main mechanism is possibly involved in the bacteria's phosphorous-solubilizing ability on the release of insoluble  $\text{Ca}_3(\text{PO}_4)_2$  accumulation and competition with *S. scabies* in growth and absorbing phosphorus. Additionally, previous reports showed that three *Bacillus* spp were used to bio-control potato or radish CS in pots and fields [7,15]. Although these *Bacillus* had a good inhibitory effect on *S. scabies*, their inhibitory efficiencies were obviously lower than that of DX-9, reduced by 20%–40% vs. 50% in infection rates. Therefore, the higher resistance of *Bacillus* DX-9 to potato CS is considered to make it suitable for potential large-scale application in potato production.

In summary, potato CS caused by pathogenic *Streptomyces* such as *S. scabies* is notorious for greatly damaging potato production. Effective protection methods against *S. scabies* and the therapeutic strategies for CS have not yet been developed. Here, we found that high phosphorus fertilizer application strengthens CS symptom. *S. scabies* growing in  $\text{Ca}_3(\text{PO}_4)_2$  containing medium produces organic acids, which decompose insoluble  $\text{Ca}_3(\text{PO}_4)_2$  into  $\text{HPO}_4^{2-}$  and promote the spore germination and hyphae growth of *S. scabies*. Moreover,  $\text{Ca}_3(\text{PO}_4)_2$  diminishes both the abundance of antagonistic bacteria and their antagonistic effect against *S. scabies*, which consequently results in severe potato CS.

#### Conflict of interest

The authors declare that they have no conflict of interest.

#### Acknowledgments

This work was supported by the Key Area Research and Development Program of Guangdong Province in China (2020B0202010005), the Strategic Priority Research Program of the Chinese Academy of Sciences (XDA28030202), the Priority Research Program of Chinese Academy of Science (XDA24020104), and the Key Technologies R & D Program of Inner Mongolia, China (2021GG0300). We thank Qiannan Tang (Shanghai Jiao Tong University, Shanghai) for valuable scientific discussion help, Dongqing Cai (Donghua University, Shanghai) for help with X-ray photoelectron spectroscopy assay.

#### Author contributions

Naiqin Zhong conceived the project. Jingjing Cao and Zhiqin Wang designed the research. Jingjing Cao, Zhiqin Wang, Chengchen Li, Xiaobo Li, Lu Liu, Yonglong Zhao performed the research. Jingjing Cao, Zhiqin Wang, Pan Zhao analyzed the data. Jiahe Wu, Jingjing Cao, and Zhiqin Wang wrote the paper. Naiqin Zhong revised the manuscript.

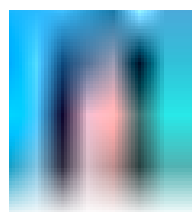
#### Appendix A. Supplementary materials

Supplementary materials to this short communication can be found online at <https://doi.org/10.1016/j.scib.2023.09.002>.

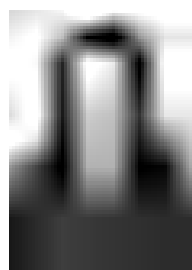
#### References

- [1] Stokstad E. The new potato. *Science* 2019;363:574–7.

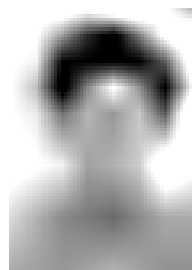
- [2] Zhang C, Yang Z, Tang D, et al. Genome design of hybrid potato. *Cell* 2021;184:3873–83.
- [3] Nguyen HP, Weisberg AJ, Chang JH, et al. *Streptomyces caniscaeii* sp. nov., which causes potato common scab and is distributed across the world. *Int J Syst Evol Microbiol* 2022;72.
- [4] Millard WA, Burr S. A study of twenty-four strains of *Aotino*myces and their relation to types of common scab of Potato. *Ann Appl Biol* 1926;13:495.
- [5] Kopecky J, Rapoport D, Sarikhani E, et al. Micronutrients and soil microorganisms in the suppression of potato common scab. *Agronomy* 2021;11:383.
- [6] Lambert DH, Powelson ML, Stevenson WR. Nutritional interactions influencing diseases of potato. *Am J Potato Res* 2005;82:309–19.
- [7] Lin C, Tsai CH, Chen PY, et al. Biological control of potato common scab by *Bacillus amyloliquefaciens* Ba01. *PLoS One* 2018;13:e0196520.
- [8] Marra LM, De Oliveira-Longatti SM, Soares CR, et al. The amount of phosphate solubilization depends on the strain, C-source, organic acids and type of phosphate. *Geomicrobiology* 2019;36:232–42.
- [9] MacDonald GK, Bennett EM, Potter PA, et al. Agronomic phosphorus imbalances across the world's croplands. *Proc Natl Acad Sci USA* 2011;108:3086–91.
- [10] Walters DR, Bingham, et al. Influence of nutrition on disease development caused by fungal pathogens: implications for plant disease control. *Ann Appl Biol* 2007;151:307–24.
- [11] Biessy A, Filion M. Biological control of potato common scab by plant-beneficial bacteria. *Biol Control* 2022;165:104808.
- [12] Li FR, Liu LL, Liu JL, et al. Abiotic and biotic controls on dynamics of labile phosphorus fractions in calcareous soils under agricultural cultivation. *Sci Total Environ* 2019;681:163–74.
- [13] Alori ET, Glick BR, Babalola OO. Microbial phosphorus solubilization and its potential for use in sustainable agriculture. *Front Microbiol* 2017;8:971.
- [14] Granada CE, Passaglia LMP, Souza EMD, et al. Is phosphate solubilization the forgotten child of plant growth-promoting rhizobacteria? *Front Microbiol* 2018;9:2054.
- [15] Han JS, Cheng JH, Yoon TM, et al. Biological control agent of common scab disease by antagonistic strain *Bacillus* sp. sunhua. *J Appl Microbiol* 2005;99:213–21.



Jingjing Cao is currently a research assistant at Institute of Microbiology, Chinese Academy of Sciences (CAS). Her research interests include agricultural microorganisms as well as prevention and control of soil-borne diseases.



Zhiqin Wang is currently a research assistant at Institute of Microbiology, CAS, and graduated from Ningxia University in 2019. Her research interests include agricultural microorganisms and prevention and control of soil-borne diseases.



Naiqin Zhong is a professor at State Key Laboratory of Plant Genomics, Deputy Director of Agricultural Microbial Advanced Technology Engineering Laboratory, Institute of Microbiology, CAS. She engages in the research on development and agricultural utilization of microbial resources.



## Article

# Effects of a Nanonetwork-Structured Soil Conditioner on Microbial Community Structure

Jingjing Cao <sup>1,2,†</sup>, Pan Zhao <sup>1,2,3,\*,†</sup> , Dongfang Wang <sup>4</sup> , Yonglong Zhao <sup>1,2</sup>, Zhiqin Wang <sup>1,2</sup>  
and Naiqin Zhong <sup>1,2,3,\*</sup>

- <sup>1</sup> State Key Laboratory of Plant Genomics, Institute of Microbiology, Chinese Academy of Sciences, Beijing 100101, China; caojingjing@im.ac.cn (J.C.); ylzhaoy97101@163.com (Y.Z.); wangzq1210@163.com (Z.W.)
- <sup>2</sup> Engineering Laboratory for Advanced Microbial Technology of Agriculture, Chinese Academy of Sciences, Beijing 100101, China
- <sup>3</sup> [The Enterprise Key Laboratory of Advanced Technology for Potato Fertilizer and Pesticide, Hulunbuir 021000, China](#)
- <sup>4</sup> College of Environmental Science and Engineering, Donghua University, Shanghai 201620, China; dfwang@dhu.edu.cn
- \* Correspondence: zhaop@im.ac.cn (P.Z.); nqzhong@im.ac.cn (N.Z.)
- † These authors contributed equally to this work.

**Simple Summary:** Soil is the basis for providing “fertile ground” for agriculture, including the growth of food and bioenergy crops. The nutrients needed by plants can be provided by chemical fertilizers. However, the heavy usage of fertilizers not only restricts crop production but also destroys the soil environment. Meanwhile, the soil microbiome, an indicator of soil quality that can affect plant growth and yield production, also changes. To solve this problem, a network-structured nanocomposite was prepared for use as a soil conditioner (SC). It was shown that this SC has a good ability to control nutrient loss; advance the agronomic traits of pepper, including growth and yield; improve soil physicochemical properties; and facilitate changes to the composition of microbial communities. With the view that the soil microbiome could develop soil function, we analyzed the correlation between network-structured nanocomposites and soil, microorganisms, and plants. In conclusion, nanonetwork-structured SC is an ideal technology that is effective for the promotion of crop growth and the improvement of the soil microbial community.



**Citation:** Cao, J.; Zhao, P.; Wang, D.; Zhao, Y.; Wang, Z.; Zhong, N. Effects of a Nanonetwork-Structured Soil Conditioner on Microbial Community Structure. *Biology* **2023**, *12*, 668. <https://doi.org/10.3390/biology12050668>

Academic Editor: Zed Rengel

Received: 15 March 2023

Revised: 25 April 2023

Accepted: 25 April 2023

Published: 28 April 2023



**Copyright:** © 2023 by the authors. Licensee MDPI, Basel, Switzerland. This article is an open access article distributed under the terms and conditions of the Creative Commons Attribution (CC BY) license (<https://creativecommons.org/licenses/by/4.0/>).

**Abstract:** Fertilizer application can increase yields, but nutrient runoff may cause environmental pollution and affect soil quality. A network-structured nanocomposite used as a soil conditioner is beneficial to crops and soil. However, the relationship between the soil conditioner and soil microbes is unclear. We evaluated the soil conditioner’s impact on nutrient loss, pepper growth, soil improvement, and, especially, microbial community structure. High-throughput sequencing was applied to study the microbial communities. The microbial community structures of the soil conditioner treatment and the CK were significantly different, including in diversity and richness. The predominant bacterial phyla were Pseudomonadota, Actinomycetota, and Bacteroidota. Acidobacteriota and Chloroflexi were found in significantly higher numbers in the soil conditioner treatment. Ascomycota was the dominant fungal phylum. The Mortierellomycota phylum was found in significantly lower numbers in the CK. The bacteria and fungi at the genus level were positively correlated with the available K, available N, and pH, but were negatively correlated with the available P. Our results showed that the loss of nutrients controlled by the soil conditioner increased available N, which improved soil properties. Therefore, the microorganisms in the improved soil were changed. This study provides a correlation between improvements in microorganisms and the network-structured soil conditioner, which can promote plant growth and soil improvement.

**Keywords:** nanocomposite microbial community; control nitrogen loss; soil properties; high-throughput sequencing

## 1. Introduction

Crop production is expanding at a remarkable rate because of increased demand for food, which is of particular necessity for the world's increasing population. Therefore, there is a need to produce more food from ever-limited land resources prepared by mixing attapulgite and PA. Soil is closely linked to agriculture-based economies, food security, and human health [1]. Plant growth and yield are limited by various factors, including soil, which is one of the most important parameters. Alterations to soil properties can result in enhanced plant production. Chemical fertilizer, which is widely used, can provide macro- and micronutrients in soil. Therefore, the application of fertilizer could promote the fast growth of crops and increase the yield of crops [2,3]. However, the amount of fertilizer used is constantly growing, and it is used in excess of what is needed. The use of extensive amounts of fertilizer has caused various negative effects on the environment; for example, excessive fertilizer use is a cause of greenhouse gas, water pollution, and soil degradation [4,5]. Synthetic nitrogen fertilizers, such as urea, contribute significantly to N<sub>2</sub>O emissions in the atmosphere [6]. Only 50–60% of nitrogen fertilizers are used by crops [7], and a portion of the rest runs off into water bodies [8]. Hence, it is important to supply nutrients to plants without damaging the environment [9]. In particular, there is an urgent need to develop fertilizers using innovative technology that can control the loss of nitrogen, increase the utilization efficiency of nitrogen, and decrease the level of environmental pollution [10].

Soil conditioners (SCs) are also called soil amendments and are an optional technology to increase crop production. An SC consists of materials that are added to soil that improve the soil conditions, especially by increasing nutrient availability [11], altering the soil physical structure [12], and stimulating microbial communities, which may enhance plant growth [13]. However, if an SC is added in excessive quantities, it may harm plant health, harm the environment, or enter the food chain [14]. Some materials used for controlled release are expensive [15], and for some materials, such as inhibitors of nitrification, actual field data are lacking [16]. Therefore, it is necessary for this new technology to not only increase the crop yield but also improve soil quality, and in particular, improve microbial communities.

In our previous study, a network-structured nanocomposite was fabricated that not only reduced the loss and effectively enhanced the utilization efficiency of nitrogen, but also modified the bacterial structure [17]. This nanocomposite, which could also be used as an SC, showed high biosafety and has the potential to reduce agricultural pollution. However, how SC causes changes in microbial communities and soil properties is unclear and needs to be studied further.

Soil microbes, including bacteria and fungi, are very important factors in an ecosystem. They are associated with many aspects of soil quality and health. Microbial communities provide different functions in soil, such as the cycling of nutrients, the degradation of various compounds, the promotion of plant growth, and the control of diseases [18,19]. A wide range of microbes have beneficial effects on soil. For example, arbuscular mycorrhizal (AM) fungi and plant-growth-promoting rhizobacteria (PGPR), including the nitrogen-fixing bacteria *Rhizobium* spp., belong to this group of beneficial microbes [19,20]. Microorganisms can mineralize soil nutrients to make them available for plants, bind soil particles together by secreting sticky polysaccharides, and coregulate the plant hormonal balance to help plants adapt to abiotic and biotic stressors [21,22]. Therefore, microbial diversity can be seen as a trait of soil quality that reflects nutrient efficiency and availability [23]. Soil microbial biomass, activity, and diversity are used as indicators of soil and ecosystem health [24].

High-throughput sequencing technology can provide deeper insight into the analysis of microbial communities [25,26]. It is an advanced method to research microbial communities because it can detect almost all species without culturing, even low-copy-number microorganisms [27]. Therefore, an in-depth analysis can be conducted from the sequencing results. This technique was used in this study to investigate microbial community changes in soil after applying SC.



Today, many studies have been reported regarding microbial community composition in soil [28]. However, the reason for the changes in microbial communities in soil treated by network-structured SC is not clear. Here, we addressed three aims: (1) evaluate the runoff of nutrients and plant growth caused by the nanonetwork-structured SC; (2) assess the effect of SC on the relationship between soil properties and microbial community structure; and (3) analyze the correlation between the network-structured SC and microorganisms. High-throughput sequencing technology was used to investigate the changes in microbial communities. The data could help understand the relationship between SC and microbial communities. We compared the changes in microbial communities at different taxonomic levels between a treatment in which the SC was administered and a treatment in which the soil was not amended. This study will help us understand the beneficial effects of our novel SC, which is a network-structured nanocomposite, on soil properties, microbial communities, and the growth of plants in greenhouses.

## 2. Materials and Methods

### 2.1. Preparation of Soil Conditioner and Leaching Assay

We purchased attapulgite powder (100–200 mesh) from Mingmei Co, Ltd. (Mingguang, China). Polyacrylamide (W. M., 5 million), urea (99%), and other chemicals were purchased from Shanghai Macklin Biochemical Co., Ltd. (Shanghai, China). Soil (20–50 mesh, pH 7.7, bulk density 1.5 g/cm<sup>3</sup>, available N 73.5 mg/kg, available P 87.8 mg/kg, available K 407.3 mg/kg) and sand (20–50 mesh, bulk density 1.5 g/cm<sup>3</sup>) were sourced from Donghua University (Shanghai, China). Deionized water was used in the experiments. Tap water was used in the greenhouse experiment.

The preparation of SC and the leaching assay were carried out as previously described [17] with minor modifications. In our previous study, the network-structured nanocomposite consisted of attapulgite, sodium humate, and polyacrylamide. Here, we modified the components. Sodium humate was removed. Briefly, SC with a weight ratio ( $W_{\text{attapulgite}}:W_{\text{polyacrylamide}} = 50:1$ ) was prepared by mixing attapulgite and PAM powders. Attapulgite and polyacrylamide in a weight ratio of 50:1 were mixed thoroughly to obtain the SC. A 50 g sand–soil mixture ( $W_{\text{soil}}:W_{\text{sand}} = 3:7$ ) was added to a 50 mL centrifuge tube with a 4 mm diameter hole at the bottom. A series of mixtures composed of urea (0.2 g) and SC (0.2 g, 0.4 g, 0.8 g) were prepared. Finally, the sand–soil mixture (10 g) covered the top of the SC–urea. A total of 50 mL of deionized water was added to the top of the system, and the urea concentration in the leachate was measured. The experiments were performed in triplicate.

### 2.2. Interaction Analyses of Soil Conditioner

A scanning electron microscope (SEM; SU8220, Hitachi High-Technologies Co., Tokyo, Japan) was used to study the morphology of the SC. A Fourier transform infrared spectrometer (FTIR, iS10, Nicolet Co., La Crosse, WI, USA) and a TTRIII X-ray diffractometer (XRD; TTRIII, Rigaku Co., Tokyo, Japan) were used to analyze the structure and chemical state of the SC. A thermogravimetric analyzer (DSCQ2000, TA Co., Valencia, CA, USA) was used for the thermal gravimetric analysis (TGA) and differential thermal analysis (DTA) of the SC. The Brunauer–Emmett–Teller (BET) specific surface areas of the attapulgite and SC were analyzed using an automatic surface area and a pore analyzer (BELSORP-max, MicrotracBEL, Osaka, Japan). The pore structure of the SC was measured based on the Barrett–Joyner–Halenda (BJH) method.

### 2.3. Greenhouse Experiment and Design

The greenhouse experiment took place in Qianbu County (36°55' N, 118°40' E), Shouguang City, Shandong Province, China. This site belongs to the Shouguang vegetable industry holding group, which is a well-known vegetable industry operator in China. To obtain a higher yield and quality of vegetables, many plastic greenhouses were constructed here over 10 years to grow cucumbers, pepper, tomatoes, and other vegetables.

The average annual temperature of the site is approximately 12.7 °C, the average annual amount of precipitation is approximately 593.8 mm, and the total amount of sunshine is 2548.8 h. The temperature of the studied greenhouse was kept at 28 °C to 30 °C, and the relative soil moisture was kept at approximately 50%. The soil's main properties were as follows: pH 7.84, available N 73.5 mg/kg, available P 87.8 mg/kg, available K 407.3 mg/kg, and organic matter 26.1 g/kg. The previous vegetable grown in our greenhouse was tomato. To investigate the soil and economic benefits that SC had on vegetable products, square pepper (*Capsicum annuum* L.) WeiLi was grown in the greenhouse in 2021.

Plots of 8.25 × 6.00 m<sup>2</sup> were used to plant the square peppers. There were three experimental treatments, and one control treatment was used based on the different amounts of SC used. Three replicates were designed for each treatment. A completely randomized experimental design was implemented. The SC needed to be mixed with base fertilizer evenly for use. The conditions were as follows: only fertilizer without soil conditioner, used as the control treatment (CK); 100 kg ha<sup>-1</sup> soil conditioner (SC1); 200 kg ha<sup>-1</sup> soil conditioner (SC2); and 400 kg ha<sup>-1</sup> soil conditioner (SC3). The base fertilizer was composed of urea (150 kg ha<sup>-1</sup>), ammonium phosphate (450 kg ha<sup>-1</sup>), and potassium sulfate (300 kg ha<sup>-1</sup>). All of these fertilizers were sprayed on the surface and tilled into the soil in a layer approximately 20 cm below the topsoil.

#### 2.4. Plant Growth, Soil Collection, and Properties

A total of 165 square pepper seedlings were transplanted into each plot. The plant distance and row distance were 50 and 60 cm, respectively. The management was the same for all treatments during the whole planting period. The experiment was performed in replicates, with 3 plots per treatment. The plant height and leaf chlorophyll content (measured using chlorophyll meter SPAD 502 Plus) were measured before the flowering stage. The fruit length and weight were measured at the end of the maturity stage. The number of earthworms in the soil was measured after the fruit stage.

Soil samples according to the "S" shape were collected after the fruit stage [29]. For the surface soil (0–20 cm) in each plot, five bulk plant soils (20 cm in depth, 5 cm in diameter) were collected. Then, the five bulk soils were pooled together to form a composite sample. There were three replicates for each treatment, so we obtained three composite samples. The soil samples were stored at 4 °C and used to analyze the soils' physiochemical properties. The following soil properties were measured: pH, total organic matter (OM), total salt (TS), available nitrogen (AN), available phosphorus (AP), available potassium (AK), soil capacity, porosity, and water retention. The soil properties were determined using previously reported methods [30].

The rhizosphere samples were collected with the soil samples in the meantime, according to the "S" shape in the previous method, with minor modifications [31,32]. The plant closest to each random point was selected. Therefore, each rhizospheric soil sample was obtained from 5 plants. The bulk soil was removed from the roots of the plants, and the soil that closely adhered to the surface of the root was collected. The soil samples were used for the microbial analysis. Three replicates were used for each treatment.

Student's *t*-test was carried out to analyze statistical significance with GraphPad Prism software (Version 9.3.0).

#### 2.5. High-Throughput Sequencing of the Microbe Communities and Data Processing

Total soil DNA was extracted using a TIANamp Soil DNA Kit (TIANGEN biotech (Beijing) Co., Ltd., Beijing, China). The purity and concentration were quantified at OD<sub>260/280</sub> nm using a NanoDrop spectrophotometer (Thermo Scientific, Waltham, MA, USA), and DNA was kept at –80 °C for further studies.

The purified DNA was amplified in the V3-V4 region of the bacterial 16S rRNA gene using the 341F (5'-CCTAYGGGRBGCASCAG-3')/806R (5'-GGACTACHVGGGTWTCTAAT-3') [33] primers and the ITS1-5F region of the fungal rDNA gene with ITS5-1737F (5'-GGAAGTAAAAGTCGTAACAAGG-3') and ITS2-2034R (5'-GCTGCGTTCTTCATCGATGC-

3') [34]. The PCR product was separated via 2% agarose gel electrophoresis and purified using a Qiagen Gel Extraction Kit (Qiagen, Germany). Library construction and sequencing were conducted by Novogene Co., Ltd. (Novogene Co., Ltd., Beijing, China, <https://www.novogene.com/>, accessed on 1 August 2022). The sequencing library was built using a TruSeq DNA PCR-Free Sample Preparation Kit (Illumina, San Diego, CA, USA). The library quality was assessed on the Qubit@ 2.0 Fluorometer (Thermo Scientific) and Agilent Bioanalyzer 2100 system. Then, the Illumina NovaSeq platform was used to sequence the library.

Paired-end reads were merged using FLASH (V1.2.7, <http://ccb.jhu.edu/software/FLASH/>, accessed on 1 August 2022) [35], and the splicing sequences were called raw reads.

The raw read data were submitted to Science Data Bank (<https://doi.org/10.57760/sciencedb.07079>, accessed on 1 August 2022. DOI:10.57760/sciencedb.07079).

To obtain high-quality clean reads, QIIME (V1.9.1, [http://qiime.org/scripts/split\\_libraries\\_fastq.html](http://qiime.org/scripts/split_libraries_fastq.html), accessed on 1 August 2022) was used to filter the raw reads following previous reports [36].

To obtain effective reads, the UCHIME algorithm ([http://www.drive5.com/usearch/manual/uchime\\_algo.html](http://www.drive5.com/usearch/manual/uchime_algo.html), accessed on 1 August 2022) was used to detect and remove chimera sequences [37].

## 2.6. Statistical Analysis

To cluster the clean reads into operational taxonomic units (OTUs) with  $\geq 97\%$  similarity, Uparse software (Uparse v7.0.1001, <http://drive5.com/uparse/>, accessed on 1 August 2022) was used. To annotate taxonomic information, bacterial OTUs were aligned against the SILVA SSUrRNA database (<https://www.arb-silva.de/>, accessed on 1 August 2022) [38]. The fungal OTUs were aligned against the UNITE database (<https://unite.ut.ee/>, accessed on 1 August 2022) [39] using QIIME software (Version 1.9.1, [http://www.drive5.com/usearch/manual/uchime\\_algo.html](http://www.drive5.com/usearch/manual/uchime_algo.html), accessed on 1 August 2022) [40].

To determine the phylogenetic relationships of different OTUs, MUSCLE software (Version 3.8.31, <http://www.drive5.com/muscle/>, accessed on 1 August 2022) was used [41]. The OTUs were standardized, and the subsequent diversity analysis was performed on the basis of the output normalized data.

To understand the changes in microbial structure, alpha diversity and beta diversity were analyzed. Alpha diversity was calculated by QIIME (Version 1.9.1). The results were displayed and differences were analyzed using R software (Version 2.15.3). A heatmap was drawn from the OTUs' relative abundance using the Vegan Package in R 2.4 (<https://cran.r-project.org/web/packages/vegan/>, accessed on 1 August 2022). QIIME software (Version 1.9.1) was used for the beta diversity analysis to calculate unweighted UniFrac distances, and R software (Version 2.15.3, R ade4 package and ggplot2 package) was used to draw graphs. The unweighted pair group method with arithmetic mean (UPGMA) was used for hierarchical clustering analysis. To reveal the variation in the microbial communities of the different samples, principal coordinate analysis (PCoA) was performed based on the unweighted UniFrac distances. Linear discriminant analysis (LDA) effect size (LEfSe) (<http://huttenhower.sph.harvard.edu/lefse/>, accessed on 13 March 2023) was used to detect the potential biomarkers by utilizing LEfSe software (LDA Score = 4). Student's *t*-test was used to calculate the differences between the different microbial abundance data. The statistical significance was set at  $p < 0.05$ .

Spearman correlation ( $p < 0.05$ ) and redundancy analysis (RDA) were used to explore the relationship between environmental factors and species richness and microbial community structure.

PICRUSt and FunGuild analyses were conducted to predict the functions of the microbial community. PICRUSt is a bioinformatics package that uses marker genes to predict the functional content of microorganisms [42]. The potential functions of each sample were predicted based on 16S rRNA sequencing data. A heat map of the Kyoto

Encyclopedia of Genes and Genomes (KEGG) level 3 functional pathways was created using the R package (Version 2.15.3). FUNGuild is a tool that can be used to obtain the ecological functions of fungi based on 18S or ITS rRNA sequencing data [43,44].

### 3. Results

#### 3.1. Effect of Controlling Urea Leaching Using the Soil Conditioner

As shown in Figure 1A, the effect of different amounts of SC on the leaching loss of urea in sand–soil mixtures was investigated. Figure 1B indicates that the concentration of urea in the leachate obviously decreased with increasing amounts of SC. An amount of 0.8 g SC was shown to have the best ability to control the loss of urea. This result illustrated that the SC possessed a strong ability to control the loss of urea and increased the utilization efficiency of urea.

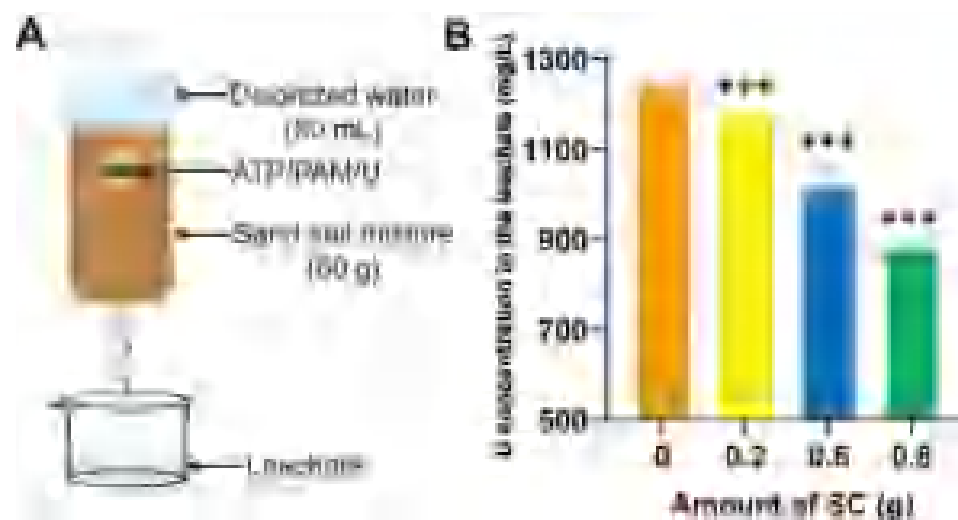


**Figure 1.** Leaching assay. (A) Schematic diagram of the leaching system. (B) Influence of the amount of SC on the leaching loss of urea from soil. Notes: ATP: attapulgite; PAM: polyacrylamide; U: urea. Asterisks indicate statistically significant differences, as determined by Student's *t*-test (\*\**p* < 0.001).

#### 3.2. Interaction Characteristics of Soil Conditioner Components

To elucidate the mechanism of the SC that enabled it to control loss ability, the microstructure of the SC system was investigated. As shown in Figure 2A,B, attapulgite nanorods aggregated to form several bunches due to the high surface activity and nanoscale effect. After it was loaded with polyacrylamide, the SC (Figure 2C,D) became a micro/nanonetwork due to bridging and netting effects, which were probably caused by the hydrogen bond between the attapulgite and polyacrylamide. Thus, it was shown that the SC possessed a high capacity to decrease the loss of urea because of the SC micro/nanonetwork.

XRD measurements were used to analyze the interactions in the SC system (Figure 3A). The characteristic peaks in the spectrum of the SC indicated that the attapulgite and polyacrylamide combined successfully. Additionally, no new characteristic peak was generated after the combination of attapulgite and polyacrylamide, indicating that intercalation did not exist between the attapulgite and polyacrylamide.

The interactions in the SC/urea system were analyzed by FTIR measurement (Figure 3B). Compared with the characteristic peaks of attapulgite and polyacrylamide, the peaks of the SC redshifted, and the intensity of the peaks decreased (Figure 3A). After the combination of SC and urea in the SC/urea system, the peaks of urea shifted, and the peak intensity decreased [17,45]. Meanwhile, the peak intensity of the SC clearly decreased in the SC/urea system. These results illustrated that hydrogen bonds probably linked the SC (-OH) and urea (N-H).

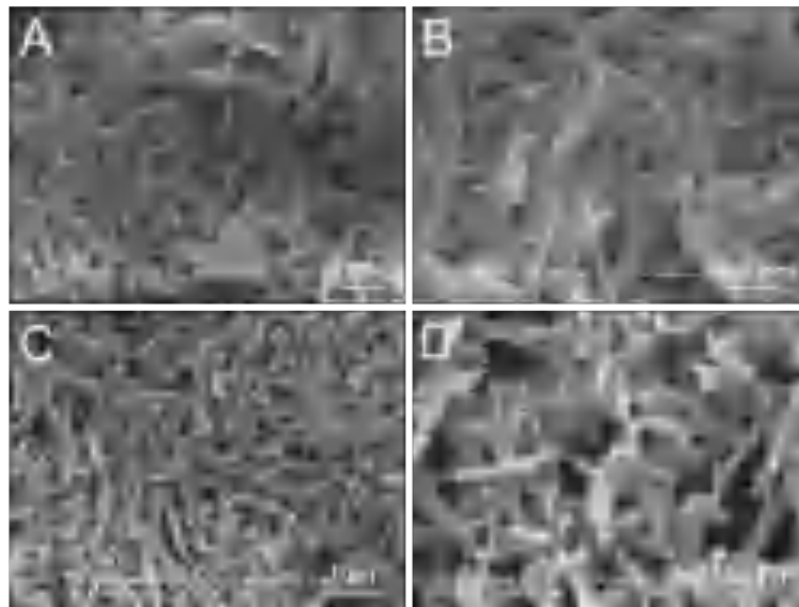


**Figure 2.** The microstructure of the SC as revealed by SEM with different magnifications: (A,B) attapulgite; (C,D) SC.

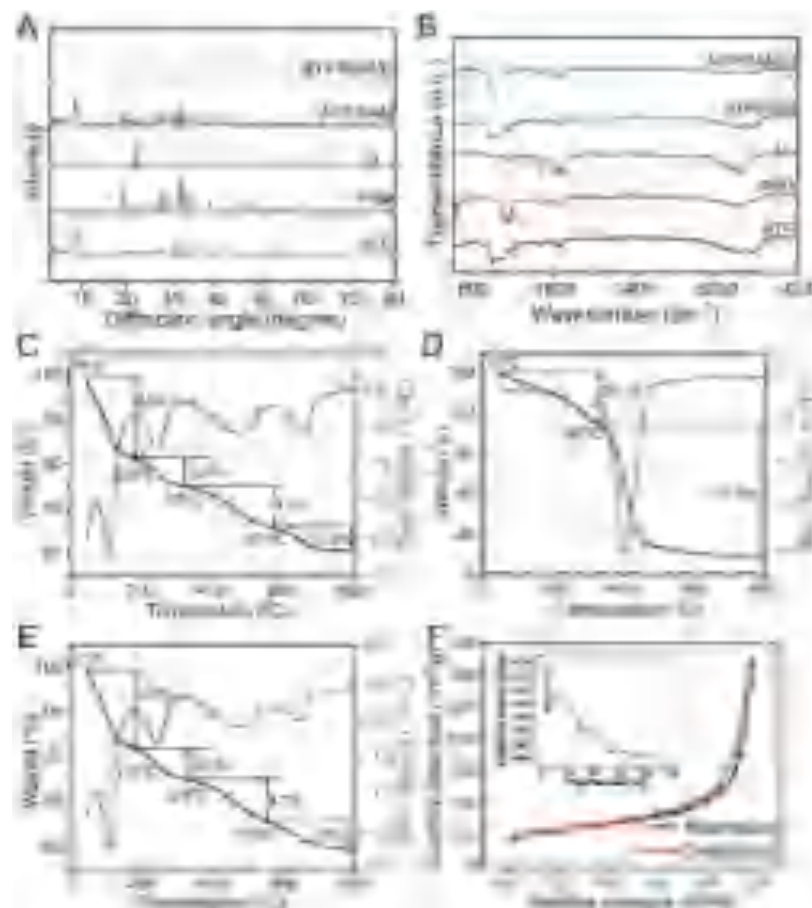


**Figure 3.** Interaction analyses of the SC system. (A) FTIR spectra of attapulgite. (B) XRD patterns of attapulgite, polyacrylamide, and SC. (C–E) TGA (black line) and DTA (blue line) curves of attapulgite, polyacrylamide, and SC. (F) N<sub>2</sub> adsorption–desorption isotherms of SC. (Inset) Pore size distribution of SC. Notes: ATP: attapulgite; PAM: polyacrylamide; U: urea; FTIR: Fourier transform infrared spectrometer; XRD: X-ray diffractometer; TGA: thermal gravimetric analysis; DTA: differential thermal analysis.



TG-DTA analysis was used to study the thermal stability of the attapulgite, polyacrylamide, and SC. As shown in Figure 3C, the initial weight loss region (51–183 °C) probably corresponded to water. The remaining weight loss regions (183–325 °C, 325–571 °C, and 571–800 °C) were probably due to organic matter degradation in the attapulgite. Figure 3D indicates that the initial weight loss (51–328 °C) may be due to water loss. The latter weight loss region (328–800 °C) was ascribed to the probable decomposition of polyacrylamide. As shown in Figure 3C–E, the weight loss regions of the SC were consistent with those of attapulgite because the SC contained 98% attapulgite. The weight loss values of attapulgite, polyacrylamide, and SC were 19.1% (Figure 3C), 92.7% (Figure 3D), and 19.5% (Figure 3E), respectively. These values illustrate that the SC included approximately 98% attapulgite, and thus, the results of the TG-DTA analysis were consistent with the weight ratio of attapulgite:polyacrylamide in the SC. As shown in Figure 3F, many pores appeared, with a size distribution of 5–60 nm in the SC (inset of Figure 3F, BJH method analysis) and a high BET specific surface area of 212.37 m<sup>2</sup>/g, which was beneficial for the adsorption of urea.

These results showed that the network structure of the SC linked the urea by hydrogen bonds.

### 3.3. Effects of Soil Conditioner on Plant Growth

A greenhouse test of the SC was performed in Shouguang City, Shandong Province, to illustrate the effects of the SC on pepper and soil. As shown in Figure S1, the SC had a significant positive influence on the growth of pepper. Figure 4A–D indicates that with the increase in the amount of SC, the plant height, SPAD, and fruit length and weight increased. These results suggested that SC can increase the yield of pepper.

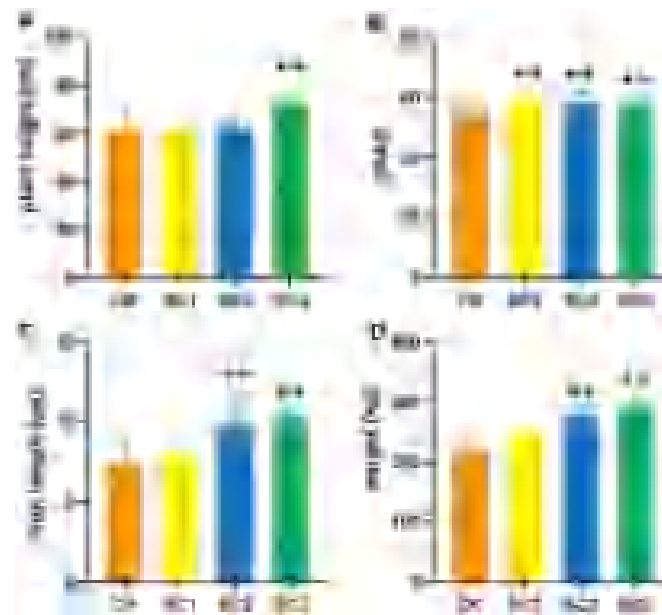


**Figure 4.** Effects of SC on plant growth. (A–D) Plant height, SPAD, and fruit length and weight when treated with different amounts of SC. Asterisks indicate statistically significant differences, as determined by Student's *t*-test (\*\*  $p < 0.01$ ).

### 3.4. Effect of Soil Conditioner on Soil Characteristics

Based on the characteristic analysis of the SC and plant growth, we selected SC3 to determine the characteristics of the soil. Table 1 shows that the SC3 soil had a high capacity to increase organic matter, available nitrogen, and potassium. This was probably because the SC possessed a nanonetwork structure that decreased the loss of nutrients and the degradation of organic matter. The SC reduced the soil capacity (4.55%) and increased the soil porosity (12.57%), indicating that the soil became loose after treatment with SC3 (Table 1). In addition, the water retention rate was enhanced by 10.04% compared to that

in the treatment without SC, probably because of the nanonetwork structure of the SC (Table 1).

**Table 1.** Soil properties after using SC.

Treatment	pH Value	Organic Matter (g/kg)	Total Salt (%)	Available Nitrogen (mg/kg)	Available Phosphorus (mg/kg)	Available Potassium (mg/kg)	Soil Capacity (g/cm <sup>3</sup> )	Porosity (%)	Water Retention Rate (%)
CK	7.86 ± 0.13	26 ± 3	0.10 ± 0.02	80 ± 7	95 ± 2	426 ± 10	1 ± 0.01	17.5 ± 0.34	23 ± 1
SC3	7.87 ± 0.06	26 ± 2	0.11 ± 0.02	97 ± 8	82 ± 4	438 ± 14	1 ± 0.01	19.7 ± 0.97	25 ± 2

The data are shown as the mean ± standard deviation (SD) of three replicates.

Earthworms can be used as indicators to assess soil quality [46,47]. The abundance of earthworms at a particular site can indicate high soil quality. We collected and recorded the number of earthworms in the different treatment soils. The number of earthworms increased gradually with the increase in the amount of SC, indicating that SC promoted the prevalence of earthworms (Figure S2A). After treatment with SC, there was a significant number of earthworms in the SC3 soil (Figure S2B).

These results illustrated that SC can be used as a promising soil conditioner in soil.

### 3.5. The Microbe Communities Identified Using High-Throughput Sequencing

Based on the results presented above, we selected SC3 to analyze the microbial communities via high-throughput sequencing.

#### 3.5.1. Alpha Diversity of the Microbial Community

After a quality control process, a total of 510,150 clean reads from the V3-V4 region of the 16S rRNA were obtained. The effectiveness of these reads was more than 91.08%. A total of 480,918 clean reads were obtained from the ITS1-5F region. The effectiveness of these reads was more than 96.07% (Table S1). The subsequent analysis was performed on the basis of the normalized data.

The Venn diagram (Figure 5) shows the differences between CK and SC3 at the OTU level. In the bacteria (Figure 5A), there were 1386 common OTUs in CK and SC3, but there were 289 unique OTUs in CK and 420 unique OTUs in SC3. In the fungi (Figure 5B), there were 517 common OTUs in CK and SC3, but there were 155 unique OTUs in CK and 178 unique OTUs in SC3. The results indicate that both the bacterial and fungal diversity in SC3 were richer than those in CK. The bacterial diversity changed more than the fungal diversity. This implies that the SC improved the soil environment to accumulate more bacterial and fungal diversity.

The rarefaction curves tended to be flat (Figure S3), suggesting that a reasonable number of individual samples were taken. The high Good's coverage values indicate that the sequencing depth was adequate for the community analysis (Table 2). Therefore, the data were sufficient for the analysis of microbial communities. Simultaneously, the rarefaction curves revealed that the microbial community richness in the SC3 samples was higher overall than that in the CK samples.

The alpha diversity indices indicated that there were significant differences between the CK and SC3 treatments (Table 2). Compared to the CK, the richness indices (including observed\_species, Chao1, and ACE) and diversity indices (including Shannon, Simpson, and PD\_whole\_tree) were higher in the treatment.

For bacteria, the Chao1, ACE, Shannon, and Simpson indices were significantly higher in SC3 than in CK. The observed\_species and PD\_whole\_tree were also higher in SC3 but were not significantly different from the CK. There was little difference in the fungi. Except for the Simpson index, which displayed no significant difference, the Chao1, ACE, Shannon, and PD\_whole\_tree were significantly higher in SC3 than in CK. From these results, the richness and diversity were significantly higher in SC3 than in CK in terms of both bacteria

and fungi. These results indicated that the diversity of the microbial community was affected by SC3.

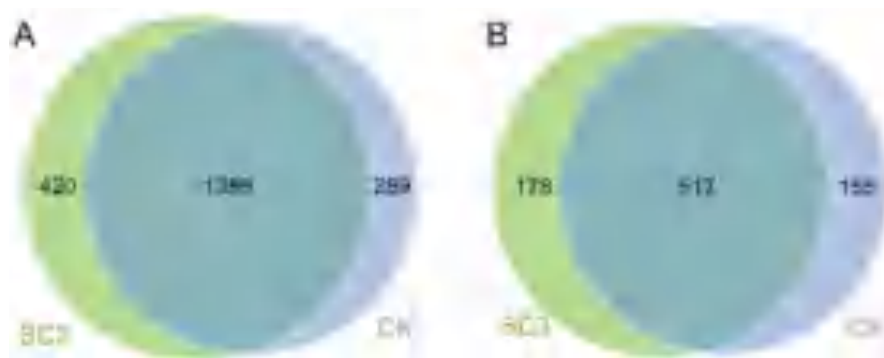


**Figure 5.** The OTUs between CK and SC3, displayed in a Venn diagram. (A) Bacteria, (B) fungi. The overlapping part shows the common OTU numbers.

**Table 2.** The alpha diversity between CK and SC3 treatments.

Treatment		Observed_Species	chao1	ACE	Shannon	Simpson	PD_Whole_Tree	Good's_Coverage
16S rRNA	CK	1240 ± 100	1336 ± 101	1346 ± 102	7.01 ± 0.19	0.96 ± 0.00	104 ± 4	0.996
	SC3	1550 ± 8	1614 ± 10 *	1604 ± 18 *	8.85 ± 0.01 ***	0.99 ± 0.00 ***	115 ± 2	0.997
ITS1-5F	CK	435 ± 22	459 ± 21	464 ± 20	4.93 ± 0.67	0.89 ± 0.07	125 ± 6	0.999
	SC3	521 ± 8 **	548 ± 11 **	549 ± 15 **	6.59 ± 0.10 *	0.97 ± 0.00	145 ± 5 **	0.999

The data are shown as the mean ± standard deviation (SD) of three replicates. Asterisks indicate statistically significant differences, as determined by Student's *t*-test (\*  $p < 0.05$ , \*\*  $p < 0.01$ , \*\*\*  $p < 0.001$ ).

### 3.5.2. Comparison of Bacterial Community Composition Based on 16S rRNA Sequencing

All bacterial sequences were classified at both the phylum and the genus level (Figure 6). The top 10 relative abundances of the bacteria in each sample at the phylum level were analyzed using the UPGMA clustering method (Figure 6A). The relative average abundance of the top 10 bacteria at the phylum level in the CK and SC3 treatments were Pseudomonadota (30.65 and 20.31%), Actinomycetota (23.75% and 17.23%), Bacteroidota (12.91% and 5.11%), Acidobacteriota (1.33% and 9.81%), Chloroflexi (2.35% and 4.62%), Gemmatimonadota (4.73% and 1.69%), Bacillota (2.36% and 3.15%), Myxococcota (2.25% and 2.54%), and Verrucomicrobiota (1.17% and 1.25%). The relative average abundance of unclassified\_Bacteria at the phylum level accounted for 14.02% in CK and 23.76% in SC3. The rest of the phyla were presented in “other phyla”, including Planctomycetota, Nitrospirota, and Cyanobacteria. Additionally, the average proportion of “other phyla” accounted for 4.49% in CK and 10.54% in SC3. The bacteria with high relative abundance, including Pseudomonadota, Actinomycetota, and Bacteroidota, were lower in SC3 than in CK. The abundance levels of Pseudomonadota, Actinomycetota, and Bacteroidota were significantly higher in SC3 than in CK ( $p < 0.05$ ). The UPGMA analysis results also showed similar samples in each treatment.

More details regarding the relative abundance of the bacterial community at the genus level are shown in a heatmap (Figure 6B). The top 35 bacteria at the genus level in the CK and SC3 treatments are presented. In SC3, *Sphingomonas*, *Blastococcus*, *RB41*, etc., were the dominant genera. In CK, the most representative genera were *Paeniglutamicibacter*, *Luteimonas*, *Pedobacter*, etc. The relative abundance levels of *Massilia*, *Sphingomonas*, *Aeromicrobium*, etc., were higher in SC3 than in CK. Meanwhile, the levels of unclassified *Gemmatimonadaceae*, *Luteimonas*, *Galbitalea*, etc., were higher in CK than in SC3. Some genera had similar average relative abundance levels between CK and SC3, such as *Flavisolibacter* (0.72% and 0.62%) and *Nocardioideis* (0.84% and 0.85%). This suggests that the changes in relative abundance occurred after the SC3 treatment. These changes may have occurred because the SC modified the soil ecosystem.



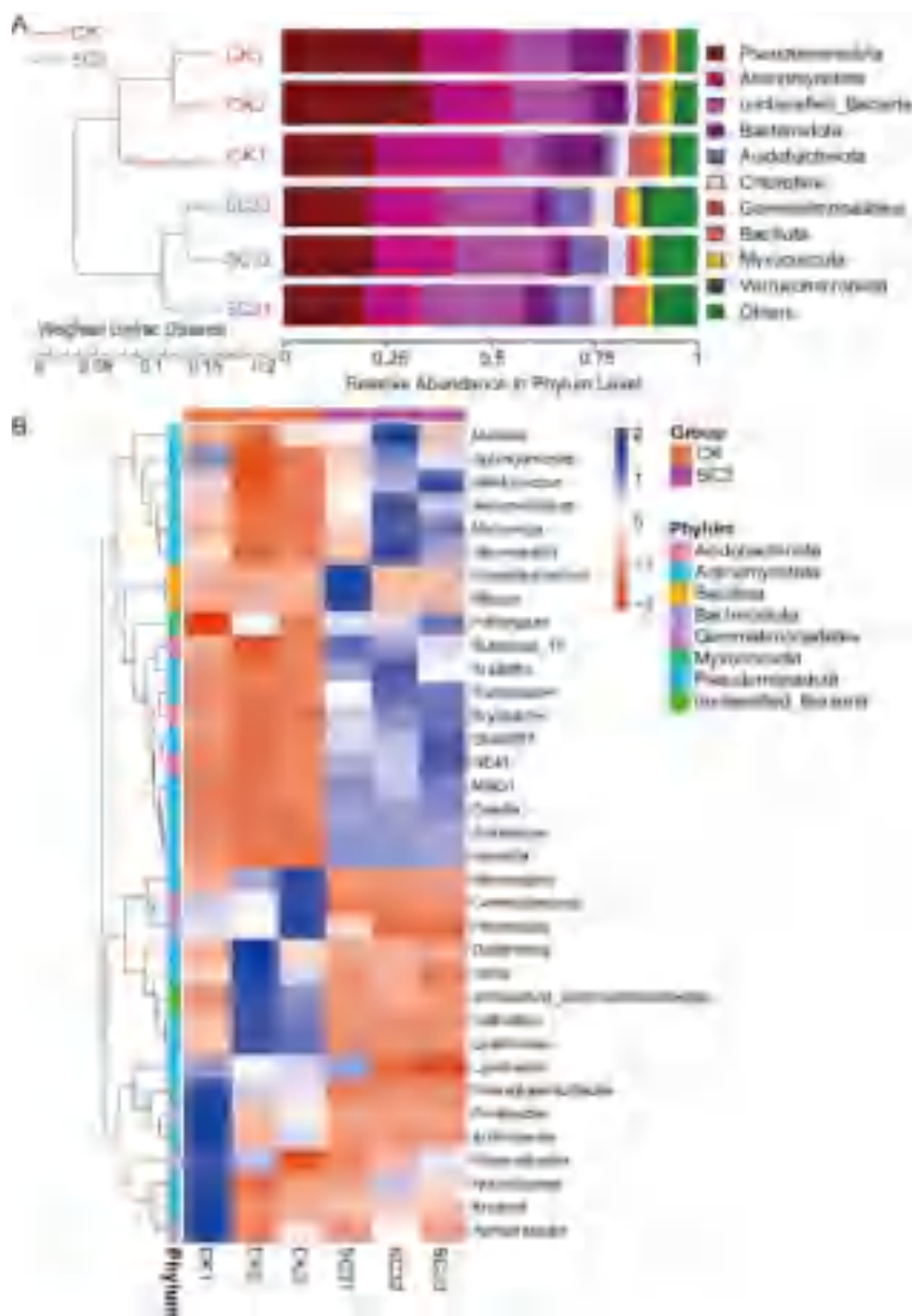


**Figure 6.** Composition and relative abundance of bacterial communities. (A) UPGMA clustering analysis showed the top 10 relative abundance levels of the bacterial community in each sample at the phylum level. (B) Clustering heat map of the relative abundance levels of the top 35 bacteria at the genus level in each sample. The “Z” value corresponding to the heat map is described by the color intensity from 2 to −2. The color gradient shifted from blue to red (from low to high abundance). CK1-CK3 represent the 3 replicates of soil without soil conditioner; SC31-SC33 represent the 3 replicates of soil with 400 kg ha<sup>-1</sup> soil conditioner.

Principal coordinate analysis (PCoA) was performed to reveal the variation in the bacterial communities among the different samples (Figure S4A). The PCoA significantly

separated the CK samples from the SC3 samples, indicating that the two treatments had their own specific characteristic microbial community. The heat map of beta diversity also indicated that the microbial communities of the samples were clearly different between CK and SC3 (Figure S4B). Both the PCoA and heatmap results showed samples that were similar in their bacterial compositions in each treatment. The bacterial compositions of the samples in the CK were different from those in SC3. The results were also the same as the results of the UPGMA analysis (Figure 6A).

To examine the taxonomic bacteria with significant abundance differences between CK and SC3, linear discriminant analysis effect size (LEfSe) was used for biomarker analysis. The results showed that there were 35 distinct bacterial taxa with LDA values greater than 4.0 (Figure 7A). In SC3, three phyla, five classes, four orders, six families, seven genera, and eight species were enriched. Meanwhile, one genus (*Luteimonas*) and one species (*Luteimonas mephitis*) were enriched in the CK. LEfSe analysis indicated that SC3 influenced the bacterial composition of the soil.

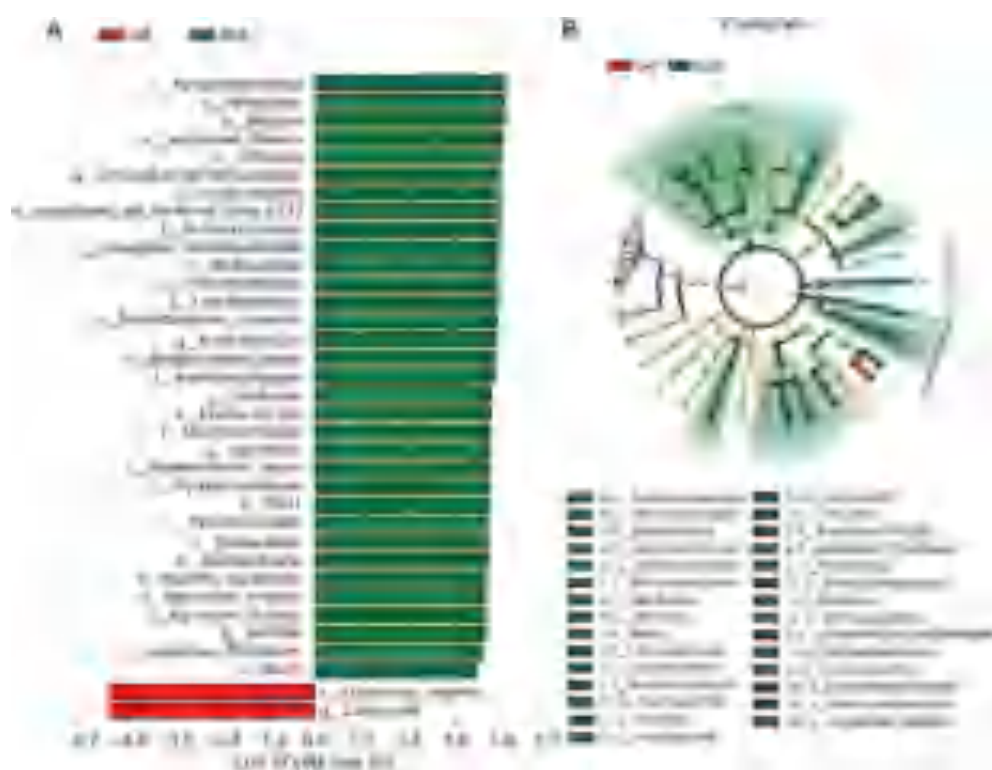


**Figure 7.** LEfSe analysis of the difference in bacterial abundance between CK and SC3. (A) LDA score between CK and SC3. The column length indicates the effect size of the bacterial lineages. (B) The cladogram of bacterial communities with differences between CK and SC3. The proportion of bacterial abundance is indicated by the circle's diameter. Red and green nodes: bacterial taxa that play a vital role in CK and SC3, respectively. Yellow: nonsignificant.

### 3.5.3. Comparison of Fungal Community Composition Based on ITS Sequencing

The relative abundance of the fungi at the phylum and genus levels is shown in Figure 8. The top 10 relative abundance levels of the fungal community in each sample at the phylum level were analyzed using the UPGMA clustering method (Figure 8A). The Ascomycota phylum was the most abundant in the two treatments (50.54% and 51.83%). The abundance of the Mortierellomycota phylum was significantly lower in CK than in SC3 (3.14% and 17.4%). Additionally, the abundance of the Basidiomycota phylum was significantly higher in the CK (14.17% and 9.42%). The average proportion of "other phyla" accounted for 30.56% in CK and 19.00% in SC3. The UPGMA analysis results also showed similar samples in each treatment.

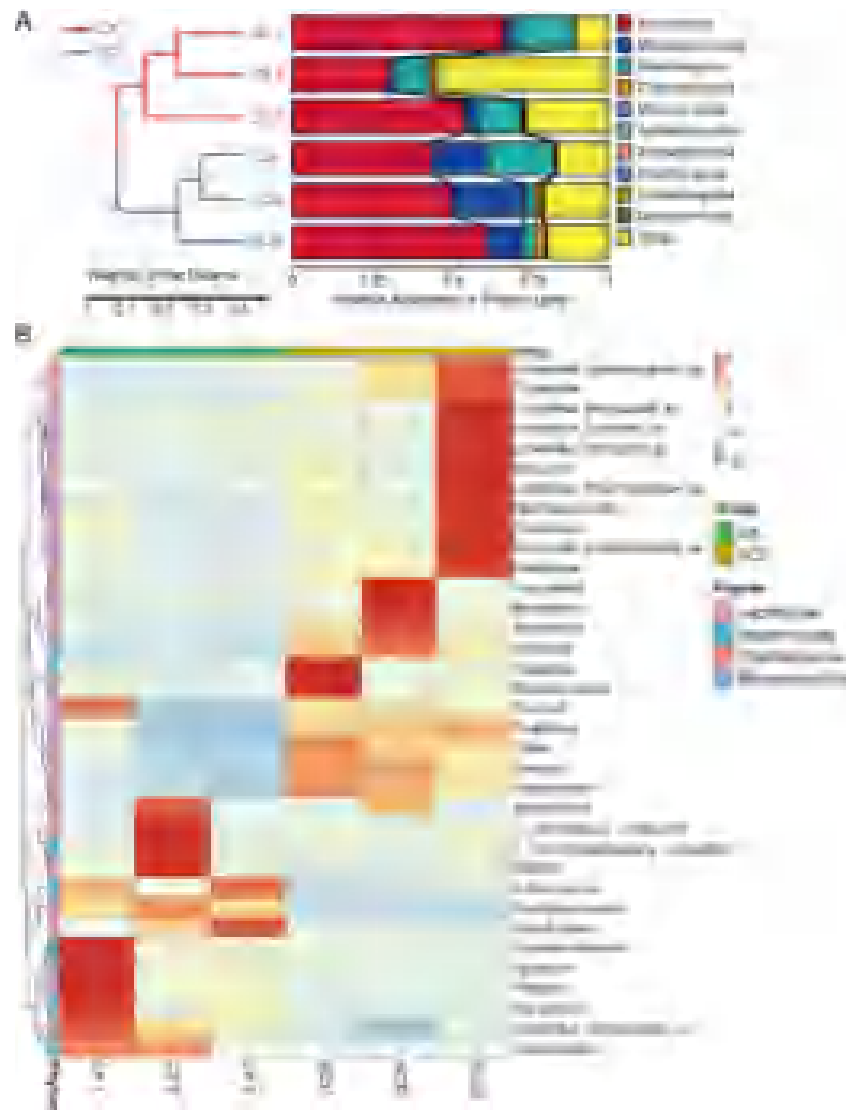


**Figure 8.** Composition and relative abundance of fungal communities. **(A)** UPGMA clustering analysis: the top 10 relative abundance levels in each sample at the phylum level. **(B)** Clustering heat map of the relative abundance of the top 35 fungi at the genus level in each sample. The corresponding value of the heat map is the “Z” value, depicted by the color intensity, ranging from 2 to  $-2$ . The gradient of color shifts from blue (low abundance) to red (high abundance). CK1-CK3 represent the 3 replicates of soil without soil conditioner; SC31-SC33 represent the 3 replicates of soil with  $400 \text{ kg ha}^{-1}$  soil conditioner.

The relative abundance levels of the top 35 fungi at the genus level in CK and SC3 are presented as a heat map (Figure 8B). In contrast to SC3, *Pseudogymnoascus*, *Thelebolus*, *Botryotrichum*, etc., were the dominant genera in the CK. In the SC3, *Mortierella*, *Thysanorea*, *Calypotella*, etc., were the dominant genera. The abundance of some fungi in SC3 was higher than that in CK, including *Alternaria*, *Acremonium*, *Mortierella*, etc. The unclassified *Eurotiales*\_sp. was only found in the SC3. This suggested that SC3 changed the relative abundance of fungi.

The variation in and relationship between fungal communities were analyzed using PCoA (Figure S5A). There was 68.72% variance in the first principal coordinate axis (PCo1) and 18.19% variance in the second principal coordinate axis (PCo2). The relationships between different samples were also the same as those shown in the UPGMA analysis (Figure 8A). The heat map of beta diversity also indicated that the fungal communities of the samples were obviously different between CK and SC3 (Figure S5B).

LEfSe was conducted to identify the taxa with significant differences between CK and SC3 (Figure 9). The results showed that there were 46 fungal taxa with distinguishable differences with LDA values greater than 4.0 (Figure 9A). From the LEfSe analysis, one phylum, two classes, five orders, five families, seven genera, and seven species were enriched in SC3, while three classes, four orders, four families, four genera, and four species were enriched in CK. These results indicated that fungal compositions in soil are influenced by the use of SC3.

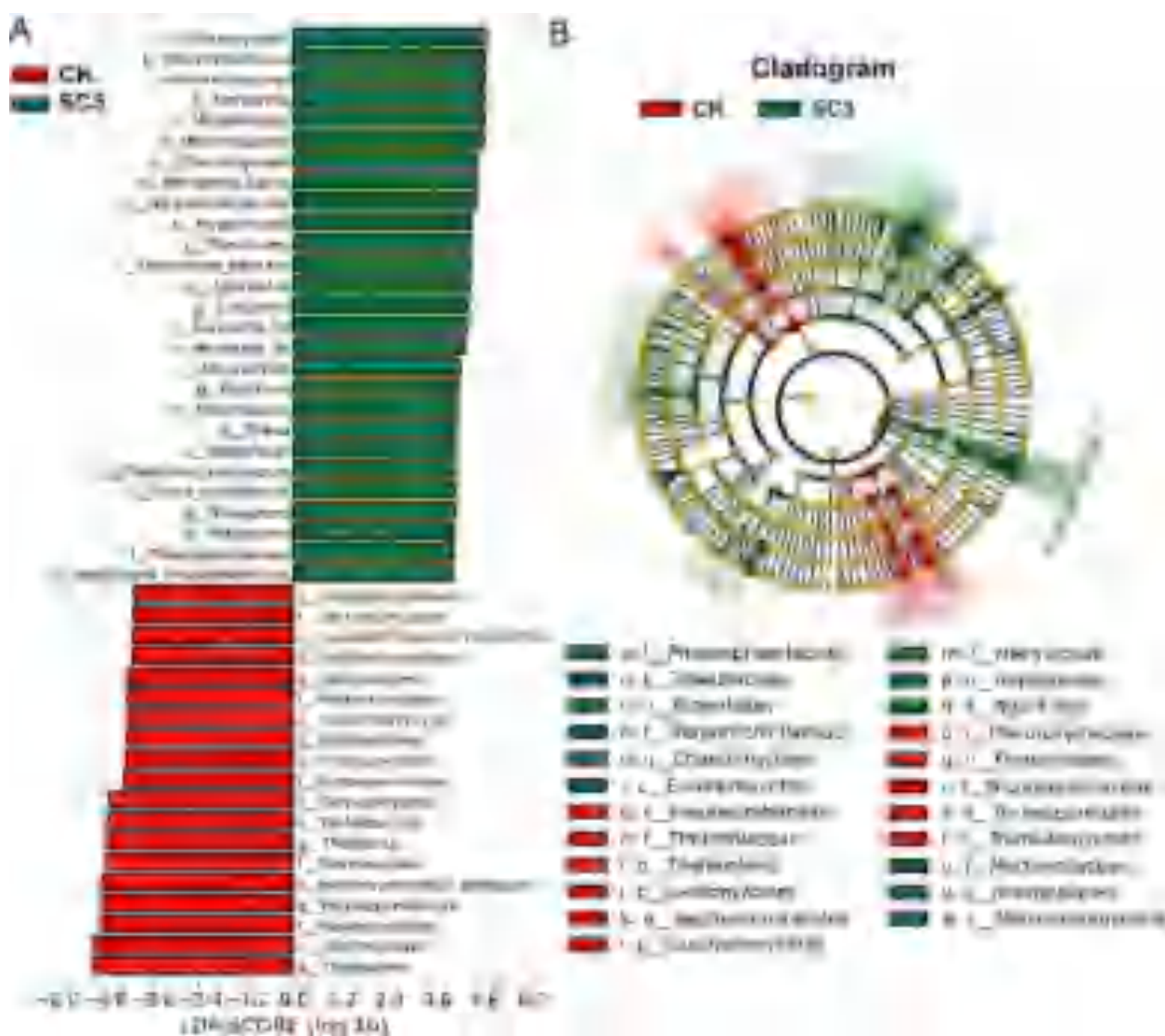


**Figure 9.** LEfSe analysis of fungal abundance between CK and SC3. (A) LDA score between CK and SC3. The column length indicates the effect size of the bacterial lineages. (B) The cladogram of fungal communities with differences between CK and SC3. The proportion of bacterial abundance is indicated by the circle’s diameter. Red and green nodes: fungal taxa that play a vital role in CK and SC3, respectively. Yellow: nonsignificant.

### 3.5.4. Correlation Analysis between Microbes and Environmental Parameters

Redundancy analysis (RDA) was conducted to identify the relationships between microbial compositions at the genus level and environmental factors (Figure 10). Four parameters—pH, available phosphorus (AP), available potassium (AK), and available nitrogen (AN)—were selected for RDA. Organic matter content was not included in our analysis because available nutrient loss could be controlled by SC3. We wanted to find

the relationships between soil properties altered by SC3's control of nutrient loss and the changes in microbial communities.

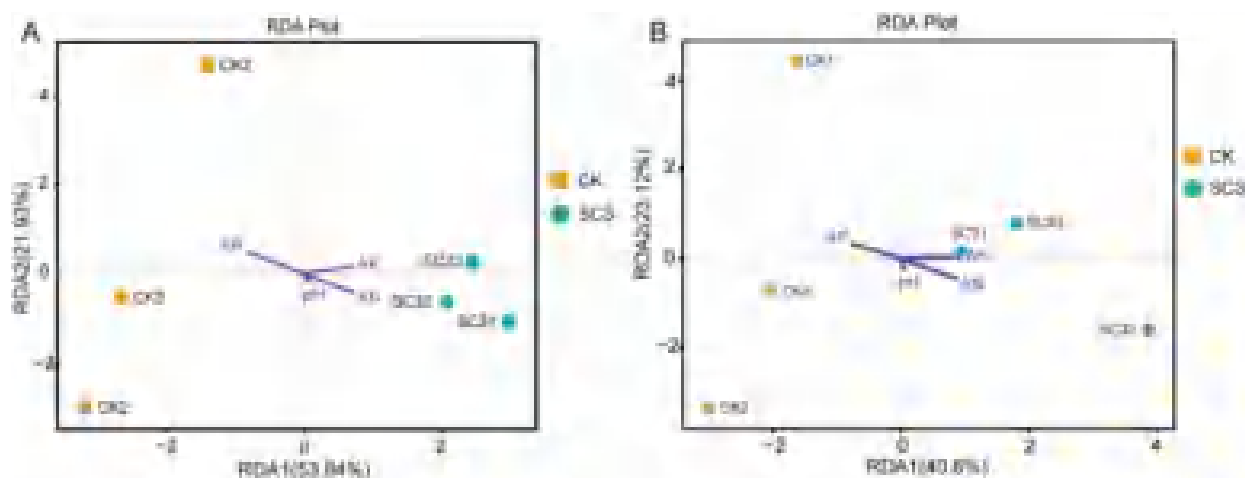


**Figure 10.** Redundancy analysis (RDA) of microbial genera and soil physical and chemical properties. (A,B) RDA of bacterial and fungal communities and environmental variables. The arrow length in the RDA plot corresponds to the strength of the correlation between a variable and the community structure. CK1–CK3 represent the 3 replicates of soil without soil conditioner; SC31–SC33 represent the 3 replicates of soil with  $400 \text{ kg ha}^{-1}$  soil conditioner.

The physicochemical properties of the soils are shown in Table 1. The AN and AK contents were higher in SC3 than in CK, while the AP content was lower in SC3 than in CK. SC3 had little effect on the soil pH value.

The compositions of bacterial genera and fungal genera in the SC3 samples were both positively correlated with AK, AN, and pH. Meanwhile, the microbial community structures in CK samples, both bacterial genera and fungal genera, were positively correlated with AP (Figure 10). Changes in microbial communities relied on the AN, AK, and AP. The results showed that microbial communities are positively correlated with AN and AK, and they may be affected by SC.

Spearman correlation analysis was used to study the correlations between environmental variables and the microbial abundance in genera (Figure 11). In terms of bacterial abundance (Figure 11A), *Massilia* and *Blautia* were positively correlated with AN, while *Pontibacter* and *Paeniglutamicibacter* were negatively correlated. *Truepera*, *Flaviaesturariibacter*, *Gemmatimonas*, *Arthrobacter*, and *Paeniglutamicibacter* were positively correlated with AP, while *Massilia* and *Blautia* had negative correlations. *Kribbella*, *Aeromicrobium*, *Massilia*, and *Blautia* were positively correlated with AK, but *Truepera*, *UTBCD1*, and *Paeniglutamicibacter* were negatively correlated with AK. In terms of fungal abundance (Figure 11B), *Myrothecium*, *Acremonium*, and *Mortierella* were positively correlated with AN, but unclassified *Leotiomyces*\_sp., *Trichosporon*, *Leucosporidium*, and *Cutaneotrichosporon* were negatively correlated. Unclassified *Leotiomyces*\_sp., *Leucosporidium*, *Solicoccozyma*, and *Thelebolus* were positively correlated with AP, while *Titaea* had a negative correlation. *Myrothecium*, *Acremonium*, and *Titaea* were positively correlated with AK, but unclassified *Leotiomyces*\_sp. and *Leucosporidium* had negative correlations with AK.

These results showed a correlation between AN, AK, AP, and the microbial community. The positive correlation between AN, AK, and the microbial community may be caused by the SC.



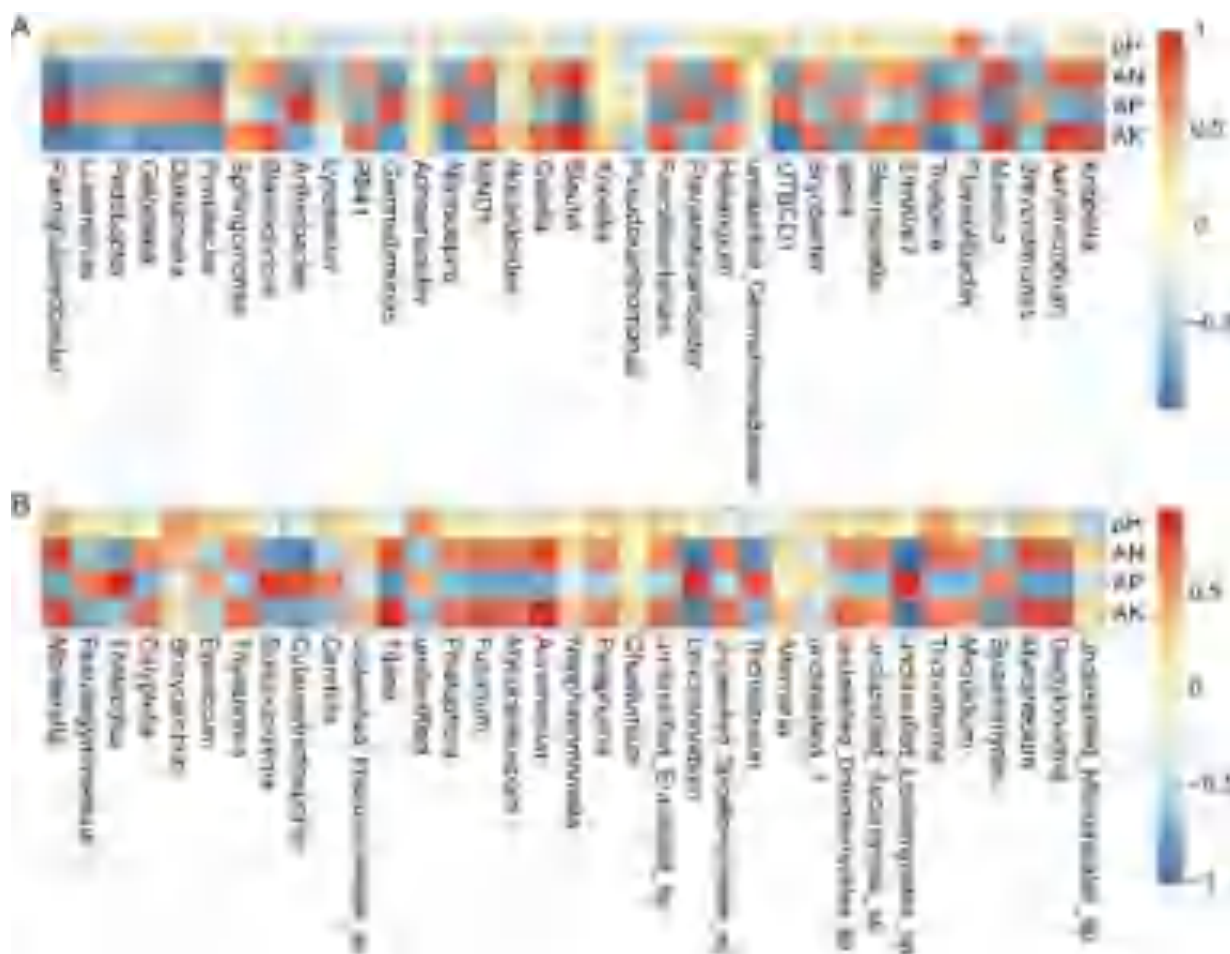


**Figure 11.** The heatmap of Spearman's rank correlation. (A,B) The correlation between the richness of bacterial and fungal genera and environmental factors, where the “r” value is between  $-1$  and  $1$ ,  $r < 0$  is a negative correlation, and  $r > 0$  is a positive correlation. Asterisks indicate statistically significant differences, as determined by Student's *t*-test (\*  $p < 0.05$ , \*\*  $p < 0.01$ ). The gradient of color shifts from blue to red (from low to high abundance).

### 3.5.5. Predicted Functional Gene Analysis for Microbial Communities

PICRUSt [42] was used to predict functional analyses for bacterial communities of all samples. A heat map of the 35 KEGG (level-2) pathways with relatively high abundance levels is shown in Figure 12A. KEGG pathways including replication and repair, nucleotide metabolism, signaling molecules and interaction, and cancers were significantly higher in abundance in the CK, while energy metabolism, metabolism of terpenoids and polyketides, metabolism of cofactors and vitamins, and endocrine system were significantly higher in abundance in the SC3 (Figures 12A and S6A).

FUNGuild [43] was used to predict functional analyses for fungal communities in all of the samples. The relative abundance levels of 26 fungal functional guilds (including others), such as Animal\_Pathogen-Soil\_Saprotroph, Endophyte-Plant\_Pathogen-Wood\_Saprotroph, and Plant\_Pathogen-Soil\_Saprotroph-Wood\_Saprotroph, were detected (Figure 12B). The “Animal\_Pathogen-Soil\_Saprotroph” guild had a significantly higher abundance level in the CK. However, the “Endophyte-Plant\_Pathogen-Wood\_Saprotroph” and “Plant\_Pathogen-Soil\_Saprotroph-Wood\_Saprotroph” guilds had relatively high abundance levels that increased significantly in SC3 (Figure 12B and Figure S6B). The predicted functional gene analyses for microbial communities from the KEGG (level-2) pathways and guilds were significantly different in CK compared with SC3.

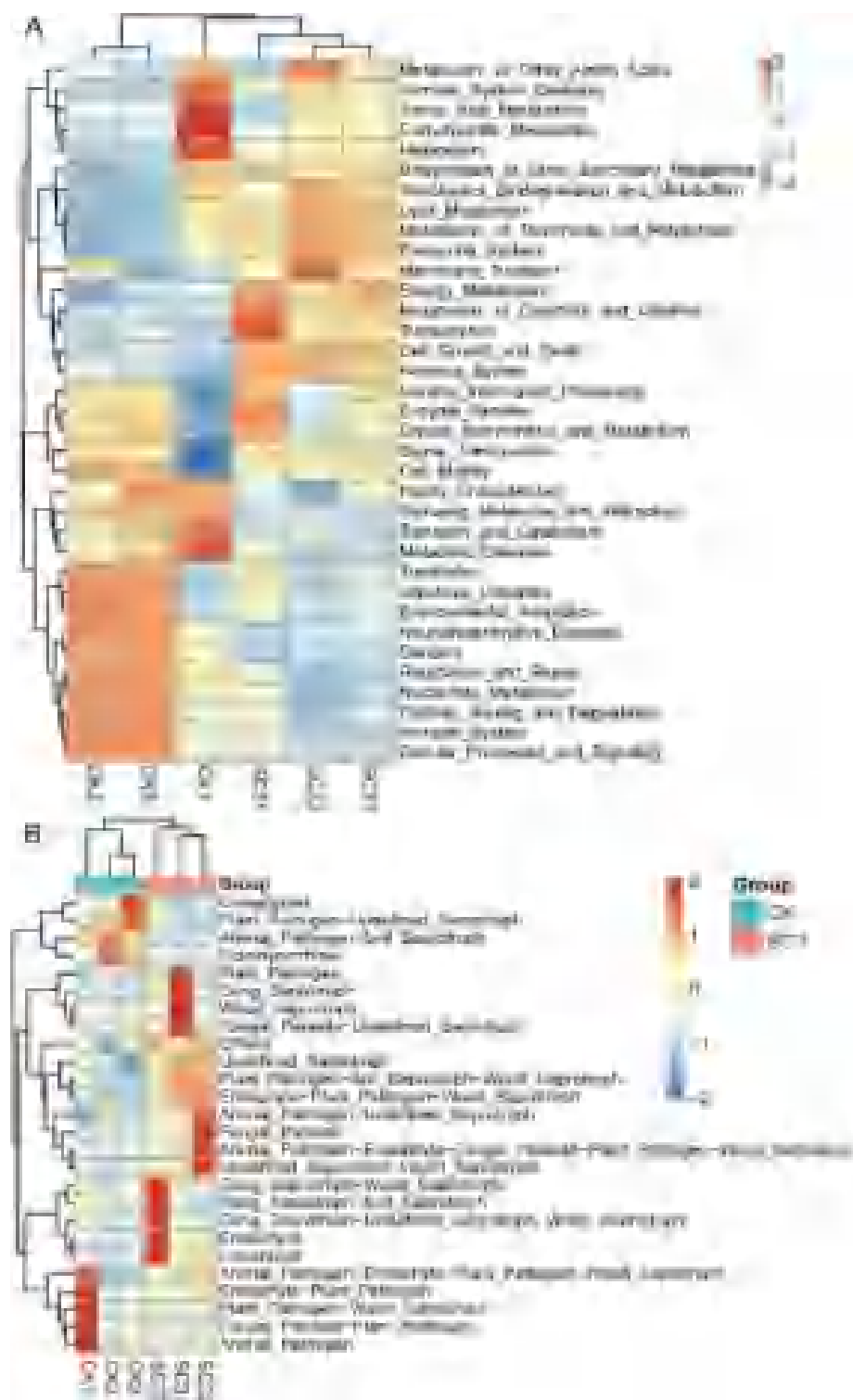


**Figure 12.** Clustering heat map of the functional pathway analyses. (A) The relative abundance of KEGG (level-2) pathways for bacterial communities of all samples. The KEGG pathways are indicated by a gradient of color from blue (low abundance) to red (high abundance). The corresponding value of the heat map is the “Z” value. (B) The relative abundance of predicted fungal functions. The corresponding value of the heat map is the “Z” value when the relative abundance was normalized. The gradient of color shifts from blue (low abundance) to red (high abundance). CK1-CK3 represent the 3 replicates of soil without soil conditioner; SC31-SC33 represent the 3 replicates of soil with 400 kg ha<sup>-1</sup> soil conditioner.

## 4. Discussion

Fertilizers represent an indispensable factor in current agriculture to sustain soil fertility and crop productivity. However, the nutrient use efficiency of fertilizers is constantly low [48]. Fertilizers left in soil due to overuse and runoff can cause a variety of environmental problems, including the pollution of water bodies and changes in soil quality [49]. The application of nanotechnology can promote the nutrient use efficiency of crops and decrease the negative effects of synthetic fertilizers in agriculture. Due to their wide-ranging environmental applications, a number of nanomaterials have been used in agriculture [50–52]. As has been reported, the application of SC is a strategy that can be used to increase crop yields and improve the quality of soil [11,53,54]. In a previous study, it was shown that a fertilizer synergist could effectively inhibit hydrolysis, reduce loss, and enhance utilization efficiency [17]. In this study, we generated a nanonetwork-structured SC composed of attapulgite and polyacrylamide and investigated the effect of the SC on pepper agronomic traits, soil properties, and the structure of microbial communities. Based on the results, we assessed and evaluated the effect on the change in microbial communities after nanomaterials were applied to control the loss of nitrogen. To our knowledge, this is the first report regarding the ability of this nanonetwork-structured SC, composed of attapulgite, to alter microbial communities. Our study provides an understanding of the mechanism that allows network-structured nanocomposites to alter microbial structures.

### 4.1. Material Characteristics of Nanostructured Soil Conditioner and Characteristics of Reducing Nitrogen Loss

We determined the effect of different amounts of SC on the control of the loss of nutrients and observed the microstructure of the SC. The amount of SC influenced the control loss efficiency (Figure 1). In view of the high surface activity and nanoscale effect, attapulgite rods tended to form several bunches with abundant small pores among the rods. After the addition of polyacrylamide, a micro/nanonetwork was formed through bridging and netting effects, probably driven by the existence of hydrogen bonds between attapulgite and polyacrylamide (Figures 2 and 3A,B). Urea could be loaded into the network to decrease the level of loss. This result is the same as our previous research regarding the microstructure of a fertilizer synergist. Our FTIR spectroscopy and XRD analyses indicated that the H bonds likely played a key role in the formation of the SC network. The thermogravimetric analysis (TGA) and differential thermal analysis (DTA) of the SC (Figure 3C–F) revealed that SC underwent a three-stage thermal decomposition process. The difference between the SC and fertilizer synergist is that sodium humate was mixed in the fertilizer synergist. Sodium humate is an efficient urease inhibitor and can be loaded into the small pores to form part of the fertilizer synergist. From previous research, it can be seen that the absence of sodium humate has no effect on the micro/nanonetwork structure of the SC [17]. These results indicated that the network structure linked by H bonds between polyacrylamide and attapulgite has a good ability to store nutrients and control nutrient loss.

### 4.2. Effect of SC on Soil Physicochemical Properties

Generally, soil conditioners are added to soil to improve its condition in terms of structure and nutrients with the goal of increasing plant growth. Therefore, we recorded the growth of pepper and the changes in soil properties. In our study, the growth of the treated peppers was advanced, and the yield was higher. The application of SC caused no change in the soil pH. The other soil properties, such as organic matter and available N and K contents, were increased through the application of SC. In particular, we compared the soil capacity, porosity, and water retention between the control and SC3 soil. These three physicochemical traits were also improved (Table 1). As the prevalence of earthworms is generally associated with good soil, we counted the number of earthworms. In the SC-improved soil, the abundance of earthworms was higher than that in the CK soil (Figure S2). As the use of nanotechnology has increased, nanomaterials have contributed



to agriculture [55]. Attapulgite has many nanoscale channels, giving it unique physical and chemical properties. It has been widely used as an additive of nanocomposites [56], as the supporter of active nanomaterials, and to control nitrogen or pesticide loss [2,17,57]. In this study, the application of SC composed of attapulgite resulted in higher nutrient availability; better soil capacity, porosity, and water retention; and increased plant yield. These results were in agreement with previous reports on soil conditioners [58,59].

For better application of SC, further research should be conducted in field conditions. The results may be different between greenhouse and field due to the different environments (soil type, pH, location, water, fertilizer, and so on). The stability of SC in controlling nutrient loss should be researched in various soils.

#### 4.3. Effect of SC on Microbial Community Structure

In this study, microbial abundance and diversity in soil, including bacteria and fungi, were assessed using high-throughput sequencing. We found that the richness and diversity of bacteria were significantly higher than those of fungi (Table 2). This implies that bacteria are dominant colonizers in this soil. The alpha diversity was also shown to differ significantly between the CK and SC treatments, both in terms of bacteria and fungi. Meanwhile, the UPGMA and PCoA results in this study indicated that there were different characteristic microbial communities between CK and SC3 (Figures 6A, S4A, 8A and S5A).

##### 4.3.1. Effect of SC on Bacterial Microorganisms

Bacterial communities are the most diverse and abundant groups in soil. Pseudomonadota, Actinomycetota, Bacteroidota, Gemmatimonadota, and Chloroflexi were the dominant phyla in CK and SC3. The predominant phyla in our study are almost the same as those in previous studies. In marine ecosystems, Pseudomonadota, Bacteroidota, and Bacillota are the dominant phyla. In apple orchard soils, Pseudomonadota, Actinomycetota, and Acidobacteria are the main phyla. On seaweed surfaces, Pseudomonadota and Bacillota are the most abundant phyla. In SC3 soil, the relative abundance levels of Pseudomonadota, Actinomycetota, Bacteroidota, and Gemmatimonadota were reduced, but the abundance levels of Acidobacteriota, Chloroflexi, Bacillota, and Myxococcota were increased (Figure 6A). Pseudomonadota are responsible for the symbiotic nitrogen fixation of legumes and biodegradation of polycyclic aromatic hydrocarbons [60,61]. Actinomycetota could be responsible for the decomposition of all sorts of organic substances, the production of bioactive metabolites, and the biological control of soil environments [62]. Bacteroidota are well-known degraders of organic matter [63]. Gemmatimonadota seem to be frequently associated with plants and the rhizosphere and have the capacity for anoxygenic photosynthesis [64]. A previous study showed that soil amendment alters the abundance of phyla. The relative abundance level of Pseudomonadota was increased, but the levels of Acidobacteria, Actinobacteria, Gemmatimonadetes, and Chloroflexi were reduced [59]. This differs somewhat from our results. At the genus level, the relative abundance levels of some bacteria, such as *Massilia*, *Sphingomonas*, *Aeromicrobium*, *Kribbella*, and *Gaiellawere*, were higher in SC3. Additionally, the relative abundance levels of *Nitrosospora*, *Luteimonas*, *Galbitalea*, and *Gemmatimonas* were lower in SC3 than in CK (Figure 6B). *Massilia* is abundant in the rhizosphere and can interact with pathogenic fungi by degrading chitin [65,66]. *Sphingomonas* functions in plant tolerance to abiotic stress and the biodegradation of environmental contaminants [67,68]. *Aeromicrobium* has been reported to possess the ability to degrade organic matter [69]. *Kribbella* and *Gaiella* [70,71] may inhibit pathogens. In the present study, soil improvement reduced the relative abundance of bacterial genera, such as *Gemmatimonas* and *Nitrosospora* [72]. Our results are similar to these reports. We noted that in our study, *Luteimonas* was enriched in the CK (Figure 7). *Luteimonas* was reported as a denitrifying genus in a wastewater treatment system [73]. These results may have shown that the soil environments were improved by the SC.

#### 4.3.2. Effect of SC on Fungal Microorganisms

Soil fungi have many functions, including as biological controllers, ecosystem regulators, and participants in the conversion of organic matter [74]. In our results, Ascomycota, Basidiomycota, and Mortierellomycota were the dominant phyla in CK and SC3 (Figure 8A). These predominant phyla in our results are consistent with the results of a previous study [75]. The Ascomycota phylum was the most dominant in all of the agricultural soil and plays an ecological role as a decomposer [76]. Basidiomycota can degrade different components of wood, and they are part of a key process in carbon recycling [77]. The abundance of the Mortierellomycota phylum in SC3 was significantly higher than that in CK. Mortierellomycota can dissolve mineral phosphorus and secrete oxalic acid to increase soil nutrient contents [78,79]. In our results, the AP content was lower in SC3 than in CK. There was a negative correlation between Mortierellomycota and AP. We speculate that the mineral phosphorus in soil was dissolved by Mortierellomycota, and then, the available P was absorbed by plants to improve their growth. This needs to be researched in future work. At the genus level, *Mortierella*, *Thysanorea*, *Calyptella*, *Pseudogymnoascus*, etc., were the dominant genera in the SC. The relative abundance levels of *Alternaria*, *Acremonium*, *Mortierella*, *Paraphoma*, and *Trichoderma* were higher in SC3 than in CK (Figure 8B). *Thysanorea* belongs to the Ascomycota phylum and may play a key role in decomposition in soils and increasing nitrogen [80]. *Calyptella* belongs to the Basidiomycota phylum and is confirmed to be an ectomycorrhizal mutualist, which protects plants [81]. *Mortierella* was shown to be the dominant fungus in fertilizer-treated soils and was affected by the nutrients in the soil. *Pseudogymnoascus* decays matter in cool environments. *Trichoderma* and *Acremonium* levels can increase in fertilized soils, and they can be used in biocontrol. In addition to beneficial fungi, the levels of pathogenic fungi such as *Fusarium*, *Alternaria*, *Botryotrichum*, and *Pseudogymnoascus* increased in SC3 (Figure 8B). We speculated that there was an increase in fungal diversity in the SC-improved soil, including beneficial and pathogenic fungi. However, the richness and diversity levels of beneficial fungi were higher than those of pathogenic fungi in the SC3 soil. Therefore, SC improves soil.

#### 4.4. Relationship between Soil Physicochemical Properties and Microbial Community after Application of SC

It was reported that microbial communities in soil strongly correlate to soil physicochemical properties [82]. In our study, the soil physicochemical properties were improved by the addition of SC (Table 1). The organic matter content was absent from our analysis because this study mainly focused on the control of the loss of available nutrients. The pH of soil significantly influences the structure of microbial communities. However, our SC did not affect the soil pH. The soil properties showed a correlation with the microbial community (Figures 10 and 11). The compositions of the bacterial genera and fungal genera in the SC3 samples were both positively correlated with AK, AN, and AP (Figure 11). At the genus level, bacteria such as *Paeniglutamibacter* (Actinomycetota phylum), *Blautia* (Firmicutes phylum), and *Massilia* (Pseudomonadota phylum) were significantly correlated with AK, AN, and AP; fungi such as *Leucosporidium* (Basidiomycota phylum), *Acremonium* (Ascomycota phylum), and *Myrothecium* (Ascomycota phylum) were significantly correlated with AK and AN. Unclassified\_Leotiomyces\_sp. (Ascomycota phylum), *Leucosporidium* (Basidiomycota phylum), *Solicoccozyma* (Basidiomycota phylum), and *Thelebolus* (Ascomycota phylum) were positively correlated with AP. We proved that SC could control the loss of nutrients (Figure 1). We speculated that the AP and AK levels were also controlled by the nanonetwork structure of the SC. The effect of soil carbon on the microbial community was not determined. In fact, microorganisms play an important role in the soil carbon cycle. Microbial biomass can increase soil carbon storage. Meanwhile, microorganisms are commonly associated with soil organic carbon degradation [83,84]. Previous reports have found that microbial interactions with soil C and N could be affected by many factors. The factors include litter input, fine roots, soil organic carbon, inorganic N, soil moisture, temperature, and pH [85,86]. SC can control the loss of nutrients that increase available

N in soil. The increased N may induce P limitation and potentially affect C cycling. We speculated that the C:N ratio was changed by the SC in soil. This may be the cause of the changes in the microbial community. This needs more study in the future.

In our study, SC affected soil fertility by controlling nutrient loss, with the potential to change the soil microbial quantity. The altered trends in the microbial community in different fields should be studied in further work.

#### 4.5. Predicted Functional Analysis for Microbial Communities

Compared with the CK, the soil properties and the bacterial community structure were altered by the administration of SC. Considering that the SC treatment's performance may have been affected by functional microorganisms, we analyzed the functional genes of the microbial communities. Bacterial results were obtained from the PICRUSt analysis. The number of genes related to cell growth and death, endocrine system, and energy metabolism in the SC treatment was significantly higher than that in the CK (Figures 12A and S6A). These functional genes may drive the compositions of bacterial communities; therefore, bacteria further improve the properties of soil. In previous studies, the composition of the bacterial community was found to be driven by functional genes rather than taxonomic or phylogenetic compositions [87,88]. We speculated that these genes promoted the related bacterial growth and development and then formed the bacterial communities in SC-treated soil. The FUNGuild analysis showed the difference in fungal functional genes between SC3 and CK (Figure 12B). The dominant fungal genera in SC3 were *Mortierella*, *Thysanoreia*, and *Calyptella* (Figure 8), which were classified as undefined saprotrophs in the FUNGuild analysis. Saprotrophic fungi are the main decomposers of litter, woody debris, and dead roots [89]. However, the functional prediction was inconsistent with the relative abundance analysis. Compared with CK, the "Endophyte-Plant\_Pathogen-Wood\_Saprotroph" and "Plant\_Pathogen-Soil\_Saprotroph-Wood\_Saprotroph" guilds were higher in SC3 (Figure S6B). This result may have been caused by the alteration in the fungal communities. We speculated that the relative abundance and richness of the saprotroph pathogens did not increase, but the number of the pathogens perhaps increased. The "Animal\_Pathogen-Soil\_Saprotroph" guild had a significantly higher abundance in the CK. This may illustrate that there were more earthworms in the SC-treated soil than in the CK. However, further studies are required to confirm the relationship between the functional prediction and fungal communities.

## 5. Conclusions

In this study, a nanonetwork-structured soil conditioner was constructed, and its effects on pepper growth, soil properties, and the construction of microbial communities were evaluated. Our results showed that SC could increase the yield of pepper and change the microbial community. The microbial abundances and diversity were higher in the SC treatment than in the CK. These microbes promote plant growth and improve soil quality. The compositions of bacterial genera and fungal genera in the SC3 samples were correlated with AK, AN, pH, and AP. Compared with the CK, the community compositions in SC3 included more metabolism-related bacterial genes. The complex changes in fungal functional genes need to be studied further. This study provides insight into the correlation between network-structured soil conditioners and soil, microorganisms, and plants. This could help us better understand the mechanism by which microorganisms are improved by network-structured SC.

**Supplementary Materials:** The following supporting information can be downloaded at: <https://www.mdpi.com/article/10.3390/biology12050668/s1>, Figure S1: Photographs of soil conditioner on pepper; Figure S2: The number of earthworms; Figure S3: The rarefaction curve of samples; Figure S4: Beta-diversity analysis showing the relatedness of bacterial communities in different samples; Figure S5: Beta-diversity analysis showing the relatedness of fungal communities in different samples; Figure S6: Difference analysis via *t*-test based on the results of functional annotation; Table S1: Sequencing statistic

**Author Contributions:** Conceptualization, P.Z. and N.Z.; methodology, D.W., P.Z., and N.Z.; software, J.C. and Z.W.; formal analysis, J.C. and Y.Z.; investigation, P.Z.; resources, N.Z. and P.Z.; data curation, D.W., J.C., and Y.Z.; writing—original draft preparation, J.C., Z.W., and P.Z.; writing—review and editing, P.Z.; visualization, J.C. and Y.Z.; supervision, P.Z.; project administration, P.Z. and Z.W.; funding acquisition, N.Z. All authors have read and agreed to the published version of the manuscript.

**Funding:** This research was supported by the Strategic Priority Research Program of the Chinese Academy of Sciences, grant number XDA28030202; the Priority Research Program of Chinese Academy of Science, grant number XDA24020104; the Key Area Research and Development Program of Guangdong province in China, grant number 2020B0202010005; and Key Technologies R & D Program of Inner Mongolia, grant number 2021GG0300.

**Institutional Review Board Statement:** Not applicable.

**Informed Consent Statement:** Not applicable.

**Data Availability Statement:** The raw read data were submitted to Science Data Bank (<https://doi.org/10.57760/sciencedb.07079>), accessed on 6 January 2023).

**Acknowledgments:** We thank D.Q. Cai (Donghua University, Shanghai) for help with SC interaction analyses.

**Conflicts of Interest:** The authors declare no conflict of interest.

## References

1. Fierer, N.; Wood, S.A.; Bueno de Mesquita, C.P. How microbes can, and cannot, be used to assess soil health. *Soil. Biol. Biochem.* **2021**, *153*, 108111. [[CrossRef](#)]
2. Cai, D.; Wu, Z.; Jiang, J.; Wu, Y.; Feng, H.; Brown, I.G.; Chu, P.K.; Yu, Z. Controlling nitrogen migration through micro-nano networks. *Sci. Rep.* **2014**, *4*, 3665. [[CrossRef](#)] [[PubMed](#)]
3. Yang, G.; Ji, H.; Sheng, J.; Zhang, Y.; Feng, Y.; Guo, Z.; Chen, L. Combining Azolla and urease inhibitor to reduce ammonia volatilization and increase nitrogen use efficiency and grain yield of rice. *Sci. Total Environ.* **2020**, *743*, 140799. [[CrossRef](#)] [[PubMed](#)]
4. Miransari, M.; Mackenzie, A. Development of a Soil N Test for Fertilizer Requirements for Corn Production in Quebec. *Commun. Soil Sci. Plant Anal.* **2011**, *42*, 50–65. [[CrossRef](#)]
5. Miransari, M.; Mackenzie, A. Development of a soil n test for fertilizer requirements for wheat. *J. Plant Nutr.* **2011**, *34*, 762–777. [[CrossRef](#)]
6. Chai, R.; Ye, X.; Ma, C.; Wang, Q.; Tu, R.; Zhang, L.; Gao, H. Greenhouse gas emissions from synthetic nitrogen manufacture and fertilization for main upland crops in China. *Carbon Balance Manag.* **2019**, *14*, 20. [[CrossRef](#)]
7. Nimmo, J. Encyclopedia of Soil in the Environment. *Fertil. Fertil.* **2004**, *3*, 295–303.
8. Singh, B.; Craswell, E. Fertilizers and nitrate pollution of surface and ground water: An increasingly pervasive global problem. *SN Appl. Sci.* **2021**, *3*, 518. [[CrossRef](#)]
9. Miransari, M. Soil microbes and plant fertilization. *Appl. Microbiol. Biotechnol.* **2011**, *92*, 875–885. [[CrossRef](#)]
10. Liu, R.; Lal, R. Potentials of engineered nanoparticles as fertilizers for increasing agronomic productions. *Sci. Total Environ.* **2015**, *514*, 131–139. [[CrossRef](#)]
11. Diacono, M.; Montemurro, F. Long-Term Effects of Organic Amendments on Soil Fertility. A Review. *Agron. Sustain. Dev.* **2010**, *30*, 401–422. [[CrossRef](#)]
12. Sohi, S.; Krull, E.; Lopez-Capel, E.; Bol, R. A Review of Biochar and Its Use and Function in Soil. *Adv. Agron.* **2010**, *105*, 47–82. [[CrossRef](#)]
13. Jagadamma, S.; Mayes, M.; Steinweg, J.M.; Schaeffer, S. Substrate quality alters microbial mineralization of added substrate and soil organic carbon. *Biogeosci. Discuss.* **2014**, *11*, 4451–4482. [[CrossRef](#)]
14. Byrne, M.; Tobin, J.; Forrestal, P.; Danaher, M.; Nkwonta, C.; Richards, K.; Cummins, E.; Hogan, S.; O’Callaghan, T. Urease and Nitrification Inhibitors—As Mitigation Tools for Greenhouse Gas Emissions in Sustainable Dairy Systems: A Review. *Sustainability* **2020**, *12*, 6018. [[CrossRef](#)]
15. Lawrencía, D.; Wong, S.K.; Low, D.Y.S.; Goh, B.H.; Goh, J.K.; Ruktanonchai, U.R.; Soottitantawat, A.; Lee, L.H.; Tang, S.Y. Controlled Release Fertilizers: A Review on Coating Materials and Mechanism of Release. *Plants* **2021**, *10*, 238. [[CrossRef](#)]
16. Dinca, L.; Grenni, P.; Onet, A.; Onet, C. Fertilization and Soil Microbial Community: A Review. *Appl. Sci.* **2022**, *12*, 1198. [[CrossRef](#)]
17. Zhou, L.; Zhao, P.; Chi, Y.; Wang, D.; Wang, P.; Liu, N.; Cai, D.; Wu, Z.; Zhong, N. Controlling the Hydrolysis and Loss of Nitrogen Fertilizer (Urea) by using a Nanocomposite Favors Plant Growth. *ChemSusChem* **2017**, *10*, 2068–2079. [[CrossRef](#)]
18. Mercado-Blanco, J.; Abrantes, I.; Barra Caracciolo, A.; Bevivino, A.; Ciancio, A.; Grenni, P.; Hrynkiewicz, K.; Kredics, L.; Proença, D.N. Belowground Microbiota and the Health of Tree Crops. *Front Microbiol.* **2018**, *9*, 1006. [[CrossRef](#)]



19. Saleem, M.; Hu, J.; Jousset, A. More Than the Sum of Its Parts: Microbiome Biodiversity as a Driver of Plant Growth and Soil Health. *Annu. Rev. Ecol. Evol. Syst.* **2019**, *50*, 145–168. [[CrossRef](#)]
20. Mohammad, M. Soil microbes and the availability of soil nutrients. *Acta. Physiol. Plant.* **2013**, *35*, 3075–3084. [[CrossRef](#)]
21. Berendsen, R.L.; Pieterse, C.M.; Bakker, P.A. The rhizosphere microbiome and plant health. *Trends. Plant Sci.* **2012**, *17*, 478–486. [[CrossRef](#)]
22. Fierer, N. Embracing the unknown: Disentangling the complexities of the soil microbiome. *Nat. Rev. Microbiol.* **2017**, *15*, 579–590. [[CrossRef](#)] [[PubMed](#)]
23. Bending, G.D.; Turner, M.K.; Rayns, F.; Marx, M.-C.; Wood, M. Microbial and biochemical soil quality indicators and their potential for differentiating areas under contrasting agricultural management regimes. *Soil. Biol. Biochem.* **2004**, *36*, 1785–1792. [[CrossRef](#)]
24. Singh, J.S.; Gupta, V.K. Soil microbial biomass: A key soil driver in management of ecosystem functioning. *Sci. Total Environ.* **2018**, *634*, 497–500. [[CrossRef](#)] [[PubMed](#)]
25. Wani, G.A.; Khan, M.A.; Dar, M.A.; Shah, M.A.; Reshi, Z.A. Next Generation High Throughput Sequencing to Assess Microbial Communities: An Application Based on Water Quality. *Bull. Environ. Contam. Toxicol.* **2021**, *106*, 727–733. [[CrossRef](#)]
26. Wang, J.X.; Liu, S.S.; Han, S.Y.; Wang, A.Y. High-throughput sequencing reveals soil bacterial community structure and their interactions with environmental factors of the grassland fairy ring. *Environ. Microbiol. Rep.* **2022**, *14*, 479–493. [[CrossRef](#)]
27. Wegner, C.E.; Richter-Heitmann, T.; Klindworth, A.; Klockow, C.; Richter, M.; Achstetter, T.; Glöckner, F.O.; Harder, J. Expression of sulfatases in *Rhodopirellula baltica* and the diversity of sulfatases in the genus *Rhodopirellula*. *Mar. Genom.* **2013**, *9*, 51–61. [[CrossRef](#)]
28. Schloter, M.; Nannipieri, P.; Sørensen, S.; van Elsas, J. Microbial indicators for soil quality. *Biol. Fertil. Soils.* **2018**, *54*, 1–10. [[CrossRef](#)]
29. Gao, Z.; Hu, Y.; Han, M.; Xu, J.; Wang, X.; Liu, L.; Tang, Z.; Jiao, W.; Jin, R.; Liu, M.; et al. Effects of continuous cropping of sweet potatoes on the bacterial community structure in rhizospheric soil. *BMC Microbiol.* **2021**, *21*, 102. [[CrossRef](#)]
30. Yao, Q.; Liu, J.; Yu, Z.; Li, Y.; Jin, J.; Liu, X. Three years of biochar amendment alters soil physiochemical properties and fungal community composition in a black soil of northeast China. *Soil. Biol. Biochem.* **2017**, *110*, 56–67. [[CrossRef](#)]
31. Lavecchia, A.; Curci, M.; Jangid, K.; Whitman, W.; Ricciuti, P.; Pascazio, S.; Crecchio, C. Microbial 16S gene-based composition of a sorghum cropped rhizosphere soil under different fertilization managements. *Biol. Fertil. Soils* **2015**, *51*, 661–672. [[CrossRef](#)]
32. Smalla, K.; Wieland, G.; Buchner, A.; Zock, A.; Parzy, J.; Kaiser, S.; Roskot, N.; Heuer, H.; Berg, G. Bulk and rhizosphere soil bacterial communities studied by denaturing gradient gel electrophoresis: Plant-dependent enrichment and seasonal shifts revealed. *Appl. Environ. Microbiol.* **2001**, *67*, 4742–4751. [[CrossRef](#)]
33. Berg, J.; Brandt, K.; Abu Al-Soud, W.; Holm, P.; Hansen, L.; Sørensen, S.; Nybroe, O. Selection for Cu-Tolerant Bacterial Communities with Altered Composition, but Unaltered Richness, via Long-Term Cu Exposure. *Appl. Environ. Microbiol.* **2012**, *78*, 7438–7446. [[CrossRef](#)] [[PubMed](#)]
34. Zhao, S.; Liu, D.; Ling, N.; Chen, F.; Fang, W.; Shen, Q. Bio-organic fertilizer application significantly reduces the *Fusarium oxysporum* population and alters the composition of fungi communities of watermelon *Fusarium* wilt rhizosphere soil. *Biol. Fertil. Soils* **2014**, *50*, 765–774. [[CrossRef](#)]
35. Magoč, T.; Salzberg, S.L. FLASH: Fast length adjustment of short reads to improve genome assemblies. *Bioinformatics* **2011**, *27*, 2957–2963. [[CrossRef](#)]
36. Caporaso, J.G.; Kuczynski, J.; Stombaugh, J.; Bittinger, K.; Bushman, F.D.; Costello, E.K.; Fierer, N.; Peña, A.G.; Goodrich, J.K.; Gordon, J.L.; et al. QIIME allows analysis of high-throughput community sequencing data. *Nat. Methods* **2010**, *7*, 335–336. [[CrossRef](#)]
37. Haas, B.J.; Gevers, D.; Earl, A.M.; Feldgarden, M.; Ward, D.V.; Giannoukos, G.; Ciulla, D.; Tabbaa, D.; Highlander, S.K.; Sodergren, E.; et al. Chimeric 16S rRNA sequence formation and detection in Sanger and 454-pyrosequenced PCR amplicons. *Genome. Res.* **2011**, *21*, 494–504. [[CrossRef](#)] [[PubMed](#)]
38. Quast, C.; Pruesse, E.; Yilmaz, P.; Gerken, J.; Schweer, T.; Yarza, P.; Peplies, J.; Glöckner, F.O. The SILVA ribosomal RNA gene database project: Improved data processing and web-based tools. *Nucleic. Acids Res.* **2013**, *41*, D590–D596. [[CrossRef](#)]
39. Altschul, S.F.; Gish, W.; Miller, W.; Myers, E.W.; Lipman, D.J. Basic local alignment search tool. *J. Mol. Biol.* **1990**, *215*, 403–410. [[CrossRef](#)]
40. Kõljalg, U.; Nilsson, R.H.; Abarenkov, K.; Tedersoo, L.; Taylor, A.F.; Bahram, M.; Bates, S.T.; Bruns, T.D.; Bengtsson-Palme, J.; Callaghan, T.M.; et al. Towards a unified paradigm for sequence-based identification of fungi. *Mol. Ecol.* **2013**, *22*, 5271–5277. [[CrossRef](#)]
41. Edgar, R.C. MUSCLE: Multiple sequence alignment with high accuracy and high throughput. *Nucleic Acids Res.* **2004**, *32*, 1792–1797. [[CrossRef](#)] [[PubMed](#)]
42. Langille, M.G.; Zaneveld, J.; Caporaso, J.G.; McDonald, D.; Knights, D.; Reyes, J.A.; Clemente, J.C.; Burkepile, D.E.; Vega Thurber, R.L.; Knight, R.; et al. Predictive functional profiling of microbial communities using 16S rRNA marker gene sequences. *Nat. Biotechnol.* **2013**, *31*, 814–821. [[CrossRef](#)] [[PubMed](#)]
43. Nguyen, N.; Song, Z.; Bates, S.; Branco, S.; Tedersoo, L.; Menke, J.; Schilling, J.; Kennedy, P. FUNGuild: An open annotation tool for parsing fungal community datasets by ecological guild. *Fungal. Ecol.* **2015**, *20*, 241–248. [[CrossRef](#)]

44. Liang, Z.; Liu, F.; Wang, W.; Zhang, P.; Sun, X.; Wang, F.; Kell, H. High-throughput sequencing revealed differences of microbial community structure and diversity between healthy and diseased *Caulerpa lentillifera*. *BMC Microbiol.* **2019**, *19*, 225. [[CrossRef](#)] [[PubMed](#)]
45. Wang, D.; Zhang, G.; Zhou, L.; Wang, M.; Cai, D.; Wu, Z. Synthesis of a Multifunctional Graphene Oxide-Based Magnetic Nanocomposite for Efficient Removal of Cr(VI). *Langmuir* **2017**, *33*, 7007–7014. [[CrossRef](#)] [[PubMed](#)]
46. Buckerfield, J.C.; Lee, K.E.; Davoren, C.W.; Hannay, J.N. Earthworms as indicators of sustainable production in dryland cropping in southern Australia. *Soil. Biol. Biochem.* **1997**, *29*, 547–554. [[CrossRef](#)]
47. Shi, Z.; Tang, Z.; Wang, C. Effect of phenanthrene on the physicochemical properties of earthworm casts in soil. *Ecotoxicol. Environ. Saf.* **2019**, *168*, 348–355. [[CrossRef](#)]
48. Singh, N.; Bhuker, A.; Jeevanadam, J. Effects of metal nanoparticle-mediated treatment on seed quality parameters of different crops. *Naunyn. Schmiedeberg's. Arch Pharm.* **2021**, *394*, 1067–1089. [[CrossRef](#)]
49. Tilman, D.; Cassman, K.G.; Matson, P.A.; Naylor, R.; Polasky, S. Agricultural sustainability and intensive production practices. *Nature* **2002**, *418*, 671–677. [[CrossRef](#)]
50. Sajjadi, M.; Ahmadpoor, F.; Nasrollahzadeh, M.; Ghafuri, H. Lignin-derived (nano)materials for environmental pollution remediation: Current challenges and future perspectives. *Int. J. Biol. Macromol.* **2021**, *178*, 394–423. [[CrossRef](#)]
51. Ma, C.; White, J.C.; Zhao, J.; Zhao, Q.; Xing, B. Uptake of Engineered Nanoparticles by Food Crops: Characterization, Mechanisms, and Implications. *Annu. Rev. Food Sci. Technol.* **2018**, *9*, 129–153. [[CrossRef](#)] [[PubMed](#)]
52. Guo, H.; White, J.C.; Wang, Z.; Xing, B. Nano-enabled fertilizers to control the release and use efficiency of nutrients. *Curr. Opin. Environ. Sci. Health* **2018**, *6*, 77–83. [[CrossRef](#)]
53. Sohi, S.P.; Krull, E.; Lopez-Capel, E.; Bol, R. Chapter 2—A Review of Biochar and Its Use and Function in Soil. In *Advances in Agronomy*; Academic Press: Cambridge, MA, USA, 2010; Volume 105, pp. 47–82.
54. Ehaliotis, C.; Cadisch, G.; Giller, K.E. Substrate amendments can alter microbial dynamics and N availability from maize residues to subsequent crops. *Soil. Biol. Biochem.* **1998**, *30*, 1281–1292. [[CrossRef](#)]
55. Kah, M. Nanopesticides and Nanofertilizers: Emerging Contaminants or Opportunities for Risk Mitigation? *Front Chem.* **2015**, *3*, 64. [[CrossRef](#)]
56. Huang, D.; Wang, W.; Xu, J.; Wang, A. Mechanical and water resistance properties of chitosan/poly(vinyl alcohol) films reinforced with attapulgite dispersed by high-pressure homogenization. *Chem. Eng. J.* **2012**, *210*, 166–172. [[CrossRef](#)]
57. Xiang, Y.; Wang, M.; Sun, X.; Cai, D.; Wu, Z. Controlling Pesticide Loss through Nanonetworks. *ACS Sustain. Chem. Eng.* **2014**, *2*, 918–924. [[CrossRef](#)]
58. Kallenbach, C.M.; Conant, R.T.; Calderón, F.; Wallenstein, M.D. A novel soil amendment for enhancing soil moisture retention and soil carbon in drought-prone soils. *Geoderma* **2019**, *337*, 256–265. [[CrossRef](#)]
59. Liang, B.; Ma, C.; Fan, L.; Wang, Y.; Yuan, Y. Soil amendment alters soil physicochemical properties and bacterial community structure of a replanted apple orchard. *Microbiol. Res.* **2018**, *216*, 1–11. [[CrossRef](#)]
60. Raymond, J.; Siefert, J.L.; Staples, C.R.; Blankenship, R.E. The natural history of nitrogen fixation. *Mol. Biol. Evol.* **2004**, *21*, 541–554. [[CrossRef](#)] [[PubMed](#)]
61. Debruyne, J.M.; Mead, T.J.; Wilhelm, S.W.; Sayler, G.S. PAH biodegradative genotypes in Lake Erie sediments: Evidence for broad geographical distribution of pyrene-degrading mycobacteria. *Environ. Sci. Technol.* **2009**, *43*, 3467–3473. [[CrossRef](#)]
62. Bhatti, A.A.; Haq, S.; Bhat, R.A. Actinomycetes benefaction role in soil and plant health. *Microb. Pathog.* **2017**, *111*, 458–467. [[CrossRef](#)]
63. Thomas, F.; Hehemann, J.H.; Rebuffet, E.; Czejek, M.; Michel, G. Environmental and gut bacteroidetes: The food connection. *Front Microbiol.* **2011**, *2*, 93. [[CrossRef](#)] [[PubMed](#)]
64. Mujakić, I.; Piwosz, K.; Koblížek, M. Phylum Gemmatimonadota and Its Role in the Environment. *Microorganisms* **2022**, *10*, 151. [[CrossRef](#)] [[PubMed](#)]
65. Tkacz, A.; Cheema, J.; Chandra, G.; Grant, A.; Poole, P.S. Stability and succession of the rhizosphere microbiota depends upon plant type and soil composition. *ISME J.* **2015**, *9*, 2349–2359. [[CrossRef](#)]
66. Bodenhausen, N.; Horton, M.W.; Bergelson, J. Bacterial communities associated with the leaves and the roots of *Arabidopsis thaliana*. *PLoS ONE* **2013**, *8*, e56329. [[CrossRef](#)]
67. Halo, B.; Khan, A.; Waqas, M.; Al-Harrasi, A.; Hussain, J.; Ali, L.; Adnan, M.; Lee, I.-J. Endophytic bacteria (*Sphingomonas* sp. LK11) and Gibberellin can improve *Solanum lycopersicum* growth and oxidative stress under salinity. *J. Plant Interact.* **2015**, *10*, 117–125. [[CrossRef](#)]
68. Asaf, S.; Numan, M.; Khan, A.L.; Al-Harrasi, A. *Sphingomonas*: From diversity and genomics to functional role in environmental remediation and plant growth. *Crit. Rev. Biotechnol.* **2020**, *40*, 138–152. [[CrossRef](#)]
69. Yoon, J.H.; Lee, C.H.; Oh, T.K. *Aeromicrobium alkaliterrae* sp. nov., isolated from an alkaline soil, and emended description of the genus *Aeromicrobium*. *Int. J. Syst. Evol. Microbiol.* **2005**, *55*, 2171–2175. [[CrossRef](#)] [[PubMed](#)]
70. Wang, D.; Le, W.; Zhang, Y.; Jiang, Y.; Wu, W.; Zu, L.; Jiang, C. A study on polyphasic taxonomy of one antifungal actinomycete strain YIM31530~(T). *J. Yunnan Univ. (Nat. Sci.)* **2004**, *26*, 265–269.
71. Fengyan, Z.; Zhang, Y.; Dong, W.; Zhang, Y.; Zhang, G.; Sun, Z.; Yang, L. Vermicompost can suppress *Fusarium oxysporum* f. sp. *lycopersici* via generation of beneficial bacteria in a long-term tomato monoculture soil. *Plant Soil* **2019**, *440*, 491–505. [[CrossRef](#)]

72. Franke-Whittle, I.; Manici, L.; Insam, H.; Stres, B. Rhizosphere bacteria and fungi associated with plant growth in soils of three replanted apple orchards. *Plant Soil* **2015**, *395*, 317–333. [[CrossRef](#)]
73. Wolff, D.; Krah, D.; Dötsch, A.; Ghattas, A.K.; Wick, A.; Ternes, T.A. Insights into the variability of microbial community composition and micropollutant degradation in diverse biological wastewater treatment systems. *Water Res.* **2018**, *143*, 313–324. [[CrossRef](#)] [[PubMed](#)]
74. Fraç, M.; Hannula, S.E.; Bełka, M.; Jędrzycka, M. Fungal Biodiversity and Their Role in Soil Health. *Front Microbiol.* **2018**, *9*, 707. [[CrossRef](#)] [[PubMed](#)]
75. Wang, S.; Cheng, J.; Li, T.; Liao, Y. Response of soil fungal communities to continuous cropping of flue-cured tobacco. *Sci. Rep.* **2020**, *10*, 19911. [[CrossRef](#)] [[PubMed](#)]
76. Ma, A.; Zhuang, X.; Wu, J.; Cui, M.; Lv, D.; Liu, C.; Zhuang, G. Ascomycota members dominate fungal communities during straw residue decomposition in arable soil. *PLoS ONE* **2013**, *8*, e66146. [[CrossRef](#)] [[PubMed](#)]
77. Zhao, R.-L.; Li, G.-J.; Sanchez-Ramirez, S.; Stata, M.; Yang, Z.-L.; Wu, G.; Dai, Y.-C.; He, S.-H.; Cui, B.-K.; Zhou, J.-L.; et al. A six-gene phylogenetic overview of Basidiomycota and allied phyla with estimated divergence times of higher taxa and a phyloproteomics perspective. *Fungal. Divers.* **2017**, *84*, 43–74. [[CrossRef](#)]
78. Spaepen, S.; Vanderleyden, J.; Remans, R. Indole-3-acetic acid in microbial and microorganism-plant signaling. *FEMS Microbiol. Rev.* **2007**, *31*, 425–448. [[CrossRef](#)]
79. Spatafora, J.W.; Chang, Y.; Benny, G.L.; Lazarus, K.; Smith, M.E.; Berbee, M.L.; Bonito, G.; Corradi, N.; Grigoriev, I.; Gryganskyi, A.; et al. A phylum-level phylogenetic classification of zygomycete fungi based on genome-scale data. *Mycologia* **2016**, *108*, 1028–1046. [[CrossRef](#)]
80. Žifčáková, L.; Větrovský, T.; Howe, A.; Baldrian, P. Microbial activity in forest soil reflects the changes in ecosystem properties between summer and winter. *Environ. Microbiol.* **2016**, *18*, 288–301. [[CrossRef](#)]
81. Phosri, C.; Pölme, S.; Taylor, A.; Kõljalg, U.; Suwannasai, N.; Tedersoo, L. Diversity and community composition of ectomycorrhizal fungi in a dry deciduous dipterocarp forest in Thailand. *Biodivers. Conserv.* **2012**, *21*, 2287–2298. [[CrossRef](#)]
82. Schreiter, S.; Ding, G.C.; Heuer, H.; Neumann, G.; Sandmann, M.; Grosch, R.; Kropf, S.; Smalla, K. Effect of the soil type on the microbiome in the rhizosphere of field-grown lettuce. *Front Microbiol.* **2014**, *5*, 144. [[CrossRef](#)] [[PubMed](#)]
83. Chu, H.; Fierer, N.; Lauber, C.L.; Caporaso, J.G.; Knight, R.; Grogan, P. Soil bacterial diversity in the Arctic is not fundamentally different from that found in other biomes. *Environ. Microbiol.* **2010**, *12*, 2998–3006. [[CrossRef](#)] [[PubMed](#)]
84. Zhu, Y.G.; Miller, R.M. Carbon cycling by arbuscular mycorrhizal fungi in soil-plant systems. *Trends Plant Sci.* **2003**, *8*, 407–409. [[CrossRef](#)] [[PubMed](#)]
85. Deng, Q.; Cheng, X.; Hui, D.; Zhang, Q.; Li, M.; Zhang, Q. Soil microbial community and its interaction with soil carbon and nitrogen dynamics following afforestation in central China. *Sci. Total Environ.* **2016**, *541*, 230–237. [[CrossRef](#)]
86. Fierer, N.; Strickland, M.S.; Liptzin, D.; Bradford, M.A.; Cleveland, C.C. Global patterns in belowground communities. *Ecol. Lett.* **2009**, *12*, 1238–1249. [[CrossRef](#)]
87. Burke, C.; Thomas, T.; Lewis, M.; Steinberg, P.; Kjelleberg, S. Composition, uniqueness and variability of the epiphytic bacterial community of the green alga *Ulva australis*. *ISME J.* **2011**, *5*, 590–600. [[CrossRef](#)]
88. Burke, C.; Steinberg, P.; Rusch, D.; Kjelleberg, S.; Thomas, T. Bacterial community assembly based on functional genes rather than species. *Proc. Natl. Acad. Sci. USA* **2011**, *108*, 14288–14293. [[CrossRef](#)]
89. Chen, L.; Xiang, W.; Wu, H.; Ouyang, S.; Lei, P.; Hu, Y.; Ge, T.; Ye, J.; Kuzyakov, Y. Contrasting patterns and drivers of soil fungal communities in subtropical deciduous and evergreen broadleaved forests. *Appl. Microbiol. Biotechnol.* **2019**, *103*, 5421–5433. [[CrossRef](#)]

**Disclaimer/Publisher’s Note:** The statements, opinions and data contained in all publications are solely those of the individual author(s) and contributor(s) and not of MDPI and/or the editor(s). MDPI and/or the editor(s) disclaim responsibility for any injury to people or property resulting from any ideas, methods, instructions or products referred to in the content.

# Alkali-Activated Potassium Persulfate Treatment of Sugarcane Filter Cake for the Rapid Production of Fulvic-like-Acid Fertilizer

Dongqing Cai, Xianghai Kong, Xiaojiang Zhang, Jinghong Ye, He Xu, Yanping Zhu, and Dongfang Wang\*



Cite This: *ACS Sustainable Chem. Eng.* 2023, 11, 13678–13687



Read Online

ACCESS |



Metrics & More

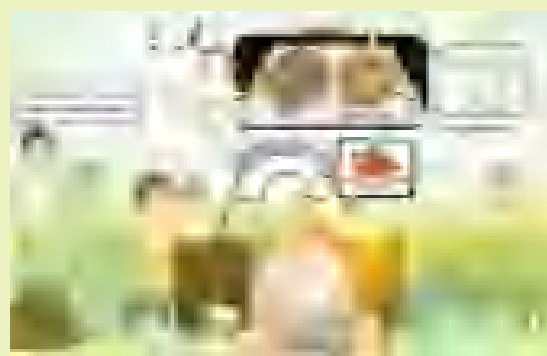


Article Recommendations



Supporting Information

**ABSTRACT:** In recent years, alkali activation for potassium persulfate (PS) treatment has been proven a promising method in the advanced oxidation processes. However, the majority of studies have focused on water pollution control and remediation processes. There are few reports on the application of PS to transform organic solid waste into a resource. In this study, the sugarcane filter cake (SFC) was treated with PS activated by calcium hydroxide (CH) to convert it into an organic fertilizer (CH-PS/SFC) with high amounts of fulvic-like acid (FLA). CH-PS/SFC could also be used to remediate the acid soil and immobilize heavy metals (HMs). Due to the simple structure and high sucrose content of SFC, the sucrose-saturated solution was to investigate the CH-PS treatment and the result was the production of a large amount of (785.7 mg/g) after 2 h. In optimal conditions, the yield of FLA in CH-PS/SFC could reach 316.8 mg/g, and the subsequent use as a fertilizer offered a germination index of over 80% and a decrease in the leachability of HMs. In addition, in the humification the maximum temperature was found to be 80.3 °C and the moisture decreased by 20% during the humification of SFC. Furthermore, pot experiments showed that CH-PS/SFC could promote Chinese cabbage growth, decrease the yellow leaves rate, and decrease the absorption of HMs by Chinese cabbage.



**KEYWORDS:** sugarcane filter cake, potassium persulfate, calcium hydroxide, fulvic-like acid, organic fertilizer

## INTRODUCTION

Sugarcane is the leading sugar crop, and its cultivation area accounts for more than 85% of the edulcorate crops area in China.<sup>1</sup> However, the fabrication of 1 t of sucrose could produce a large number of organic wastes, such as 2.5 t of bagasse, 800 kg of molasses, and 250 kg of sugarcane filter cake (SFC).<sup>2</sup> Therein, most SFCs are mechanically dewatered and then landfilled or incinerated, resulting in very low utilization efficiency of SFCs.<sup>3</sup> Actually, SFCs contain sucrose, crude fiber, sugarcane wax colloid, crude protein, metal salt, and other substances, showing them as a promising fertilizer source.<sup>4</sup> However, SFCs have the problems of high water content, long humification time, low fertilizer efficiency, and foul smell. These problems are key factors restricting the sustainable development of the sucrose industry. Therefore, it is important to develop a fast, safe, and high-quality method to deal with SFC to protect the environment, create a circular economy, and improve agricultural products' quality.

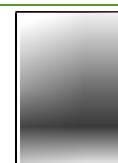
Generally, composting means that microbial metabolism can convert organic matter into stable humus. However, the composting process is prolonged and sensitive to temperature, humidity, pH, and other conditions.<sup>5</sup> In addition, incomplete composting in the organic fertilizer could produce harmful bacteria, which is detrimental to plant growth.<sup>6,7</sup> Therefore, it

is sensible to apply advanced oxidation processes (AOPs) to overcome the problems of traditional composting, such as long compost time, high running expense, and large occupation of land. In the AOPs, the free radicals are strong oxidants and could enhance the composting process (i.e., Le Chatelier's principle). At the same time, the macromolecular substances in the SFC could be rapidly decomposed to produce small molecular substances<sup>8</sup> and most of the harmful bacteria are eliminated.<sup>9,10</sup> Because the composition (carboxylic acid, amino acids, quinones, and aromatic hydroxyl) and properties of small molecular substances are similar to those of fulvic acid (FA), they are named fulvic-like acid (FLA).<sup>11</sup> Meanwhile, the abundant FLA could meet the needs of plants and reduce the activity of heavy metals (HMs) in SFC.<sup>12</sup> Compared with traditional compost, AOPs have the advantages of short humification time, simple process, and low cost.<sup>13,14</sup> Therefore,

**Received:** June 12, 2023

**Revised:** August 18, 2023

**Published:** September 1, 2023





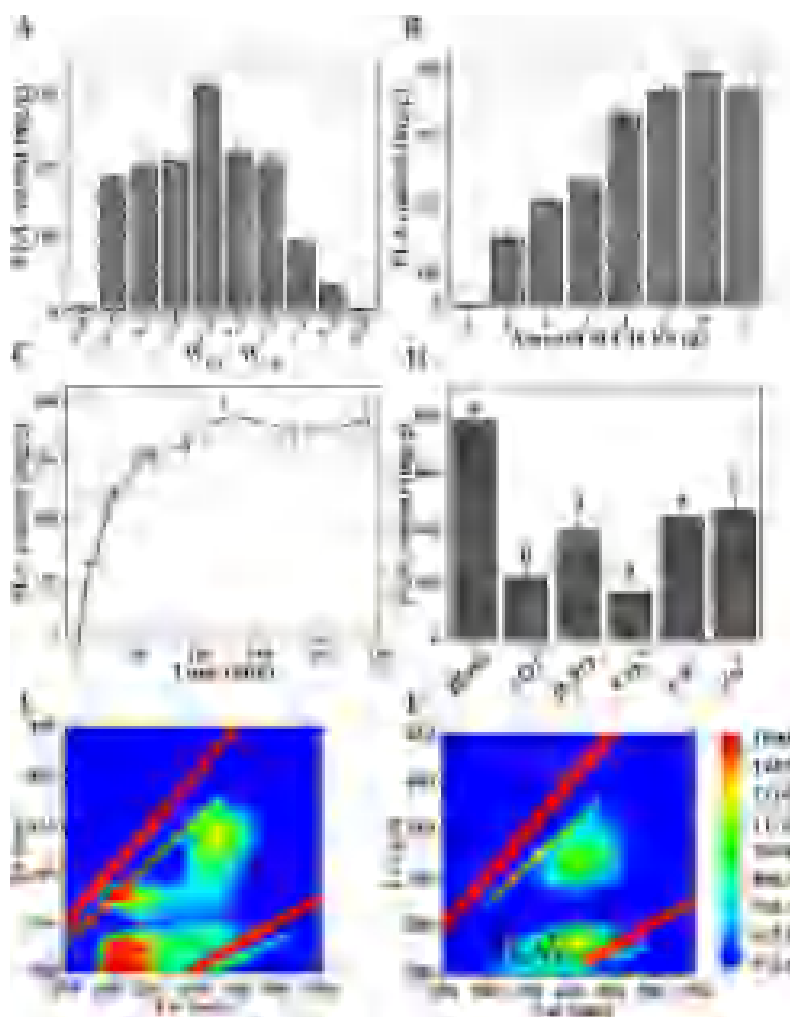


**Figure 1.** (A) Effect of CH-PS (2.0 g) with different  $W_{\text{CH}}/W_{\text{PS}}$  on the conversion of sucrose to FLA content for 2 h. (B) Effect of the CH-PS amount on the conversion of sucrose to the FLA content ( $W_{\text{CH}}/W_{\text{PS}} = 1:1$ ) for 2 h. (C) Influence of reaction time on the FLA content of CH-PS/sucrose ( $W_{\text{CH}}/W_{\text{PS}} = 1:1$ , 4.0 g). (D) Effect of coexisting ions (0.25 mM/g) on the FLA content of CH-PS/sucrose ( $W_{\text{CH}}/W_{\text{PS}} = 1:1$ , 4.0 g) for 2 h. Significance was accepted if  $p < 0.05$ . Different letters (a and b) denote statistical differences across treatments. (E, F) 3D-EEM for FLA in sucrose and CH-PS/sucrose.

the application of AOPs for treating SFC has the prospect of wide application.<sup>15</sup>

Among AOPs, potassium peroxydisulfate (PS) is investigated widely because it can produce sulfate radicals ( $\text{SO}_4^{\bullet-}$ ), which have a high oxidative power and long half-life.<sup>16</sup> Typically, PS could be activated by various types of activators, such as metal ions,<sup>9</sup> metal oxides,<sup>17</sup> carbon materials,<sup>18</sup> ultraviolet irradiation,<sup>10</sup> and thermal activation.<sup>19</sup> Due to the complex activated process and high-cost limitations, a kind of new activated process for PS in SFC is quite necessary.

In this work, PS was activated by calcium hydroxide (CH) to get PS-CH, and then PS-CH was applied to humify sucrose for the first time. Due to the high sucrose content of SFC, the sucrose-saturated solution was used as a model to investigate the conversion regularity of SFC to FLA fertilizer. This work had three outstanding highlights: (1) SFC could be humified by PS-CH rapidly in 2 h to get an FLA organic fertilizer; (2) PS-CH/SFC could be used to remediate the acidic soil and immobilize HMs; and (3) PS-CH/SFC could promote the growth of Chinese cabbage significantly. Therefore, this work

provided a rapid-humification, low-cost ( $\sim 30$  \$/ton), and high-value way to deal with SFCs.

## MATERIALS AND METHODS

**Materials.** SFC was purchased from the Guangxi Sugar Industry Group Co., Ltd., (Nanning, China). PS, CH, methanol (MeOH, 99.5%), *tert*-butanol (TBA, 99.5%), histidine (His, 99.8%), sodium carbonate ( $\text{Na}_2\text{CO}_3$ , 99.8%), hydrochloric acid (HCl, 37.2%), copper chloride ( $\text{CuCl}_2$ , 99.8%), cadmium chloride ( $\text{CdCl}_2$ , 99.8%), zinc chloride ( $\text{ZnCl}_2$ , 99.8%), sodium sulfate ( $\text{Na}_2\text{SO}_4$ , 99.8%), monosodium phosphate ( $\text{NaH}_2\text{PO}_3$ , 99.8%), and lead chloride ( $\text{PbCl}_2$ , 99.8%) were analytical reagent grade and provided by Sinopharm Chemical Reagent Company (Shanghai, China). The deionized water was used in all of the experiments except for the pot experiment and was made by an ultrapure water machine (Qclean, China). Cucumber seeds and Chinese cabbage seeds were purchased from He Xian Huahe Seed Industry Co., Ltd., (Maanshan, China). Soil and sand were taken from Songjiang Campus of Donghua University (Shanghai, China). All of the experiments were performed in triplicate in the following experiments.

**Sucrose and SFC Humifying Experiments.** CH (2.0 g) and PS (2.0 g) were added to 20 g of sucrose-saturated solution orderly and the resulting solution was stirred (200 rpm) for 2 h at 25 °C to obtain

CH-PS/sucrose. Therein, sucrose (250 g) was added to deionized water (100 mL) and the resulting solution was stirred (200 rpm) for 2 h at 25 °C. Then, the solution was filtrated to get the sucrose-saturated solution. Subsequently, 1 mL of methanol (a free radical quencher) was added to 10 mL of CH-PS/Sucrose for 1 h and the mixed solution was diluted 10 times. After stirring for 5 min, the solution was centrifuged at 10,000 rpm for 10 min, and the supernatant was filtered with a fiber membrane (0.45 μm). After that, FLA was detected by three-dimensional fluorescence excitation–emission (3D-EEM) matrix spectroscopy and a UV–vis spectrophotometer in the filtrate,<sup>8</sup> and the details of 3D-EEM could be found in S1. Additionally, the influences of the ratio CH to PS, the amount of CH-PS, time, and coexisting ions for FLA content were investigated. Meanwhile, the exploration of coexisting ions (0.25 mM/g) was the same as that of the sucrose humifying experiment, except for the addition of Na<sub>2</sub>SO<sub>4</sub>, NaH<sub>2</sub>PO<sub>3</sub>, Na<sub>2</sub>CO<sub>3</sub>, CdCl<sub>2</sub>, and ZnCl<sub>2</sub> in the sucrose-saturated solution.

CH (2.0 g) and PS (2.0 g) were added in 20.0 g of SFC (75.2% of moisture content) orderly and mixed well. Then, the mixture was humified in the style of strip compost for 2 h at 25 °C to get CH-PS/SFC. After that, 100 mL of deionized water was added to CH-PS/SFC (10.0 g) for stirring (160 rpm, 1 h). Meanwhile, the detection method of FLA was the same as that of the sucrose humifying experiment. In addition, organic matter, pH, and moisture of CH-PS/SFC were also detected and the descriptions of the procedures followed can be found in the Supporting Information (S2–S4).

**Analysis of Maturity of CH-PS/SFC.** Deionized water (100.0 mL) was added to CH-PS/SFC (10.0 g) for stirring (160 rpm, 1 h) at 25 °C. After that, the resulting solution was centrifuged at 10,000 rpm for 10 min, and the supernatant was filtered with a fiber membrane (0.45 μm). Subsequently, 2 pieces of filter paper (diameter = 8.0 cm) and 5 mL of the filtrate were placed on the Petri dishes (diameter = 9.0 cm) orderly and 10 cucumber seeds were added evenly on the surface of the filter paper. Then, the resulting system was placed in an incubator (dark, 25 °C, SRG-800C, China) for 48 h. After that, the germination rate and root length were measured. Germination index (GI) was calculated according to eqs 1 and 2

$$\text{germination percentage} = \frac{\text{number of germinated seeds}}{\text{total number of seeds}} \times 100\% \quad (1)$$

$$GI = \frac{A_1 + B_1}{A_2 + B_2} \times 100\% \quad (2)$$

where  $A_1$  and  $A_2$  were referred to as the average root length and  $B_1$  and  $B_2$  were germination percentages of cultivated seeds in the experimental and control groups, respectively.

**Pot Experiment.** The description of the preparation of the acidic soil (AS) with a pH of 4.8 can be found in S5. AS (500 g) was put in a plastic pot (trapezoidal shape, height 8.5 cm, diameter 10.0 cm (top), and 7.3 cm (bottom)), and then CH-PS/SFC (2.0 g) was spread on the surface of the AS. Subsequently, four seedlings of Chinese cabbage (length of 5.0–7.0 cm, diameter of 0.5–1.5 mm) were evenly planted in the AS. Afterward, all samples were kept in a greenhouse (humidity of 70%, light for 12 h every day) at 25 °C and HM solution (30 mL, 2 mg/L of Cu(II), Pd(II), and Cd(II), respectively) was sprayed to the system every 3 days. After 25 days, the height, yellow leaf ratio, chlorophyll content, length of root, and HM content of Chinese cabbages were measured and HMs detection is detailed in S6.

**Characterizations.** The morphology was measured by using a scanning electron microscope (SEM, FEI, Quanta250), and elemental analysis was performed by using SEM-energy-dispersive X-ray (SEM-EDX) (surface scanning, time = 100 s). X-ray photoelectron spectroscopy (XPS, Hitachi, S-4800, Japan) was performed by using Al K $\alpha$  radiation to analyze the chemical states of the elements of the samples. The structural and composition analyses were conducted on a TTR-III X-ray diffractometer (XRD, Hitachi, D/max-2550 PC, Japan) with the diffraction angles of 3–90° and a Fourier transform infrared spectrometer (FTIR, Thermo Fisher, Nicolet 6700) in the ranges of 400–4000 cm<sup>-1</sup>. The thermal stability of CH-PS/SFC was

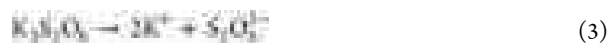
analyzed by thermal gravimetric analysis (TGA, Clarus, SQ8-STA8000, Netherlands) in the temperature ranges of 50–800 °C. The concentrations of FLA in CH-PS/sucrose and CH-PS/SFC were detected on a UV–vis spectrophotometer (Shimadzu, UV-1900i, Japan) at 262 nm. The chlorophyll contents in corn leaves were determined by a chlorophyll meter (YSI, 600CHL). FLA was detected using 3D-EEM matrix spectroscopy (Hitachi, F-7000, Japan) to confirm the generation and transformation. The composition of SFC was verified by gas chromatography–mass spectrometry (GC/MS, Shimadzu, QP2020, Japan) and is detailed in S7.

## RESULTS AND DISCUSSION

**Effects of CH-PS on Sucrose.** The effect of CH-PS with different mass ratios was investigated to obtain the conversion regularity of sucrose to FLA. As shown in Figure 1A, the FLA content did not increase at the addition of PS only compared with sucrose. With the increase of the CH amount ( $W_{PS}/W_{CH} = 4:1$ ), it was found that the FLA content (185.6 mg/g) improved. It was probably because PS could be activated by CH according to eqs 3–5,<sup>20</sup> which was beneficial for the production of FLA. As the proportion of CH increased, the content of FLA increased sequentially and the content of FLA reached the maximum value of 314.5 mg/g at  $W_{PS}/W_{CH} = 1:1$ . With the increase of CH proportion, the content of FLA began to decrease, probably because of the mineralization of FLA and the production of insufficient free radicals.<sup>21</sup> Therefore,  $W_{PS}/W_{CH} = 1:1$  was selected as the optimal ratio in the humifying process of sucrose. Figure 1B shows that the FLA content increased gradually with the addition of CH-PS before 6.0 g. Notably, the growth rate of FLA reached the maximum at 4.0 g of CH-PS. With the increase of the CH-PS amount (7.0 g), the content of FLA began to decrease, probably because of the mineralization of FLA.<sup>22</sup> Thus, the optimal amount of CH-PS was 4.0 g from the viewpoint of CH-PS utilization efficiency and economy. Meanwhile, the optimal humifying condition for sucrose was named CH-PS/sucrose ( $W_{PS}/W_{CH} = 1:1$ , 20% of CH-PS, and 2 h).

In addition, it can be seen from Figure 1C that the FLA content increased significantly before 1 h and reached a maximum value of 785.7 mg/g at 2 h. After that, the FLA content decreased slightly, which might be due to the excessive reaction leading to FLA mineralization. This result was also consistent with previous studies. As shown in Figure 1D, the effect of coexisting ions on the FLA content was also investigated. The FLA content decreased significantly after the addition of SO<sub>4</sub><sup>2-</sup>, H<sub>2</sub>PO<sub>4</sub><sup>-</sup>, and CO<sub>3</sub><sup>2-</sup> probably because the generation of free radicals could be inhibited by SO<sub>4</sub><sup>2-</sup> and H<sub>2</sub>PO<sub>4</sub><sup>-</sup>, according to eqs 3–5<sup>20,23</sup> and Le Chatelier's principle. In addition, the free radicals could be quenched by CO<sub>3</sub><sup>2-</sup>, which was disadvantageous for the generation of FLA.<sup>24</sup> The FLA content decreased significantly in the existence of Cd<sup>2+</sup> and Zn<sup>2+</sup>, probably because Cd<sup>2+</sup> and Zn<sup>2+</sup> could be chelated by FLA, which would influence the detection of FLA.<sup>25</sup>

Subsequently, the existence of FLA could be confirmed by 3D-EEM, and its characteristic peak positions were located at  $E_x/E_m = 230\text{--}250/370\text{--}430$  nm.<sup>8,26</sup> As shown in Figures 1E,F the content of FLA increased after CH-PS treatment, and thus CH-PS was beneficial for the humification of sucrose and the generation of FLA.



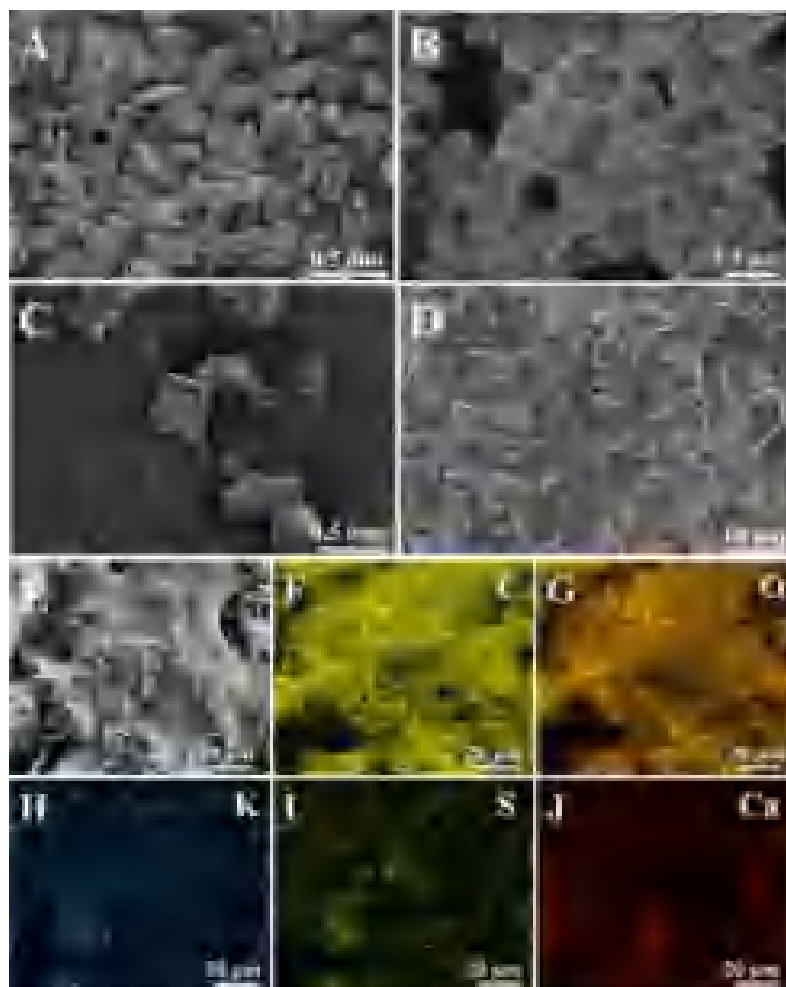


**Figure 2.** SEM images of (A–C) PS, CH, sucrose, and (D, E) CH-PS/sucrose. (F–J) Distribution maps of C, O, K, S, and Ca in CH-PS/sucrose.

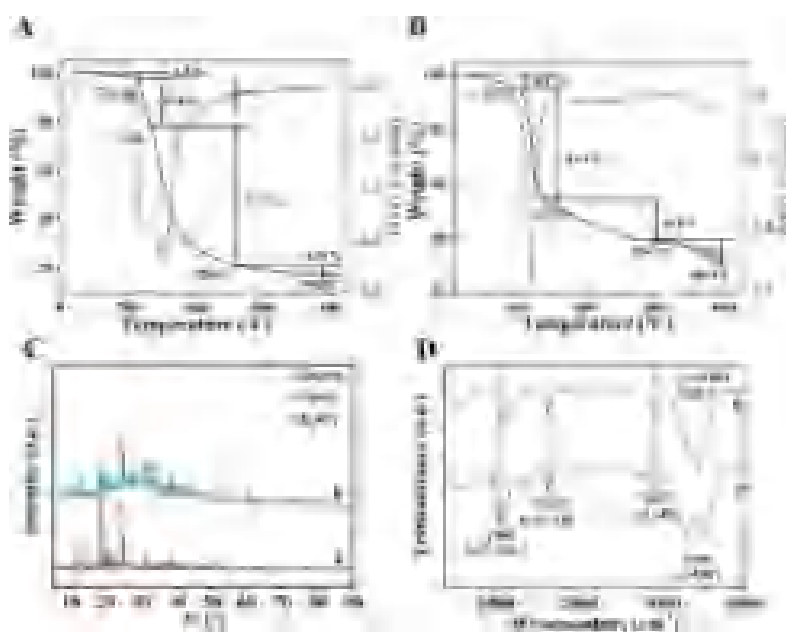


**Figure 3.** TGA (black) and DTG (blue) curves of (A) sucrose and (B) CH-PS/sucrose. (C) XRD spectra and (D) FTIR spectra of sucrose (a) and CH-PS/sucrose (b).

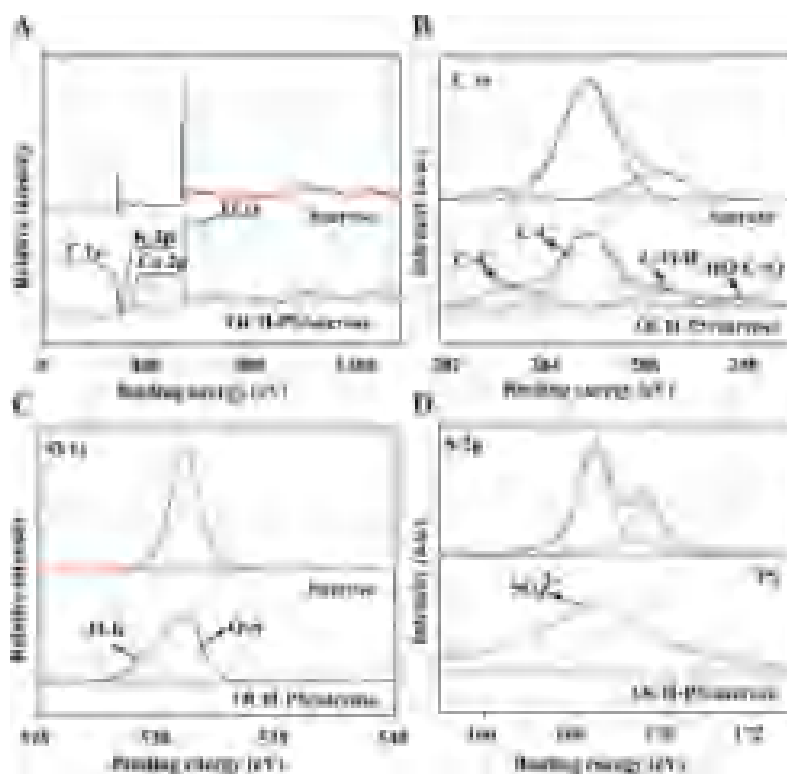


Figure 4. (A) Full-range XPS spectra of sucrose and CH-PS/sucrose. (B–D) XPS spectra of C 1s, O 1s, and S 2p.

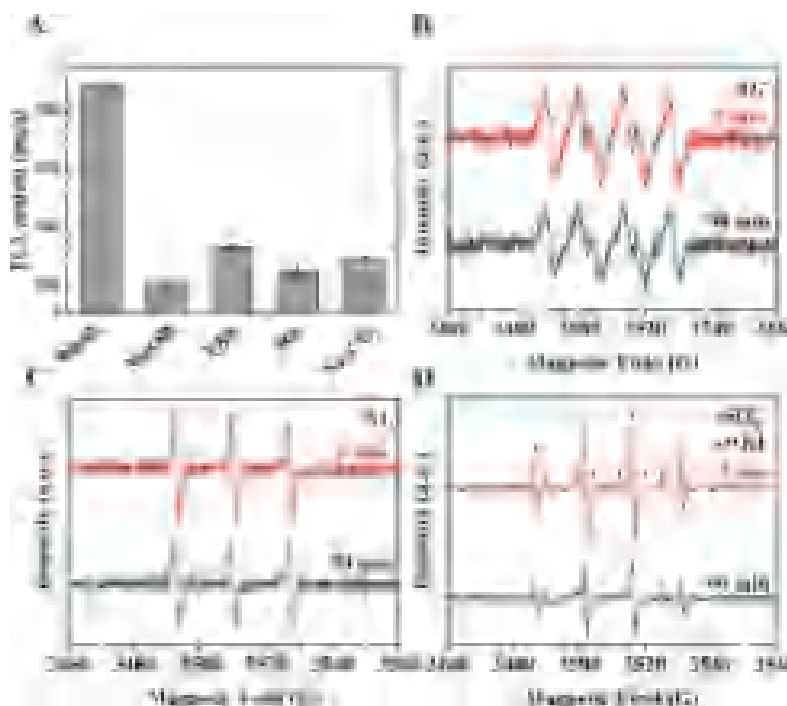


Figure 5. (A) Influence of quenching reagents for FLA content in the CH-PS/sucrose system (quenching reagent/PS = 10:1). EPR spectra at different time intervals using DMPO and TEMP as spin-trapping reagents for (B)  $\text{SO}_4^{\bullet-}$  and  $\bullet\text{OH}$ , (C)  $^1\text{O}_2$ , and (D)  $\bullet\text{O}_2^-$ .



(5)

**Mechanism of the Investigation of CH-PS on the Humification of Sucrose.** In order to study the humification mechanism of sucrose by CH-PS, the morphologies of CH-PS/sucrose were observed. After the treatment of sucrose by PS

(Figure 2A) and CH (Figure 2B), the particle size decreased from 500  $\mu\text{m}$  to less than 10  $\mu\text{m}$ , indicating that sucrose (Figure 2C) could be decomposed into smaller particles by CH-PS in CH-PS/sucrose (Figure 2D,E). As shown in Figure 2F–J, the elements of C (36.9%), O (48.6%), K (4.2%), S (2.2%), and Ca (8.1%) were uniformly distributed on the

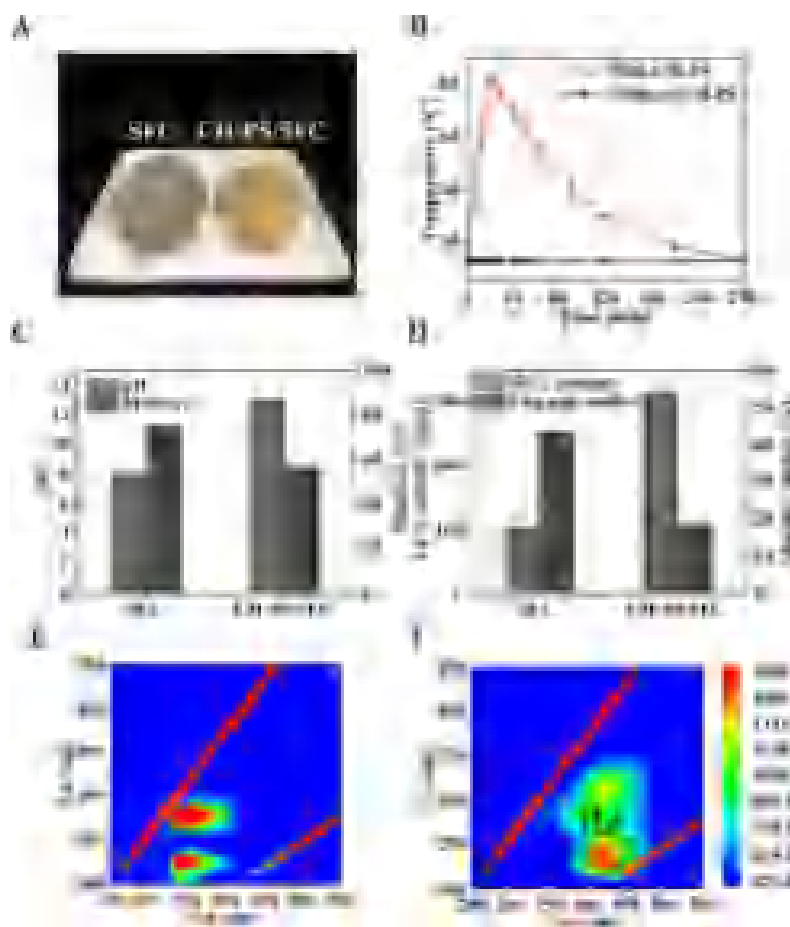


**Figure 6.** (A) Digital photograph of SFC and CH-PS/SFC. (B) Changes of temperature with time during the humification process of SFC. (C, D) FLA content, organic matter content, pH, and moisture in SFC and CH-PS/SFC. (E, F) 3D-EEM for FLA in SFC and CH-PS/SFC. Reaction conditions:  $m_{\text{SFC}} = 20$  g,  $W_{\text{PS}}/W_{\text{CH}} = 1:1$ ,  $m_{\text{CH-PS}} = 4.0$  g, and time = 4 h.

surface of CH-PS/sucrose (Table S1). Moreover, the percentage of K–S–Ca could reach 14.5%, which was advantageous for improving fertilizers' efficiency.

TG-differential thermal analysis (TG-DTA) was also performed to further investigate the humification mechanism of sucrose by CH-PS. As shown in Figures 3A and 4B, the first weight loss regions of sucrose (below 227.9 °C) and CH-PS/sucrose (below 207.0 °C) were 1.8 and 4.8%, respectively, because CH-PS/sucrose possessed more hydrophilic groups (–COOH and –OH) than sucrose, which was consistent with the FTIR results in Figure 3C. The second weight loss of CH-PS/sucrose (41.4%) was significantly higher than that of sucrose (19.8%), illustrating that sucrose was humified to smaller molecules such as FLA (furan, ketone, and esters) with a lower thermal stability. This could also be proved by the results of GC-MS for CH-PS/sucrose (Figure S1). Additionally, the characteristic peak of C–O–C (1064  $\text{cm}^{-1}$ ) of CH-PS/sucrose became weaker compared with sucrose, while the peaks of C=O (1639  $\text{cm}^{-1}$ ) and –OH (3438  $\text{cm}^{-1}$ ) became stronger, likely suggesting that C–O–C was transformed to –COOH through the oxidation of radicals. In addition, XRD measurements were applied to analyze the humification mechanism of sucrose. As shown in Figure 3C,  $\text{K}_2\text{SO}_4$  and  $\text{CaSO}_4$  were found in CH-PS/sucrose after the humification of sucrose, indicating that  $\text{S}_2\text{O}_8^{2-}$  was transferred to  $\text{SO}_4^{2-}$  after

the reaction. Thus,  $\text{SO}_4^{\bullet-}$  could be produced according to eqs 3 and 4.

The XPS spectra were also employed to analyze the structure change and the humification mechanism of the sucrose and CH-PS/sucrose. As shown in Figures 4A and S2, the peaks of K, Ca, and S appeared in the CH-PS/sucrose spectrum, indicating that CH-PS was mixed with sucrose evenly. For the C 1s spectrum of CH-PS/sucrose (Figure 4B), four peaks with binding energies of 283.2, 284.8, 285.4, and 288.5 eV were observed, corresponding to C=C, C–C, C–O–R, and O=C–OH.<sup>27</sup> Thus, the oxygen-containing groups increased in the CH-PS/sucrose spectrum compared with sucrose, and sucrose was humified by CH-PS successfully. As for the O 1s spectrum of CH-PS/sucrose, the peak at 529.7 eV was the same as PS, which revealed that PS still existed after the humification of sucrose (Figures 4B and S3). In addition, the S 2p spectrum of CH-PS/sucrose revealed that the peak at 168.5 eV corresponded to  $\text{SO}_4^{2-}$ .<sup>28</sup> Therefore, this result also illustrated that  $\text{S}_2\text{O}_8^{2-}$  was transferred to  $\text{SO}_4^{2-}$  after the reaction.

**Identification of Reactive Oxygen Species.** The quenching experiments were adopted to further explore the mechanism of sucrose humification by CH-PS. Therein, MeOH, TBA, His, and  $\text{Na}_2\text{CO}_3$  were used as free radical quenchers to remove  $\text{SO}_4^{\bullet-}$ ,  $\bullet\text{OH}$ ,  $^1\text{O}_2$ , and  $\bullet\text{O}_2^-$ ,

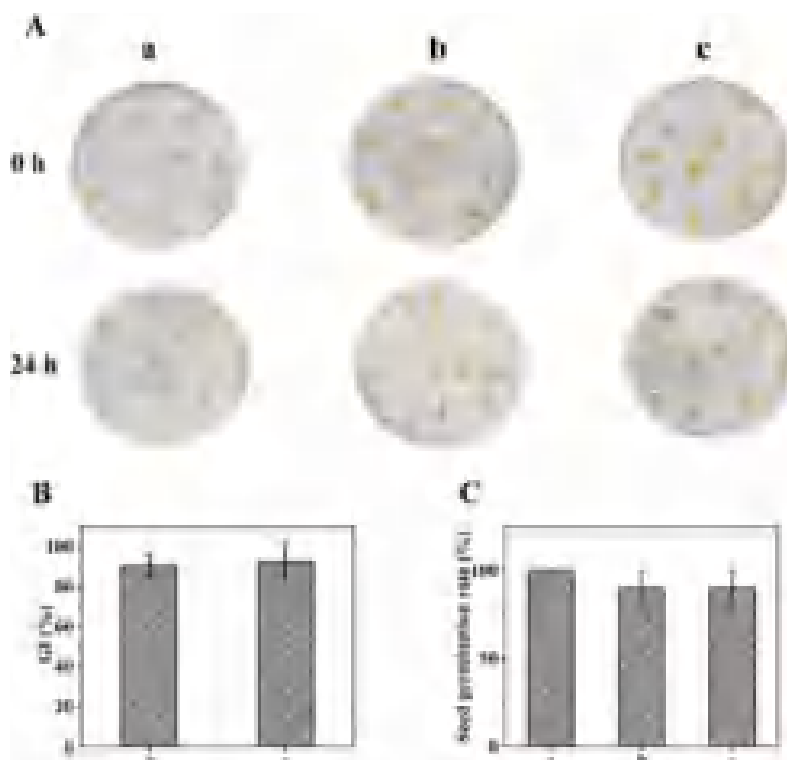


**Figure 7.** (A) Digital photographs of the germination test of cucumber seeds. (B, C) Germination rate and GI of cucumber seeds. (a) Deionized water, (b) CH-PS/SFC filtrate, and (c) CH-PS/SFC filtrate diluted 10 times.

**Table 1. Comparison of GI and Germination Rate of Different Samples Made from Different Raw Materials and Methods**

s.no.	plant	raw material	method	times	GI (%)	germination rate (%)	refs
1	wheat	wheat straw	compost	50 days	92	98	31
2	corn	peanut shells	compost	7 days	29	90	32
3	Chinese cabbage	bagasse	compost	90 days	25		37
4	pakchoi	food waste	hydrothermal/ compost	34 days	91		38
5	radish	food waste	compost	15 days	94		39
6	cucumber	SFC	AOPs	2 h	85	83	this work

respectively.<sup>24</sup> Furthermore, the free radicals of  $\cdot\text{OH}$  and  $\text{SO}_4^{\cdot-}$  could be strongly inhibited by MeOH simultaneously.<sup>29</sup>

As shown in Figure 5A, the FLA content decreased by 682.7, 560.95, 643.4, and 597.35 mg/g, respectively, with the addition of MeOH, TBA, His, and  $\text{Na}_2\text{CO}_3$ . This result proved that the free radicals ( $\text{SO}_4^{\cdot-}$ ,  $\cdot\text{OH}$ , and  $\cdot\text{O}_2^-$ ) and nonfree radical ( $^1\text{O}_2$ ) existed in the humification process of sucrose, which was also consistent with eqs 3–6.<sup>30</sup> In addition, the humification contribution of radicals could be listed as  $\cdot\text{OH} + \text{SO}_4^{\cdot-} \geq ^1\text{O}_2 \geq \cdot\text{OO}_2^- \geq \cdot\text{OH}$ . Figure 5B–D could also demonstrate the existence of four active substances and these could be detected at 90 min still. This result was also consistent with XPS spectra (Figure 4C). Thus, these radicals had a high utilization efficiency because of the slow production in the CH-PS/sucrose system.<sup>21</sup>



**Humification Process and Mechanism of SFC.** To elucidate the practical application of CH-PS, SFC, with a large amount of sucrose, was chosen as a typical substance. Figure 6A shows that the color of the SFC was changed from dark green to yellow, probably because of FLA. The maximum temperature of CH-PS/SFC could reach 80.3 °C at 20 min

(Figure 6B) during the humification process. Thus, the heating rate was excellent compared to traditional compost.<sup>31,32</sup> Furthermore, the moisture of SFC was reduced by 20%, probably due to the high temperature of SFC humification by CH-PS (Figure 6C). Also, the pH of SFC was increased significantly from 8 to 13 after the CH-PS treatment and the main reason was the addition of CH (Figure 6C). Thus, CH-PS/SFC could be used to remediate AS. As shown in Figure 6D, the FLA content in SFC was 102.5 mg/g and that of CH-PS/SFC increased to 316.8 mg/g, which was nearly 3 times that of SFC. Simultaneously, the content of organic matter decreased remarkably after the humification of SFC, likely because of the addition of CH-PS. In addition, the content of K was increased from 3.5 to 64.0 g/kg and the HM content was in accordance with the international standard for organic fertilizers after the humification of SFC (Table S2).<sup>33</sup> It was probably due to the passivation of CH-PS and the chelation of FLA for HMs. Interestingly, the crude protein and crude fat contents were decreased dramatically, and the 17 amino acids and fatty acid content were significantly increased in CH-PS/SFC (Figures S4 and S5).<sup>34</sup> Furthermore, the contents of phenol and furan were distinctly increased in CH-PS/SFC, indicating that the crude fiber in SFC could be degraded by



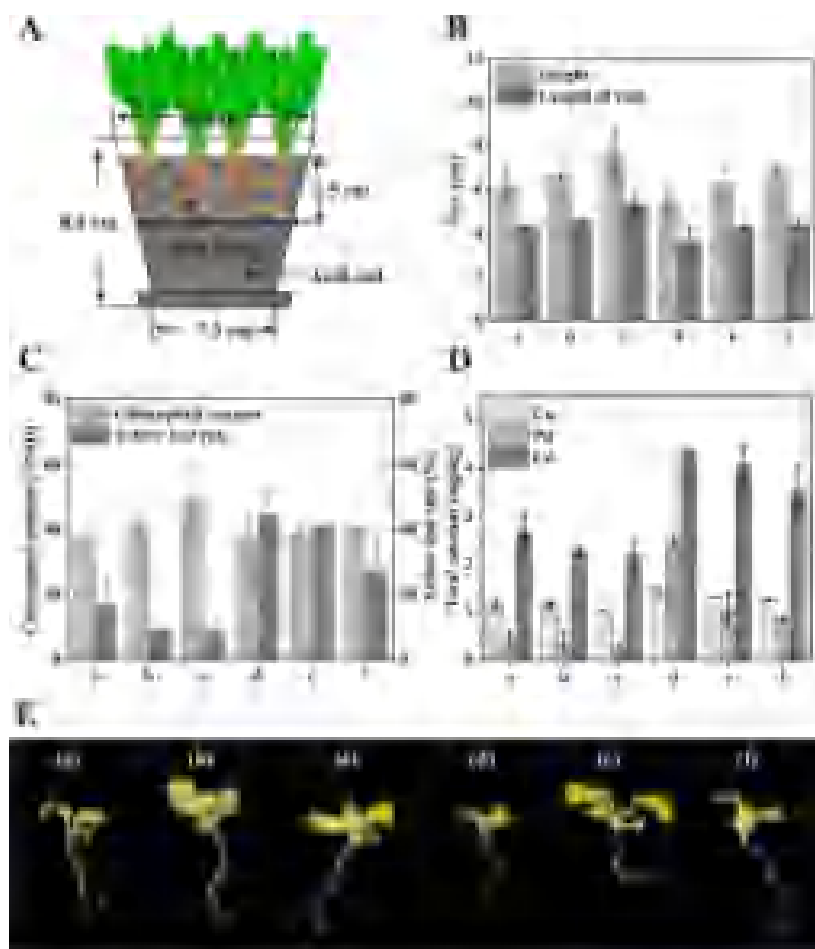


**Figure 8.** (A) Schematic diagram of the pot experiment system. (B, C) Height, length of root, chlorophyll content, and yellow leaf rate of Chinese cabbage with different treatments. (D) Total amounts of Cu, Pb, and Cd in the Chinese cabbage with different treatments. (E) Digital photographs of Chinese cabbage. (a) AS (pH = 4.8), (b) AS + CH-PS/SFC (1.0 g), (c) AS + CH-PS/SFC (2.0 g), (d) AS/HMs, (e) AS/HMs + CH-PS/SFC (1.0 g), and (f) AS/HMs + CH-PS/SFC (2.0 g).

CH-PS (Figures S5 and S6 and Table S3).<sup>35</sup> At the same time, Figure 6E,F illustrates that FLA was successfully fabricated by CH-PS. These results elucidated that the humification process of SFC by CH-PS was rapid and high temperature, which could produce an organic fertilizer with nutrient-rich (FLA), nonhazardous (immobilization HMs), and high pH.

**Maturity Test of CH-PS/SFC.** The toxicity and maturity of CH-PS/SFC were evaluated by the GI of cucumber seeds. As shown in Figure 7, the germination rate of cucumber seeds was nearly 100% and the GI was over 80%, indicating complete humification of SFC and CH-PS/SFC could act as a rich-FLA organic fertilizer.<sup>36</sup> Compared with the previous studies (Table 1), it could be found that the humification time of SFC was the shortest.

**Pot Experiments.** Due to the high pH value of CH-PS/SFC organic fertilizer (a large number of FLA and nutritious elements), CH-PS/SFC could be taken as a kind of AS and HM remediation agent. As shown in Figure 8A–C, the height, length of root, and chlorophyll content increased markedly and the yellow leaf rate of Chinese cabbage decreased significantly at the existence of CH-PS/SFC compared with AS and AS/HMs alone. Additionally, the pH of AS improved from 5.5 to 7.0 after adding CH-PS/SFC (Figure S7). Thus, CH-PS/SFC could not only remediate AS but also reduce the HM toxicity for Chinese cabbage. Furthermore, the total amounts of Cu,

Pb, and Cd were decreased distinctly in Chinese cabbage at the existence of CH-PS/SFC compared with AS and AS/HMs alone and that of HMs decreased gradually with the increase of the CH-PS/SFC amount (Figure 8D). Therefore, CH-PS/SFC could inhibit the uptake of HMs by Chinese cabbage and promote the growth of Chinese cabbage (Figure 8E).

In this work, SFC was treated with CH-PS to convert it into a fertilizer with high amounts of FLA, AS remediation, and HM immobilization. The sucrose-saturated solution was a model to investigate first. The sucrose was humified quickly by CH-PS to produce a large amount of FLA for 2 h. After 2 h, SFC was also humified to produce an organic fertilizer with abundant FLA. In addition, the maximum temperature could reach 80.3 °C and the water was removed by about 20% during the humification of SFC. Furthermore, pot experiments showed that CH-PS/SFC could promote the growth of Chinese cabbage in height, length of root, and chlorophyll content and decrease the yellow leaves rate. Moreover, the HM content reduced significantly in Chinese cabbage and the pH value of AS improved apparently after the treatment of CH-PS/SFC. Therefore, this work provides a rapid-humification, low-cost (30 \$/t), and high-value way to deal with SFC.



## ■ ASSOCIATED CONTENT

## SI Supporting Information

The Supporting Information is available free of charge at <https://pubs.acs.org/doi/10.1021/acssuschemeng.3c03511>.

Compositions analysis of CH-PS/sucrose based on GC-MS; mass ratios of C, O, S, Ca, and K elements on sucrose and CH-PS/sucrose based on the XPS spectra; XPS spectrum of O 1s for PS; composition analysis of SFC and CH-PS/SFC based on GC-MS; the effect of CH-PS/SFC on the acid soil pH; the element proportion of CH-PS/sucrose based on SEM-EDX; effect of CH-PS on the elemental contents of SFC and CH-PS/SFC; and basic physical and chemical properties of the experimental original soil (PDF)

## ■ AUTHOR INFORMATION

## Corresponding Author

**Dongfang Wang** – College of Environmental Science and Engineering, Donghua University, Shanghai 201620, People's Republic of China; Shanghai Institute of Pollution Control and Ecological Security, Shanghai 200092, People's Republic of China; [orcid.org/0000-0003-3720-8297](https://orcid.org/0000-0003-3720-8297); Phone: +86-21-67792625; Email: [dfwang@dhu.edu.cn](mailto:dfwang@dhu.edu.cn)

## Authors

**Dongqing Cai** – College of Environmental Science and Engineering, Donghua University, Shanghai 201620, People's Republic of China; Shanghai Institute of Pollution Control and Ecological Security, Shanghai 200092, People's Republic of China

**Xianghai Kong** – College of Environmental Science and Engineering, Donghua University, Shanghai 201620, People's Republic of China

**Xiaojiang Zhang** – College of Environmental Science and Engineering, Donghua University, Shanghai 201620, People's Republic of China

**Jinghong Ye** – College of Environmental Science and Engineering, Donghua University, Shanghai 201620, People's Republic of China

**He Xu** – College of Environmental Science and Engineering, Donghua University, Shanghai 201620, People's Republic of China; Shanghai Institute of Pollution Control and Ecological Security, Shanghai 200092, People's Republic of China; [orcid.org/0000-0003-2225-4725](https://orcid.org/0000-0003-2225-4725)

**Yanping Zhu** – College of Environmental Science and Engineering, Donghua University, Shanghai 201620, People's Republic of China; Shanghai Institute of Pollution Control and Ecological Security, Shanghai 200092, People's Republic of China

Complete contact information is available at: <https://pubs.acs.org/doi/10.1021/acssuschemeng.3c03511>

## Author Contributions

D.C. wrote, reviewed, and edited the manuscript and supervised the study. X.K. was responsible for conceptualization and methodology. X.Z. performed the methodology and software. J.Y. was responsible for data curation and software. H.X. performed the project administration and supervision. Y.Z. was responsible for data curation and methodology. D.W. performed the formal analysis and writing, reviewing, and editing the manuscript.

## Notes

The authors declare no competing financial interest.

## ■ ACKNOWLEDGMENTS

The authors acknowledge financial support from the Fundamental Research Funds for the Central Universities (22D111317 and 2232020D-22), the Key R&D Program of Guangdong Province (2020B0202010005), the Plan for Anhui Major Provincial Science & Technology Project (202203a06020001), the National Natural Science Foundation of China (52000025), the Key R&D Program of Shandong Province (2022SFGC0302), the Key R&D Program of Inner Mongolia Autonomous Region (2021GG0300), the Key Program (Achievement Transformation) of "Revitalizing the City by Science and Technology" of Hulun Buir (2022HZXX008), and the Science and Technology Service Programs of Chinese Academy of Sciences (KFJ-STZ-QYZD-199).

## ■ REFERENCES

- (1) Xu, Q.; Ji, T.; Gao, S. J.; Yang, Z.; Wu, N. Characteristics and applications of sugar cane bagasse ash waste in cementitious materials. *Materials* **2018**, *12*, No. 39.
- (2) Raza, Q.-U.-A.; Bashir, M. A.; Rehim, A.; Sial, M. U.; Ali Raza, H. M.; Atif, H. M.; Brito, A. F.; Geng, Y. Sugarcane industrial byproducts as challenges to environmental safety and their remedies: A Review. *Water* **2021**, *13*, No. 3495.
- (3) González, L. M. L.; Reyes, I. P.; Dewulf, J.; Budde, J.; Heiermann, M.; Vervaeren, H. Effect of liquid hot water pretreatment on sugarcane press mud methane yield. *Bioresour. Technol.* **2014**, *169*, 284–290.
- (4) Carpanez, T. G.; Moreira, V. R.; Assis, I. R.; Amaral, M. C. S. Sugarcane vinasse as organo-mineral fertilizers feedstock: Opportunities and environmental risks. *Sci. Total Environ.* **2022**, *832*, No. 154998.
- (5) Alengebawy, A.; Mohamed, B. A.; Jin, K.; Liu, T.; Ghimire, N.; Samer, M.; Ai, P. A comparative life cycle assessment of biofertilizer production towards sustainable utilization of anaerobic digestate. *Sustainable Prod. Consumption* **2022**, *33*, 875–889.
- (6) de Melo, A. L. F.; Rossato, L.; dos Santos Barbosa, M.; Palozi, R. A. C.; Alfredo, T. M.; Antunes, K. A.; Eduvirgem, J.; Ribeiro, S. M.; Simionatto, S. From the environment to the hospital: How plants can help to fight bacteria biofilm. *Microbiol. Res.* **2022**, *261*, No. 127074.
- (7) He, P.; Wei, S.; Shao, L.; Lü, F. Aerosolization behavior of prokaryotes and fungi during composting of vegetable waste. *Waste Manage.* **2019**, *89*, 103–113.
- (8) Cai, D.; Yao, X.; Wu, Q.; Ye, J.; Zhang, J.; Guo, M.; Xu, H.; Wang, D. Gel-based nanocomposite using persulfate-activated bread crumbs for fulvic acid release and Pb(II) removal. *Chem. Eng. J.* **2022**, *446*, No. 137002.
- (9) Wang, X.; Xia, J.; Ding, S.; Zhang, S.; Li, M.; Shang, Z.; Lu, J.; Ding, J. Removing organic matters from reverse osmosis concentrate using advanced oxidation-biological activated carbon process combined with Fe<sup>3+</sup>/humus-reducing bacteria. *Ecotoxicol. Environ. Saf.* **2020**, *203*, No. 110945.
- (10) Zhang, Y.; Zhao, Y. G.; Yang, D.; Zhao, Y. Insight into the removal of tetracycline-resistant bacteria and resistance genes from mariculture wastewater by ultraviolet/persulfate advanced oxidation process. *J. Hazard. Mater. Adv.* **2022**, *7*, No. 100129.
- (11) Lv, D.; Sun, H.; Zhang, M.; Li, C. Fulvic acid fertilizer improves garlic yield and soil nutrient status. *Gesunde Pflanz.* **2022**, *74*, 685–693.
- (12) Cui, H.; Wen, X.; Wu, Z.; Zhao, Y.; Lu, Q.; Wei, Z. Insight into complexation of Cd(II) and Cu(II) to fulvic acid based on feature recognition of PARAFAC combined with 2DCOS. *J. Hazard. Mater.* **2022**, *440*, No. 129758.

- (13) Xing, R.; Yang, X.; Sun, H.; Ye, X.; Liao, H.; Qin, S.; Chen, Z.; Zhou, S. Extensive production and evolution of free radicals during composting. *Bioresour. Technol.* **2022**, *359*, No. 127491.
- (14) Sun, R.; Fu, M.; Ma, L.; Zhou, Y.; Li, Q. Iron reduction in composting environment synergized with quinone redox cycling drives humification and free radical production from humic substances. *Bioresour. Technol.* **2023**, *384*, No. 129341.
- (15) Wang, C.; Kim, J.; Malgras, V.; Na, J.; Lin, J.; You, J.; Zhang, M.; Li, J.; Yamauchi, Y. Metal-Organic frameworks and their derived materials: emerging catalysts for a sulfate radicals-based advanced oxidation process in waterpurification. *Small* **2019**, *15*, No. 1900744.
- (16) Li, L.; Yuan, X.; Zhou, Z.; Tang, R.; Deng, Y.; Huang, Y.; Xiong, S.; Su, L.; Zhao, J.; Gong, D. Research progress of photocatalytic activated persulfate removal of environmental organic pollutants by metal and nonmetal based photocatalysts. *J. Cleaner Prod.* **2022**, *372*, No. 133420.
- (17) Wang, T.; Xu, K. M.; Yan, K. X.; Wu, L. G.; Chen, K. P.; Wu, J. C.; Chen, H. L. Comparative study of the performance of controlled release materials containing mesoporous MnOx in catalytic persulfate activation for the remediation of tetracycline contaminated groundwater. *Sci. Total Environ.* **2022**, *846*, No. 157217.
- (18) Chen, J.; Jiang, X.; Zhang, Y.; Zhang, Y.; Sun, Y.; Zhang, L. Organic matter conversion and contributors to bioavailability in biogas slurry treated by biochar/persulfate during the oxidation pond process. *J. Cleaner Prod.* **2022**, *355*, No. 131770.
- (19) Arvaniti, O. S.; Ioannidi, A. A.; Mantzavinos, D.; Frontistis, Z. Heat-activated persulfate for the degradation of micropollutants in water: A comprehensive review and future perspectives. *J. Environ. Manage.* **2022**, *318*, No. 115568.
- (20) Preethi; Banu, J. R.; Sharmila, V. G.; Kavitha, S.; Varjani, S.; Kumar, G.; Gunasekaran, M. Alkali activated persulfate mediated extracellular organic release on enzyme secreting bacterial pretreatment for efficient hydrogen production. *Bioresour. Technol.* **2021**, *341*, No. 125810.
- (21) Yang, X.; Ding, X.; Zhou, L.; Fan, H. H.; Wang, X.; Ferronato, C.; Chovelon, J. M.; Xiu, G. New insights into clopyralid degradation by sulfate radical: Pyridine ring cleavage pathways. *Water Res.* **2020**, *171*, No. 115378.
- (22) Liang, R.; Van Leuwen, J. C.; Bragg, L. M.; Arlos, M. J.; Li Chun Fong, L. C. M.; Schneider, O. M.; Jaciw-Zurakowsky, I.; Fattahi, A.; Rathod, S.; Peng, P.; Servos, M. R.; Zhou, Y. N. Utilizing UV-LED pulse width modulation on TiO<sub>2</sub> advanced oxidation processes to enhance the decomposition efficiency of pharmaceutical micro-pollutants. *Chem. Eng. J.* **2019**, *361*, 439–449.
- (23) Wang, J.; Wang, C.; Guo, H.; Ye, T.; Liu, Y.; Cheng, X.; Li, W.; Yang, B.; Du, E. Crucial roles of oxygen and superoxide radical in bisulfite-activated persulfate oxidation of bisphenol AF: Mechanisms, kinetics and DFT studies. *J. Hazard. Mater.* **2020**, *391*, No. 122228.
- (24) Gao, L.; Guo, Y.; Zhan, J.; Yu, G.; Wang, Y. Assessment of the validity of the quenching method for evaluating the role of reactive species in pollutant abatement during the persulfate-based process. *Water Res.* **2022**, *221*, No. 118730.
- (25) Wang, D.; Li, J.; Yao, X.; Wu, Q.; Zhang, J.; Ye, J.; Xu, H.; Wu, Z.; Cai, D. Tobacco waste liquid-based organic fertilizer particle for controlled-release fulvic acid and immobilization of heavy metals in soil. *Nanomaterials* **2022**, *12*, No. 2056.
- (26) Chen, W.; Westerhoff, P.; Leenheer, J. A.; Booksh, K. Fluorescence excitation-emission matrix regional Integration to quantify Spectra for dissolved organic matter. *Environ. Sci. Technol.* **2003**, *37*, 5701–5710.
- (27) Zhang, Y.; Zhang, B. T.; Teng, Y.; Zhao, J.; Sun, X. Heterogeneous activation of persulfate by carbon nanofiber supported Fe<sub>3</sub>O<sub>4</sub>@carbon composites for efficient ibuprofen degradation. *J. Hazard. Mater.* **2021**, *401*, No. 123428.
- (28) Zhao, T.; Jiang, L.; Liu, J.; Wu, H.; Qin, N.; Qian, L. Potassium persulfate as an effective oxidizer for chemical mechanical polishing of GCr15 bearing steel. *J. Appl. Electrochem.* **2021**, *51*, 803–814.
- (29) Bian, C.; Ge, D.; Wang, G.; Dong, Y.; Li, W.; Zhu, N.; Yuan, H. Enhancement of waste activated sludge dewaterability by ultrasound-activated persulfate oxidation: Operation condition, sludge properties, and mechanisms. *Chemosphere* **2021**, *262*, No. 128385.
- (30) Zhang, H.; Yan, Z.; Wan, J.; Wang, Y.; Ye, G.; Huang, S.; Zeng, C.; Yi, J. Synthesis of Fe-Nx site-based iron-nitrogen co-doped biochar catalysts for efficient removal of sulfamethoxazole from water by activation of persulfate: Electron transfer mechanism of non-free radical degradation. *Colloids Surf., A* **2022**, *654*, No. 130174.
- (31) Liu, D.; Xie, B.; Dong, C.; Liu, G.; Hu, D.; Qin, Y.; Li, H.; Liu, H. Effect of fertilizer prepared from human feces and straw on germination, growth and development of wheat. *Acta Astronaut.* **2018**, *145*, 76–82.
- (32) Bibi, F.; Ilyas, N.; Arshad, M.; Khalid, A.; Saeed, M.; Ansar, S.; Batley, J. Formulation and efficacy testing of bio-organic fertilizer produced through solid-state fermentation of agro-waste by Burkholderia cenocepacia. *Chemosphere* **2022**, *291*, No. 132762.
- (33) Hai, D. M.; Qiu, X.; Xu, H.; Honda, M.; Yabe, M.; Kadokami, K.; Shimasaki, Y.; Oshima, Y. Contaminants in Liquid Organic Fertilizers Used for Agriculture in Japan. *Bull. Environ. Contam. Toxicol.* **2017**, *99*, 131–137.
- (34) Wang, M. L.; Harrison, M. L.; Tonniss, B. D.; Pinnow, D.; Davis, J.; Irish, B. M. Total leaf crude protein, amino acid composition and elemental content in the USDA-ARS bamboo germplasm collections. *Plant Genet. Resour.* **2018**, *16*, 185–187.
- (35) Bu, Q.; Chen, K.; Xie, W.; Liu, Y.; Cao, M.; Kong, X.; Chu, Q.; Mao, H. Hydrocarbon rich bio-oil production, thermal behavior analysis and kinetic study of microwave-assisted co-pyrolysis of microwave-torrefied lignin with low density polyethylene. *Bioresour. Technol.* **2019**, *291*, No. 121860.
- (36) Yang, Y.; Wang, G.; Li, G.; Ma, R.; Kong, Y.; Yuan, J. Selection of sensitive seeds for evaluation of compost maturity with the seed germination index. *Waste Manage.* **2021**, *136*, 238–243.
- (37) Meunchang, S.; Panichsakpatana, S.; Weaver, R. W. Co-composting of filter cake and bagasse; by-products from a sugar mill. *Bioresour. Technol.* **2005**, *96*, 437–442.
- (38) Xie, T.; Zhang, Z.; Zhang, D.; Wei, C.; Lin, Y.; Feng, R.; Nan, J.; Feng, Y. Effect of hydrothermal pretreatment and compound microbial agents on compost maturity and gaseous emissions during aerobic composting of kitchen waste. *Sci. Total Environ.* **2023**, *854*, No. 158712.
- (39) Xin, L.; Li, X.; Bi, F.; Yan, X.; Wang, H.; Wu, W. Accelerating Food Waste Composting Course with Biodrying and Maturity Process: A Pilot Study. *ACS Sustainable Chem. Eng.* **2021**, *9*, 224–235.



# Accelerated spent coffee grounds humification by heat/base co-activated persulfate and products' fertilization evaluation

Yanping Zhu<sup>a</sup>, Keyi Zhang<sup>a</sup>, Qing Hu<sup>a</sup>, Weijia Liu<sup>a</sup>, Yi Qiao<sup>a</sup>, Dongqing Cai<sup>a</sup>, Pengjin Zhu<sup>b</sup>, Dongfang Wang<sup>a</sup>, He Xu<sup>a</sup>, Shihu Shu<sup>a,\*</sup>, Naiyun Gao<sup>c</sup>

<sup>a</sup> College of Environmental Science and Engineering, Donghua University, Shanghai 201620, China

<sup>b</sup> Guangxi Subtropical Crops Research Institute, Nanning 530000, China

<sup>c</sup> State Key Laboratory of Pollution Control Reuse, Tongji University, Shanghai 200092, China

## ARTICLE INFO

### Keywords:

Artificial humification  
Persulfate-based advanced oxidation  
Biowaste  
Fulvic acid  
Fertilization effect

## ABSTRACT

Coffee, as the second most common beverage in the world, produced 60% of spent coffee grounds (SCG) with per ton of coffee beans processed. SCG is a typical lignocellulosic-rich organic waste and mainly disposed via composting or incineration. In this study, a rapid humification approach was proposed for the recycling of SCG using heat/base co-activated persulfate (heat/KOH/PS) advanced oxidation process. The yields of humic-like acid (HLA) and fulvic-like acid (FLA) reached 45 (3.96%) and 192 mg/g (19.2%) under the optimal humification conditions of 1% PS and 4% KOH at 100 °C in 1 h. The typical active groups of -OH and -COOH in FA standard were observed with higher amounts in the product compared to SCG, which may be related to occurrence of hydroxylation, carboxylation and Maillard reactions during humification. Radicals of  $\bullet\text{OH}$  and  $\text{SO}_4^{\bullet-}$  were identified in heat/KOH/PS system and made significant contribution to SCG humification. A slow-release nano FLA fertilizer (SNFF) was prepared by mixing treated SCG with attapulgite and showed good slow-release behaviors of HLA and FLA. In pot experiments with acid soil, SNFF increased the average root length of chickweeds by 233% compared with blank. Meanwhile, SNFF also contributed to increased abundance and richness of soil microbial community as well as a pH rise from 5 to 6.7, which was conducive to acid soil amendment. The earthworm test indicated positive ecological safety of SNFF. Overall, this study highlights an efficient humification method for the recycling of organic biowaste such as SCG in green agriculture.

## 1. Introduction

Coffee is the second most popular beverage in the world, with an estimated global consumption of 10 million tons in 2020 and a

*Abbreviations:* 3D-EEM, three dimensional-excitation emission matrix; AOP, advanced oxidation process; ASO, aminosilicone oil; ATP, attapulgite; BET, Brunauer-Emmett-Teller; DMPO, 5,5-Dimethyl-1-pyrroline-N-oxide; EPR, electron paramagnetic resonance; EtOH, ethanol anhydrous; FA, fulvic acid; FLA, fulvic-like acid; FRI, fluorescence regional integration; HLA, humic-like acid; NMR, nuclear magnetic resonance; PS, K2S2O8; SCG, spent coffee grounds; SEM, scanning electron microscope; SHA, soluble humic acid; SNFF, slow-release nano fulvic-like acid fertilizer; TBA, *tert*-butanol; TSCG, treated spent coffee grounds; XG, xanthan gum; XPS, X-ray photoelectron spectroscopy; XRD, X-ray diffraction.

\* Corresponding author.

E-mail address: [ShihuShu@163.com](mailto:ShihuShu@163.com) (S. Shu).

<https://doi.org/10.1016/j.eti.2023.103393>

Received 6 August 2023; Received in revised form 4 October 2023; Accepted 5 October 2023

Available online 7 October 2023

2352-1864/© 2023 The Authors. Published by Elsevier B.V. This is an open access article under the CC BY-NC-ND license (<http://creativecommons.org/licenses/by-nc-nd/4.0/>).

production of approximately 6.5 million tons spent coffee grounds (SCG) (Murthy and Naidu, 2012). SCG is a typical biowaste with the main components of hemicellulose (30–40%), lignin (25–33%), cellulose (8.6–13.3%), oil (10–20%), and proteins (6.7–13.6%) (Stylianou et al., 2018). Currently, it is usually treated by direct landfill or incineration, causing wide environmental concerns and a waste of resource (Das et al., 2022a; 2022b). Recent research regarding the valorization of SCG mainly includes the extraction of food ingredients, plant nutrients, bioenergy, and using as environmental pollution remediation or photothermal materials after modification (Chen et al., 2023; Gebreeyessus, 2022; Hsieh et al., 2023). Considering the relatively high contents of organic matter (90.5%) and nitrogen (1–2.5%) in SCG, some attempts have been made for its utilization as a biofertilizer/soil amendment directly or after composting (Gebreeyessus, 2022). Therein, its direct application in agriculture is not recommended because it may inhibit seed germination and crop growth due to the ecotoxicity of caffeine, tannins, and polyphenols in SCG (Ciesielczuk et al., 2018; Hardgrove and Livesley, 2016; Mussatto et al., 2011). Comparatively, composting has been found effective in realizing humification as well as detoxification of SCG (Yamane et al., 2014), with derived products showing plant growth-promoting effects (Horgan et al., 2023). However, its application was hindered because of the slow decomposition rate of the recalcitrant lignocellulosic components in SCG (Bhatia et al., 2020). Consequently, it is crucial to develop rapid humification technology for the conversion of such lignocellulosic biowastes (e.g. SCG) into biofertilizer.

Abiotic humification technology has become a new frontier in the management and recycling of lignocellulosic biowastes, mainly including acid/base hydrothermal treatment and catalytic oxidation (Huang et al., 2022; Shao et al., 2023; Wei et al., 2022). The main humification mechanism of the former has been proposed to be a two-step top-down pathway: 1) hydrolysis and dehydration of organic macromolecules into reactive monomeric substances (e.g. furan derivatives, organic acids and phenolic monomers) as a function of heat and acid/base catalysis; 2) these reactive monomeric substances, as important precursors, polymerize to form humic-like acid (HLA)/fulvic-like acid (FLA) through auto-polycondensation and recombination (Fukuchi et al., 2010). As for the latter, radicals (e.g.  $\bullet\text{OH}$ ,  $\text{SO}_4^{\bullet-}$ ) produced by the catalytic oxidation played key roles in the humification process (Jeong et al., 2018; Yang et al., 2023). Specifically, radicals converted the macromolecules into reactive radical intermediates as bricks to build up HLA and/or FLA via radical-initiated polymerization reactions (Hunkeler, 1991; Waggoner et al., 2015). Though the above two approaches were effective in humification, their practical applications were challenged by drawbacks such as the rigid reaction conditions, long duration, and incorporation of expensive catalysts.

Inspired by this, we developed a novel approach to accelerate the humification of SCG based on synergistic heat/base co-activated persulfate (heat/KOH/PS) advanced oxidation process (AOP) (Checa-Fernández et al., 2021; Sonawane et al., 2022). This approach integrated heat/base and radicals in one system to compensate the above drawbacks of individual methods. That is, heat/base could not only catalyze the hydrolysis of macromolecules, but also activate PS to produce radicals (e.g.  $\bullet\text{OH}$  and  $\text{SO}_4^{\bullet-}$ ). The existing studies on PS-based AOP are regarding its application in the degradation of micropollutants (Lee et al., 2020), while those in biowaste humification are scarce. Those radicals were reported with extremely high reactivity towards a wide range of organic components (kinetic rates varied in  $10^7$ – $10^9 \text{ M}^{-1}\text{s}^{-1}$ ) (Wojnarovits and Takacs, 2019) and could induce a series of oxidation and polymerization reactions (Buback et al., 2023), thus may boost the humification process under relatively mild reaction conditions, overcoming the above-mentioned drawbacks in traditional catalytic oxidation and hydrothermal processes. The objectives of this study include (1) optimization of humification conditions, (2) characterization and quantification of produced HLA and FLA, (3) identification of radicals and related humification mechanism, (4) fabrication of slow-release nano FLA fertilizer (SNFF) using treated SCG (TSCG), and (5) evaluation of SNFF's release performance, plant promotion effects, and eco-safety (Fig. 1). Overall, this work highlights an innovative and efficient artificial humification technology for the recycling of SCG as a high-quality organic fertilizer, and remaining K in the product would also function as an important nutrient, which may overcome the above-mentioned drawbacks in traditional catalytic oxidation and hydrothermal processes, with the product being a potential organic-inorganic complex fertilizer.

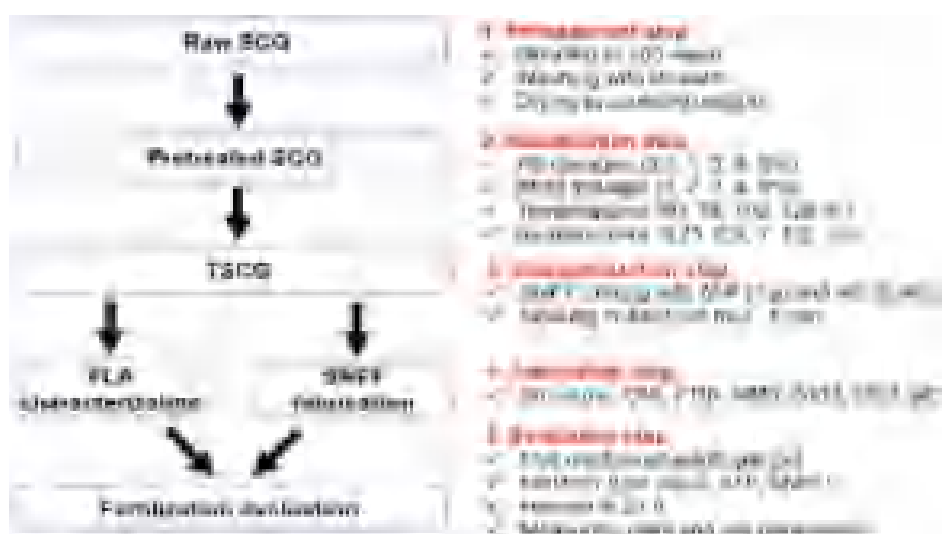


Fig. 1. Scheme of SNFF synthesis, characterization, and fertilization evaluation.



## 2. Materials and methods

### 2.1. Reagents and materials

All chemicals used were of analytical grade without further purification. KOH (purity  $\geq 95\%$ ),  $K_2S_2O_8$  (PS, purity  $\geq 99.5\%$ ), hydrochloric acid (36.0–38.0%), Anhydrous ethanol (EtOH,  $C_2H_6O$ , 99.5%), *tert*-butanol (TBA,  $C_4H_{10}O$ ,  $\geq 99\%$ ) were purchased from Sinopharm Chemical Reagent Company (Shanghai, China). Standard fulvic acid (FA) was provided from International Humic Acid Association (Florida, USA). ATP, xanthan gum (XG) and aminosilicone oil (ASO) were provided by Fufeng Biotechnology Co., Ltd (Inner Mongolia, China). SCG was obtained from a Starbucks' store in Shanghai. Chickweed seeds were purchased from Shanghai Vegetable Seed Company. Adult earthworms (*Eisenia fetida*) were provided by Ruizhou Fishing Tackle Co., Ltd (Jiangsu province, China). Acid soil was collected from a typical acid soil district of Guigang in Guangxi Province (China). Deionized water was used throughout the work except for pot experiments.

### 2.2. Experimental section

#### 2.2.1. Humification of SCG

Before humification, SCG was ground to 100-mesh and washed with deionized water for several times until dissolved organic carbon in elution was below detection (0.3 mg C/L). Afterwards, the SCG was dried in an oven at 60 °C to a constant weight. Deionized water (2 mL) was added to the dried SCG (1 g) to obtain SCG mud with moisture of 66.7%. Then both PS and KOH were evenly added with dosages of 0–0.15 g to SCG mud and the mixture was heated (50–125 °C, 0–1.5 h) to achieve humification (Fig. 1).

#### 2.2.2. Extraction and quantitative analyses of HLA and FLA in the TSCG

After the characterization of HLA and FLA in the TSCG via three dimensional-excitation emission matrix (3D-EEM) fluorescence spectrum, their amounts were quantified through the fluorescence regional integration (FRI) (Xiao et al., 2022). The TSCG was mixed with deionized water at a weight ratio of 1:10 and the mixture (pH around 10.5) was shaken (300 rpm) for 20 mins at room temperature (Said-Pullicino et al., 2007). The insoluble non-humic substances (sediment 1) in the resulting system were separated from soluble humic acid (SHA, a mixture of HLA and FLA) through centrifugation (12,000 rpm) for 15 min, which referred to product. Subsequently, the pH of SHA supernatant was adjusted to pH  $1 \pm 0.1$  using 6 M hydrochloric acid, and the insoluble substance (HLA, sediment 2) was obtained after centrifugation (12,000 rpm, 15 min) followed by standing overnight. The FLA in the supernatant was extracted using resins of Supelite DAX-8 and IR120: firstly absorbed to an acidified hydrophobic resin Supelite DAX-8, then desorbed with 0.1 M NaOH, and finally protonated using a IR120 hydrogen form exchange resin. The TSCG and sediments (1 and 2) were dried to constant weights at 60 °C. The HLA and FLA contents were quantified according to Eqs. (1)–(4).

$$W_{SHA} = W_{TSCG} - W_1 - W_2 \quad (1)$$

$$W_{FLA} = W_{SHA} - W_{HLA} \quad (2)$$

$$HLA\% = (W_{HLA} / W_{TSCG}) \times 100\% \quad (3)$$

$$FLA\% = (W_{FLA} / W_{TSCG}) \times 100\% \quad (4)$$

Where  $W_{TSCG}$ ,  $W_{SHA}$ , and  $W_{FLA}$  referred to the dry weights of TSCG, SHA, and FLA, respectively. Besides,  $W_1$  and  $W_2$  were the weights of sediment 1 and  $K_2SO_4$  stoichiometrically quantified based on complete consumption of PS.

#### 2.2.3. Radical identification

•OH and  $SO_4^{\bullet-}$  produced during the process were determined on an electron paramagnetic resonance (EPR) spectrometer using 5,5-Dimethyl-1-pyrroline-N-oxide (DMPO) as the spin-trapping agent. Additionally, quenching experiments were carried out by adding 0.3 mol EtOH and TBA (around 100 times of PS and KOH dosages) to 1 g SCG before PS and KOH to obtain the contributions of those radicals (Gao et al., 2022).

#### 2.2.4. Fabrication of SNFF and release behavior

The TSCG (1 g) as-prepared under the optimum condition (0.03 g PS, 0.12 g KOH, 1 h, 100 °C) was mixed with ATP (1 g) and XG (0.08 g) and the mixture was granulated to get spheric fertilizer with size of approximately 3 mm. Then, the fertilizer particles were soaked in ASO (25 mL) for 5 min to get SNFF after air-drying.

The as-prepared SNFF (2 g) or SCG (1 g, equal amount to that in SNFF) was placed in 1 L deionized water (adjusted to initial pHs of 3 and 7). After different intervals, 5 mL solution was sampled to determine the HLA and FLA contents in the system as well as pH.

The SHA content was monitored using UV-vis spectrophotometry at 267 nm (the maximum absorbing wavelength). As the solubility of SHA was closely related to pH, the product solution at different pHs (3, 4, 5, 6, 7, 8 and 9) was filtered, quantified through weight method, and diluted to get the standard curves. Similarly, the FLA content was measured based on its standard curve at 241 nm (the maximum absorbing wavelength). A standard curve of FLA was consistently used with a pH range of 3–9 because of its pH-independent solubility.

Three kinetic models were used to illustrate the release mechanism of FLA from SRNFF including First-order, Ritger-Peppas, and

Parabolic diffusion according to Eqs. (5)–(7) (Liu et al., 2021):

$$\ln(1-RR_t) = -kt \tag{5}$$

$$RR_t = kt^n \tag{6}$$

$$\frac{RR_t}{t} = kt^{0.5} + b \tag{7}$$

where  $RR_t$  (%) referred to the RR of the FLA at time  $t$ ,  $k$  was the kinetic constant related to structural and geometric characteristics of release system,  $b$  was a constant, and  $n$  was release exponent of the release mechanism: Fickian diffusion ( $n < 0.43$ ) and non-Fickian or anomalous diffusion ( $0.43 < n < 1.0$ ).

2.2.5. Pot experiment

Considering the alkaline property of SNFF, its remediation ability on soil acidification was investigated via pot experiment (Fig. S1). Acid soil (pH 5, 300 g) with humidity of 30% was placed in a pot (height of 8.5 cm, bottom width and length of 7 cm, top width and length of 10 cm). Then five chickweed seeds were planted evenly in the soil with depth of approximately 1 cm. The SCG (0.75 g), ATP (0.75 g), or SNFF (1.5 g, containing 0.75 g TSCG and 0.75 g ATP) was spread evenly to the soil surface. Afterwards, the pots were kept in an incubator (25 °C) at humidity of 60%. Tap water (20 mL) was sprayed evenly to the soil every two days. soil pH was measured on day 1, 7, 14, and 21. After harvest in 21 d, plant (wet weight, dry weight, plant height, chlorophyll content, root

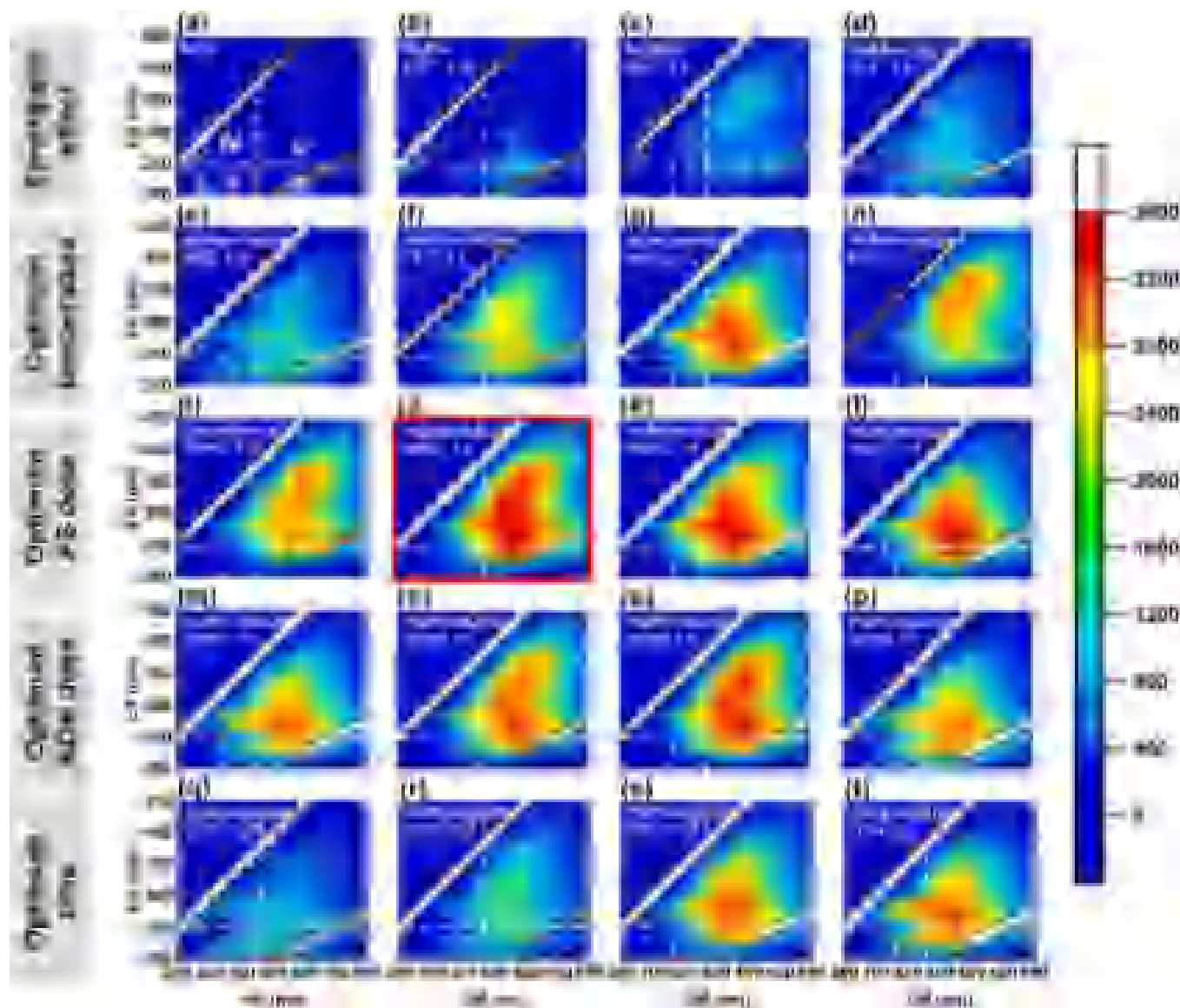


Fig. 2. 3D-EEM fluorescence spectra of SCG treated by KOH/PS under different conditions: (a-d) synergistic effect of KOH and PS, (e-t) effect of temperature, dosage, and reaction time. Conditions: SCG = 1 g, DI water volume= 2 mL, PS or KOH dosage= 0–5%, heating temperature= 50–125 °C, and reaction time= 0–2 h.

length, survival rate) and soil parameters (total N, total P, total K, available N, available P, available K, organic matter, bacterial communities) were measured according to standard procedures reported previously (Wang et al., 2022a).

In addition, the biosafety of SNFF on earthworms was explored (Hoeffner et al., 2019). Acid soil (pH 5, 200 g) was placed in plastic containers with five earthworms each. The experimental set was same with the pot experiment. The lengths and weights of earthworms were recorded at different intervals.

### 2.3. Characterizations

The compositional changes of SCG during the humification process were preliminarily analyzed through 3D-EEM fluorescence spectrum measurement on a fluorescence spectrophotometer (F-7000, Hitachi High-Technologies Co., Japan) after filtered through a 0.45- $\mu\text{m}$  membrane. The functional groups and element components of the freeze-dried product were compared with standard FA on X-ray photoelectron spectroscopy (XPS, ESCALAB 250, Thermo-VG Scientific Co., USA), Fourier transform infrared spectrometer (FTIR, NEXUS-670, Nicolet Co., USA) and solid-state  $^{13}\text{C}$  nuclear magnetic resonance (NMR, Bruker-400, Bruker Co., Germany). A scanning electron microscope (SEM, S4800, Hitachi High-Technologies Co., Japan) with an accelerating voltage of 0.5–30 kV was used to observe the morphologies of the TSCG and SNFF. The crystal structure of samples was analyzed using an X-ray diffraction (XRD, D/max-2550VB/PC, Rigaku Co., Japan). Brunauer-Emmett-Teller (BET) specific surface areas were determined by physisorption of  $\text{N}_2$  using an automatic surface area and a pore analyzer (Tristar II 3020 M, Micromeritics, USA). The pore volume and size distribution were measured through the Barrett-Joyner-Halenda method. An EPR spectrometer (Magnetech MS5000, Germany) was employed to identify radicals. The soil microbial community was characterized through 16 S rDNA high-throughput sequencing technology.

### 2.4. Statistical analysis

All experiments were performed in triplicates with data presented as mean  $\pm$  standard deviation. All statistical analyses were done with one-way analysis of variance (ANOVA) and Duncan's multiple range test using SPSS package version 9.2 (2010, SAS Institute Cary, NC).

## 3. Results and discussion

### 3.1. Humification of SCG by heat/KOH/PS treatment

#### 3.1.1. Optimization of heat/KOH/PS treatment condition

3D-EEM was applied to analyze the composition changes of SCG with treatment under different conditions (Fig. 2). Fluorescence spectra included five regions: I (EM < 330 nm, EX < 250 nm) and II (EM=330–380 nm, EX < 250 nm) corresponded to small aromatic proteins, III (EM > 380 nm, EX < 250 nm) and V (EM > 380 nm, EX > 250 nm) were attributed to FLA and HLA, IV (EM < 380 nm, EX > 250 nm) referred to soluble microbial product (Chen et al., 2003). Additionally, FRI approach was used to quantify EEM results (Table S1) based on the fluorescence intensity and percent fluorescence response in each region (Chen et al., 2003). Fig. 2a showed that no significant fluorescence of SCG was found. After treatment with PS or KOH alone (Fig. 2b and 2c), the fluorescence appeared in regions III and V especially with KOH, implying the generation of HLA/FLA likely via oxidation and alkaline hydrolysis effect (Boczkaj and Fernandes, 2017). Notably, the fluorescence further moved towards regions III (FLA) and V (HLA) after the simultaneous addition of PS and KOH (Fig. 2d). Specifically, the sum of  $P_{\text{III}}$  and  $P_{\text{V}}$  of KOH/PS-treated SCG (0.7355) was higher compared with PS (0.6691) and KOH (0.6509) alone, proving their synergistic effect on the SCG humification (Shao et al., 2023).

The combination of heating and KOH/PS showed further promotion effect on the degree of SCG humification (Shao et al., 2023). With the increase of temperature, the fluorescence intensities (Fig. 2d-h) and percent fluorescence responses of regions III and V (Table S1) increased initially from 22 to 100  $^{\circ}\text{C}$ , and then decreased from 100 to 125  $^{\circ}\text{C}$ , achieving the optimal temperature of 100  $^{\circ}\text{C}$ . This was probably because of the decomposition of generated HLA/FLA at higher temperature (Cai et al., 2022; Cao et al., 2023; Yang et al., 2019). The humification was probably induced by the coactivation of KOH and heat on PS according to Eqs. (8–10).



In order to maximize the degree of SCG humification, the dosages of PS and KOH and reaction time were optimized at 100  $^{\circ}\text{C}$ . With the increase of PS dosage from 0.5% to 5%, the fluorescence intensities (Fig. 2g, i-l) of regions III and V also showed a trend of first increase followed by decrease, achieving the maximum at 1%. As for KOH, the fluorescence intensities (Fig. 2j, m-p) of regions III and V rised with the dosage from 1% to 4% while remained almost unchanged with further increasing to 5%. Considering the high cost of KOH, 4% was chosen as the suitable dosage. Besides, with the increase of reaction time, the fluorescence intensities (Fig. 2j, q-t) of regions III and V continuously increased in the first 1 h and then stayed unchanged in the next hour. Overall, the optimum humification conditions were selected at 100  $^{\circ}\text{C}$  for 1 h and dosages of 1% PS/4% KOH, showing the  $P_{\text{III}}$  and  $P_{\text{IV}}$  of 0.2929 and 0.4748 respectively (Table S1). Additionally, weight method was used to precisely quantify HLA, FLA and SHA (HLA+FLA) in the TSCG under optimal



condition, obtaining their yields of 45 (3.96%), 192 (19.20%), and 237 mg/g (23.26%) respectively. Notably, the yield of FLA in this work was much higher than the reported results (less than 12.7%) via hydrothermal treatment of organic wastes (Cai et al., 2022; Wang et al., 2023a). The much higher yields and reaction efficiency in this work compared with reported artificial humification studies confirmed the application value of this humification technology (Wei et al., 2022).

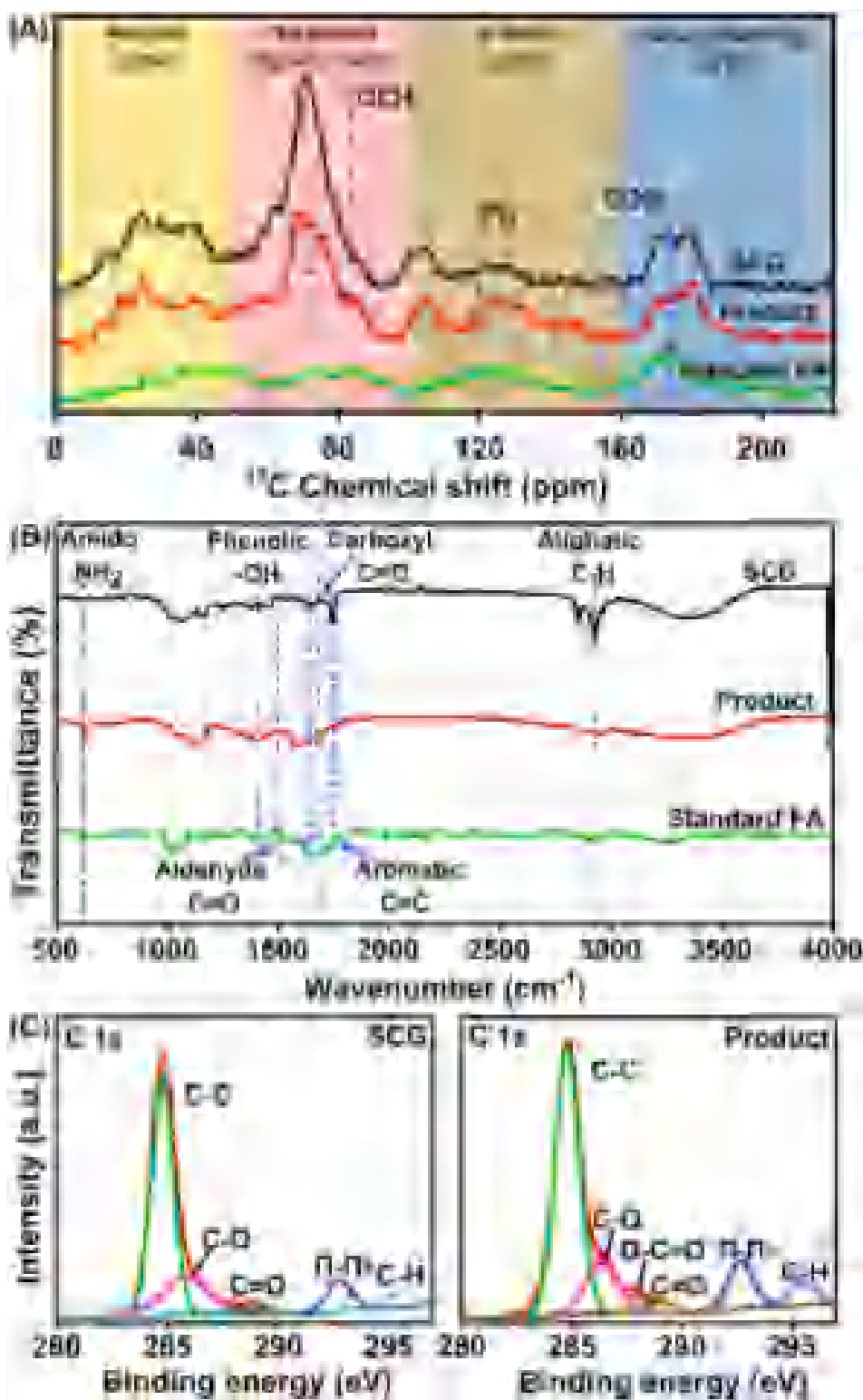


Fig. 3. (A)  $^{13}\text{C}$  NMR and (B) FTIR spectra of SCG, product and standard FA. (C) XPS spectra of C1s for SCG and product. Humification conditions: SCG = 1 g, DI water volume = 2 mL, PS dosage = 1%, KOH dosage = 4%, heating temperature = 100  $^{\circ}\text{C}$ , and reaction time = 1 h.

### 3.1.2. Characterization of HLA/FLA

As shown in Fig. 3 A, compared with the  $^{13}\text{C}$  NMR spectrum of SCG, the percentage of aliphatic C in 0–50 ppm was slightly lower in product, along with a higher percentage of aromatic C in 110–160 ppm, which may evidence the occurrence of aromatization reaction during humification. The oxygenated aliphatic C (60–100 ppm) in 60–100 ppm appeared much weaker in product compared to SCG, accompanied by higher peak intensities in carboxyl C (160–185 ppm) (Xiaoli et al., 2008), indicating that carboxylation may be involved relevant to radical oxidation (Zhang et al., 2023). Besides, typical peaks of aromatic C (110–160 ppm) and carboxyl C (160–185 ppm) are also appeared in the spectrum of FA standard, suggesting the formation of FLA.

FTIR characterization results were presented in Fig. 3B. The peaks in the region of  $1650\text{--}1500\text{ cm}^{-1}$ , representing valence oscillations of  $\text{C}=\text{C}$ -aromatic structure, were enhanced in product compared with SCG. Meanwhile, the typical band at around  $2923\text{ cm}^{-1}$  in the spectrum of SCG, assigned to the valence vibrations of aliphatic C-H group, was almost disappeared in product. These differences possibly indicated increased aromaticity during humification (Karabaev et al., 2012). The peak at  $1745\text{ cm}^{-1}$  (aldehyde  $\text{C}=\text{O}$  stretching) observed in SCG's spectrum was weakened in the product, while the peak at  $1670\text{ cm}^{-1}$  (carboxyl  $\text{C}=\text{O}$  stretching) was stronger in the product, reflecting the occurrence of carboxylation. The appearance of the peak at  $617\text{ cm}^{-1}$  (amido  $\text{NH}_2$ ) in product may be related to a previously proposed humification route of Maillard reaction considering the presence of sugar and protein in SCG (Stylianou et al., 2018; Zhang et al., 2019). A significant increase in the phenolic hydroxyl group ( $1410\text{ cm}^{-1}$ ) in the product indicates the formation of quinone. To be noted, peaks of active groups including aliphatic/phenolic  $\text{-OH}$  and  $\text{-COOH}$  were consistently observed in the product and FA standard, proving the successful synthesis of FLA (Crespilho et al., 2005).

XPS spectra in Fig. 3C showed that the  $\text{C}1\text{s}$  peaks of SCG can be deconvoluted into peaks at 284.8, 287.8, 289.08, 292.68 and 295.48 eV, corresponding to C-C, C-O,  $\text{C}=\text{O}$ ,  $\text{II-II}^*$  and C-H (Zhu et al., 2017), respectively. In comparison, a new peak at 286.38 eV referring to  $\text{O-C}=\text{O}$  emerged in the spectrum of product, confirming the aforementioned carboxylation during humification.

In general, the above characterization results proved the presence of typical FA active groups such as  $\text{-COOH}$  and  $\text{-OH}$  in the product and the possible occurrence of hydroxylation, carboxylation and Maillard reactions, all of which evidenced the humification of SCG.

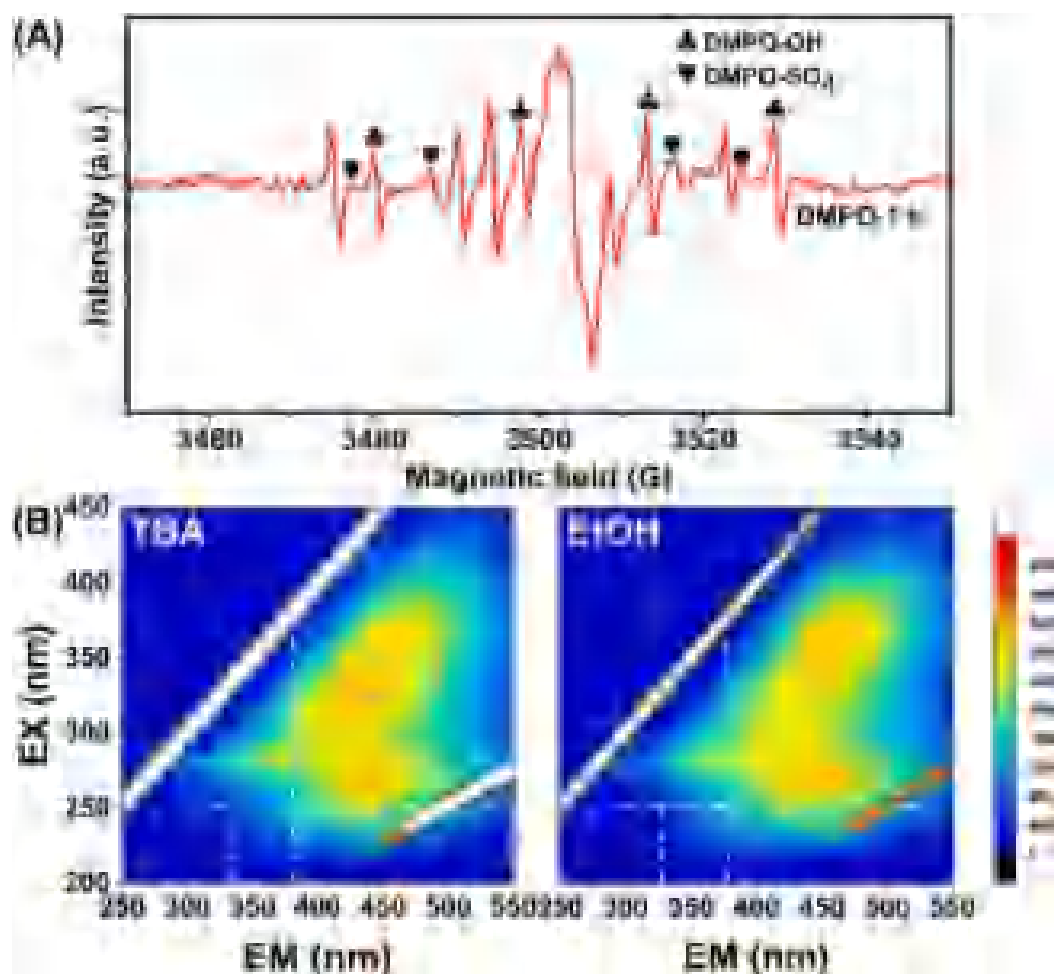


Fig. 4. (A) EPR spectra of  $\bullet\text{OH}$  and  $\text{SO}_4^{\bullet-}$  during the treatment of SCG by heat/KOH/PS. (B) 3D-EEM spectra of heat/KOH/PS-treated SCG with addition of different quenchers. Conditions: SCG = 1 g, DI water volume = 2 mL, PS dosage = 1%, KOH dosage = 4%, heating temperature =  $100\text{ }^\circ\text{C}$ , reaction time = 1 h, DMPO = 1 mmol, TBA dosage = 0.3 mol, EtOH dosage = 0.3 mol.

### 3.1.3. Role of radicals in humification

Radicals such as  $\bullet\text{OH}$  and  $\text{SO}_4^{\bullet-}$  have been reported involved in either degradation or polymerization of organics (Jeong et al., 2018; Zhang et al., 2023; Zhang et al., 2020). EPR and quenching experiments were conducted to investigate the role of radicals in the humification of SCG by heat/KOH/PS. Fig. 4 A showed that peaks of  $\bullet\text{OH}$  and  $\text{SO}_4^{\bullet-}$  appeared in EPR spectra of the humification system after 1 h, likely because of PS decomposition via heat/base activation (Ma et al., 2017). In quenching experiments, TBA was applied to quench  $\bullet\text{OH}$  ( $k_{\bullet\text{OH}/\text{EtOH}} = (3.8\text{--}7.6) \times 10^8 \text{ M}^{-1} \text{ s}^{-1}$ ), and EtOH as quenchers of both  $\bullet\text{OH}$  and  $\text{SO}_4^{\bullet-}$  ( $k_{\bullet\text{OH}/\text{EtOH}} = 1.6 \times 10^7 \text{ M}^{-1} \text{ s}^{-1}$ ,  $k_{\text{SO}_4^{\bullet-}/\text{EtOH}} = 1.9 \times 10^9 \text{ M}^{-1} \text{ s}^{-1}$ ) (Wang et al., 2023b). 3D-EEMs of these quenchers were also presented to exclude their influence (Fig. S2). As shown in Fig. 4B, the addition of TBA and EtOH decreased the fluorescence intensities of EEM peaks in regions III and V, suggesting a lower humification degree of SCG and the significant role of these radicals. The radical-involved humification here may be related to reported radical-induced polymerization in polymer synthesis (Hunkeler, 1991). The occurrence of humification in the quenching systems indicated the possible contribution of heat/base catalyzed hydrolysis (Wang et al., 2023a).

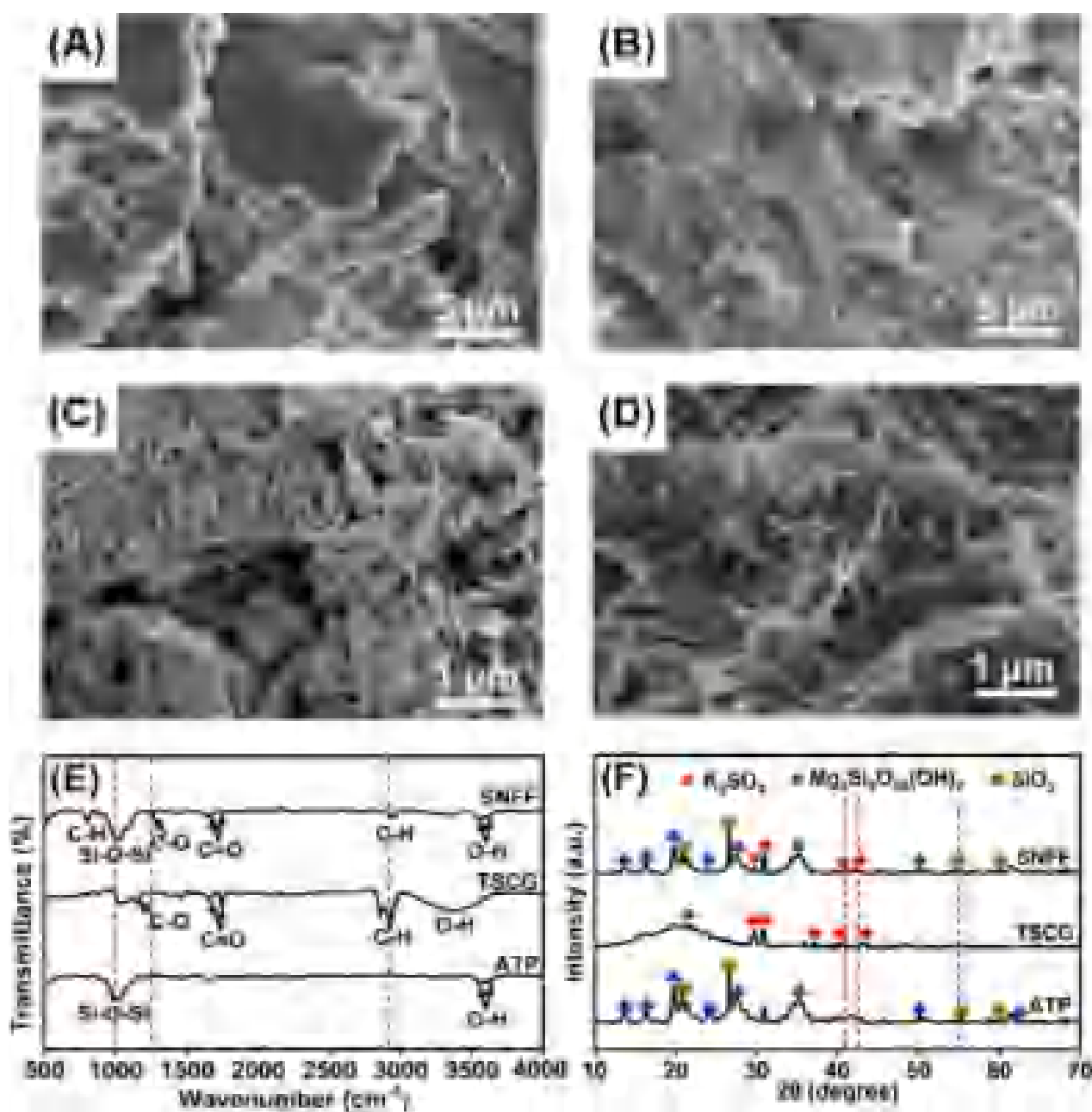


Fig. 5. SEM images of (A) SCG, (B) TSCG, (C) ATP, and (D) SNFF. (E) FTIR and (F) XRD spectra of ATP, TSCG and SNFF. Humification conditions: SCG = 1 g, DI water volume = 2 mL, PS dosage = 1%, KOH dosage = 4%, heating temperature = 100 °C, and reaction time = 1 h.

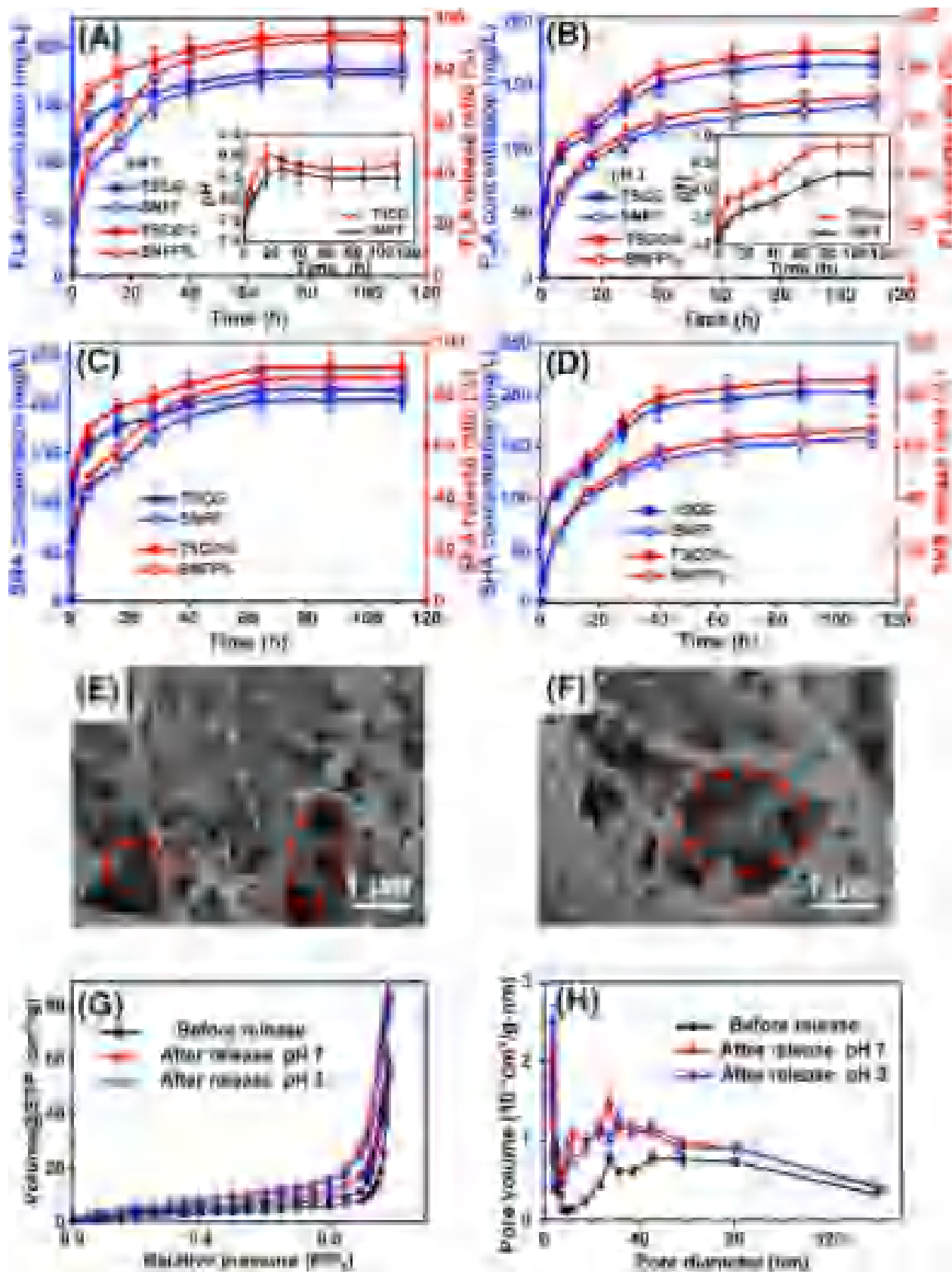


Fig. 6. Cumulative released concentration and release ratio of FLA and SHA from TSCG and SNFF at (A, C) pH 7 and (B, D) pH 3. Inserts in (A) and (B) refer to pH variation during slow-release at pH 7 and 3, respectively. SEM images of SNFF surface after release at (E) pH 7 and (F) pH 3. (G) N<sub>2</sub> adsorption-desorption isotherms and (H) pore size distributions of SNFF before and after release. Conditions: [SNFF]<sub>0</sub> = 2 g/L, [SCG]<sub>0</sub> = 1 g/L, initial pH = 3 or 7, ambient temperature = 22 ± 1 °C. Error bars refer to the standard deviations from triplicate experiments.

3.2. Characterization and slow-release behavior of SNFF

3.2.1. SNFF characterization

In order to improve the application convenience and HLA/FLA utilization efficiency, TSCG was well mixed with XG and ATP to fabricate SNFF with size of approximately 3–5 mm. Fig. 5A and 5B showed that both SCG and TSCG exhibited rough morphologies. As shown in Fig. 5C, ATP showed a nanonetworks morphology formed by crosslinking of micro-nano rods, favoring the loading of HLA/FLA. Comparatively, a great many of organic substances were found evenly on ATP rods surface and micro-nano pores in Fig. 5D, suggesting the successful loading of HLA/FLA. Such nanonetworks structure of SNFF was beneficial to the slow release of HLA/FLA.

Fig. 5E illustrated that the FTIR characteristic peaks of TSCG (1660 and 1740 for C=O, 2923 cm<sup>-1</sup> for C-H) and ATP (988 for Si-O-Si, 3617 and 3555 cm<sup>-1</sup> for O-H) could be found in the spectrum of SNFF (Xiang et al., 2018), indicating the loading of TSCG in ATP. Besides, the peak intensity at 988 cm<sup>-1</sup> for Si-O-Si in SNFF became stronger compared with ATP alone. The C-O peak at 1260 cm<sup>-1</sup> of SNFF red-shifted compared with TSCG. These results likely implied the existence of hydrogen bonds between Si-O-Si of ATP and C-O of HLA/FLA (Cai et al., 2022), facilitating the slow-release of SNFF. Besides, rare new peak was found in the spectrum of SNFF compared with ATP and TSCG, probably suggesting the dominant physical interaction between ATP and TSCG.

Fig. 5 F demonstrated that the characteristic peaks of K<sub>2</sub>SO<sub>4</sub> appeared in the XRD spectrum of TSCG based on standard atlas in JADE, illustrating that K<sub>2</sub>SO<sub>4</sub> was the dominant crystal component. The generation of K<sub>2</sub>SO<sub>4</sub> was probably resulted from the reactions between PS and KOH (Eqs. 8, 9 and 10). The peaks of Mg<sub>5</sub>(SiAl<sub>8</sub>)O<sub>20</sub>, SiO<sub>2</sub> and K<sub>2</sub>SO<sub>4</sub> appeared in spectrum of SNFF, also proving the adsorption of TSCG on ATP. Noteworthily, the peaks at 41° and 42.5° of K<sub>2</sub>SO<sub>4</sub> in SNFF right- and left-shifted respectively compared with TSCG, probably owing to the variation of K<sub>2</sub>SO<sub>4</sub> crystal orientation by ATP. The peak at 55° in SNFF red-shifted compared with ATP, likely owing to the intercalation of HLA/FLA or K<sub>2</sub>SO<sub>4</sub> into ATP crystal layers, conducive to the slow-release of SNFF.

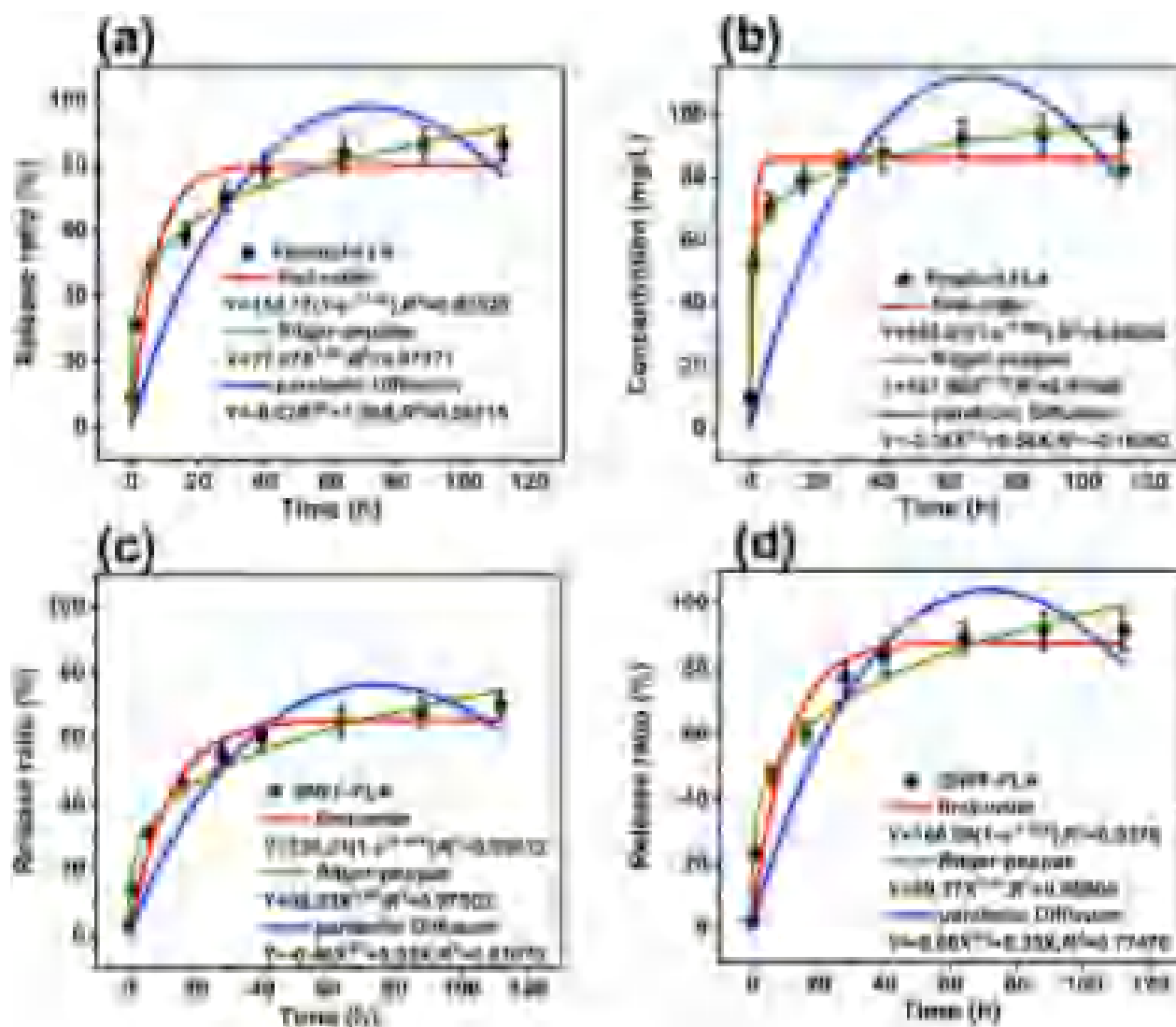
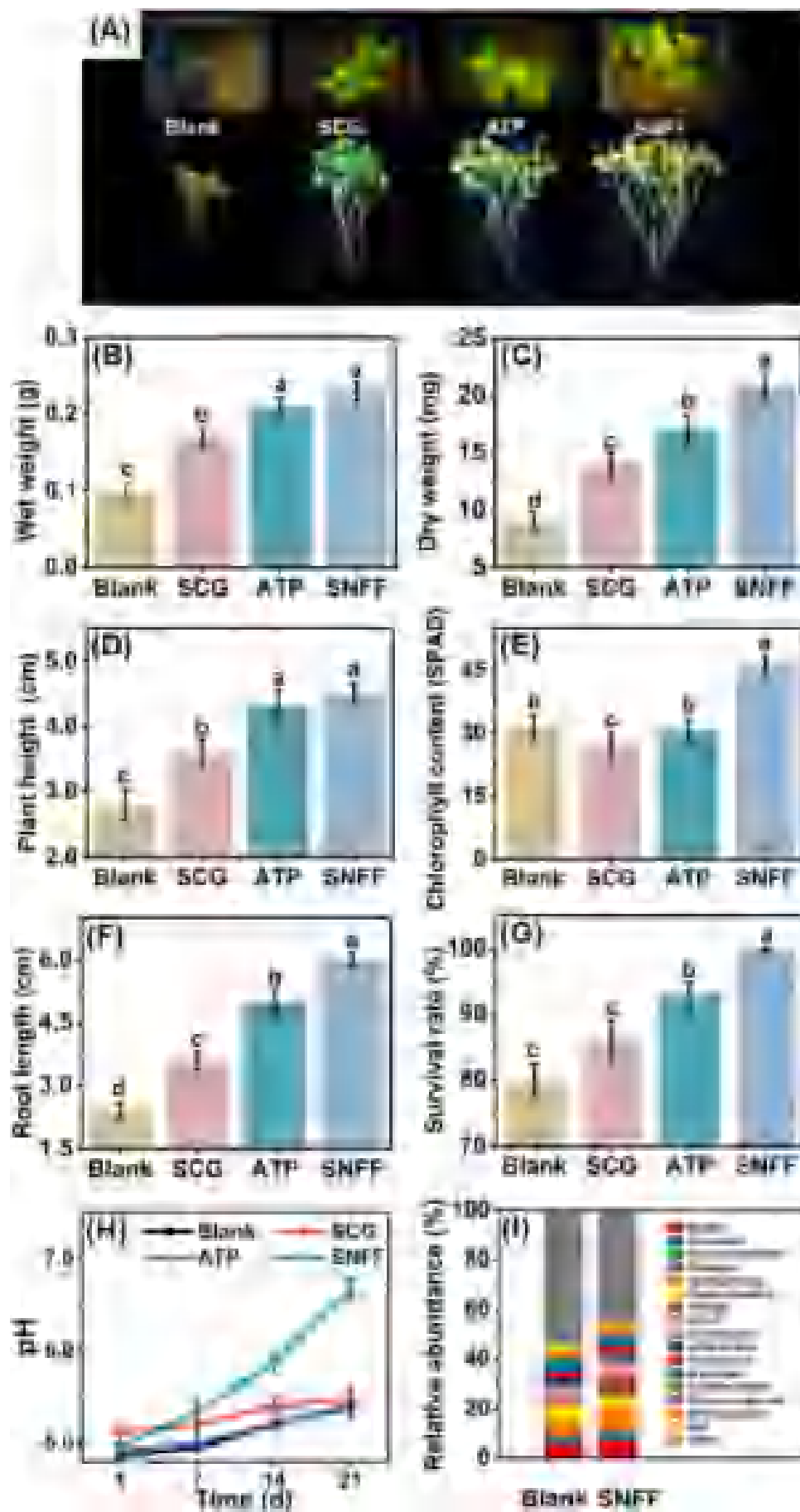


Fig. 7. Plots of different kinetic models for FLA release from product at (a) pH 7 and (b) 3, SNFF at (c) pH 3 and (d) 7.



(caption on next page)



**Fig. 8.** (A) Photographs, (B) wet weight, (C) dry weight, (D) plant height, (E) I chlorophyll content, (F) root length, and (G) survival rate of chickweeds with different treatments. (H) Soil pH variation curve during cultivation. (I) Bacterial communities at genus level in soil of blank and SNFF groups after harvest. Blank, SCG, ATP, and SNFF represent groups containing 300 g acid soil alone, 300 g soil+ 0.75 g ATP, 300 g soil+ 0.75 g SCG, and 300 g soil+ 1.5 g SNFF, respectively. A total of 5 seeds were added to each pot and triplicates were conducted for each group. Error bars represent the standard deviations. Different letters refer to significant differences at  $p < 0.05$ .

### 3.2.2. Slow-release behavior of SNFF

Since the alkalinity of TSCG may contribute to improving the pH of acidic soil, the FLA/HLA release performance of SNFF was explored in aqueous solution at pH 3 in comparison with 7. The respective loading amounts of SHA and FLA in SNFF were measured to be 118.5 and 96 mg/g. The standard curves of SHA and FLA at different pHs were used to obtain their cumulative release concentrations (RCs) (Fig. S3). The release ratio (RR) was obtained based on Eq. (11). Fig. 6A and 6C showed that, at pH 7, both SHA and FLA in SNFF exhibited slower release than those in TSCG especially within the initial 40 h and reached equilibrium in 88 h. The maximum cumulative RCs of SHA and FLA were achieved to be 204 (RR=86%) and 176 mg/L (RR=91%), respectively. Fig. 6B and 6D illustrated a similar but slower release trend at pH 3 with RCs of 160 mg SHA/L and 135 mg FLA/L in 112 h, reflecting the pH dependence property of their release. The kinetics fitting results indicated that FLA release corresponded best to the Ritger-Peppas release model ( $R^2 > 0.97$ ) (Fig. 7), indicated that the slow-release mechanism was non-Fickian or anomalous diffusion (Dai et al., 2015).

$$RR(\%) = (RC \times V) / (M_1 \times M_2) \times 100\% \quad (11)$$

Where  $V$  was the volume of deionized water,  $M_1$  was the loading amount of FLA/SHA for 1 g SNFF, and  $M_2$  was the dose of SNFF.

In addition, the pH of the aqueous solution raised with the release of FLA/HLA, finally reaching 8.5 and 4.3 respectively, implying the application value of SNFF in acidic soil amendment. After release, both BET surface areas and pore volumes of SNFF increased respectively at pH 7 and 3 (Fig. 6G and 6H), which was consistent with the SEM images (Fig. 6E and 6F).

### 3.3. The potential agricultural effect of SNFF

As shown in Fig. 8A, the growth of chickweed with different treatments in pot experiment followed an order of SNFF > ATP > SCG > Blank. The promotion effect of raw SCG and ATP on chickweed' growth may be related to their positive soil amendment effects and/or nutrients carrier performance reported previously (Gebreyessus, 2022; Kwon et al., 2022; Pagliarini et al., 2023). According to Fig. 8B-G, the addition of SNFF showed significant promotion on indexes of dry weight, plant height, root length, and survival rate. Specifically, the average root length of all the chickweeds in one pot with SNFF (6 cm) increased by 233% compared with the blank (1.8 cm), which was consistent with the widely reported root promotion of HLA/FLA (Olaetxea et al., 2015). Overall, the greater significant promotion of SNFF than SCG and ATP proved that the fertilization effect of SCG was improved after humification treatment and ATP could be used as an ideal carrier for the product (Lee et al., 2019). Besides, SNFF could significantly improve the soil pH from 5 to 6.7 compared with blank, ATP and SCG (Fig. 8H), demonstrating its function in acidic soil remediation, which was similarly observed in previous studies using biochar as acidic soil amendment (Das and Ghosh, 2022a; 2022b).

The soil bacterial structure variation of the pot experiment was analyzed using 16 S rRNA high-throughput sequencing. As shown in Table 1, compared with the blank, SNFF group showed higher Ace, Chao 1 and Sobs, revealing that SNFF could effectively improve the bacterial richness. Similarly, the increase of Shannon and decrease of Simpson in SNFF-treated soil reflected that SNFF may contribute to enhanced bacterial diversity. Fig. 8I (detailed in Fig. S4) showed that the relative abundances of plant growth-promoting bacteria (PGPB) including *Bacillus*, *Sinomonas*, *Sphingomonas*, and *Massilia* in SNFF-treated soil consistently increased from 6.52, 1.41, 5.71, and 1.65–7.84%, 2.51%, 11.13%, and 7.66% respectively (Alves et al., 2022). Therein, *Massilia* was reported capable of quinone respiration (Holochoová et al., 2020), and the stimulation of quinone respiratory bacteria by humic acid has been observed previously (Wang et al., 2022b). Meanwhile, after SNFF treatment, the relative abundances of *Acidobacteriales* and *Ralstonia* decreased from 2.99 and 1.22–1.55% and 0.14%, respectively. Therein, *Acidobacteriales* was usually abundant in acidic soil, and the *Ralstonia* could suppress soil nitrogen metabolism (Malkan et al., 2009; Wang et al., 2021). These results indicated that SNFF addition was favorable to soil bacterial structure. Besides, the results of soil physicochemical indexes (Table S2) reflected the increase of total and available N/P/K and organic matter in soil with the addition of SNFF. To be noted, the organic matter content increased from 5.81 to 13 g/kg due to SNFF addition, suggesting its unignorable potential in soil carbon sequestration, which was consistent with the reported superior soil carbon sequestration performance of diverse biomass-derived biochar (Das et al., 2023; 2022a).

Conclusively, SNFF exhibited excellent growth promotion and soil improvement effect. Therein, the soil amendment mechanism may be attributed to the slow-release of OH<sup>-</sup> and soil carbon supplement by SNFF. Plant-growth promotion was probably ascribed to the simultaneous slow-release and possible synergistic effects of HLA/FLA and K<sup>+</sup>. Besides, soil improvement may also be positively

**Table 1**

Richness and diversity estimators of the microbial communities in soil of blank and SNFF groups.

Group	Ace	Chao 1	Shannon	Simpson	Coverage	Sobs
Blank	1005 ± 80b	1005 ± 16b	5.9 ± 0.22b	0.007 ± 0.0a	1.0 ± 0.0	1005 ± 11b
SNFF	1329.1 ± 30a	1306.4 ± 11a	6.3 ± 0.08a	0.004 ± 0.0b	1.0 ± 0.0	1297 ± 20a

Note: the standard deviations were derived from triplicate tests. Different letters in the same column represent significant differences at  $p < 0.05$ .

correlated to the plant-growth promoting effect.

Besides, according to the growth of earthworms in soil with different treatments (Table S3), the increase of earthworms' length and weight within 14 d followed the same order with the growth of chickweed in Fig. 8A. Specifically, earthworms' length and weight were increased by 3 cm and 0.43 g due to SNFF addition, indicating the soil biosafety of SNFF.

#### 4. Conclusion

In this study, heat/base co-activated PS AOP was used in the humification of SCG to produce TSCG within 1 h. The contents of HLA and FLA in TSCG reached 45 (3.96%) and 192 mg/g (19.2%), respectively. EPR and quenching experiment results revealed the generation and contribution of  $\bullet\text{OH}$  and  $\text{SO}_4^{\bullet-}$  to humification as well as heat/base catalyzed hydrolysis. Structural and component characterization results evidenced the increase of active groups -COOH and -OH in the structure of TSCG and the possible occurrence of hydroxylation, carboxylation and Maillard reaction during humification. SNFF was prepared by mixing TSCG with ATP and showed good slow-release behavior of HLA/FLA especially at pH 3. The pot experiment results in acid soil confirmed that SNFF exhibited significant plant promotion and soil amendment effects. The earthworm test indicated SNFF's positive soil ecological security. This study provides an efficient route for artificial humification of lignocellulosic-rich organic wastes induced by PS-based AOP, which may be of significance in the management and recovery of organic biowastes. In future, the related humification and fertilization mechanism should be further explored.

#### CRediT authorship contribution statement

**Yanping Zhu:** Conceptualization, Formal analysis, Data curation, Software, Investigation, Writing – original draft, Visualization. **Keyi Zhang:** Investigation, Data curation, Writing – original draft, Visualization. **Qing Hu:** Investigation, Data curation, Writing – original draft, Visualization. **Weijia Liu:** Data curation, Writing – original draft, Visualization. **Yi Qiao:** Data curation, Writing – original draft, Visualization. **Dongqing Cai:** Investigation, Writing – review & editing, Supervision. **Pengjin Zhu:** Investigation, Writing – review & editing. **Dongfang Wang:** Investigation, Writing – review & editing. **He Xu:** Investigation, Writing – review & editing. **Shihu Shu:** Writing – review & editing, Supervision, Project administration, Funding acquisition. **Naiyun Gao:** Writing – review & editing.

#### Declaration of Competing Interest

The authors declare the following financial interests/personal relationships which may be considered as potential competing interests: Yanping Zhu reports financial support was provided by the National Natural Science Foundation of China. Yanping Zhu reports financial support was provided by the Key R&D Program of Guangxi Province. Yanping Zhu reports financial support was provided by Science and Technology Commission of Shanghai Municipality. Yanping Zhu reports financial support was provided by the Key R&D Program of Guangdong Province. Yanping Zhu reports financial support was provided by the Science and Technology Service Program of Chinese Academy of Science. Yanping Zhu reports financial support was provided by the Key R&D Program of Inner Mongolia Autonomous Region. Yanping Zhu reports financial support was provided by the National Natural Science Foundation of China. Yanping Zhu reports financial support was provided by Revitalizing the City by Science and Technology of Hulun Buir.

#### Data Availability

Data will be made available on request.

#### Acknowledgements

This work was supported by the National Natural Science Foundation of China (No. 52000023), the Key R&D Program of Guangxi Province (No. GuikeAB23026061), the Shanghai Committee of Science and Technology (No. 19DZ1204400), the Key R&D Program of Guangdong Province (No. 2020B0202010005), the Science and Technology Service Program of Chinese Academy of Science (KFJ-STQYZD-199), the Key R&D Program of Inner Mongolia Autonomous Region (2021GG0300), the National Natural Science Foundation of China (52000025), and the Key Program (Achievement Transformation) of "Revitalizing the City by Science and Technology" of Hulun Buir (2022HZZX008).

#### Appendix A. Supporting information

Supplementary data associated with this article can be found in the online version at [doi:10.1016/j.eti.2023.103393](https://doi.org/10.1016/j.eti.2023.103393).

## References

- Alves, A.R.A., Yin, Q., Oliveira, R.S., Silva, E.F., Novo, L.A.B., 2022. Plant growth-promoting bacteria in phytoremediation of metal-polluted soils: current knowledge and future directions. *Sci. Total Environ.* 838. <https://doi.org/10.1016/j.scitotenv.2022.156435>.
- Bhatia, S.K., Jagtap, S.S., Bedekar, A.A., Bhatia, R.K., Patel, A.K., Pant, D., Rajesh Banu, J., Rao, C.V., Kim, Y.-G., Yang, Y.-H., 2020. Recent developments in pretreatment technologies on lignocellulosic biomass: effect of key parameters, technological improvements, and challenges. *Bioresour. Technol.* 300. <https://doi.org/10.1016/j.biortech.2019.122724>.
- Boczkaj, G., Fernandes, A., 2017. Wastewater treatment by means of advanced oxidation processes at basic pH conditions: a review. *Chem. Eng. J.* 320, 608–633. <https://doi.org/10.1016/j.cej.2017.03.084>.
- Buback, M., Hutchinson, R.A., Lacić, I., 2023. Radical polymerization kinetics of water-soluble monomers. *Prog. Polym. Sci.* 138. <https://doi.org/10.1016/j.procpolymsci.2022.101645>.
- Cai, D.Q., Yao, X., Wu, Q.C., Ye, J.H., Zhang, J., Guo, M.X., Xu, H., Wang, D.F., 2022. Gel-based nanocomposite using persulfate-activated bread crumbs for fulvic acid release and Pb(II) removal. *Chem. Eng. J.* 446, 137002. <https://doi.org/10.1016/j.cej.2022.137002>.
- Cao, Y.Y., Jin, H.M., Zhu, N., Zhou, Z.M., 2023. High-efficiency fungistatic activity of vegetable waste-based humic acid related to the element composition and functional group structure. *Process Saf. Environ. Prot.* 169, 697–705. <https://doi.org/10.1016/j.psep.2022.11.028>.
- Checa-Fernández, A., Santos, A., Romero, A., Domínguez, C.M., 2021. Remediation of real soil polluted with hexachlorocyclohexanes ( $\alpha$ -HCH and  $\beta$ -HCH) using combined thermal and alkaline activation of persulfate: optimization of the operating conditions. *Sep. Purif. Technol.* 270, 118795. <https://doi.org/10.1016/j.seppur.2021.118795>.
- Chen, W., Westerhoff, P., Leenheer, J.A., Booksh, K., 2003. Fluorescence excitation– emission matrix regional integration to quantify spectra for dissolved organic matter. *Environ. Sci. Technol.* 37 (24), 5701–5710. <https://doi.org/10.1021/es034354c>.
- Chen, X.-E., Mangindaan, D., Chien, H.-W., 2023. Green sustainable photothermal materials by spent coffee grounds. *J. Taiwan Inst. Chem. Eng.* 137, 104259. <https://doi.org/10.1016/j.jtice.2022.104259>.
- Ciesielczuk, T., Rosik-Dulewska, C., Poluszynska, J., Milek, D., Szewczyk, A., Sławińska, I., 2018. Acute toxicity of experimental fertilizers made of spent coffee grounds. *Waste Biomass Valoriz.* 9 (11), 2157–2164. <https://doi.org/10.1007/s12649-017-9980-3>.
- Crespihlo, F.N., Zucolotto, V., Siqueira, J.R., Constantino, C.J., Nart, F.C., Oliveira, O.N., 2005. Immobilization of humic acid in nanostructured layer-by-layer films for sensing applications. *Environ. Sci. Technol.* 39 (14), 5385–5389. <https://doi.org/10.1021/es050552n>.
- Dai, C.-F., Tian, D.-Y., Li, S.-P., Li, X.-D., 2015. Methotrexate intercalated layered double hydroxides with the mediation of surfactants: Mechanism exploration and bioassay study. *Mater. Sci. Eng.: C* 57, 272–278. <https://doi.org/10.1016/j.msec.2015.07.040>.
- Das, S.K., Ghosh, G.K., 2022a. Conversion of biomass into low-cost biochar along with organic manure improved soil hydro-physical environment through technological intervention for sandy soil restoration. *Biomass Convers. Biorefinery.* <https://doi.org/10.1007/s13399-022-02724-6>.
- Das, S.K., Ghosh, G.K., 2022b. Soil hydro-physical properties affected by biomass-derived biochar and organic manure: a low-cost technology for managing acidic mountain sandy soils of north eastern region of India. *Biomass Convers. Biorefinery.* <https://doi.org/10.1007/s13399-022-03107-7>.
- Das, S.K., Ghosh, G.K., Avasthe, R., 2022a. Biochar and organic manures on produce quality, energy budgeting, and soil health in maize-black gram system. *Arab. J. Geosci.* 15. <https://doi.org/10.1007/s12517-022-10790-3>.
- Das, S.K., Ghosh, G.K., Choudhury, B.U., Hazarika, S., Mishra, V.K., 2022b. Developing biochar and organic nutrient packages/technology as soil policy for enhancing yield and nutrient uptake in maize-black gram cropping system to maintain soil health. *Biomass Convers. Biorefinery.* <https://doi.org/10.1007/s13399-022-02300-y>.
- Das, S.K., Choudhury, B.U., Hazarika, S., Mishra, V.K., Laha, R., 2023. Long-term effect of organic fertilizer and biochar on soil carbon fractions and sequestration in maize-black gram system. *Biomass Convers. Biorefinery.* <https://doi.org/10.1007/s13399-023-04165-1>.
- Fukuchi, S., Miura, A., Okabe, R., Fukushima, M., Sasaki, M., Sato, T., 2010. Spectroscopic investigations of humic-like acids formed via polycondensation reactions between glycine, catechol and glucose in the presence of natural zeolites. *J. Mol. Struct.* 982 (1), 181–186. <https://doi.org/10.1016/j.molstruc.2010.08.032>.
- Gao, L., Guo, Y., Zhan, J., Yu, G., Wang, Y., 2022. Assessment of the validity of the quenching method for evaluating the role of reactive species in pollutant abatement during the persulfate-based process. *Water Res.* 221. <https://doi.org/10.1016/j.watres.2022.118730>.
- Gebreyessus, G.D., 2022. Towards the sustainable and circular bioeconomy: insights on spent coffee grounds valorization. *Sci. Total Environ.* 833. <https://doi.org/10.1016/j.scitotenv.2022.155113>.
- Hardgrove, S.J., Livesley, S.J., 2016. Applying spent coffee grounds directly to urban agriculture soils greatly reduces plant growth. *Urban For. Urban Green.* 18, 1–8. <https://doi.org/10.1016/j.ufug.2016.02.015>.
- Hoeffner, K., Santonja, M., Cluzeau, D., Monard, C., 2019. Epi-aneic rather than strict-aneic earthworms enhance soil enzymatic activities. *Soil Biol. Biochem.* 132, 93–100. <https://doi.org/10.1016/j.soilbio.2019.02.001>.
- Holochová, P., Mašláňová, I., Sedláček, I., Švec, P., Králová, S., Kovařovic, V., Busse, H.-J., Staňková, E., Barták, M., Pantůček, R., 2020. Description of *Massilia rubra* sp. nov., *Massilia aquatica* sp. nov., *Massilia mucilaginoso* sp. nov., *Massilia frigida* sp. nov., and one *Massilia* genomospecies isolated from Antarctic streams, lakes and regoliths. *Syst. Appl. Microbiol.* 43 (5) <https://doi.org/10.1016/j.syapm.2020.126112>.
- Horgan, F., Floyd, D., Mundaca, E.A., Crisol-Martinez, E., 2023. Spent coffee grounds applied as a top-dressing or incorporated into the soil can improve plant growth while reducing slug herbivory. *Agric. Basel* 13 (2), 257. <https://doi.org/10.3390/agriculture13020257>.
- Hsieh, P.-C., Chen, Y.-C., Zheng, N.-C., Mangindaan, D., Chien, H.-W., 2023. A low-cost and environmentally-friendly chitosan/spent coffee grounds composite with high photothermal properties for interfacial water evaporation. *J. Ind. Eng. Chem.* 126, 283–291. <https://doi.org/10.1016/j.jiec.2023.06.019>.
- Huang, M.Q., Wang, X.L., Zhu, C.Y., Zhu, F.X., Liu, P., Wang, D.X., Fang, G.D., Chen, N., Gao, S.X., Zhou, D.M., 2022. Efficient chlorinated alkanes degradation in soil by combining alkali hydrolysis with thermally activated persulfate. *J. Hazard. Mater.* 438. <https://dx.doi.org/10.1016/j.jhazmat.2022.129571>.
- Hunkeler, D., 1991. Mechanism and kinetics of the persulfate-initiated polymerization of acrylamide. *Macromolecules* 24 (9), 2160–2171. <https://doi.org/10.1021/ma00009a004>.
- Jeong, H.J., Cha, J.Y., Choi, J.H., Jang, K.S., Lim, J., Kim, W.Y., Seo, D.C., Jeon, J.R., 2018. One-pot transformation of technical lignins into humic-like plant stimulants through fenton-based advanced oxidation: accelerating natural fungus-driven humification. *ACS Omega* 3 (7), 7441–7453. <https://doi.org/10.1021/acsomega.8b00697>.
- Karabaev, S., Gainullina, I., Harchenko, A., Satarova, M., Lugovskoy, S., Pendin, A., 2012. Solvation excess of urea over water in humic acid in three-component solutions saturated with the biopolymer. *J. Solut. Chem.* 41 (6), 1013–1019. <https://doi.org/10.1007/s10953-012-9842-3>.
- Kwon, S., Yoon, H.Y., Phong, N.T., Lee, G.Y., Jang, K.-S., Joe, E.-N., Lee, Y., Jeon, J.-R., 2022. Humic-like crop stimulatory activities of coffee waste induced by incorporation of phytotoxic phenols in melanoidins during coffee roasting: linking the Maillard reaction to humification. *Food Res. Int.* 162. <https://doi.org/10.1016/j.foodres.2022.112013>.
- Lee, J., von Gunten, U., Kim, J.-H., 2020. Persulfate-based advanced oxidation: critical assessment of opportunities and roadblocks. *Environ. Sci. Technol.* 54 (6), 3064–3081. <https://doi.org/10.1021/acs.est.9b07082>.
- Lee, J.G., Yoon, H.Y., Cha, J.-Y., Kim, W.-Y., Kim, P.J., Jeon, J.-R., 2019. Artificial humification of lignin architecture: top-down and bottom-up approaches. *Biotechnol. Adv.* 37 (8) <https://doi.org/10.1016/j.biotechadv.2019.107416>.
- Liu, B., Zhang, J., Chen, C., Wang, D., Tian, G., Zhang, G., Cai, D., Wu, Z., 2021. Infrared-light-responsive controlled-release pesticide using hollow carbon microspheres@Polyethylene glycol/ $\alpha$ -cyclodextrin gel. *J. Agric. Food Chem.* 69 (25), 6981–6988. <https://doi.org/10.1021/acs.jafc.1c01265>.
- Ma, J., Li, H.Y., Chi, L.P., Chen, H.K., Chen, C.Z., 2017. Changes in activation energy and kinetics of heat-activated persulfate oxidation of phenol in response to changes in pH and temperature. *Chemosphere* 189, 86–93. <https://doi.org/10.1016/j.chemosphere.2017.09.051>.
- Malkan, A.D., Strollo, W., Scholand, S.J., Dudrick, S.J., 2009. Implanted-port-catheter-related sepsis caused by *Acidovorax avenae* and methicillin-sensitive *Staphylococcus aureus*. *J. Clin. Microbiol.* 47 (10), 3358–3361. <https://doi.org/10.1128/jcm.01093-09>.

- Murthy, P.S., Naidu, M.M., 2012. Sustainable management of coffee industry by-products and value addition - a review. *Resour. Conserv. Recycl.* 66, 45–58. <https://doi.org/10.1016/j.resconrec.2012.06.005>.
- Mussatto, S.I., Machado, E.M.S., Martins, S., Teixeira, J.A., 2011. Production, composition, and application of coffee and its industrial residues. *Food Bioprocess Technol.* 4 (5), 661–672. <https://doi.org/10.1007/s11947-011-0565-z>.
- Olaetxea, M., Mora, V., Bacaicoa, E., Garnica, M., Fuentes, M., Casanova, E., Zamarreño, A.M., Iriarte, J.C., Etayo, D., Ederria, I., Gonzalo, R., Baigorri, R., García-Mina, J.M., 2015. Abscisic acid regulation of root hydraulic conductivity and aquaporin gene expression is crucial to the plant shoot growth enhancement caused by rhizosphere humic acids. *Plant Physiol.* 169 (4), 2587–2596. <https://dx.doi.org/10.1104/pp.15.00596>.
- Pagliarini, E., Totaro, G., Sacconi, A., Gaggia, F., Lancellotti, I., Di Gioia, D., Sisti, L., 2023. Valorization of coffee wastes as plant growth promoter in mulching film production: a contribution to a circular economy. *Sci. Total Environ.* 871. <https://doi.org/10.1016/j.scitotenv.2023.162093>.
- Said-Pullicino, D., Erriquens, F.G., Gigliotti, G., 2007. Changes in the chemical characteristics of water-extractable organic matter during composting and their influence on compost stability and maturity. *Bioresour. Technol.* 98 (9), 1822–1831. <https://doi.org/10.1016/j.biortech.2006.06.018>.
- Shao, Y.C., Bao, M.G., Huo, W.Z., Ye, R., Ajmal, M., Lu, W.J., 2023. From biomass to humic acid: Is there an accelerated way to go. *Chem. Eng. J.* 452. <https://doi.org/10.1016/j.cej.2022.139172>.
- Sonawane, S., Rayaroth, M.P., Landge, V.K., Fedorov, K., Boczkaj, G., 2022. Thermally activated persulfate-based advanced oxidation processes - recent progress and challenges in mineralization of persistent organic chemicals: a review. *Curr. Opin. Chem. Eng.* 37. <https://doi.org/10.1016/j.coche.2022.100839>.
- Stylianou, M., Agapiou, A., Omirou, M., Vyrides, I., Ioannides, I.M., Maratheftis, G., Fasoula, D., 2018. Converting environmental risks to benefits by using spent coffee grounds (SCG) as a valuable resource. *Environ. Sci. Pollut. Res.* 25 (36), 35776–35790. <https://doi.org/10.1007/s11356-018-2359-6>.
- Waggoner, D.C., Chen, H.M., Willoughby, A.S., Hatcher, P.G., 2015. Formation of black carbon-like and alicyclic aliphatic compounds by hydroxyl radical initiated degradation of lignin. *Org. Geochem.* 82, 69–76. <https://doi.org/10.1016/j.orggeochem.2015.02.007>.
- Wang, J.L., Liu, K.L., Zhao, X.Q., Zhang, H.Q., Li, D., Li, J.J., Shen, R.F., 2021. Balanced fertilization over four decades has sustained soil microbial communities and improved soil fertility and rice productivity in red paddy soil. *Sci. Total Environ.* 793. <https://doi.org/10.1016/j.scitotenv.2021.148664>.
- Wang, L.X., Chi, Y., Du, K., Zhou, Z.Z., Wang, F., Huang, Q.X., 2023. Hydrothermal treatment of food waste for bio-fertilizer production: Regulation of humus substances and nutrient (N and P) in hydrochar by feedwater pH. *Waste Biomass Valoriz.* 1–15. <https://doi.org/10.1007/s12649-023-02033-7>.
- Wang, X., Yao, Y., Wang, G., Li, H., Ma, J., Zhang, M., Chen, X., Yin, C., Mao, Z., 2022. Controlled-release diammonium phosphate alleviates apple replant disease: an integrated analysis of soil properties, plant growth, and the soil microbiome. *J. Agric. Food Chem.* 70, 8942–8954. <https://doi.org/10.1021/acs.jafc.2c01630>.
- Wang, X.Z., Chen, Z.G., He, Y.T., Yi, X.H., Zhang, C., Zhou, Q., Xiang, X.Z., Gao, Y.A., Huang, M.Z., 2023. Activation of persulfate-based advanced oxidation processes by 1T-MoS<sub>2</sub> for the degradation of imidacloprid: Performance and mechanism. *Chem. Eng. J.* 451. <https://doi.org/10.1016/j.cej.2022.138575>.
- Wang, Z.B., Zhang, Y.Z., Bo, G.D., Zhang, Y.P., Chen, Y., Shen, M.C., Zhang, P., Li, G.T., Zhou, J., Li, Z.F., Yang, J.M., 2022. *Ralstonia solanacearum* infection disturbed the microbiome structure throughout the whole Tobacco Crop Niche as well as the nitrogen metabolism in soil. *Front. Bioeng. Biotechnol.* 10. <https://doi.org/10.3389/fbioe.2022.903555>.
- Wei, S.X., Li, Z.C., Sun, Y., Zhang, J.M., Ge, Y.Y., Li, Z.L., 2022. A comprehensive review on biomass humification: recent advances in pathways, challenges, new applications, and perspectives. *Renew. Sustain. Energy Rev.* 170. <https://doi.org/10.1016/j.rser.2022.112984>.
- Wojnarovits, L., Takacs, E., 2019. Rate constants of sulfate radical anion reactions with organic molecules: a review. *Chemosphere* 220, 1014–1032. <https://doi.org/10.1016/j.chemosphere.2018.12.156>.
- Xiang, Y.B., Zhang, G.L., Chen, C.W., Liu, B., Cai, D.Q., Wu, Z.Y., 2018. Fabrication of a pH-responsively controlled-release pesticide using an attapulgite-based hydrogel. *ACS Sustain. Chem. Eng.* 6 (1), 1192–1201. <https://doi.org/10.1021/acssuschemeng.7b03469>.
- Xiao, K.K., Horn, H., Abbt-Braun, G., 2022. "Humic substances" measurement in sludge dissolved organic matter: a critical assessment of current methods. *Chemosphere* 293. <https://doi.org/10.1016/j.chemosphere.2022.133608>.
- Xiaoli, C., Shimaoka, T.Y., Qiang, G., Youcai, Z., 2008. Characterization of humic and fulvic acids extracted from landfill by elemental composition, <sup>13</sup>C CP/MAS NMR and TMAH-Py-GC/MS. *Waste Manag.* 28 (5), 896–903. <https://doi.org/10.1016/j.wasman.2007.02.004>.
- Yamane, K., Kono, M., Fukunaga, T., Iwai, K., Sekine, R., Watanabe, Y., Iijima, M., 2014. Field evaluation of coffee grounds application for crop growth enhancement, weed control, and soil improvement. *Plant Prod. Sci.* 17 (1), 93–102. <https://doi.org/10.1626/pp.17.93>.
- Yang, F., Zhang, S.S., Cheng, K., Antonietti, M., 2019. A hydrothermal process to turn waste biomass into artificial fulvic and humic acids for soil remediation. *Sci. Total Environ.* 686, 1140–1151. <https://doi.org/10.1016/j.scitotenv.2019.06.045>.
- Yang, S.Q., Liu, Z.Q., Cui, Y.H., Wang, M.K., 2023. Organics abatement and recovery from wastewater by a polymerization-based electrochemically assisted persulfate process: promotion effect of chloride ion and its mechanism. *J. Hazard. Mater.* 446. <https://doi.org/10.1016/j.jhazmat.2022.130658>.
- Zhang, H.X., Xie, C.H., Chen, L., Duan, J., Li, F., Liu, W., 2023. Different reaction mechanisms of SO<sub>4</sub><sup>•-</sup> and •OH with organic compound interpreted at molecular orbital level in Co(II)/peroxymonosulfate catalytic activation system. *Water Res.* 229. <https://doi.org/10.1016/j.watres.2022.119392>.
- Zhang, X.C., Wu, S.H., Jia, S.Y., Wang, C., Sun, S.W., Wang, X.M., Meng, Z.H., Lin, Y.Y., Liu, Y., Ren, H.T., Han, X., 2020. Turning thiophene contaminant into polymers from wastewater by persulfate and CuO. *Chem. Eng. J.* 397. <https://doi.org/10.1016/j.cej.2020.125351>.
- Zhang, Y.C., Yue, D.B., Wang, X., Song, W.F., 2019. Mechanism of oxidation and catalysis of organic matter abiotic humification in the presence of MnO<sub>2</sub>. *J. Environ. Sci. (China)* 77, 167–173. <https://doi.org/10.1016/j.jes.2018.07.002>.
- Zhu, Y.Y., Chen, M.M., Li, Q., Yuan, C., Wang, C.Y., 2017. High-Yield humic acid-based hard carbons as promising anode materials for sodium-ion batteries. *Carbon* 123, 727–734. <https://doi.org/10.1016/j.carbon.2017.08.030>.

ICS 67.100

CCS B23

# T/SDIFST

山东省食品科学技术学会团体标准

T/SDIFST 0003—2021

## 马铃薯抗性淀粉质量通则

General quality of potato resistant starch

2022-10-22 发布

2022-10-22 实施

山东省食品科学技术学会 发布

## 前 言

本文件按照GB/T 1.1—2020《标准化工作导则 第1部分：标准化文件的结构和起草规则》的规定起草。

请注意本文件的某些内容可能涉及专利，本文件的发布机构不承担识别专利的责任。

本文件由青岛农业大学提出。

本文件由山东省食品科学技术学会归口。

本文件起草单位：青岛农业大学、呼伦贝尔农垦集团（集团）股份有限公司、呼伦贝尔瑞源生物科技有限公司、呼伦贝尔恒能马铃薯产业研究院有限公司。

本文件主要起草人：孙庆杰、李楠、董楠燕、代蕾、鹿娜、曹静、袁惠昆、郭志军、董悦。

本文件为首次发布。



# 马铃薯抗性淀粉质量通则

## 1 范围

本文件规定了马铃薯抗性淀粉的术语和定义，规定了其技术要求、检验规则、包装、标识、运输和贮存。

本文件适用于粮食工业作为原料使用或直接冲调食用的马铃薯抗性淀粉的生产、检验及销售。

## 2 规范性引用文件

下列文件中的内容通过文中的规范性引用而构成本文件必不可少的条款。其中，注日期的引用文件，仅该日期对应的版本适用于本文件；不注日期的引用文件，其最新版本（包括所有的修改单）适用于本文件。

- GB/T 191 包装储运图示标志
- GB 1886.44 食品安全国家标准 食品添加剂 抗坏血酸钠
- GB 1886.174 食品安全国家标准 食品添加剂 食品工业用酶制剂
- GB 1886.235 食品安全国家标准 食品添加剂 柠檬酸
- GB 2709 食品安全国家标准 食品添加剂使用标准
- GB 4789.1 食品安全国家标准 食品微生物学检验 总则
- GB 4789.2 食品安全国家标准 食品微生物学检验 菌落总数测定
- GB 4789.3 食品安全国家标准 食品微生物学检验 大肠菌群计数
- GB 4789.4 食品安全国家标准 食品微生物学检验 沙门氏菌检验
- GB 4789.10 食品安全国家标准 食品微生物学检验 金黄色葡萄球菌检验
- GB 4789.15 食品安全国家标准 食品微生物学检验 霉菌和酵母计数
- GB 4806.7 食品安全国家标准 食品接触用塑料材料及制品
- GB 4806.9 食品安全国家标准 食品接触用金属材料及制品
- GB 5009.3 食品安全国家标准 食品中水分的测定
- GB 5009.4 食品安全国家标准 食品中灰分的测定
- GB/T 5491 粮食、饲料检验 取样、分样法
- GB 5749 生活饮用水卫生标准
- GB 7101 食品安全国家标准 饮料
- GB 7718 食品安全国家标准 预包装食品标签通则
- GB/T 8891 食用马铃薯淀粉
- GB 28050 食品安全国家标准 预包装食品营养标签通则
- GB 29921 食品安全国家标准 预包装食品中致病菌限量
- GB 31437 食品安全国家标准 食用淀粉
- LS/T 3106 马铃薯
- SB/T 10753 马铃薯雪花全粉
- JJF 1070 定量包装商品净含量计量检验规则
- 国家市场监督管理总局令第75号 《定量包装商品计量监督管理办法》

## 3 术语和定义

下列术语和定义适用于本文件。

### 3.1

马铃薯抗性淀粉 (potato resistant starch)

以鲜马铃薯、马铃薯淀粉、马铃薯雪花全粉等为原料，适量添加柠檬酸、抗坏血酸钠和食品工业用酶制剂，经前处理、热糊化（或不糊化）、酶解、回生、干燥、筛分、包装而成，含有抗性淀粉的产品。

#### 4 技术要求

##### 4.1 原辅料要求

###### 4.1.1 马铃薯

应符合 LS/T 3106 的规定。

###### 4.1.2 马铃薯淀粉

应符合 GB/T 8884 的规定。

###### 4.1.3 马铃薯雪花全粉

应符合 SB/T 10752 的规定。

###### 4.1.4 加工用水

应符合 GB5749 的要求。

###### 4.1.5 食品添加剂

加工用柠檬酸应符合 GB 1886.235 的要求，抗坏血酸钠应符合 GB 1886.44 的要求，食品工业用酶制剂应符合 GB 1886.171 的要求，其他添加剂应符合 GB 2760 的要求。

##### 4.2 感官要求

感官要求应符合表 1 规定。

表1 感官要求

项目	要求	检验方法
色泽	呈产品应有的色泽，洁白至浅黄色	取适量样品置于洁净、干燥的白色盘（或同类型器皿）中，在自然光线下，肉眼辨别。
滋味和气味	无异味、无异味	
组织状态	呈干燥疏松粉末状，无结块，无霉变	
杂质	正常视力下无可见外来物质	

##### 4.3 理化要求

应符合表 2 规定。

表2 理化要求

项目	指标要求		检验方法
	一级	二级	
水分, % ≤	9.0		GB 5009.3
灰分(干燥), % ≤	6.0		GB 5009.4
抗性淀粉(干基), % ≥	55	40	见附录B

##### 4.4 微生物指标

应符合 GB 7101、GB 29921 和 GB 31637 的规定，具体要求见表 3。

表3 微生物限量要求

项目	采样方案 <sup>a</sup> 及限量 <sup>b</sup>				检验方法
	n	c	m	M	
菌落总数/(CFU/g)	5	2	10 <sup>4</sup>	10 <sup>5</sup> / 10 <sup>6</sup> / 10 <sup>7</sup>	GB 4789.2
大肠菌群/(CFU/g)	5	2	10 <sup>3</sup> / 10 <sup>4</sup>	10 <sup>4</sup> / 10 <sup>5</sup>	GB 4789.3
金黄色葡萄球菌/(CFU/g)	5	1	10 <sup>2</sup>	10 <sup>3</sup>	GB 4789.10
沙门氏菌 (CFU/25g)	5	0	0	—	GB 4789.6
霉菌与酵母/(CFU/g) M	M <sup>c</sup> (10 <sup>3</sup> )				GB 4789.15

<sup>a</sup> 样品的采样及处理按照 GB 4789.1 执行。n 为同一批次产品应采样的样品数量；c 为最大可允许超出 m 值的样品数；m 为致病微生物可接受水平的限量值；M 为致病微生物的最高安全限量值。

<sup>b</sup> 括号中限制适用于直接冲泡食用的与碎薯粒性淀粉。

<sup>c</sup> 括号中的限制仅是对原型的限制。

#### 4.5 净含量要求

应符合《定量包装商品计量监督管理办法》的规定，净含量检测应按照 GB 10770 的规定执行。

### 5 检验规则

#### 5.1 批次

同一批原料，同一批次、同一生产线生产和包装的，且同一品种，同一等级，同一规格产品为一批。

#### 5.2 抽样

按照 GB/T 5491 规定执行。

#### 5.3 原辅料入库检验

原辅料应经过质检部门按照原辅料要求进行检查，合格后方可入库。

#### 5.4 出厂检验

每批次出厂检验按照本标准要求进行，包括感官要求、水分、菌落总数、大肠菌群、净含量、检验合格并签发产品合格证后方可出厂。

#### 5.5 型式检验

5.5.1 正常生产时，每半年进行一次型式检验，有下列情况之一时，也应进行型式检验：

- 新产品鉴定时；
- 原辅材料产地或供应商、生产工艺发生较大改变时；
- 停产半年以上，恢复生产时；
- 出厂检验的结果与上次型式检验的结果有较大差异时；
- 国家质量监督机构或主管部门提出要求时；
- 更换生产设备时。

5.5.2 型式检验项目包括本文件中规定的全部项目。

#### 5.6 判定规则

5.6.1 出厂检验项目或型式检验项目全都符合本文件时，则该批产品检验合格。

5.6.2 检验结果中若微生物指标中有一项检验不合格，则判该批产品检验不合格，不得复检。

5.6.3 若出厂检验项目或型式检验中其它项目检验不合格，允许加倍抽样，对不合格项目进行复检，复检合格，则该批产品检验合格。

### 6 包装

包装材料应符合 GB 1806.7 和 GB 1806.9 的要求，非标准产品的等级

## 7 标识

产品图示标志应符合 GB/T 191 的规定；产品标签应符合 GB 7714 和 GB 26030 的规定。

## 8 运输

运输工具要干净、无异味，运输中要避免受潮、受压、暴晒，注意防震、轻卸，不得与有毒、有害、有异味物品混装运输。

## 9 贮存

产品应贮存于专用的食品成品库，库内要清洁、通风、阴凉、干燥、防尘、防蝇、防虫、防鼠，并应离地离墙，不得与有毒、有害、有异味等影响产品品质的物品共同存放。

在本标准规定的运输、贮存条件下，保质期 18 个月。

## 附录 A (规范性) 抗性淀粉含量测定

### A.1 仪器设备

- a) 离心机。
- b) 水浴振荡器。
- c) 水浴锅。
- d) 涡旋混匀器。
- e) 磁力搅拌器。
- f) 天平。
- g) 计时器。
- h) 分析天平。
- i) 分光光度计。
- j) 100  $\mu$ L 移液器及一次性枪头。
- k) 温度计：能够读取  $37 \pm 0.1^\circ\text{C}$  和  $50 \pm 0.1^\circ\text{C}$ 。
- l) 容量瓶，100ml、200ml、500ml、1L、2L。

### A.2 试剂

除非另有说明，本方法所用水为蒸馏水，试剂为分析纯。

- a) 淀粉葡萄糖苷酶 (3000 U/ml)：根据淀粉葡萄糖苷酶活力，称取适量，用 pH 5 醋酸钠缓冲液配制成 3000 U/ml， $4^\circ\text{C}$  下可保存 5 年。
- b) 胰  $\alpha$ -淀粉酶 (10mg/ml，含 30 U/ml 淀粉葡萄糖苷酶)：称取 1 g 胰  $\alpha$ -淀粉酶，用 100 mL 马来酸纳缓冲液，悬浮，振荡 5 分钟，加入 1 mL 300 U/ml 淀粉葡萄糖苷酶，充分混合，15000g 离心 10 分钟，取上清液，现配现用。
- c) GODPO (glucose oxidase/peroxidase) 试剂缓冲液。
- d) GODPO (glucose oxidase/peroxidase) 试剂酶。
- e) D-葡萄糖标准品。
- f) 两丁磺二酸钠 (马来酸纳) 缓冲液 (100mM, pH6.0)：准确称取 23.2 g 马来酸，加 1000 mL 水溶解后，用 2M 氢氧化钠溶液调 pH 至 6.0，再加入 0.6 g 二水合氯化钙溶解并定容至 1L，该溶液在  $4^\circ\text{C}$  下可保存 1 年。
- g) 醋酸钠缓冲液 (1.2M, pH3.8)：将 69.6mL 的冰醋酸 (1.05g/mL) 加至 800mL 的蒸馏水中，用 1M 氢氧化钠调节 pH 至 pH3.8，用蒸馏水定容至 1L。
- h) 醋酸钠缓冲液 (100mM, pH4.5)：将 5.8mL 的冰醋酸加至 900mL 的蒸馏水中，用 1M 氢氧化钠调节 pH 至 pH4.5，用蒸馏水定容至 1L。
- i) 氢氧化钠溶液 (2M)。
- j) 含水乙醇 (大约 50%v/v)：将 500mL 乙醇 (95%v/v 或者 99%v/v) 加至 500mL 的水中混匀。
- k) 空白试剂：通过混匀 0.1mL 的 100mM 醋酸钠缓冲液 (pH4.5) 和 3.0mL 的 GODPO 试剂。

### A.3 检测方法

#### A.3.1 样品准备

##### A.3.1.1 水解非抗性淀粉

准确称取 100mg ( $\pm 5$  mg) 样品直接倒入有编号的试管里，轻柔的拍打试管以保证样品集中在底部。每个试管中加入 4.0mL 胰  $\alpha$ -淀粉酶 (10mg/ml) 其中含有淀粉葡萄糖苷酶 (30 U/ml)，盖紧试管盖子，用涡旋振荡器混匀，放入振荡水浴器，连续振荡 (200 r/min)， $37^\circ\text{C}$  孵育，精确孵育时间为 16 小时，孵育结束后，打开试管盖子，加入 4.0mL 乙醇 (99%v/v)，离心 10 分钟，小心倒出上清液，加入 2mL

50%乙醇重悬浮，用涡旋器涡旋，再加入6ml 50%乙醇混合，离心10分钟，重复上述重悬浮和离心步骤，小心倒出上清液，翻转试管，吸取余余的液体。

### A.3.1.2 抗性淀粉含量测定

将试管冰冻，再向每个试管中加入磁力搅拌棒和3ml 2M的KOH，用磁力搅拌棒在冰浴/水浴状态下搅拌20分钟，以重悬浮状物和溶解抗性淀粉。向每个试管中加入8ml 1.2M的醋酸钠缓冲液(pH 8)，并用磁力搅拌棒搅拌，立即加入0.1ml淀粉葡萄糖苷酶(3300U/ml)，混匀，并放入50℃水浴孵育30min。对于抗性淀粉含量>10%的样品，用水洗瓶定量转移试管里的样品至100ml容量瓶，当用洗瓶冲洗试管中的溶液时用外磁铁保持试管中的磁力棒，用蒸馏水定容至100ml，并混匀。1500g离心10分钟。对于抗性淀粉含量<10%的样品，直接1500g离心10分钟(非稀释)。对于这些样品，试管里的最终体积大约为10.3ml。将上述上清液分别以0.1ml为单位转移至玻璃试管(16×100mm)，一式两份，加入3.0ml G0P00试剂，50℃孵育30分钟。测量每一个溶液在510nm下相对于空白试剂的吸光度值。

### A.3.2 计算公式

$$a = \Delta A_1 \times A \times 100 \times 0.9 \times \frac{100}{W} \quad \text{----- (A.1)}$$

$$b = \Delta A_1 \times A \times 10.3 \times 0.9 \times \frac{100}{W} \quad \text{----- (A.2)}$$

式中:

$a$  ——抗性淀粉(g/100g样品) (样品包含≥10%抗性淀粉);

$b$  ——抗性淀粉(g/100g样品) (样品包含<10%抗性淀粉);

$\Delta A_1$  ——相对于空白试剂的吸光度值;

$A$  ——100  $\mu$ g D-葡萄糖的G0P00吸光度值;

100 ——抗性淀粉含量≥10%的样品最终定容体积;

$W$  ——分析样本的干重=重量×(100-含水量)/100;

0.9 ——从测定获得的游离D-葡萄糖转换到淀粉中存在的脱水-D-葡萄糖的因子;

$\frac{100}{W}$  ——抗性淀粉在样品重量中百分比;

10.3 ——抗性淀粉含量<10%的样品最终体积。

注：本测试是根据国际先进标准 AOAC 2002.02「淀粉与植物性基质中的抗性淀粉 酶消化法」而制定。



全国团体标准信息平台

310013

浙江省杭州市西湖区竞舟路1号筑品金座501室 杭州天勤知识产权  
代理有限公司  
韩聪(0571-87755913)

发文日:

2023年10月27日



申请号: 202311409297.2

发文序号: 2023102702003610

## 专利申请受理通知书

根据专利法第28条及其实施细则第38条、第39条的规定,申请人提出的专利申请已由国家知识产权局受理。现将确定的申请号、申请日等信息通知如下:

申请号: 2023114092972

申请日: 2023年10月27日

申请人: 青岛农业大学

发明人: 李杨,吴雪颖,刘永新,孙庆杰,姬娜

发明创造名称: 一株戊糖片球菌 LWQ1 及其应用

经核实,国家知识产权局确认收到文件如下:

权利要求书 1份1页,权利要求项数: 10项

说明书 1份17页

说明书附图 1份8页

说明书摘要 1份1页

专利代理委托书 1份2页

遗传资源来源披露登记表 1份1页

生物材料存活证明 1份2页

生物材料保藏证明 1份2页

S26 标准序核苷酸或氨基酸序列列表 1份2页

发明专利请求书 1份5页

实质审查请求书 文件份数: 1份

申请方案卷号: 23127F1728

提示:

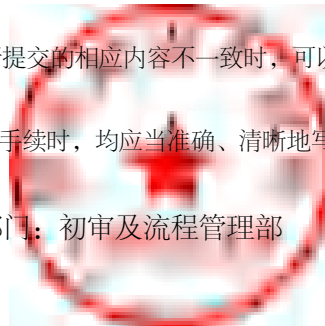
1.申请人收到专利申请受理通知书之后,认为其记载的内容与申请人所提交的相应内容不一致时,可以向国家知识产权局请求更正。

2.申请人收到专利申请受理通知书之后,再向国家知识产权局办理各种手续时,均应当准确、清晰地写明申请号。

审查员: 自动受理

联系电话: 010-62356655

审查部门: 初审及流程管理部



310013

浙江省杭州市西湖区竞舟路1号筑品金座501室 杭州天勤知识产权  
代理有限公司  
韩聪(0571-87755913)

发文日:

2023年10月27日



申请号: 202311409402.2

发文序号: 2023102702015860

## 专利申请受理通知书

根据专利法第28条及其实施细则第38条、第39条的规定,申请人提出的专利申请已由国家知识产权局受理。现将确定的申请号、申请日等信息通知如下:

申请号: 2023114094022

申请日: 2023年10月27日

申请人: 青岛农业大学

发明人: 李杨,吴雪颖,刘永新,孙庆杰,杨洁

发明创造名称: 一株植物乳杆菌 LWQ17 及其应用

经核实,国家知识产权局确认收到文件如下:

权利要求书 1份2页,权利要求项数: 10项

说明书 1份16页

说明书附图 1份6页

说明书摘要 1份1页

专利代理委托书 1份2页

遗传资源来源披露登记表 1份1页

生物材料存活证明 1份2页

生物材料保藏证明 1份2页

S26 标准序核苷酸或氨基酸序列列表 1份2页

发明专利请求书 1份5页

实质审查请求书 文件份数: 1份

申请方案卷号: 23127F1730

提示:

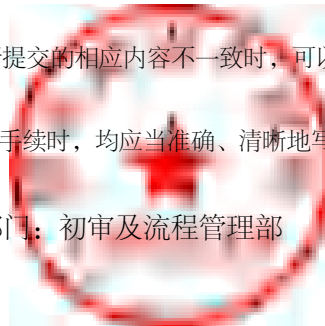
1.申请人收到专利申请受理通知书之后,认为其记载的内容与申请人所提交的相应内容不一致时,可以向国家知识产权局请求更正。

2.申请人收到专利申请受理通知书之后,再向国家知识产权局办理各种手续时,均应当准确、清晰地写明申请号。

审查员: 自动受理

联系电话: 010-62356655

审查部门: 初审及流程管理部



100040

北京市石景山区石景山路 23 号 22 号楼七层 716 室 北京大田律师事  
务所  
姜义民(18600039757)

发文日:

2023 年 05 月 06 日



申请号: 202310499446.2

发文序号: 2023050600392730

## 专利申请受理通知书

根据专利法第 28 条及其实施细则第 38 条、第 39 条的规定, 申请人提出的专利申请已由国家知识产权局受理。现将确定的申请号、申请日等信息通知如下:

申请号: 2023104994462

申请日: 2023 年 05 月 06 日

申请人: 中国科学院微生物研究所

发明人: 赵盼, 仲乃琴, 汪志琴, 曹晶晶

发明创造名称: 植物抗性诱导制剂及其应用

经核实, 国家知识产权局确认收到文件如下:

权利要求书 1 份 1 页, 权利要求项数: 4 项

说明书 1 份 10 页

说明书摘要 1 份 1 页

专利代理委托书 1 份 2 页

发明专利请求书 1 份 5 页

实质审查请求书 文件份数: 1 份

申请方案卷号: IMCAS20230046

提示:

1. 申请人收到专利申请受理通知书之后, 认为其记载的内容与申请人所提交的相应内容不一致时, 可以向国家知识产权局请求更正。

2. 申请人收到专利申请受理通知书之后, 再向国家知识产权局办理各种手续时, 均应当准确、清晰地写明申请号。

审查员: 王善雯

联系电话: 010-62356655

审查部门: 初审及流程管理部



# 国家知识产权局

100040

北京市石景山区石景山路 23 号 22 号楼七层 716 室 北京大田律师事  
务所  
姜义民(18600039757)

发文日:

2023 年 09 月 11 日



申请号: 202311160441.3

发文序号: 2023091100621870

## 专利申请受理通知书

根据专利法第 28 条及其实施细则第 38 条、第 39 条的规定, 申请人提出的专利申请已由国家知识产权局受理。现将确定的申请号、申请日等信息通知如下:

申请号: 2023111604413

申请日: 2023 年 09 月 08 日

申请人: 中国科学院微生物研究所

发明人: 仲乃琴, 曹晶晶, 汪志琴, 赵盼

发明创造名称: 磷酸根盐在制备促疮痂链霉菌生长的菌剂中的应用

经核实, 国家知识产权局确认收到文件如下:

权利要求书 1 份 2 页, 权利要求项数: 9 项

说明书 1 份 14 页

说明书附图 1 份 3 页

说明书摘要 1 份 1 页

专利代理委托书 1 份 2 页

发明专利请求书 1 份 5 页

申请方案卷号: IMCAS20230126

提示:

1. 申请人收到专利申请受理通知书之后, 认为其记载的内容与申请人所提交的相应内容不一致时, 可以向国家知识产权局请求更正。

2. 申请人收到专利申请受理通知书之后, 再向国家知识产权局办理各种手续时, 均应当准确、清晰地写明申请号。

审查员: 刘承骏

联系电话: 010-62356655

审查部门: 初审及流程管理部



200101  
2022.10

纸件申请, 回函请寄: 100088 北京市海淀区蓟门桥西土城路 6 号 国家知识产权局专利局受理处收  
电子申请, 应当通过专利业务办理系统以电子文件形式提交相关文件。除另有规定外, 以纸件等其他形式提交的文件视为未提交。



## OCTROOINUMMER 2031145

Octrooi Centrum Nederland verklaart dat op grond van octrooiaanvraag 2031145, ingediend op 2 maart 2022 octrooi is verleend aan:

Qingdao Agricultural University te Qingdao City, China

Uitvinder(s):  
Qingjie Sun te Qingdao City, China  
Congli Cui te Qingdao City, China  
Na ji te Qingdao City, China  
Qianzhu Lin te Qingdao City, China  
Kaili Qin te Qingdao City, China  
Han Jiang te Qingdao City, China  
Liu Jiong te Qingdao City, China

Voor: SLOWLY DIGESTIBLE STARCH AS WELL AS PREPARATION METHODS AND APPLICATIONS THEREOF

Aan dit bewijs is een exemplaar van het octrooi-schrift gehecht met nummer 2031145 en  
dattekening 8 september 2023.

De maximale beschermingsduur van het octrooi loopt tot en met 1 maart 2042.

Uitgereikt te Den Haag, 14 september 2023

De Directeur van Octrooi Centrum Nederland,

dr M.H. Spigt







## OCTROOINUMMER 2031143

Octrooi Centrum Nederland verklaart dat op grond van octrooiaanvraag 2031143, ingediend op 2 maart 2022, deftaal is verleend aan:

Qingdao Agricultural University te Qingdao City, China

UITVINDERS: Qingjie Sun te Qingdao City, China  
Xiaoyu Chen te Qingdao City, China  
Jin Gao te Qingdao City, China  
Na Ji te Qingdao City, China  
Yang Qin te Qingdao City, China  
Yanfei Wang te Qingdao City, China  
Man Li te Qingdao City, China  
Liu Kiong te Qingdao City, China

Voor: ANNEALING TREATMENT BASED MODIFIED STARCH AND PREPARATION  
METHOD AND APPLICATION THEREOF

Aan dit bewijs is een exemplaar van het octrooijschrift gehecht met nummer 2031143 en  
datstempeling 8 september 2023.

De maximale beschermingsduur van dit octrooi loopt tot en met 1 maart 2042.

Uitgereikt te Den Haag, 14 september 2023

De Directeur van Octrooi Centrum Nederland,

dr M.H. Spigt





## OCTROOINUMMER 2031144

Octrooiencentrum Nederland verklaart dat op grond van octrooiaanvraag 2031144, ingediend op 2 maart 2022 octrooi is verleend aan:

Qingdao Agricultural University te Qingdao City, China

**Uitvinder(s):**  
Qingjie Sun te Qingdao City, China  
Zihan Xu te Qingdao City, China  
Xuehai Wang te Qingdao City, China  
Lei Dai te Qingdao City, China  
Xuyan Dong te Qingdao City, China  
Liu Xiong te Qingdao City, China  
Na ji te Qingdao City, China

**Voor:** MAGNETIC MICROSPHERIC IMMOBILIZED PROTEASE, INSTANT HIGH-NITROGEN-SOLUBILITY-INDEX VEGETABLE PROTEIN PREPARED FROM SAME AND PREPARATION METHOD

Aan dit bewijs is een exemplaar van het octrooischrift gehecht met nummer 2031144 en slagtekening 8 september 2023.

De maximale beschermingsduur van dit octrooi loopt tot en met 1 maart 2042.

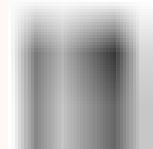
Uitgereikt te Den Haag, 14 september 2023

De Directeur van Octrooiencentrum Nederland,

Dr M.H. Spijt



证书号第5767334号



# 发明专利证书

发明名称：一种微生物菌剂、制备方法及其应用

发明人：汲恩民;仲乃琴;钞亚鹏;宋双伟;赵盼;刘宁;郝长虹  
赵广明;吴建强

专利号：ZL 2018 1 0113513.1

专利申请日：2018年02月05日

专利权人：呼伦贝尔恒屹农牧业股份有限公司

地址：021000 内蒙古自治区呼伦贝尔市陈巴尔虎旗宝日希勒镇  
奋斗居委

授权公告日：2023年03月07日

授权公告号：CN 110117554 B

国家知识产权局依照中华人民共和国专利法进行审查，决定授予专利权，颁发发明专利证书并在专利登记簿上予以登记。专利权自授权公告之日起生效。专利权期限为二十年，自申请日起算。

专利书记载专利权登记时的法律状况。专利权的转移、质押、无效、终止、恢复和专利权人的姓名或名称、国籍、地址变更等事项记载在专利登记簿上。

\* 2018101135131 \*

局长  
申长雨

申长雨



证书号 第5767334号

专利权人应当依照专利法及其实施细则规定缴纳年费。本专利的年费应当在每年02月05日前缴纳。未按照规定缴纳年费的，专利权自应当缴纳年费期满之日起终止。

申请日时本专利记载的申请人、发明人信息如下：

申请人：

呼伦贝尔恒屹农牧业股份有限公司

发明人：

汲恩民;仲乃琴;钞亚鹏;宋双伟;赵盼;刘宁;郝长虹;赵广明;吴建强

## 呼伦贝尔市“科技兴市”行动项目任务书

项目编号： 2022HZZX008

项目名称： 呼伦贝尔地区畜禽粪污及农作物秸秆  
快速腐熟技术研发与应用

任务下达单位（甲方）：呼伦贝尔市科学技术局

项目承担单位（乙方）：呼伦贝尔恒屹马铃薯产业研究院有限公司

主持单位：呼伦贝尔恒屹马铃薯产业研究院有限公司

合作单位：东华大学

归口管理单位（丙方）：陈巴尔虎旗农牧和科技局  
(旗市区科技管理部门, 主管部门)

项目执行期：2022年10月至2024年10月

呼伦贝尔市科学技术局

任务下达单位	单位名称	(盖章)		
	法定代表人	(盖章)	委托代理人	(盖章)
	通讯地址	呼和浩特市赛罕区腾飞大厦B座		
	联系人	张雷	电话	8252703
法人单位代码	11221060112902100	单位邮政编码	021000	
任务接收单位	单位名称	呼伦贝尔德昂特房产开发有限公司 (盖章)		
	法定代表人	(盖章)	委托代理人	(盖章)
	通讯地址	呼和浩特市赛罕区腾飞大厦B座		
	联系人	志恒	电话	13909703429
	开户银行	中国银行股份有限公司 呼伦贝尔市河东支行	账号	162402210280
法人单位代码	91150221MAA000100	单位邮政编码	021000	
窗口管理单位	单位名称	呼伦贝尔德昂特房产开发有限公司		
	法定代表人	徐蒙 (盖章)	委托代理人	(盖章)
	通讯地址	呼和浩特市赛罕区腾飞大厦B座		
	联系人	车力木格	电话	13948400284
	法人单位代码	91150221MAA000100	单位邮政编码	021000

任务下达单位业务科室意见:

同意

负责人(签字或盖章):



任务下达单位财务科意见:

同意

负责人(签字或盖章):



## 技术（植物新品种）实施许可协议

许可方（甲方）：定西马铃薯研究所（普通合伙）

住所地：甘肃省定西市安定区香泉镇陈家沟村

统一社会信用代码：91621102784015621E

法定代表人：李进福

项目联系人：李华圣 联系电话：18693553185

通讯地址：甘肃省定西市安定区香泉镇陈家沟村

被许可方（乙方）：呼伦贝尔恒屹农牧业股份有限公司

住所地：内蒙古自治区呼伦贝尔市海拉尔区神宝小区10号楼7号门市

统一社会信用代码：911507005888238409

法定代表人：波恩民

项目联系人：那长江 联系电话：13948703133

通讯地址：内蒙古自治区呼伦贝尔市海拉尔区神宝小区10号楼7号门市

本协议乙方呼伦贝尔恒屹农牧业股份有限公司经甲方定西马铃薯研究所（普通合伙）授权，将其拥有的马铃薯新品种生产经营予以授权，乙方受让并向甲方支付相应的使用费。双方经过平等协商，在真实、充分地表达各自意愿的基础上，根据《中华人民共和国民法典》的规定，达成如下协议，并由双方共同恪守。

第一条：本协议许可实施的植物新品种

1. 登记编号：GPD马铃薯（2023）620010



2. 作物种类：马铃薯

3. 品种名称：甘引9号

4. 育种者：定西马铃薯研究所（普通合伙）

5. 品种来源：AGRIA 突然结实实生苗

6. 适宜种植区域及季节：适宜在北部马铃薯一作区内蒙古鄂尔多斯地区，乌兰察布地区，河北张家口地区夏季种植。

7. 发证日期：2023年6月12日

8. 公告号：中华人民共和国农业农村部公告第678号

第二条：甲方在本协议生效前实施或转让本项植物新品种的状况：

1. 甲方实施本项植物新品种的状况：已授权区域内蒙古锡林郭勒盟。

2. 甲方许可他人本项植物新品种的状况：甲方向乙方授权并非独家授权，可以将本项植物新品种授权本协议之外的其他区域生产经营等。

第三条：乙方应以如下范围，方式和期限实施本项植物新品种：

1. 实施范围：仅仅在内蒙古呼伦贝尔区域内。

2. 实施方式：自主生产经营，非经书面许可，不得向他人另行授权。

3. 实施期限：2023年8月1日至2033年7月31日。

第四条：为保证乙方有效实施本项植物新品种，甲方应向乙方提交以下实物或技术资料：

联系事宜，一方变更项目联系人的，应当及时以书面形式通知另一方。未及时通知并影响本协议履行或造成损失的，应承担相应的责任。

第十五条：双方确定，出现下列情形，致使本协议的履行成为不必要或不可能的：可以解除本协议：

1. 发生不可抗力；
2. 双方约定解除协议。
3. 任何一方发生违约行为，经合理催告仍不改正的。

第十六条：双方因履行本协议而发生的争议，应协商、调解解决。协商、调解不成的，依法向甲方所在地人民法院提起诉讼。

第十七条：本协议一式四份，双方各执两份，具有同等法律效力。

第十八条：本协议经双方签字盖章后生效，有效期至本协议所有义务履行完毕。未尽事宜，双方另行协商签订补充协议，补充协议与本协议具有同等法律效力。

甲方：（盖章）  
法定代表人/委托代理人：

2023年 8 月 1 日

乙方：（盖章）  
法定代表人/委托代理人：

2023年 8 月 1 日



合同登记编号：

--	--	--	--	--	--	--	--	--	--	--	--	--	--	--	--	--	--	--	--

## 技 术 开 发 合 同

项目名称：马铃薯肥药高效技术开发示范推广

委托人（甲方）：呼伦贝尔农垦薯业（集团）股份有限公司

受托人（乙方）：中国科学院微生物研究所

签订地点：北京市

签订日期：2021年03月01日

有效期限：2021年03月01日至2025年12月31日



依据《中华人民共和国民法典》及其他相关法律法规的规定，合同双方就马铃薯肥药高效技术开发示范推广项目的技术开发经协商一致，签订本合同。

### 一、标的技术的内容、范围及要求

1. 本合同标的技术属于农业领域，依托甲方已有的“马铃薯肥料农药高效利用技术企业重点实验室”和院士工作站，开展马铃薯“肥-药-病-防”等相关技术开发。

2. 甲方委托乙方提供《马铃薯肥药高效技术开发推广示范方案》，技术开发内容包括马铃薯病毒检测，化肥农药减施增效技术，马铃薯土传病害防控，功能菌剂开发以及相关高效栽培技术开发推广等。

### 二、应达到的技术指标和参数

1. 为“马铃薯肥药减施增效剂技术示范”工作提供技术开发支撑，大田示范中化肥减施 10%，农药减施 10%，马铃薯不减产；等肥等药条件下，马铃薯增产 5%。

2. 乙方指导甲方技术人员开展马铃薯病毒检测，利用 PCR 技术鉴定马铃薯样品的病毒含量。同时培训相关技术人员 1-2 名，使其能够保障病毒检测技术的顺利进行。

3. 鉴定马铃薯块茎病在该区域的主要致病微生物，针对性展开功能菌剂的防控试验。

### 三、研究开发计划

2021 年 3 月 1 日至 2021 年 12 月 31 日：依托甲方“马铃薯肥料农药高效利用技术企业重点实验室”和院士工作站，鉴定种植区域马铃薯块茎病主要致病源，分析土壤理化性质，制定防控方案；

2022 年 3 月 1 日至 2023 年 12 月 31 日：对马铃薯种苗、种薯、土壤进行病害、病毒等检测，严控种苗、种薯质量；同时开展肥药减施增效、土传病害防控等功能菌剂技术开发，进行技术的展示及应用，培训相关技术人员 1-2 名。

#### 四、研究开发经费及其支付或结算方式

(一)本项目研究开发经费为人民币 150 万元(大写:壹佰伍拾万元整), 税费 0 元, 共计 150 万元。

##### (二)支付方式

1. 甲方应于合同期间按照工作计划, 分5年支付, 即于每年3月15日以前(付款具体时间为2021年3月15日前, 2022年3月15日前, 2023年3月15日前, 2024年3月15日前, 2025年3月15日前)向乙方支付当年研究经费 30 万元(大写:叁拾万元整)(含相应税费); 乙方于甲方按时足额支付该笔费用后开始工作;

2. 乙方于甲方按时足额支付每笔费用后15个工作日内向甲方开具等额增值税普通发票。

五、利用研究开发经费购置的设备、器材、资料的所有权归乙方所有。

#### 六、履行期限、地点和方式

(一)本合同履行期限为 2021 年 3 月 1 日至 2025 年 12 月 31 日。

(二)本合同在呼伦贝尔农垦种业(集团)股份有限公司所在地履行。

(三)本合同的履行方式为乙方向甲方交付:

1. 技术实施方案, 包括马铃薯病毒检测、化肥农药减施增效技术研发、马铃薯土传病害防控以及相关高效栽培技术等。

2. 在甲方或乙方所在地, 对甲方人员进行分子检测技术的培训。

#### 七、技术情报和资料的保密

(一)未经对方书面同意, 甲乙双方必须对本项目技术开发所涉及到的合同文本、项目经费、甲方书面明确要求的研究内容等资料保密。

(二)双方约定不论本协议是否变更、解除或终止, 协议的保密条款不受其限制而继续有效, 双方均应继续承担保密条款约定的保密义务。

(三)保密期限: 自合同签订之日起至合同履行完毕, 合同解除, 合同终止后两年内。

(四)如果合同解除或合同终止, 乙方有权本合同技术内容与第三方继续合作, 甲方不再承担的相应保密义务。

## 八、技术协作和技术指导的内容

在履行本合同过程中，甲方应对乙方提供乙方所需技术协作和技术指导，所产生的全部费用由甲方承担。

## 九、技术成果的归属和分享

### （一）专利申请权：

为履行本合同所产生的新技术、新设计的申请专利的权利，专利申请权及专利权归乙方所有。

### （二）发明人署名权

本合同所产生的专利申请文本、专利文本的发明人由乙方确定。

### （三）技术秘密的所有权、使用权

为履行本合同所产生的技术秘密的所有权归乙方所有，甲方可以使用。

### （四）后续改进的权利

乙方有权在完成本合同约定的研究开发工作后，利用该项研究开发成果进行后续改进，由此产生的具有实质性或创造性技术进步特征的新的技术成果，归乙方所有。

## 十、验收的标准和方式

研究开发所完成的技术成果，达到了本合同第二条所列技术指标，按标准，采用总结报告方式验收，由甲方在 10 个工作日内出具技术项目验收证明。甲方逾期不出具验收证明，或者验收不合格但未给出具体证据、理由或可行性改进意见，则视为验收合格。

## 十一、风险责任的承担

在履行本合同的过程中，确因在现有水平和条件下难以克服的技术困难，非因乙方故意或重大过失导致研究开发部分或全部失败所造成的损失，风险责任由甲方承担。

甲方已支付的所有费用不予退回，除非甲方已支付费用无法承担乙方已支出的人力、物力、财力成本，乙方不再要求甲方支付其他费用，合同终止。

## 十二、违约金或者损失赔偿额的计算

违反本合同约定，违约方应按照《中华人民共和国合同法》有关条款的规定承担违约责任。

(一)违反本合同第四条约定，甲方未经乙方书面同意而逾期付款的，按每日合同总金额的1%支付逾期违约金，甲方逾期30个工作日未足额支付相应费用，合同终止，甲方已向乙方支付的费用，乙方不予退还，由此给乙方造成的损失由甲方承担，乙方有权利用履行本合同所获得的技术成果与第三方继续合作。

(二)违反本合同第二、六条约定，甲方付款后乙方未能交付相关材料时，应承担以下违约责任：乙方按比例退还已收取的该部分研发经费，以乙方收到甲方支付费用扣除发生成本后的数额为上限。

### 十三、解决合同纠纷的方式

在履行本合同的过程中发生争议，双方当事人和解或调解不成，可采取仲裁程序解决，双方同意由北京仲裁委员会仲裁。


### 十四、其他

(一)甲方不得将乙方名称、标识、乙方人员姓名、职务等用于对外宣传、产品推广等活动，如甲方在对外宣传或产品推广过程中需要使用乙方名称、标识、乙方人员姓名、职务，则需书面通知乙方并将具体宣传推广方式、草案、文案等交于乙方审核，经乙方书面同意后方可使用。

(二)本合同所涉及乙方义务由乙方仲乃琴实验室团队承担，项目负责人为赵盼，乙方其他实验室团队不受本合同条款约束。

(三)本合同自甲乙双方签字盖章之日起生效，本合同一式肆份，甲乙双方各执贰份，具有同等法律效力。



委托人 (甲方)	名称 (或姓名)	呼伦贝尔农垦乳业 (集团) 股份有限公司 (盖章)			 技术合同专用章 单位公章
	法定代表人	汲恩民 			
	委托代理人	汲恩民 			
	联系 (经办) 人	志恒 (盖章)			
	住所 (通讯地址)	海拉尔区巴彦托	邮政	021000	
		海路中天大厦	编码		
	电话	13904703429	传真	0470-8348811	
	开户银行	中国银行股份有限公司呼伦贝尔市河套支行			
帐号	154064482014				
研究开发人员 (乙方)	名称 (或姓名)	中国科学院微生物研究所 (盖章)			 技术合同专用章 合同专用章
	法定代表人	钱韦 			
	委托代理人	赵盼 (盖章)			
	联系 (经办) 人	赵盼 (盖章)			
	住所 (通讯地址)	北京市朝阳区	邮政	100101	
		北辰西路1号院	编码		
	电话	13693010861	传真		
	开户银行	北京市工行海淀西区支行			
帐号	02000041090689117425				

印花稅票粘貼處

~~~~~

登記機關審查登記欄：

經辦人：

技術合同登記處機關（專用章）

年 月 日

合同登记编号：

|  |  |  |  |  |  |  |  |  |  |  |  |  |  |  |  |  |  |  |  |
|--|--|--|--|--|--|--|--|--|--|--|--|--|--|--|--|--|--|--|--|
|  |  |  |  |  |  |  |  |  |  |  |  |  |  |  |  |  |  |  |  |
|--|--|--|--|--|--|--|--|--|--|--|--|--|--|--|--|--|--|--|--|

## 技 术 开 发 合 同

项目名称：马铃薯病毒检测技术开发示范推广

委托人（甲方）：呼伦贝尔农垦薯业（集团）股份有限公司

受托人（乙方）：中国科学院微生物研究所

签订地点：北京市

签订日期：2021年5月6日

有效期限：2021年5月6日至2025年12月31日

依据《中华人民共和国民法典·合同编》及其他相关法律法规的规定，合同双方就马铃薯病毒检测技术开发示范推广项目的技术开发经协商一致，签订本合同。

### 一、标的技术的内容、范围及要求

1. 本合同标的技术属于农业领域，依托甲方已有的院士工作站，甲方委托乙方开展马铃薯病毒检测等相关技术开发。

2. 甲方委托乙方提供《马铃薯病毒检测技术方案》，技术开发内容包括马铃薯病毒检测。开发标的包括引物设计、检测试剂盒开发升级、马铃薯质量检测、品质鉴定（包括淀粉含量、Vc、蛋白质）。

### 二、应达到的技术指标和参数

1. 乙方指导甲方技术人员开展马铃薯病毒检测，利用 PCR 技术鉴定马铃薯样品的病毒含量。

(1) 设计特定 6 种病毒引物 18 对

(2) 升级试剂盒 1 个

(3) 检测病毒含量 > 10ng

(4) 培训相关技术人员 1-2 名，使其掌握病毒检测技术的操作程序。

### 三、研究开发计划

2021 年 5 月 6 日至 2021 年 12 月 31 日：依托甲方“马铃薯肥料农药高效利用技术企业重点实验室”和院士工作站，鉴定种植区域马铃薯病毒病主要病源，设计病毒引物，升级试剂盒。

2022 年 1 月 1 日至 2025 年 12 月 31 日：对马铃薯种薯、种薯、土壤进行病毒检测，严控种苗，种薯质量；培训相关技术人员 1-2 名。

### 四、研究开发经费及其支付或结算方式

(一) 本项目研究开发经费为人民币 100 万元（大写：壹佰万元整），税费 0 元，共计 100 万元。

(二) 支付方式

按照研究开发计划，甲方分 5 年向乙方支付研究开发经费。

1. 甲方应于合同签订后十个工作日内一次性向乙方支付第一笔研究经费人民币 20 万元（大写：贰拾万元整）（含相应税费），乙方于甲方按时足

额支付该笔费用后开始工作；

2. 甲方应连续四年于每年5月15日以前（即2022年5月15日、2023年5月15日、2024年5月15日、2025年5月15日）向乙方支付当年研究经费人民币20万元/年（大写：贰拾万元整/年）（含相应税费），乙方于甲方按时足额支付该笔费用后开始工作；

3. 乙方于甲方按时足额支付每笔费用后15个工作日内向甲方开具等额增值税普通发票。

**五、利用研究开发经费购置的设备、器材、资料的所有权归乙方所有。**

#### **六、履行期限、地点和方式**

（一）本合同履行期限为2021年5月6日至2025年12月31日；

（二）本合同在甲方或乙方所在地履行。

（三）本合同的履行方式为乙方向甲方交付：

1. 技术实施方案，包括马铃薯病毒检测以及相关高效栽培技术等。
2. 在甲方或乙方所在地，对甲方人员进行分子检测技术的培训。

#### **七、技术情报和资料的保密**

（一）未经对方书面同意，甲乙双方必须对本项目技术开发所涉及到的合同文本、项目经费、甲方书面明确要求的研究内容等资料保密。

（二）双方约定不论本协议是否变更、解除或终止，协议的保密条款不受其限制而继续有效，双方均应继续承担保密条款约定的保密义务。

（三）保密期限：自合同签订之日起至合同履行完毕、合同解除、合同终止后两年内。

#### **八、技术协作和技术指导的内容**

在履行本合同过程中，甲方对乙方提供乙方所需技术协作和技术指导，所产生的相关费用由甲方另行承担。

#### **九、技术成果的归属和分享**

（一）专利申请权：

为履行本合同所产生的新技术、新设计、申请专利的权利，专利申请权及专利权归甲乙双方共同所有。

（二）发明人署名权

本合同所产生的专利申请文本，专利文本的发明人由甲乙双方商定确定。

### （三）技术秘密的所有权、使用权

乙方为履行本合同所产生的技术秘密的所有权归乙方所有，甲方可以使用。

### （四）后续改进的权利

乙方有权在完成本合同约定的研究开发工作后，利用该项研究开发成果进行后续改进，由此产生的具有实质性或创造性技术进步特征的新的技术成果，归乙方所有。

### （五）培育人署名权

本合同所产生的植物新品种权的培育人由乙方确定。

### （六）论文与奖项

乙方或乙方技术人员有权将履行本合同所产生的技术成果发表论文；乙方或乙方技术人员有权单独享有履行本合同所产生的技术成果所获得的奖项，包括但不限于依法取得荣誉称号、奖章、奖励证书、奖金等等。

## 十、验收的标准和方式

研究开发所完成的技术成果，达到了本合同第二条所列技术指标，按标准，采用总结报告方式验收，由甲方在 10 个工作日内出具技术项目验收证明。甲方逾期不出具验收证明，或者验收不合格但未给出具体证据、理由或可行性改进意见，则视为验收合格。

## 十一、风险责任的承担

在履行本合同的过程中，确因在现有水平和条件下难以克服的技术困难，非因乙方故意或重大过失导致研究开发部分或全部失败所造成的损失，风险责任由甲方承担。

甲方已支付的所有费用不予退回，除非甲方已支付费用无法承担乙方已支出的人力、物力、财力成本，乙方不再要求甲方支付其他费用，合同终止。

## 十二、违约金或者损失赔偿额的计算

违反本合同约定，违约方应按照《中华人民共和国合同法·合同编》有关条款的规定承担违约责任。

(一) 违反本合同第四条约定，甲方未经乙方书面同意而逾期付款的，按每日合同总金额的 1% 支付逾期违约金，甲方逾期 30 个工作日未足额支付相应费用，乙方有权终止合同，乙方将合同终止通知函邮寄至甲方工商登记地址，无论甲方是否签收，本合同即告终止。甲方已向乙方支付的费用，乙方不予退还，由此给乙方造成的损失由甲方承担。本合同所产生的知识产权全部归乙方所有，乙方有权利用履行本合同所获得的技术成果与第三方继续合作。

(二) 违反本合同第二、六条约定，甲方付款后乙方因故意或重大过失未能交付相关材料时，应承担以下违约责任：乙方按比例退还已收取的该部分研发经费，以乙方收到甲方支付费用扣除发生成本后的数额为上限。如由于甲方原因造成结果不合约定内容，责任由甲方承担，甲方已支付的款项乙方不必退回，并且甲方需按合同提供乙方全部剩余款。

### 十三、解决合同纠纷的方式

在履行本合同的过程中发生争议，双方当事人和解或调解不成，可采取仲裁程序解决，双方同意由北京仲裁委员会仲裁。

### 十四、其他

(一) 甲方不得将乙方名称、标识、乙方人员姓名、职务等用于产品描述、包装或对外宣传、产品推广等活动。如甲方在产品描述、包装、对外宣传或产品推广过程中需要使用乙方名称、标识、乙方人员姓名、职务，需书面通知乙方并将具体使用方式、草案、文案、范围等交予乙方审核，经乙方书面同意后方可使用。甲方如违反该约定，则乙方有权单方解除本合同，已收到款项乙方将不予退还，甲方应承担赔礼道歉、消除影响、恢复名誉等等责任，并承担乙方因此受到的全部损失。(二) 本合同所涉及乙方义务由乙方 方荣祥 实验室团队承担，项目负责人为 张玉清，乙方其他实验室团队不受本合同条款约束。

(三) 本合同自甲乙双方签字盖章之日起生效，本合同一式肆份，甲乙双方各执贰份，各份具有同等法律效力。



|             |                     |                              |         |                                                                                                             |              |
|-------------|---------------------|------------------------------|---------|-------------------------------------------------------------------------------------------------------------|--------------|
| 委托人 (甲方)    | 名称 (或姓名)            | 呼伦贝尔农垦乳业 (集团) 股份有限公司<br>(盖章) |         | <br>技术合同专用章<br>或<br>单位公章 |              |
|             | 法定代表人               | 汲惠民 (盖章)                     |         |                                                                                                             |              |
|             | 委托代理人               | 汲惠民 (盖章)                     |         |                                                                                                             |              |
|             | 联系 (经办) 人           | 志 恒 (盖章)                     |         |                                                                                                             |              |
|             | 住所<br>(通讯地址)        | 海拉尔区巴彦托海路中天大厦                | 邮 政 编 码 |                                                                                                             | 021000       |
|             | 电 话                 | 13904703429                  | 传 真     |                                                                                                             | 0470-8348811 |
|             | 开户银行                | 中国银行股份有限公司呼伦贝尔市河东支行          |         |                                                                                                             | 2024年5月6日    |
|             | 帐 号                 | 15406448201                  |         |                                                                                                             |              |
| 研究开发人员 (乙方) | 名称 (或姓名)            | 中国科学院微生物研究所 (盖章)             |         | 技术合同专用章<br>或<br>单位公章                                                                                        |              |
|             | 法定代表人               | 钱 颖 (盖章)                     |         |                                                                                                             |              |
|             | 委托代理人               | 方荣祥 (盖章)                     |         |                                                                                                             |              |
|             | 联系 (经办) 人           | 张玉清 (盖章)                     |         |                                                                                                             |              |
|             | 住所<br>(通讯地址)        | 北京市朝阳区<br>北辰西路1号院3号          | 邮 政 编 码 |                                                                                                             | 100101       |
|             | 电 话                 | 13601220373                  | 传 真     |                                                                                                             | 010-64806543 |
|             | 开户银行                | 中国工商银行北京海淀西区支行营业室            |         |                                                                                                             | 2024年5月6日    |
| 帐 号         | 0200004309089117425 |                              |         |                                                                                                             |              |

印花稅票粘貼處



技術合同登記處

登記機關審查登記柱：

經辦人：

技術合同登記處機關（專用章）

年 月 日

## 合作框架协议

甲方：呼伦贝尔恒屹农牧业股份有限公司

乙方：呼伦贝尔市农牧业科学研究所

为发挥自治区马铃薯联合发展企业重点实验室的辐射带动作用，提升自治区原始创新能力，实现优势互补，甲乙双方就合作事宜达成如下协议。

### 一、合作内容及时间

1. 合作内容：甲乙双方就优质马铃薯淀粉加工品种的选育、育种基地建设及育种体系建设、重大项目申报及实施等开展深度合作。

2. 合作时间：2023年7月至2025年7月，第一合作周期暂定为2年。

### 二、职责

#### 1. 甲方职责：

为乙方提供科研试验必要的场所、科研辅助人员、试验材料和相关物质条件，提供必要的住宿等后勤保障。

根据甲方现有条件，全力配合乙方科研试验工作计划的安排落实。

#### 2. 乙方职责

协助开展合作内容，协助甲方建立育种基地，并提供全方位技术服务和指导，开展育种相关技术培训；为甲方马铃薯育种体系建设、重大项目开展进行技术性把关，视甲方需要，组织相关专家开展技术攻关和学术研讨活动。

开展优质马铃薯淀粉加工品种的选育工作，合作期间根据甲方需求筛选出多个马铃薯优质新品种系。

### 三、其他相关事宜

1. 各方应相互尊重，承担保密责任，在进行交流时，涉及他方的研究内容，未经同意不得向第三方透露。

2. 在协议到期前两个月，双方在良好合作的基础上协商续签协议事项。

3. 本协议未尽事宜，双方协商解决，协商一致后签订书面补充协议。本协议设正式文本一式两份，双方各持一份。

甲方：呼伦贝尔顺泰农牧业股份有限公司  
(盖章)



甲方代表(签字):

*[Handwritten signature]*

乙方：呼伦贝尔市畜牧科学研究所  
(盖章)



乙方代表(签字):

*[Handwritten signature]*

签订日期: 2024.7.21

签订日期: 2024.7.21

